POLYMERIC MATERIALS FOR THE QUANTITATIVE AND REVERSIBLE ABSORPTION OF ORGANIC AND INORGANIC WATER CONTAMINANTS

UNIVERSITÀ DEGLI STUDI DI MILANO
FACOLTÀ DI SCIENZE E TECNOLOGIE

Doctorate School of Chemical Sciences and Technologies
Doctorate Thesis in Industrial Chemistry

ELENA FERRARI

Co-ordinator: Prof. Dominique Roberto

Tutor: Dr. Amedea Manfredi

Co-tutor: Prof. Elisabetta Ranucci

ABSTRACT

Water pollution is one of the most serious environmental problems the world faces today.

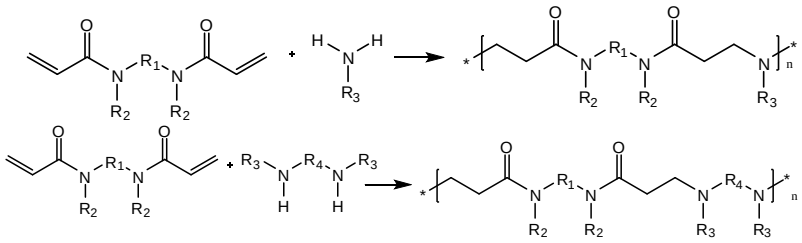

Scheme 1. PAA syntheses.

Due to a progressive change in environmental perception in developed countries, great attention is currently given to specific pollutants, both of natural and human origin, often labeled as organic and inorganic micropollutants. Micropollutants can have severe implications both on ecology and human health even in very low concentration in water, being potentially toxic and carcinogenic, and are included in the EU PP (Priority Pollutants) list. Inorganic micropollutants include many heavy metal ions, such as for instance Pb^{2+}, Cd^{2+} and Ni^{2+}. Organic micropollutants include a huge range of organohalides, aromatic hydrocarbons and other chemicals. The current water purification treatments are affected by many limitations and do not significantly lower the concentration of micropollutants, unless the treatment is carried out, if technically possible, to such an extent to become not economically sustainable. [1] In this context, the aim of this PhD thesis is the development and characterization of polymeric absorbing materials for the quantitative and reversible removal of organic and inorganic micro-pollutants from water. These materials are based on poly(amidoamine)s (PAAs), oligosaccharides

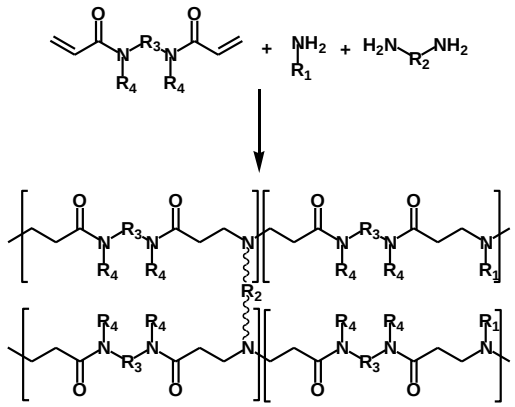

Scheme 2. Synthetic pathway leading to cross-linked PAAs.

such as cyclodextrins, as well as renewable resources such as hemicelluloses and guar gum.

PAAs are a family of versatile synthetic polymers obtained by 1,4-polyaddition of aliphatic primary amines or secondary bisamines to bisacrylamides (Scheme 1). The synthetic process is cheap and environmentally friendly as it proceeds in water, at room temperature and without added catalysts. Cross-linked PAA hydrogels can be prepared using multifunctional amines as cross-linking agents (Scheme 2) or by radical polymerization of acrylamide end-capped PAA oligomers, pre-synthesized employing a controlled excess of bisacrylamide. Both linear and cross-linked PAAs proved good absorbers for different heavy metal ions, such as Co^{2+}, Ni^{2+} and Cu^{2+}.This property is related to their complexing ability due to the presence of tert-amine groups regularly distributed along their backbone, which in connection with the neighboring amide groups act as chelating functions. Further chelating groups such as, for example, -COOH can also be introduced as side substituents. Moreover, pH modulation affords reversibility and selectivity in heavy metal complexation, since ion coordination by PAAs is pH-dependent. In particular, metal ion desorption is obtained by lowering the pH. [2]

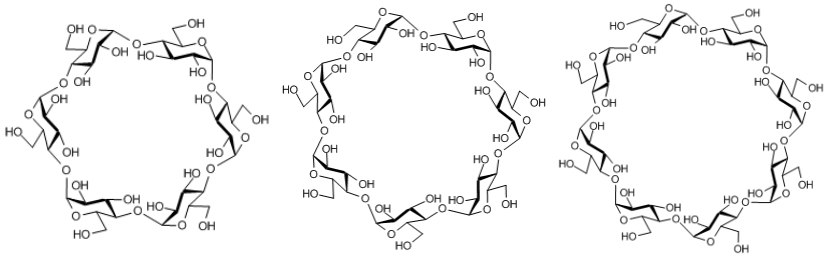

Figure 1. Structural features of cyclodextrins.

Cyclodextrins (CDs) are oligosaccharides made of glucopyranoside units α(1-4) linked to form a toroidal structure endowed with a hydrophobic cavity (Figure 1). CDs come with three different cavity sizes (0.57 nm for α-CD, 0.78 nm for β-CD and 0.95 nm for γ-CD) according to the number of glucopyranoside units (6, 7, 8 for α, β, and γ-CD, respectively) and interact with many different inorganic and organic compounds through host-guest interactions, and with a dimensional selectivity due to the different sizes of their inner cavity. CD-containing polymers, either linear or immobilized on solid supports and crosslinked CD hydrogels have been extensively studied as sorbents of organic pollutants with removal efficacy ranging within ample limits. [3] Since 1998, when the term was first used by Li and Ma, hyper-crosslinked CD in which CD units are linked by many short moieties are commonly referred to as nanosponges. Nanosponges represent supermolecular structures in which CD units are connected by nanochannels forming a cage-like architecture. They are nanoporous by definition and this is the reason why they

show very high inclusion constants with several organic pollutants, including aromatic and chlorinated ones. Nanosponges are usually obtained from β-CD, the cheapest one, and only relatively few examples of α- and γ-CD nanosponges, characterized by different dimensional selectivity, are reported. [4] [5]

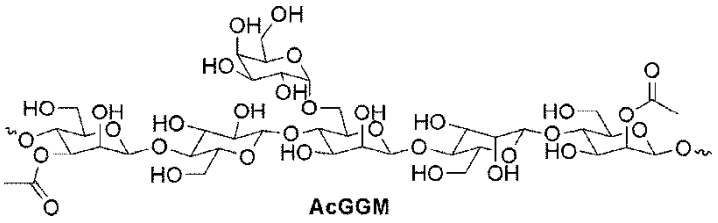

Figure 2. Structural features of AcGGM.

Hemicelluloses are amorphous polysaccharides located in the secondary cell wall of woods and grasses and the 2nd most common polysaccharides in nature, representing about 20-35%$^{w}/_{w}$ of lignocellulosic biomass. Dependent on their biological origin, hemicelluloses consist of varying amounts of xylan, mannan, β-glucan, and xyloglucan. Whereas hardwood hemicelluloses contain mostly xylans, softwood hemicelluloses contain mostly glucomannans. Lignocellulosic materials have sorption capacity for a wide range of solutes, particularly divalent metal cations, which derives from their constituent polymers and structure, including hemicelluloses. [6] In recent years, the interest in hemicellulose as a renewable resource has rapidly grown, and it has been used for the preparation of value-added products such as, for example, films, [7] bio-based fuels [8] and hydrogels. [9] In this thesis, a particular softwood hemicellulose, namely O-acetyl-galactoglucomannan (AcGGM, Figure 2), primarily found in the lignified secondary cell wall of softwoods such as spruce (*picea abies*), and representing up to 20%$^{w}/_{w}$ of the dry wood, was used for the preparation of hydrogels with PAAs. [10] Besides AcGGM, which is a highly purified fraction, also its less fractionated form, namely hydrolyzate, was employed.

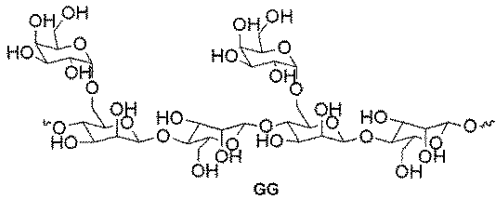

Figure 3. Structural features of GG.

Guar gum (GG) is a naturally occurring galactomannan polysaccharide extracted from the seed of the leguminous shrub *Cyamopsis tetragonoloba*. It is made up of a linear chain of β-D-mannopyranose joined by β-(1-4) linkage to which α-D-galactopyranosyl units are linked at every second mannose to give short side-branches (Figure 3). GG hydrates in cold water to form a highly viscous solution where the single polysaccharide chains interact with each other in a complex way. [11] Since GG is a low-cost, easily available and non-toxic polysaccharide, it is widely applied in many industrial fields. [12]

An adverse property of GG is its susceptibility for biodegradation therefore it is rarely used in its natural form. To enhance the application spectrum, GG modification has been reported by grafting, derivatization, and network formation. [13] GG-graft copolymers, nanocomposite materials as well as hydrogels have found application also in the environmental field. In particular, they proved efficient flocculants and sorbents for the treatment of industrial wastewater containing heavy metal ions such as Cr^{6+}, Pb^{2+}, Cd^{2+}, Zn^{2+}, Cu^{2+}, and Fe^{2+}. [14] [15] [16] [17]

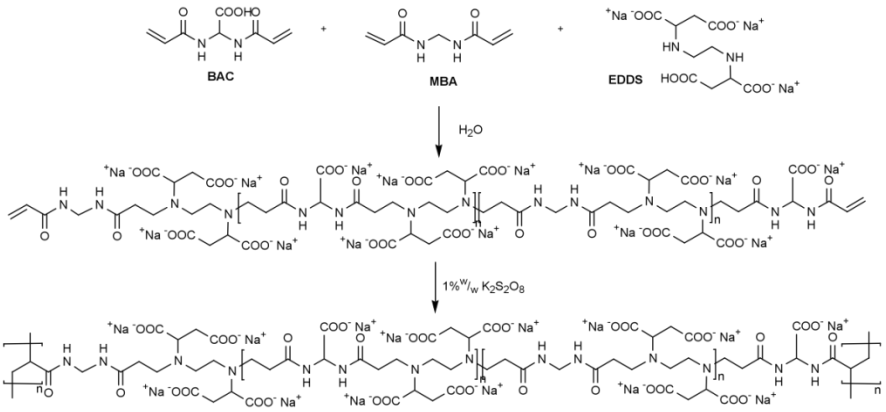

Scheme 3. Synthetic procedure leading to LMT85 hydrogel.

1. PAA hydrogels as inorganic pollutants absorbers [18] [19]

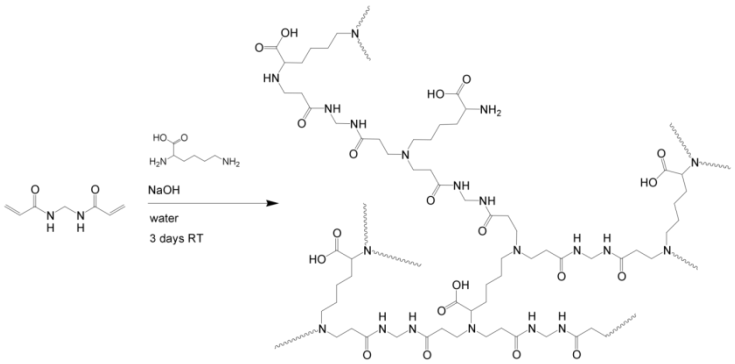

Scheme 4. Synthetic pathway leading to LYMA hydrogel.

As mentioned above, PAAs proved able to interact with many heavy metal ions. Based on this premise, a series of PAA hydrogels for the absorption of inorganic micro-pollutants such as Cu^{2+}, Co^{2+}, Ni^{2+}, Zn^{2+}, Cd^{2+}, Pb^{2+} and Mn^{2+} was developed.

The first material, labeled LMT85, was prepared by polyaddition of ethylenediamine-N,N'-disuccinic acid (EDDS) to 2,2-bisacrylamidoacetic acid (BAC) and N,N'-methylenebisacrylamide (MBA), following the synthetic pathway reported in Scheme 3. The second hydrogel, LYMA, was prepared by polyaddition of L-lysine (Lys) to MBA following the synthetic procedure reported in Scheme 4.

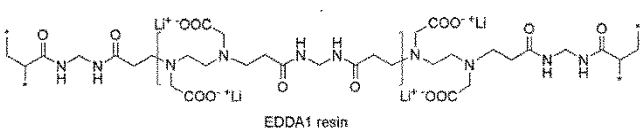

Figure 4. EDDA1 structure.

The third hydrogel developed for the absorption of inorganic micropollutants, labeled EDDA1 (Figure 4), was prepared following the same synthetic procedure described for LMT85 (Scheme 3) but employing N,N'-ehtylendiaminodiacetic acid (EDDA) and MBA. The same pathway was followed for the preparation of the fourth hydrogel, EDDA2 (Figure 5), employing EDDA, BAC and MBA. The hydrogels were successfully synthesized as shown by elemental and FTIR analyses. Their swelling degrees were evaluated in H_2O and buffers at pH 2, 7.4 and 9 according to Eq. 1:

$$SD\ [\%] = \frac{V_{eq}}{V_0}\ x\ 100 \quad \text{(Eq. 1)}$$

where V_{eq} is the volume of the sample at equilibrium and V_0 the volume of the dry sample.

LMT85 displayed high hydrophilicity with swelling degrees above 3000%, LYMA swelled up to 400%, EDDA1 up to 480% and EDDA2 up to 890%. According to differential scanning calorimetry (DSC) and thermogravimetric (TG) analyses, EDDA1, EDDA2, LYMA and LMT85 hydrogels were thermally stable up to 200 °C.

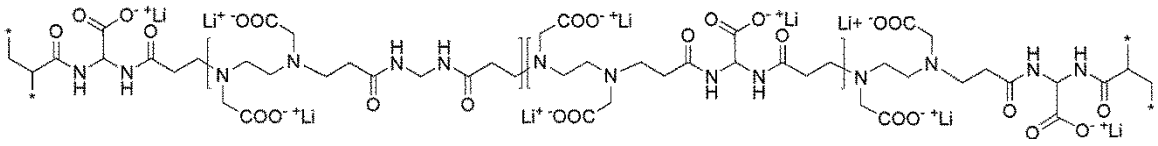

Figure 5. EDDA2 structure.

Electrochemical characterizations aimed to study the complexing ability of PAA hydrogels towards inorganic micro-pollutants were carried out in collaboration with Prof. Mussini's research group, University of Milan, Dept. of Chemistry. PAA hydrogels were tested towards heavy metal ions such as Mn^{2+}, Co^{2+}, Zn^{2+}, Pb^{2+}, Cd^{2+}, Ni^{2+} and Cu^{2+} and their uptake ability was monitored via Anodic Stripping Voltammetry (ASV). The same technique was used for studying metal ion desorption when lowering the pH for hydrogels regeneration. EDDA1 and EDDA2 were studied for Co^{2+} and Cu^{2+} absorption and showed able to efficiently remove the metal ions from their 1 ppm aqueous solutions. In particular, in the presence of both Cu^{2+} and Co^{2+} EDDA2 showed selectivity towards

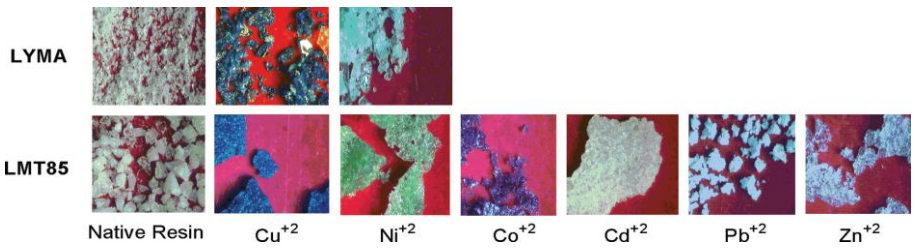

Figure 6. The chromatic changes of LYMA and LMT85 hydrogels upon ion absorption are shown as an example.

Co^{2+}. LMT85 proved able to efficiently absorb Mn^{2+}, Co^{2+}, Zn^{2+}, Pb^{2+}, Cd^{2+}, Ni^{2+} and Cu^{2+} while LYMA was selective for Cu^{2+}, Ni^{2+} and Mn^{2+}. The absorption capacities of the PAA hydrogels, corresponding to 100-500 mg Me^{2+} g^{-1} hydrogel, depending on the metal atomic weights, were competitive with the literature data for other absorbing materials, considering both the absorption capacity and, in the case of LMT85, the wide range of metal ions efficiently absorbed that can be reasonably expected to extend far beyond the model metal series considered in this study. The same experiment also gave indication about the chromatic changes of the hydrogels upon metal absorption. As shown in Figure 6, in some cases, particularly with Cu^{2+}, Co^{2+}, and Ni^{2+}, the absorption process resulted in intense and fast coloring (blue, pink/violet, and green, respectively). This feature may be in principle exploited in diagnostic kits or, if the hydrogels are used for water purification, adopted as indicator of their degree of exhaustion and, therefore, of the regeneration timing. With all of the hydrogels the absorption process was easily reversed by acidifying with excess mineral acids down to pH ≈ 1. This feature is particularly attractive for metal recover and/or hydrogel recycle after use.

2. CD nanosponges as organic micro-pollutants absorbers

CD-based nanosponges capable to entrap organic micropollutants were obtained by two different synthetic approaches: by free radical graft polymerization of methacrylic acid (MA) onto CDs in the presence of acrylamido end-capped PAA oligomers as crosslinkers, and by Michael polyaddition of amines and CD to bis-acrylamides.

2.1 PAA-MA-CD nanosponges

PAA-MA-CD nanosponges were prepared by free radical graft polymerization of MA onto either α- or β-CD followed by crosslinking in the presence of MBAMP oligomers, presynthesized by polyaddition of 2-methylpiperazine (MP) to a controlled excess of MBA (Figure 7), and $Na_2S_2O_8/Na_2S_2O_5$ as initiator according to the procedure shown in Scheme 5. Various PAA/MA/CD ratios were employed. It is known for many polysaccharides that the radicals resulting from the radical initiator generate active centers on the substrate abstracting hydrogens from the hydroxyl groups to form alkoxy radicals. These active centers radically initiate the polymerization of MA and since a crosslinking agent, e.g. MBAMP, is present in the system, the final product is a hydrogel. [20] The materials were successfully synthesized as demonstrated by elemental and FTIR analyses and showed swelling degrees between 270% and 1250%. PAA-MA-CD nanosponges proved thermally stable up to 200 °C, with weight losses due to dehydration up to 6.7%. As showed by *in situ* Square Waved Voltammetry (SWV), PAA-MA-CD nanosponges exhibited sorption capacities toward chlorinated volatile organic compounds such as chloroform, halothane and

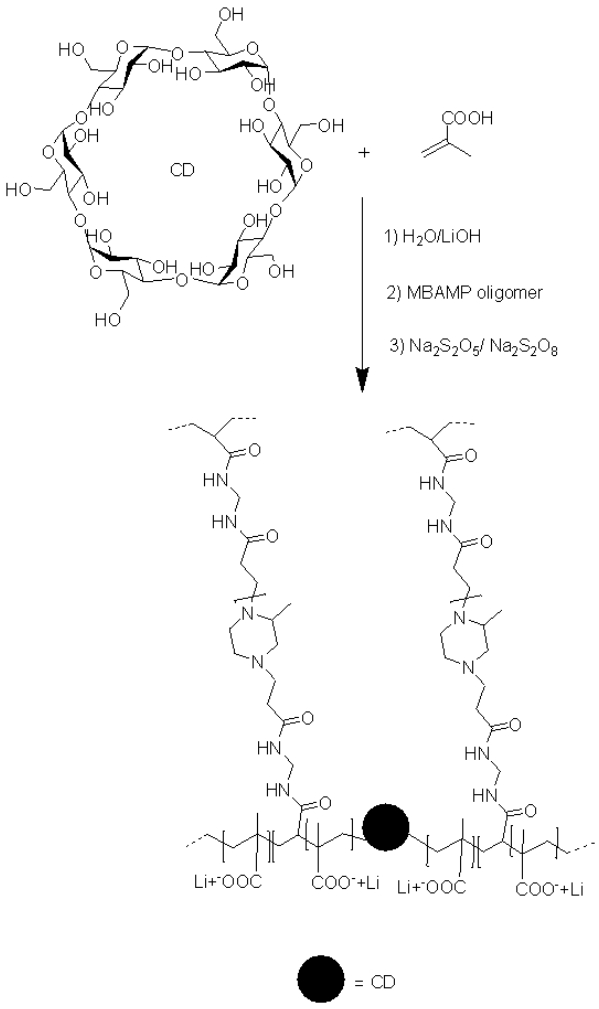

Scheme 5. Synthesis of PAA-MA-CD nanosponges.

tetrachloroethylene, between 5 and 116 mg g^{-1}, depending on the molecular weight of the absorbed species. Thanks to their different cavity volumes, CDs gave the chance of designing materials specifically tailored for the absorption of pollutants of different sizes. In fact, due to the small dimensions of the organic molecules chosen as a benchmark, PAA-MA-CD nanosponges containing α-CD showed higher absorption capacities than those prepared with β-CD. Apparently, the tighter α-CD cavity accommodated the small organohalides better than that of β-CD. Furthermore, the sorption capacities of PAA-MA-CD hydrogels were up to 2 x 10^3 times higher than those of the soluble parent CDs, and competitive with other materials employed to the same purpose. [21] [22]

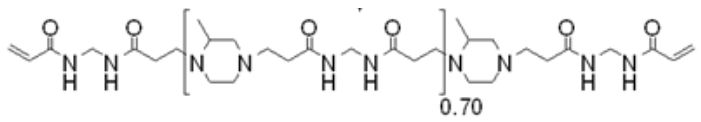

Figure 7. MBAMP structure.

2.2 CD nanosponges

Previous studies demonstrated that CDs hydroxyl groups give polyaddition to bisacrylamides at pH>11. CDs act in this way as multifunctional co-monomers giving cross-linked CD nanosponges. [23] Based on these findings, and following the synthetic procedure reported in Scheme 6, α, β or γ-CDs were reacted together with either BAC, bis(acryloylpiperazine) (BISPIP) or an acryloyl end-capped PAA oligomer named ISA23. The cross-linked materials were successfully synthesized as shown by FTIR and elemental analyses and characterized by swelling degrees between 200% and 1700%. DSC and TG analyses showed that CD nanosponges were thermally stable up to 150 °C, with a maximum 4.5% weight loss due to dehydration. Like PAA-MA-CD nanosponges, one of the potential applications of CD nanosponges is the absorption of organic micropollutants from water. To this purpose, their absorption capacities were studied by Linear Sweep Voltammetry

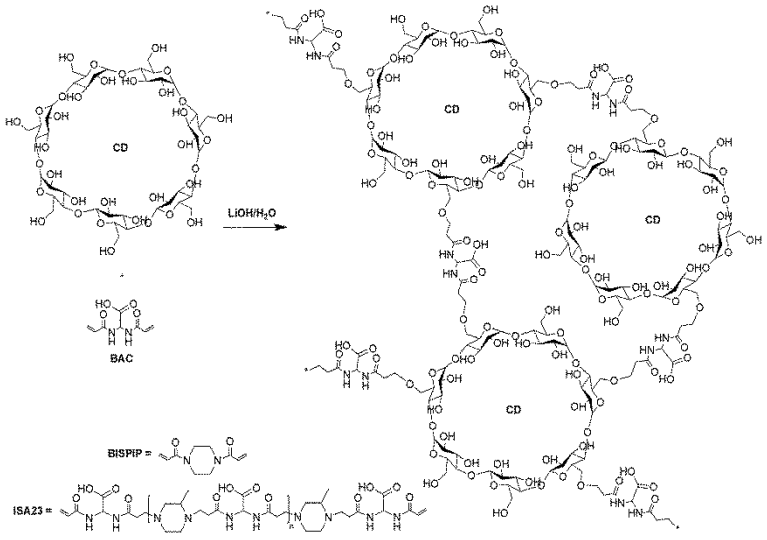

Scheme 6. Synthesis of BAC-CD, BISPIP-CD, ISA23-CD nanosponges. As an example the reaction of β-CD is shown.

(LSV) towards o-toluidine, an organic molecule classified by the International Agency for Research on Cancer (IARC) as 'carcinogenic to humans', and whose efficient removal from water is highly required. CD nanosponges proved efficient o-toluidine absorbers, especially those containing β-CD due to its cavity size, and showed absorption capacities up to 21.32 mg g^{-1} even after the regeneration treatment, carried out by methanol extraction. The results obtained were competitive with those reported in literature for other materials employed to the same purpose. [24]

3. PAA-Hemicellulose hydrogels as inorganic micropollutant absorbers

This part of the work was carried out at the Royal Institute of Technology, Stockholm, Sweden. PAA-Hemicellulose hydrogels were prepared by free radical graft polymerization of MA onto AcGGM, either purified or in its less fractionated form called Hydrolyzate, followed by crosslinking in the presence of PAA oligomers and $(NH_4)_2S_2O_8/Na_2S_2O_5$ as redox initiator (Scheme 7), employing various PAA/MA/AcGGM ratios and leading to PAA-MA-AcGGM hydrogels. The PAA portions stemmed from either MBAMP (Figure 7) or MBAGD oligomer (Figure 9), prepared by polyaddition of glycine and N,N'-dimethylethylenediamine (N,N'-DMEDA) to a controlled excess of MBA. FTIR, elemental and dynamic mechanical analyses showed that all of the hydrogels were successfully synthesized. Their swelling degrees varied between 220% and 1480% and, in general, hydrogels prepared with AcGGM swelled more than those containing Hydrolyzate. This was probably due to a higher crosslink density. DSC and TG analyses proved that the hydrogels were thermally stable up to 200 °C, with weight losses due to dehydration not exceeding 1.2%. Preliminary investigations concerning their heavy metal ion absorption capacity were carried out in batch, incubating swollen hydrogel samples with single heavy metal ion aqueous solutions until equilibrium concentrations were achieved. The initial and final ion concentrations of Cd^{2+}, Pb^{2+}, Zn^{2+}, Ni^{2+}, Cu^{2+} and Co^{2+} were determined via complexometric titration with

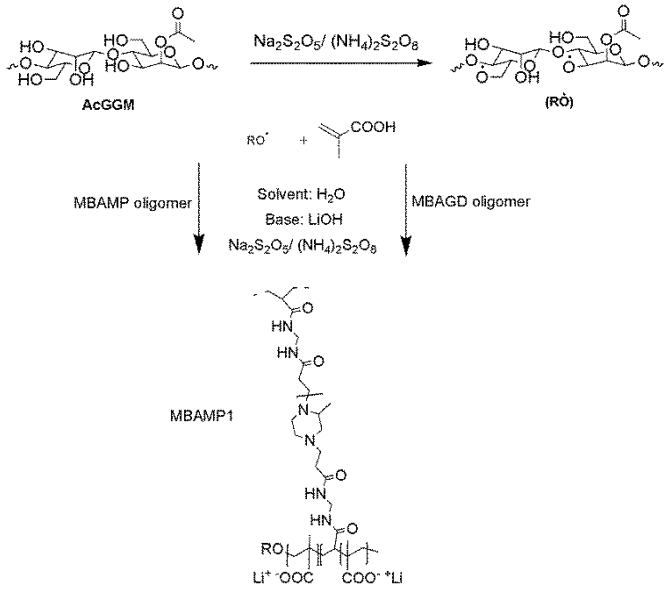

Scheme 7. Synthesis of PAA-MA-AcGGM hydrogels. As an example the synthesis of MBAMP1 is shown.

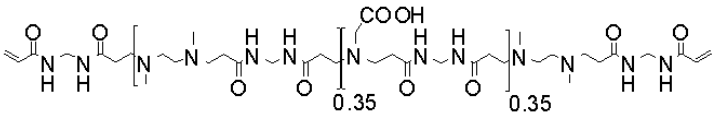

Figure 9. MBAGD structure.

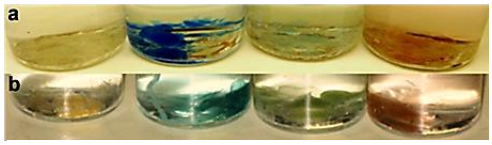

Figure 8. Chromatic changes of MBAGD1 (a) and AcGGM4 (b) upon Cu^{2+}, Ni^{2+} and Co^{2+} absorption. Native hydrogels on the left.

ethylenediaminetetraacetic acid (EDTA), while those of CrO_4^{2-} were determined by UV-vis spectrophotometry. The initial heavy metal concentrations were 700 ppm, for determining the maximum uptake, and 50 ppm, for studying the absorption performance in diluted solutions. For CrO_4^{2-}, particularly noxious species, a concentration of 4 ppm was tested. The absorption capacities ranged 76.3-1.1 mg g^{-1}, depending on the atomic weight of the metal ion considered, with removal percentages up to 54%, quite competitive with the values reported in literature for other absorbing materials. [25] [26] [27] As shown in Figure 8, in some cases and particularly with Cu^{2+}, Ni^{2+} and Co^{2+} the sorption process resulted in intense and fast coloring (blue, green, and pink, respectively). This feature may be in principle exploited in diagnostic kits, or adopted as indicator of the degree of exhaustion if the hydrogels are used for water purification.

4. PAA-GG hydrogels as inorganic micropollutant absorbers

The synthetic route employed for the preparation of PAA-GG hydrogels capitalized on the general reactivity of bisacrylamides in Michael addition, known to proceed with both primary and secondary amines at pH>7 and with alcohols at pH>11. [23] GG acted in this way as a multifunctional co-monomer in PAA synthesis giving PAA-GG cross-linked products. In particular, the devised process consisted in the reaction, carried out in aqueous solutions, of GG with either MBA or BAC and, as amine counterparts, MP, N,N-dymethylehtylenediamine (DMEDA), N,N'-DMEDA, EDDS or Lys (Scheme 8). The PAA portions, though not always specifically endowed with remarkable ion complexing properties, represent good models of either cationic or amphoteric cost-effective PAAs. FTIR and elemental analyses proved that PAA-GG

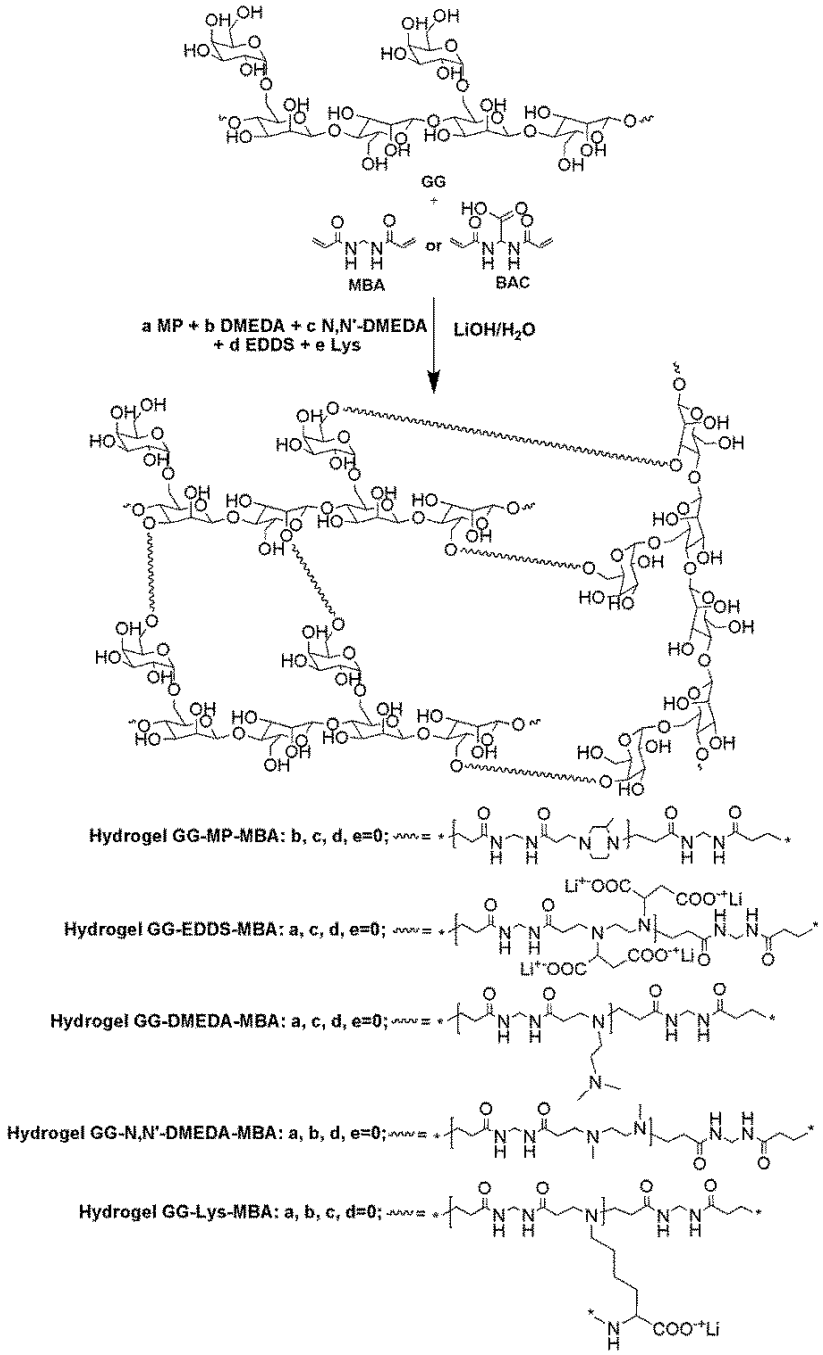

Scheme 8. Synthesis of GG-PAA hydrogels. As examples, only products prepared with MBA as a bisacrylamide are shown.

hydrogels were successfully synthesized. The products showed swelling degrees between 1300% and 5700% and DSC and TG analyses proved that they were thermally stable up to 200 °C, with weight losses up to 13.2% due to dehydration. Preliminary investigations for determining the absorption capacities of PAA-GG hydrogels towards Cd^{2+}, Pb^{2+}, Zn^{2+}, Ni^{2+}, Cu^{2+} and Co^{2+} were carried out in batch, incubating swollen hydrogel samples with single heavy metal ion aqueous solutions until equilibrium concentrations were achieved. The initial and final ion concentrations were determined via complexometric titration with EDTA. The Me^{2+} uptake was evaluated from 1000 ppm and 50 ppm solutions. The absorption capacities of PAA-GG hydrogels ranged 132.1-8 mg g^{-1}, depending on the atomic weight of the metal ion considered, with removal efficiencies up to 100% in 50 ppm Me^{2+} solutions. The results were quite competitive with other data reported in literature. [25] [28] [15] The same experiments gave also indications on the chromatic changes of the hydrogels upon metal ion absorption. With Cu^{2+}, Co^{2+}, and Ni^{2+}, the absorption process resulted in intense and fast coloring (blue, pink, and green, respectively). As an example, in Figure 10 the chromatic changes of a PAA-GG hydrogel, labeled GG-EDDS-BAC and prepared by polyaddition of GG and EDDS to BAC, are shown. This feature may be in principle exploited in diagnostic kits or, if the hydrogels are used for water purification, adopted as indicator of their degree of exhaustion and, therefore, of the regeneration timing. The absorption performance of PAA-GG hydrogels was studied also on a series of four consecutive absorption-desorption cycles. Between each absorption cycle, the material was regenerated washing with 0.01 M HCl, thoroughly rinsed with water hence re-employed for the absorption of the selected metal ion from fresh 1000 ppm aqueous solution. The absorption capacities slightly decreased after the initial absorption cycle, probably due to the extraction of soluble residues that contributed to enhance the absorption performance of the hydrogels, and remained unchanged for the following absorption cycles thus indicating that reuse had little influence on the heavy metal ions absorption behavior of PAA-GG hydrogels.

Figure 10. Chromatic changes of GG-EDDS-BAC upon ion absorption. Native hydrogel (A), hydrogel upon Cu^{2+} (B), Co^{2+} (C) and Ni^{2+} (D) adsorption.

References

[1] R. P. Schwarzenbach, B. I. Escher, K. Fenner, T. B. Hofstetter, C. A. Johnson, U. von Gunten, B. Wehrli, *Science,* vol. 313, pp. 1072-1077, 2006.

[2] P. Ferruti, *J. Polym. Sci. Pol. Chem.,* vol. 51, pp. 2319-2353, 2013.

[3] G. Crini, M. Morcellet, *J. Sep. Sci.,* vol. 25, pp. 789-813, 2002.

[4] D. Li, M. Ma, «Cyclodextrin polymer separation materials». Patent WO9822197, 28 May 1998.

[5] S. D. Mhlanga, B. B. Mamba, R. W. Krause, T. J. Malefetse, *J. Chem. Technol. Biotechnol.,* vol. 82, pp. 382-388, 2007.

[6] A. Demirbas, *J. Hazard. Mater.,* vol. 157, pp. 220-229, 2008.

[7] J. Hartman, A.-C. Albertsson, M. S. Lindblad, J. Sjöberg, *J. Appl. Polym. Sci.,* vol. 100, pp. 2985-2991, 2006.

[8] J. Lundqvist, A. Jacobs, M. Palm, G. Zacchi, O. Dahlman, H. Stålbrand, *Carbohyd. Polym.,* vol. 51, pp. 203-211, 2003.

[9] J. Voepel, U. Edlund, A. C. Albertsson, *J. Polym. Sci. Pol. Chem.,* vol. 47, pp. 3595-3606, 2009.

[10] D. Fengel, G. Wegener, Wood: chemistry, ultrastructure, reactions, Berlin: de Gruyter, 1984.

[11] R. H. W. Wientjes, M. G. H. Duits, R. J. J. Jongschaap, J. Mellema, *Macromolecules,* vol. 33, pp. 9594-9605, 2000.

[12] P. A. Todd, P. Benfield, Goa, K. L., *Drugs*, vol. 39, pp. 917-928, 1990.

[13] R. Barbucci, D. Pasqui, R. Favaloro, G. Panariello, *Carbohyd. Res.,* vol. 343, pp. 3058-3065, 2008.

[14] R. K. S. Lalita, *Carbohyd. Polym.,* vol. 83, pp. 1929-1936, 2011.

[15] K. Chauhan, G. S. Chauhan, J.-H. Ahn, *Bioresource Technol.,* vol. 100, pp. 3599-3603, 2009.

[16] V. Singh, S. Pandey, S. K. Singh, R. Sanghi, *Sep. Purif. Technol.,* vol. 67, pp. 251-261, 2009.

[17] V. Singh, S. K. Singh, S. Pandey, R. Sanghi, *Int. J. Bio. Macromol.,* vol. 49, pp. 233-240, 2011.

[18] A. Manfredi, E. Ranucci, S. Morandi, P. R. Mussini, P. Ferruti, *J. Polym. Sci. Pol. Chem.,* vol. 51, pp. 769-773, 2013.

[19] P. Ferruti, E. Ranucci, A. Manfredi, N. Mauro, E. Ferrari, R. Bruni, F. Colombo, P. Mussini, M. Rossi, *J. Polym. Sci. Pol. Chem.,* vol. 50, pp. 5000-5010, 2012.

[20] G. Gurdag, M. Yasar, M. A. Gurkaynak, *J. Appl. Polym. Sci.,* vol. 66, pp. 929-934, 1997.

[21] I. Abe, T. Fukuhara, J. Maruyama, H. Tatsumoto, S. Iwasaki, *Carbon,* vol. 39, pp. 1069-1073, 2001.

[22] H. Zhao, K. L. Nagy, J. S. Waples, G. F. Vance, *Environ. Sci. Technol. ,* vol. 34, pp. 4822-4827, 2000.

[23] S. Swaminathan, R. Cavalli, F. Trotta, P. Ferruti, E. Ranucci, I. Gerges, A. Manfredi, D. Marinotto, P. R. Vavia, *J. Incl. Phenom. Macrocycl. Chem.,* vol. 68, pp. 183-191, 2010.

[24] Z.-Y. Sun, M.-X. Shen, G.-P. Cao, J. Deng, Y. Liu, T. Liu, *J. Appl. Polym. Sci.,* vol. 118, pp. 2176-2185, 2010.

[25] G. Crini, *Prog. Polym. Sci.,* vol. 30, pp. 38-70, 2005.

[26] S. K. R. Yadanaparthi, D. Graybill, R. von Wandruszka, *J. Hazard. Mater.,* vol. 171, pp. 1-15, 2009.

[27] K. G. Bhattacharyya, S. S. Gupta, *Adv. Colloid Interfac.,* vol. 140, pp. 114-131, 2008.

[28] J. Tripathy, D. K. Mishra, A. Srivastava, M. M. Mishra, K. Behari, *Carbohyd. Polym.,* vol. 72, pp. 462-472, 2008.

LIST OF PAPERS

This thesis is a summary of the following papers:

I L-lysine and EDTA polymer mimics as resins for the quantitative and reversible removal of heavy metal ion water pollutants. P. Ferruti, E. Ranucci, A. Manfredi, N. Mauro, E. Ferrari, R. Bruni, F. Colombo, P. R. Mussini, M. Rossi (2012). *Journal of Polymer Science Part A: Polymer Chemistry, 50*(24), 5000-5010.

II Cyclodextrin nanosponges as o-toluidine absorbents.
Manuscript

III Synthesis and characterization of hybrid poly(amidoamine)/hemicellulose hydrogels.
Manuscript

IV Synthesis and characterization of guar gum/poly(amidoamine) hydrogels.
Manuscript

TABLE OF CONTENTS

INTRODUCTION 23

Water pollution 25

Macropollutants 25

Micropollutants 25

Micropollutants sources 26

Water Treatment technologies 29

Polymeric materials for water and wastewater treatment 30

Poly(amidoamine)s 35

Functionalization of poly(amidoamine)s 36

Acid-base properties of poly(amidoamine)s 37

Biocompatibility and degradation of poly(amidoamine)s 37

Poly(amidoamine)-based hydrogels 38

Poly(amidoamine)s complexes with heavy metal ions 40

Polysaccharides 42

Cyclodextrins 43

Hemicelluloses 47

Guar gum 49

References 50

CHAPTER 1 59

EDDA, L-LYSINE AND EDTA POLYMER MIMICS AS HYDROGELS FOR THE QUANTITATIVE AND REVERSIBLE REMOVAL OF HEAVY METAL ION WATER POLLUTANTS 61

Introduction 61

Experimental 62

Results and discussion 69

Conclusions 94

References 95

CHAPTER 2 97

SYNTHESIS AND CHARACTERIZATION OF CYCLODEXTRIN-GRAFT-METHACRYLIC ACID-POLYAMIDOAMINE NANOSPONGES 99

Introduction 99

Experimental 101

Results and discussion 104
Conclusions 115
References 116
CYCLODEXTRIN NANOSPONGES AS O-TOLUIDINE ABSORBENTS 121
Introduction 121
Experimental 122
Results and discussion 127
Conclusions 140
References 141
CHAPTER 3 145
SYNTHESIS AND CHARACTERIZATION OF HYBRID POLY(AMIDOAMINE)/HEMICELLULOSE HYDROGELS 147
Introduction 147
Experimental 148
Results and discussion 153
Conclusions 167
Acknowledgments 168
References 168
CHAPTER 4 171
SYNTHESIS AND CHARACTERIZATION OF GUAR GUM/POLY(AMIDOAMINE) HYDROGELS 173
Introduction 173
Experimental 175
Results and discussion 178
Conclusions 194
References 194

INTRODUCTION

WATER POLLUTION [1] [2]

Water pollution is one of the most serious environmental problems the world faces today. With respect to human health, the most direct and most severe impact is the lack of improved sanitation, and related to it is the lack of safe drinking water, which currently affects more than a third of the people in the world. Additional threats include, for example, exposure to pathogens or to chemical toxicants via the food chain (e.g., the result of irrigating plants with contaminated water and of bioaccumulation of toxic chemicals by aquatic organisms, including seafood and fish) or during recreation (e.g., swimming in polluted surface water). Chemical water pollutants can be divided into two categories: macro- and micro-pollutants.

Macropollutants represent a relatively small number of pollutants and typically occur at the milligram per liter level. They include nutrients such as nitrogen and phosphorous species as well as natural organic constituents. The sources and impacts of these common classical pollutants are reasonably well understood, but designing sustainable treatment technologies for them remains a scientific challenge. Technical and political strategies to cope with these classical problems have been already extensively discussed in the literature.

Micropollutants are thousands of synthetic and natural trace contaminants that are present in natural water at the nanogram to microgram per liter level and may exert toxic effects even at such low concentrations, particularly when present as mixtures. Due to their potential toxicity and carcinogenicity they are included in the EU PP (Priority Pollutants) list. Micropollutants can be divided into two main categories: inorganic and organic micropollutants.

Inorganic micropollutants include heavy metals (e.g., Cr, Ni, Cu, Zn, Cd, Pb, Hg, U, Pu) and metalloids (e.g., Se, As). The main challenge in assessing their environmental risks is related to their contrasting behavior under different redox conditions. These elements are not subject to degradation like many organic pollutants and the major processes that determine their transport and their bioavailability include oxidation/reduction, complexation, adsorption, and precipitation/dissolution reactions. Furthermore, most metallic elements exhibit widely different solubility in the presence of oxygen and under reducing conditions. This complicates the environmental assessment of metal pollution and limits the ability to predict and quantify adverse effects of inorganic pollutants on aquatic life and human health.

Organic micropollutants are mainly represented by fertilizers, pesticides and synthetic organic chemical compounds. The general characteristics of organic pollutants are: presence of one or more cyclic ring either of aromatic or aliphatic nature, lack of polar functional groups and a variable number of halogen substitutions, usually chlorine. The major challenge is to cope with the large number and the great variety of chemicals covering a wide range in physical-chemical properties and, as a consequence, a very different transport and phase transfer behavior in the environment. Moreover, depending on the environmental conditions (e.g., pH, redox potential, type of surfaces present), a given compound may react by various pathways and/or at very different rates further complicating the issue. [3]

As a consequence to the large number and great structural variety of micropollutants, it is usually very difficult to assess their adverse effects, which often are not acute but subtle and chronic. This contrasts with the common acute health effects of the rather small number of well-known pathogens that may be present in polluted water. Furthermore, owing to the enormous variability of micropollutants, mitigating a given chemical water pollution problem is commonly a quite challenging task. Each case requires its own interdisciplinary scientific knowledge and methods, and each has its own technical, economical, and societal dimensions.

Micropollutants sources

Understanding the origin of organic and inorganic micropollutants is a crucial requirement for better facing the environmental issue. The sources of micropollutants are diverse. About 30% of the globally accessible renewable freshwater is used by industry and municipalities, generating together an enormous amount of wastewaters containing numerous chemicals in varying concentrations. About 300 million tons of synthetic compounds annually used in industrial and consumer products partially find their way into waters. In the European Union, for instance, there are more than 100,000 registered chemicals, of which 30,000 to 70,000 are in daily use (EINECS, European Inventory of Existing Chemical Substances). Other important sources of micropollutants include inputs from agriculture, which applies several million tons of pesticides each year; from oil and gasoline spills; and from the human-driven mobilization of naturally occurring geogenic toxic chemicals, such as heavy metals and metalloids. Additional natural micropollutants are biologically produced (Table 1). There are also millions of municipal and,

particularly, hazardous waste sites, including abandoned industrial and former military sites, from which toxic chemicals may find their way into natural water, especially into groundwater. As an example, a range of micropollutants of toxicological concern in listed detail in Table 2. Some chemicals are not degraded at all (e.g., heavy metals) or only very slowly (e.g., persistent organic pollutants such as polychlorinated biphenyls). They can therefore be transported via water or air to locations hundreds or even thousands of kilometers away from their source. Those compounds that are less persistent and not prone to long range transport may still be of concern if they are continuously emitted or form problematic (bio)transformation products.

Table 1. Dimensions of water problems: water use and macro- and micropollutant fluxes.

Human appropriation of freshwater supply (km^3/year)	
Total global runoff	40,700
Accessible global runoff	12,500
Water withdrawals (total)	4,430
Agriculture	2,880
Industry	975
Municipalities	300
Reservoir losses	275
Fluxes of macropollutants with world rivers (10^6 tons/year)	
Total inorganic nitrogen (~75% anthropogenic)	21
Total phosphorus (60% anthropogenic)	5.6
Anthropogenic inputs of heavy metals to aquatic systems (10^6 tons/year)	
Zn, Cr, Ni, Pb, Cu, Cd, Hg	0.3-1
Anthropogenic fluxes affecting water quality (10^6 tons/year)	
Global fertilizer production (2000)	140
Global pesticide production	5
Synthetic organic chemicals production	300
Oil spills (average 1980-2000)	0.4

Table 2. Examples of ubiquitous water micropollutants.

Origin/usage	**Class**	**Selected examples**	**Related problems**
Industrial chemicals	Solvents	Tetrachloromethane	Drinking-water contamination
	Intermediates	Methyl-*t*-butylether	
	Petrochemicals	BTEX (benzene,	

Origin/usage	Class	Selected examples	Related problems
		toluene, xylene)	
Industrial products	Additives	Phthalates	Biomagnification, long-range transport
	Lubricants	PCBs (polychlorinated biphenyls)	
	Flame retardants	Polybrominated diphenylethers	
Consumer products	Detergents	Nonylphenol ethoxylates	Endocrine active transformation product (nonylphenol)
	Pharmaceuticals	Antibiotics	Bacterial resistance, nontarget effects
	Hormones	Ethinyl estradiol	Feminization of fish
	Personal-care products	Ultraviolet filters	Multitude of (partially unknown) effects
Biocides	Pesticides	DDT	Toxic effects and persistent metabolites
		Atrazine	Effects on primary producers
	Nonagricultural biocides	Tributyltin	Endocrine effects
		Triclosan	Nontarget effects, persistent degradation product (methyl-triclosan)
Geogenic/natural chemicals	Heavy metals	Lead, cadmium, mercury	
	Inorganics	Arsenic, selenium, fluoride, uranium	Risks for human health
	Taste and odor	Geosmin, methylisoborneol	Drinking-water–quality problems
	Cyanotoxines	Microcystins	
	Human hormones	Estradiol	Feminization of fish
Disinfection/oxidation	Disinfection by-products	Trihalomethanes, haloacetic acids, bromate	Drinking-water–quality, human health problems
Transformation products	Metabolites from all above	Metabolites of perfluorinated compounds	Bioaccumulation despite low hydrophobicity
		Chloroacetanilide herbicide metabolites	Drinking-water–quality problems

Water Treatment technologies

In many parts of the world, including emerging economies, water and wastewater are still untreated or undergo treatments that do not effectively remove the majority of the micropollutants present. [4] The latter also holds for municipal wastewater in industrialized countries. Demand for clean water is steadily rising therefore there is an increasing need for more powerful strategies to mitigate water contamination. To this purpose, there are various available technologies including chemical precipitation, coagulation, solvent extraction, ultra filtration, biological systems, electrolytic processes, reverse osmosis, oxidation with ozone/hydrogen peroxide, membrane filtration, ion exchange, photo catalytic degradation, and adsorption. These technologies can be divided into three main categories: biological, chemical and physical. Currently, the major methods of water and wastewater treatment involve physical and/or chemical processes. To date, there is no single process capable of adequate treatment, mainly due to the complex nature of the effluents and a combination of different processes is often used to achieve the desired water quality in the most economical way.

Biological treatment is often the most economical alternative when compared with other physical and chemical processes. Biodegradation and bioaugmentation are commonly applied for the treatment of organic pollutants and are based on the ability of many microorganisms such as bacteria, yeasts, algae and fungi to accumulate and degrade several organic species. However, their application is often restricted because of technical constraints such as low flexibility in design and operation. [5]

Chemical methods include coagulation or flocculation combined with flotation and filtration, precipitation, oxidation methods, irradiation or electrochemical processes. These chemical techniques are often expensive and although the toxic pollutants are removed, accumulation of concentrated sludge creates a disposal problem.

Different physical methods are also widely used, such as membrane-filtration processes (for example nanofiltration, reverse osmosis, electrodialysis) and adsorption techniques. The major disadvantage of the membrane process is that of a limited lifetime due to membrane fouling, and the cost of periodic replacement can be very high. In accordance with the abundant literature data, liquid-phase adsorption is one of the most popular methods for the removal of toxic pollutants from water and wastewater, since proper design of the adsorption process will produce a high quality treated effluent. This process provides an attractive alternative for the treatment of contaminated water, especially if the

adsorbent is not expensive and does not require any additional pre-treatment step before its application. Adsorption has been found to be superior compared to the other techniques in terms of initial cost, flexibility and simplicity of design as well as ease of operation. [5] In fact, the water treatment costs usually range from 10-450 US$ per cubic meter of treated water but for adsorption they are 5.0-200 US$ per cubic meter of water. Furthermore, adsorption does not result in the formation of harmful substances and can remove both inorganic and organic pollutants as well as both soluble and insoluble species with removal capacities up to 100%. [6] Moreover, adsorbents can often be regenerated. [5]

The most popular adsorbent is activated carbon (AC). Its usefulness derives mainly from the high surface area but the depleted source of commercial coal-based AC results in increasing price. This, together with AC loss during the regeneration process, restricts its applications therefore searching less expensive alternatives is of great concern. To date, hundreds of studies on the use of less expensive adsorbents have been published. These adsorbents are produced on the basis of low-cost materials or even wastes such as agricultural wastes, industrial byproducts and natural substances (mainly carbohydrates), and seem economically attractive for practical application. [7] [6] [8] [9] However, their adsorption capacities, mechanical strength, and other properties need further improvement for wider application. In the past decades, polymeric adsorbents emerged as a potential alternative due to their chemico-physical properties and feasible regeneration under mild conditions and numerous publications are available on the topic. [10]

Polymeric materials for water and wastewater treatment [10]

Traditional polymeric adsorbents were first developed in the 1960s. They were originally used in gel permeation chromatography, but their outstanding physical properties made them a very popular material for adsorption and filtration processes. To date, they are widely used for the removal of organic and inorganic pollutants from industrial wastewaters or natural waters. Among the ubiquitous organic pollutants adsorbed there are phenolic compounds, organic acids, aromatic or polyaromatic hydrocarbons, alkanes and their derivatives. To improve their adsorption performance toward specific pollutants, their modification and functionalization proved effective approaches. As compared to AC, exhausted polymeric adsorbents can undergo efficient regeneration under mild conditions employing different desorption reagents depending on the adsorbed pollutants.

[11] [12] The main polymeric adsorbents employed so far for water and wastewater treatment are based on polystyrene (PS) or polyacrylic ester matrixes, either modified or not, and their preparations are extensively described in literature. [10] Some examples on their applications for the adsorption of organic pollutants are reported in Table 3. As for the adsorption mechanism, hydrophobic interaction, ionic attraction, hydrogen bonding, and even complex formation possibly occur under different operation conditions. [13]

Table 3. Polymeric adsorbents for organic micropollutants removal from aqueous media.

Polymeric adsorbents	**Type**	**Organic chemicals**	**Maximum sorption capacities**
XAD-16	Polystyrene	Phenol, *p*-chlorophenol	1.5029 mmol/g (phenol), 2.2702 mmol/g (*p*-CP)
XAD-1600	Polystyrene	Dichloromethane	27 mmol/g
XAD-2, 4	Polystyrene	Benzene	730 mg/g (XAD-2), 1400 mg/g (XAD-4)
XAD-2, 4	Polystyrene	Carbon tetrachloride	1250 mg/g (XAD-2), 2600 mg/g (XAD-4)
Duolite ES-861	Polystyrene	*m*-Cresol	141 mg/g
XAD-4, 16	Polystyrene	Phenol	Not available
XAD-2, 4	Polystyrene	Phenol, 4-chlorophenol, 2,4-dichlorophenol	≈0.4–2.5 mmol/g
NDA-701	Hypercrosslinked PS	4-Nitrophenol	≈600 mg/g
NJ-8	Hypercrosslinked PS	Phenol, *p*-cresol, *p*-chlorophenol, *p*-nitrophenol	1.455 mmol/g (phenol), 2.489 mmol/g (*p*-cresol), 2.891 mmol/g (*p*-CP), 2.364 mmol/g (*p*-NP)
Sample 390	Hypercrosslinked PS	Aniline, phenol	1.931 mmol/g (aniline), 1.390 mmol/g (phenol)
Hypersol-Macronet MN-200	Hypercrosslinked PS	Phenol, 2-chlorophenol, 3-chlorophenol, 4-chlorophenol	0.922 mmol/g (phenol), 1.060 mmol/g (2-CP), 1.355 mmol/g (3-CP), 1.270 mmol/g (4-CP)

Polymeric adsorbents	**Type**	**Organic chemicals**	**Maximum sorption capacities**
XAD-7, 8	Polyacrylic ester	2-Naphthylamine	232.5 mg/g (XAD-7), 263.2 mg/g (XAD-8)
		1-Naphthol	278.0 mg/g (XAD-7), 296.5 mg/g (XAD-8)
		1-Naphthylamine	256.4 mg/g (XAD-7), 267.1 mg/g (XAD-8)
XAD-7		Dichloromethane	17.76 mmol/g
		Phenol	78.7 mg/g
		Diethyl phthalate	480 ± 49.9 mg/g
		Phenol, 4-chlorophenol	0.84 mmol/g (phenol), 1.31 mmol/g (4-CP)

For the specific removal of heavy metal ions polymeric chelating adsorbents were developed. The specific interactions are generally interpreted by Lewis acid–base principle, where the chelating groups can be taken as Lewis bases while the heavy metal ions as Lewis acids. Some of the recent developments on polymeric chelating adsorbents employed for heavy metals removal are summarized in Table 4. [10]

Table 4. Polymeric chelating adsorbents for selective heavy metals removal from aqueous media.

Polymeric adsorbents	**Chelating groups**	**Targeted pollutants**	**Maximum sorption capacities**
Iminodiacetate chelating resins	Iminodiacetate groups	Cu^{2+},Co^{2+}, Ni^{2+}	3.257 mmol/g (Cu), 2.6 mmol/g (Co), 2.809 mmol/g (Ni)
Chelex 100	Iminodiacetic acid groups	Ni^{2+}, Cu^{2+}	2.15 mmol/g (Ni), 1.6 mmol/g (Cu)
GMA/DVB magnetic resin	Iminodiacetic acid groups	Pb^{2+}, Cd^{2+}, Zn^{2+}, C^{a2+}, Mg^{2+}	2.3 mmol/g (Pb), 2.0 mmol/g (Cd), 1.65 mmol/g (Zn), 1.60 mmol/g (Ca), 1.48 mmol/g (Mg)

Polymeric adsorbents	**Chelating groups**	**Targeted pollutants**	**Maximum sorption capacities**
Dowex M 4195	Bispicolylamine groups	Cr^{6+}	29.7 mg/g (Cr)
PASP chelating resin	Aspartate groups	Cu^{2+}, Cd^{2+}	1.40 mmol/g (Cu), 1.28 mmol/g (Cd)
Benzothiazole-based chelating resin	Benzothiazole groups	Cu^{2+}, Cd^{2+}, Pb^{2+}	5.68 mmol/g (Cu), 1.03 mmol/g (Cd), 1.55 mmol/g (Pb)
PGLY chelating resin	Glycine groups	Cu^{2+}, Ni^{2+}, Cd^{2+}	1.22 mmol/g (Cu), 1.07 mmol/g (Ni), 0.96 mmol/g (Cd)

Hybrid polymeric adsorbents are also widely employed. They are prepared impregnating or coating fine environmentally benign inorganic particles, namely, metal (hydr)oxides (e.g., Fe(III), Mn(IV), and $M(HPO_4)_2$ where M = Zr, Ti, Sn) onto the porous supports of larger particle size. One of the basic reasons for designing these hybrid adsorbents relied on the fact that fine or ultrafine inorganic particles were unusable in fixed beds or any flow-through systems because of excessive pressure drops and poor mechanical strength, though most of them exhibit specific affinity toward target pollutants in waters. Thus, they had to be impregnated into porous supports of larger particle size to overcome the technical bottleneck, and porous polymeric materials seemed more attractive than activated carbon, cellulose, alginate, diatomite, and sand due to their adjustable chemico-physical properties.

Table 5 summarizes the applications of some typical hybrid adsorbents based on polymeric materials. [10]

Table 5. Polymer-based hybrid adsorbents for inorganic pollutants removal.

Polymeric substrate	**Inorganic nanoparticles**	**Targeted pollutants**	**Detailed performance**
Polymeric cation exchanger	$Zr(HPO_4)_2$	Pb^{2+}	Pb^{2+} removed from 40 to <0.05 mg/L
Polymeric anion exchangers	Hydrous ferric oxide	Arsenic	As^{5+} removed from 23 to <0.5 ppb
Polymeric cation exchanger	$Zr(HPO_3S)_2$	Pb^{2+}, Cd^{2+}, Zn^{2+}	Pb^{2+} removed from 50-130 to <10 ppb, Cd^{2+} removed from 80–140 to <3 ppb
Polymeric cation exchanger	Hydrous ferric oxide	Pb^{2+}, Cu^{2+}, Cd^{2+}	Metal ions removal from 1 ppm to <5 ppb
Polymeric cation exchanger D-001, 001 × 7; D-113	Hydrous manganese oxide	Pb^{2+}, Cd^{2+}, Zn^{2+}	20-800 times faster adsorption as compared to host exchangers, sorption capacities increased by 50–300%

POLY(AMIDOAMINE)S

Poly(amidoamine)s (PAAs) represent a family of biodegradable and biocompatible polymers with proved potential application in both biomedical and environmental field. The first extensive studies on PAA synthesis have been published in 1970 and their chemical properties and applications reviewed in several instances.

General synthesis and structures

PAAs are obtained by stepwise Michael type polyaddition reaction of primary or bis-secondary amines to bisacrylamides. The polymer obtained presents tert-amino and amido groups regularly arranged along the main chain (Scheme 9).

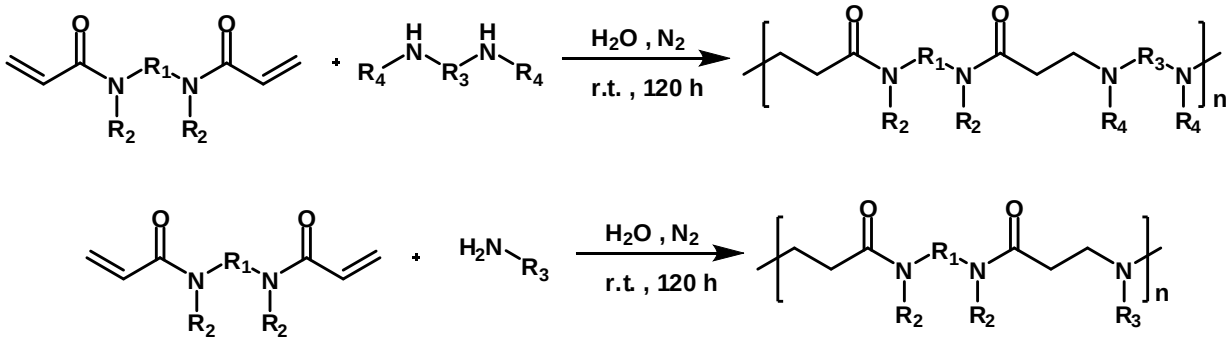

Scheme 9. Synthesis of linear PAAs. R_1, R_2, R_3 and R_4 can be any alkyl residues eventually containing carboxyl, amide, ester, ether groups.

Polymerization reaction takes place in solvents carrying mobile protons, such as water or alcohols, without added catalysts (Scheme 10). [14] [15] [16] The number-average and weight-average molecular weights of the PAAs usually range between 5,000-40,000 and 10,000-70,000 respectively, with a polydispersity index around 1.5-2 depending on the isolation method.

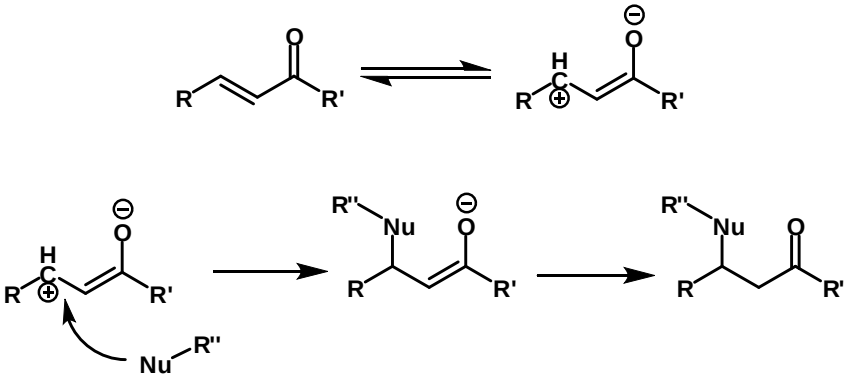

Scheme 10. Michael type addition mechanism.

The reaction is considerably influenced by the temperature. High temperatures accelerate the polyaddition reaction rate but the resulting polymers showed lower molecular weights because of the increase of hydrolysis reaction rate. Pioneering studies previously performed showed that high molecular weight polymers can only be obtained in organic solvents bearing mobile hydrogens such as alcohols; indeed aprotic solvents give always poor results irrespective of their polarity. [14] Recently, further study showed that mobile hydrogens play a key role in the reaction mechanism of Michael addition, and hydrogen mobility strongly influences reaction kinetics. [17] It is possible to obtain amphoteric PAAs using carboxyl containing starting monomers, carboxyl groups in fact, do not influence the polyaddition reaction. In this case, a stoichiometric amount of base (inorganic such as lithium or sodium hydroxide, or organic, such as triethylamine) must be added to the monomers mixture in order to prevent amine protonation by the acid groups. Amphoteric PAAs show remarkable biological properties as will reported later in this chapter.

Non amphoteric PAAs are soluble in water as well as in chloroform, lower alcohols, dimethyl sulfoxide and other polar solvents. However, amphoteric PAAs dissolve only in water. [18] The intrinsic viscosities of PAAs in organic solvents or aqueous media usually range from about 0.15 to 1 dl/g. As a rule, PAAs exhibit relatively large hydrodynamic volumes in solution if compared with vinyl polymers of similar molecular weight, indicating a tendency to assume an extended chain conformation in solution.

Functionalization of poly(amidoamine)s

PAAs are inherently highly functional polymers, however, further functionalization of PAAs may be useful for special purposes. Functional groups not capable of undergoing Michael addition under the conditions of PAA synthesis, for instance hydroxy, tert-amino, allyl, amido and ether groups, do not compete with the polymerization reaction. Therefore, the introduction of these additional functions in PAAs as side substituents can be simply achieved by using monomers properly functionalised. Chemical groups capable of reacting with activated double bonds under the conditions of PAA synthesis such as -SH, $-NH_2$, -NHR and $-PH_2$, if unprotected, cannot as a rule be introduced directly as side substituents in PAAs. However, it is possible to obtain these types of functional groups by functionalization of purposely pre-synthesised polymers. [19]

Acid-base properties of poly(amidoamine)s

All PAAs contain tert-amino groups in their main chain and therefore can be classified as polyelectrolytes. [20] [21] Normally, the values of the protonation constants (log K) of polyelectrolytes depend on the degree of protonation of the whole macromolecule. They follow the modified Henderson-Hasselbach equation:

$$logK_i = logK_i^o + (n-1)\log\left[\frac{(1-\alpha)}{\alpha}\right] \qquad \text{Eq. 1}$$

where $logK^0_i$ is the protonation constant of a group present in a completely unionized polymer and α is the protonation degree. The protonation constants of polyelecrolites are usually referred to as "apparent" constants, as opposed to the "real" constants of non-macromolecular acids and bases. However, in most PAAs the results of the potentiometric titrations are consistent with n values very close to 1. This means that in PAAs the tendency of the amine nitrogen atoms of each repeating unit to assume a proton does not depend on the degree of protonation of the whole macromolecule. Therefore, real or "quasi real" basicity constants can be determined. As a consequence, non ampohoteric PAAs behave as polycations and show the same number of basicity constant of the amino groups present in their repeating unit. [22]

Differently from non-amphoteric PAAs, amphoteric PAAs deriving from amino acids and therefore carrying both carboxyl and amino groups attached to the same monomer, tend to exhibit a typical polyelectrolite behavior. In solution, they change their net average charge as a function of pH.

By a proper choice of the starting monomers, the acid and basic strength of the amino and the carboxyl groups can be controlled in such a way that the polymer passes from a prevailingly anionic to a prevailingly cationic state as a consequence of relatively modest pH changes. [19]

Biocompatibility and degradation of poly(amidoamine)s

Cationic PAAs are usually one or two order or magnitude less cytotoxic (IC_{50} between 0.5 and 3 mg/ml) than other common polycations such as poly-L-lysine (IC_{50} 0.012 mg/ml) and poly(ethyleneimine) (IC_{50} 0.01 mg/ml) while amphoteric PAAs are often non-cytotoxic (IC_{50} above 5 mg/ml, similar to dextran, nontoxic reference). All PAAs containing in their main chain tertiary amine in β to amidic bonds are degradable in aqueous solution. The degradation of several PAAs has been extensively studied in

physiological conditions (37 °C and phosphate buffer pH=7.4) by means of viscosimetry and chromatographic techniques. [23] [24] It has been demonstrated that the degradation rate of PAAs in aqueous media is strongly influenced by basic pH and increasing temperatures (40-60 °C), as well as by the structure of both amine and amide moieties. The mechanism of PAAs degradation seems to be purely hydrolytic as no vinyl groups, such as those which would have derived from a β-elimination reaction, could be determined. [25] Furthermore, degradation seems not to be affected by the presence of isolated lysosomal enzymes at pH 5.5. The cytotoxicity of different PAAs degradation products has been also tested, always leading to IC_{50} values similar to those of the native polymers. [26]

Poly(amidoamine)-based hydrogels

Crosslinked PAAs can be easily obtained by different methods. So far, the most often employed method to achieve this is to introduce into the polymerization mixture multifunctional amines as crosslinking agents. [27] For example, primary diamines carry four different mobile hydrogens and hence behave as tetrafunctional monomers in PAA synthesis (Scheme 11). Cross-linked PAAs are typical hydrogels, absorbing large amounts of water if their cross-linking degree is not too high.

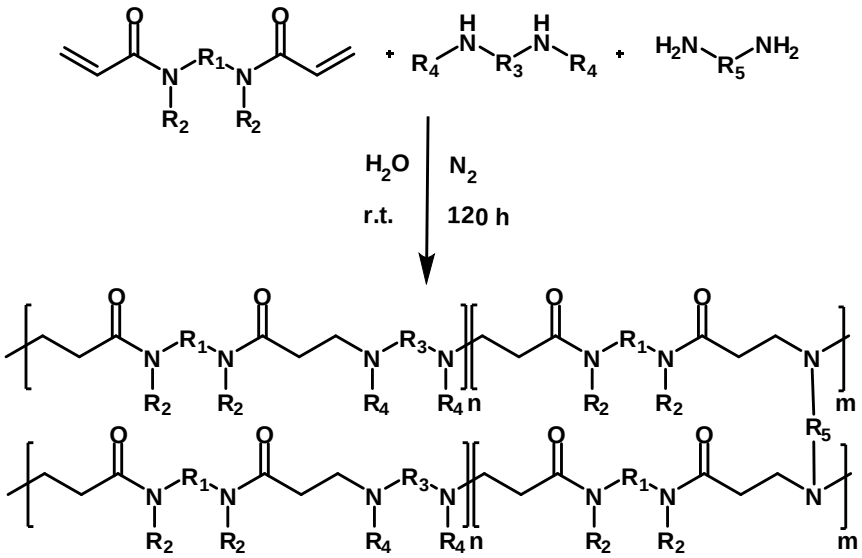

Scheme 11. General synthesis of PAA-based hydrogels.

Another synthetic procedure leading to PAA hydrogels involves the preparation of a linear amphoteric PAA carrying primary amino pendants (NH_2–BAC) by the polyaddition of monoprotonated ethylenediamine (EDA) to 2,2-bis(acrylamido)acetic acid (BAC). [28]

This PAA can be used in the place of diamines as a multifunctional crosslinking agent for preparing PAA hydrogels; in fact, it gives rise to intersegmented networks with PAAs of different structures. [29]

PAA hydrogels can also be synthesized via free radical polymerization of presynthesized acrylamide endcapped PAA oligomers, prepared employing a controlled excess of bisacrylamide. The synthesis can be performed in the presence of a redox couple, a thermal initiator or UV radiation. [19]

The water content in a hydrogel is a very important property defined as:

$$SD\ (\%) = \frac{W_{swollen} - W_{dry}}{W_{dry}} \times 100 \qquad \text{Eq. 2}$$

If the water content is higher than 90% the hydrogel is defined as "super absorbent". Different factors influence the water content of hydrogels such as the osmotic potential, strong interactions with water, a high free volume, a high chain flexibility, and a low density of the crosslinking points. Swelling tests demonstrated that all hydrogels had a high swelling capability. This property, not unexpected considering the hydrophilic and ionic nature of all investigated PAA-hydrogels, ensures an efficient diffusion of low molecular weight substances, thus facilitating purification processes that consisted in extensive extraction with water. However, the mechanical strength of the hydrogels in the swollen form was scarce and the materials appeared relatively fragile. The swelling behaviour of PAA hydrogels protonated with different acids is still very high and not significantly different from that of the corresponding free bases, with the exception of sulfates, slightly less swollen.

PAA hydrogels proved to be cyto/biocompatible both as free bases and as salts with different strong or medium-strong acids. Their biological performance was independent of the nature of the counterions. Degradation tests carried out with selected PAA hydrogels under conditions mimicking the body fluids (pH 7.4 and 37 °C) revealed that they degrade fast, since they completely dissolved within ten day from the beginning of the experiments. Furthermore, their degradation products proved to be completely non-toxic. [19]

Poly(amidoamine)s complexes with heavy metal ions

In early studies, many linear PAAs proved to form coordination complexes with some heavy metal ions, namely Cu^{2+}, Ni^{2+},Co^{2+} and as with protonation, "real" stability constants could be determined for the complexes. [30] [31] [32] [33]

More recently, several basic and amphoteric poly(amido-amine)s containing carboxyl and tertiary amino groups as well as peptide nitrogens proved able to easily complex Cu^{2+} ions by amino nitrogens in a stable five-member ring showing complex species of different stoichiometries on the whole range of pH investigated (from 3 to 11). [34] Compared to some previously studied homologous PAAs, [35] the basic polymers showed lower basicity constants and increased polyelectrolyte behavior. Polyampholytes were able to bind Cu^{2+} ions through peptide sites at low pHs (> 3) while the basic PAAs needed to reach pH > 5. [34] It is noteworthy that metal complexation, similarly to protonation, led to a stiffening of the PAA conformation in solution. [36]

In the absence of additional side amine or carboxyl groups, only PAAs carrying at least two amine nitrogens per unit that neither belonged to a cyclic structure nor were separated by more than three carbon atoms showed complexing ability. The electronic and electron paramagnetic resonance (EPR) spectra of both polymeric and non-polymeric complexes, obtained from PAA models, were similar and consistent with an octahedral tetragonally distorted structure, in agreement with the substantial independence of the polymer repeating units in complex formation. [19]

It was quite early ascertained that crosslinked PAAs [37] [38] [39] and PAA-grafted materials, for example silica, [40] [41] [42] [43] retained the ion-complexing ability of their linear counterparts. This concept was more recently resumed by studying crosslinked amphoteric PAAs as specific heavy metal ion absorbers for water purification from inorganic pollutants. An amphoteric PAA with inter-segmented structure (Figure 12) obtained by synthesizing ISA23 (Figure 11) in the presence of a second pre-synthesized PAA carrying primary amino groups as side substituents that acted as a macromolecular crosslinking agent was studied as a Co^{2+}, Ni^{2+}, and Cu^{2+}-sorbing material. This resin exhibited a remarkable sorption capacity and sorption rate for the three ions considered, which were in situ monitored by cyclic voltammetry. The metal-ion uptake was very fast and quantitative. Dilute acids quantitatively eluted the absorbed metal ions, thus allowing metal recovering and resin regeneration. [29]

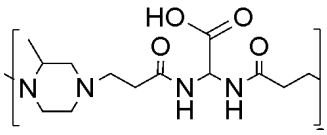

Figure 11. Structure of the PAA dubbed ISA23.

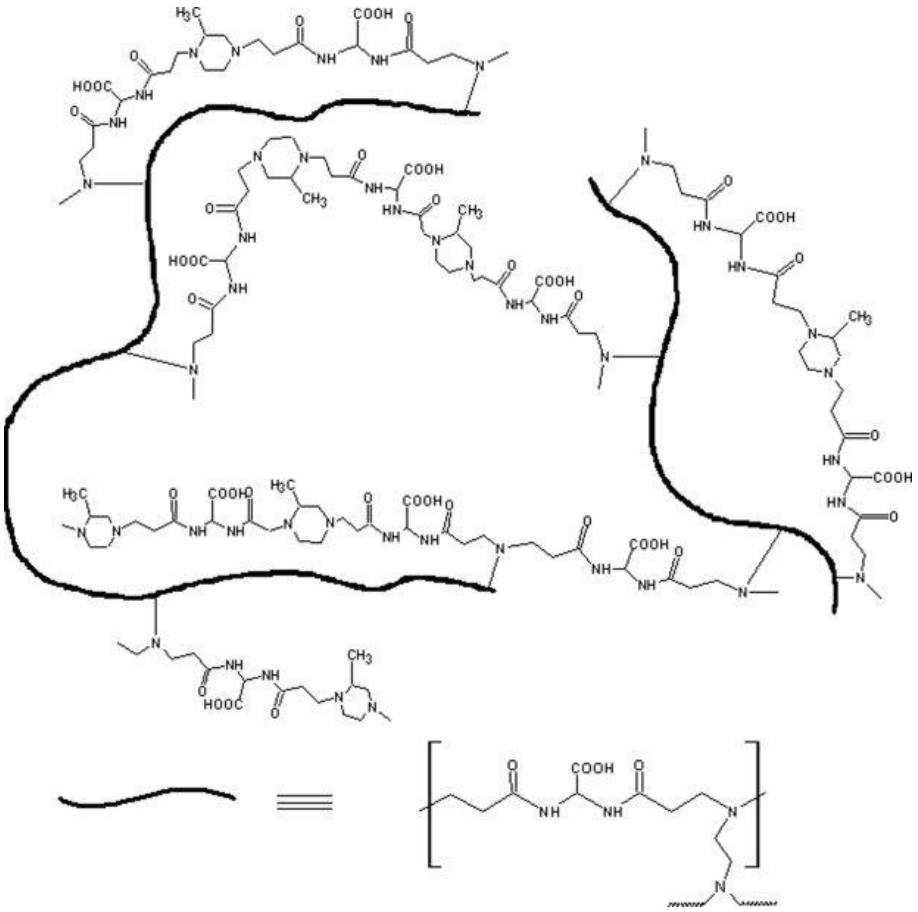

Figure 12. Structure of the intersegmented hydrogel called INT-PAA1.

POLYSACCHARIDES [44]

Recently, numerous approaches have been studied for the development of cheaper and more effective adsorbents containing natural polymers. Among these, polysaccharides such as, for example, chitin, starch, guar gum, lignocellulosic materials, cyclodextrins and their derivatives deserve particular attention. These natural polymers, referred to as biopolymers, represent an interesting and attractive alternative as adsorbents because of their particular structure, physico-chemical characteristics, chemical stability, high reactivity and excellent selectivity towards aromatic compounds and metals. Furthermore, they are inexpensive, widely available in many countries, renewable resources, stable and hydrophilic as well as modifiable. They also have biological and chemical properties such as non-toxicity, biocompatibility, biodegradability, polyfunctionality, high chemical reactivity, chirality, chelation and adsorption capacities. The excellent adsorption behavior of polysaccharides towards a wide variety of molecules is mainly attributed to the high hydrophilicity of the polymer due to the presence of hydroxyl groups which are also highly reactive, together with the flexibility of the polymer structure. Moreover, due to the unique structure of the macromolecule combined with their polyfunctionality, polysaccharides have the ability to form crosslinked networks, gels and macroreticular resins. These materials are easy to prepare, relatively inexpensive and practical to use for water treatment since they can be easily separated from the liquid phase after their use. Crosslinked materials, in particular cyclodextrins polymers, possess an amphiphilic character. It is precisely this character that makes these sorbents so appealing. In fact, they are hydrophilic enough to considerably swell in water allowing fast diffusion processes for the adsorbates while possessing at the same time highly hydrophobic sites, which efficiently trap non-polar pollutants. Adsorption on polysaccharide derivatives can be a low-cost approach for protecting the environment and the increasing number of publications on the topic shows that there is a great interest in the synthesis of new polysaccharide-containing adsorbent materials. To this purpose, in this PhD thesis part of the work was carried out employing three classes of carbohydrates, namely cyclodextrins, hemicelluloses and guar gum.

Cyclodextrins

Origin, structure, properties and applications of cyclodextrins

Cyclodextrins (CDs) are seminatural cyclic oligosaccharides produced in thousands of tons per year from starch by a relatively simple enzymic conversion. CDs comprise a family of three well known industrially produced and several rare minor cyclic oligosaccharides. Due to steric reasons, CDs built from less than six glucose units do not exist. The most commonly used are α-, β- and γ-CD, although larger CDs have been reported as well. [45] [46] They are crystalline, homogeneous substances, with a torus-like macro-ring structure built up from glucopyranose units. α-CD comprises six glucopyranose units, β-CD comprises seven such units, and γ-CD eight (Figure 13).

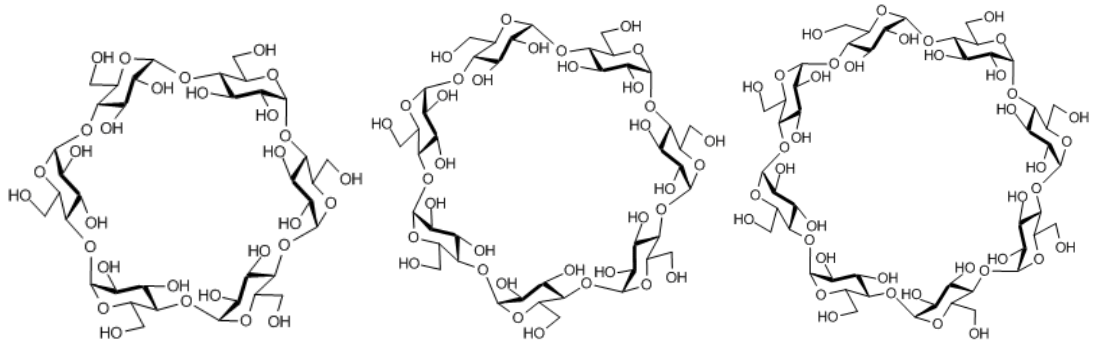

Figure 13. From left to right: structures of α-, β-, and γ-CD molecules.

As a consequence of the $^4C_1$ conformation of the glucopyranose units, all secondary hydroxyl groups are situated on one of the two edges of the ring, whereas all the primary ones are placed on the other edge. The ring is a conical cylinder frequently characterized as a doughnut or wreath-shaped truncated cone. The cavity is lined by the hydrogen atoms and the glycosidic oxygen bridges, respectively. The nonbonding electron pairs of the glycosidic oxygen bridges are directed toward the inside of the cavity producing a high electron density and lending to it some Lewis base characteristics. The C-2-OH group of one glucopyranoside unit can form a hydrogen bond with the C-3-OH group of the adjacent glucopyranose unit. In the β-CD molecule, a complete secondary belt is formed by these H bonds, therefore the β-CD is a rather rigid structure. This intramolecular hydrogen bond formation is probably the reason why β-CD has the lowest water solubility of all CDs. The hydrogen-bond belt is incomplete in the α-CD molecule while γ-CD has a noncoplanar, more flexible structure, andit is the more soluble of the

three CDs. On the side where the secondary hydroxyl groups are situated, the diameter of the cavity is larger than on the side with the primary hydroxyls, since free rotation of the latter reduces the effective diameter of the cavity. [47]

Because of their hydrophobic interior cavity, CDs can either partially or entirely accommodate suitably sized lipophilic molecules. The main driving forces behind the formation of these host-guest inclusion complexes are hydrophobic and van der Waals interactions, although other factors also play a role, including release of CD ring strain, changes in solvent-surface tensions, and hydrogen bonding with CD's hydroxyl groups. [48] The structure of CD molecules gives rise to the remarkable ability to form inclusion complexes with inorganic, ionic,[49] [50] and organic [51] [52] [53] compounds as well as with polymers. [54] [55] [56] [57] [58] [59]

Due to their capability to form inclusion complexes, low price, and availability, CDs have found applications in many fields such as pharmacy, [48] [47] [60] [61] [62] analytical sciences,[63] catalysis,[64][65] cosmetic,[66] textile,[67] food,[68] and packaging industries,[69][70][71] as well as separation processes, including applications for environmental protection. [72] [73]

To date, numerous studies on sorbents containing CD molecules to use in the environmental field are reported in literature. The first results were published in the 1960s by Solms and Egli [74] when β-CD-containing hydrogels showed strong adsorptive properties and formed specific inclusion complexes with benzaldehyde, aniline, nitrophenol isomers, pyridine, iodine, Congo red, and methylene blue. Later in the 1990s, reviews and books published on CDs and their practical applications further stimulated numerous works on CD-based materials and their use for environmental applications. [75] After 1998, when the term was first used by Li and Ma, [76] [77] those materials in which CD units are linked by many short moieties, are commonly referred to as nanosponges. Nanosponges represent supermolecular structures in which CD units are connected by nanochannels forming a cage-like architecture.[78] [79] [80] They are nanoporous by definition and this is the reason why they show very high inclusion constants with several organic pollutants, including aromatic and chlorinated ones. [77] [81] [82] Nanosponges are usually obtained from β-CD, the cheapest one, and only relatively few examples of α- and γ-CD nanosponges, characterized by different dimensional selectivity, are reported. [83] However, the use of a support containing CD molecules in the reduction of environmental pollution is based in all cases on the formation of inclusion complexes between CDs and the unwanted substances.[44]

To date, the list of pollutants investigated on CD-containing materials is very large and includes dye molecules, aromatics, chlorophenols, naphthalene derivatives, dibenzofuran molecules, polychlorinated biphenyls, pesticides, nonionic and ionic surfactants, detergents, metals and also rare earth metal ions.[84] [50] [85] [75] CD-based insoluble crosslinked polymers and copolymers were also employed for the removal of other aromatic derivatives such as chloro and nitro phenols, beta-naphtol, nitroaniline, toluidine, cresol, benzoic acid derivatives and dyes from aqueous solutions. In some cases the sorption behavior resulted comparable to those of commercial porous polymeric materials.[72]

The sorption properties of CD cross-linked materials were also improved by chemical modification, for example with the introduction of carboxyl groups which conferred the matrix the ability to adsorb cationic dyes onto polymer beads. [86] [87] In this case, the sorption mechanism was based on the presence of CD cavities as well as on electrostatic interactions and van der Waals forces due to new reactive groups present on the surface of the polymer particles.[88] Furthermore, when ionic groups such as COOH sites were covalently linked to the (co)polymer, the interactions between the matrix and the contaminants were supplemented with salt formation, with different kinds of interactions acting simultaneously (e.g. inclusion, chemisorption, physical sorption by the polymer network). [75]

Particular interest has been devoted also to amphoteric pH-sensitive CD-based sorbents capable of swelling in both acidic and basic media, without requiring modification of the pH. Amphoteric CD-containing insoluble materials bearing in the polymer network tertiary amine and pendant carboxyl groups were proposed as complexing resins for the removal of organic matter, metals, boron and fluoride ions from industrial wastewater. Furthermore, they simultaneously removed cations, anions, and organics. [75]

In order to keep the process costs down and recover the pollutant extracted from the solution, the regeneration of the sorbent is of crucial importance. To this purpose, the reproducibility of the sorption properties and the regeneration after saturation of CDs polymers was studied by many authors. Since the interactions between the pollutant and CD are driven mainly by hydrophobic interactions, organic solvents such as ethanol or methanol were mainly used for the treatment. As a result, the materials were easily regenerated and showed unchanged sorption capacities. In some cases also weak acidic treatments proved effective. Moreover, it was showed that the repeated cycling of some

CD-based sorbents was more advantageous than that of commercial AC in practical use. [44] [72] [88] [89] [90]

Hemicelluloses

Origin, structure, properties and applications of hemicelluloses

Hemicelluloses are amorphous polysaccharides located in the secondary cell wall of woods and grasses. They are the second most common polysaccharides in nature and represent about 20–35 $^{w}/_{w}$% of lignocellulosic biomass. Unlike cellulose, hemicelluloses are not chemically homogeneous. Their amount and composition in the living tree differs in the different macroscopic parts of the tree (branches, knots, tops, roots). [91] [92] There are also variations within the tree stem; between earlywood and latewood, between sapwood and heartwood, between normal wood and compression wood, and between different fibers and parts of fibers. [93] [91] [94] [95] [96] [97] [92] [98] Dependent on their biological origin, hemicelluloses consist of varying amounts of xylan, mannan, β-glucan, and xyloglucan and [99] whereas hardwood hemicelluloses contain mostly xylans, softwood hemicelluloses contain mostly glucomannans. [100] For this thesis, part of the work involves the use of a particular softwood hemicellulose, namely *O*-acetyl-galactoglucomannan (AcGGM),which is primarily found in the lignified secondary cell wall of softwoods such as spruce (*picea abies*) and can constitute up to 20 $^{w}/_{w}$% of the dry wood. [101] The main structural features of spruce AcGGM are outlined in Figure 14. It has a backbone of randomly distributed β-(1→4)-D-Mannopyranosyl and β-(1→4)-D-Glucopyranosyl residues with α-(1→6)-D-Galactopyranosyl and acetyl side groups. About 20–30 $^{w}/_{w}$% of the backbone units are substituted by acetyl groups [102] on the C-2 and C-3 positions (one acetyl per 3–4 backbone hexose units). [96] [103]

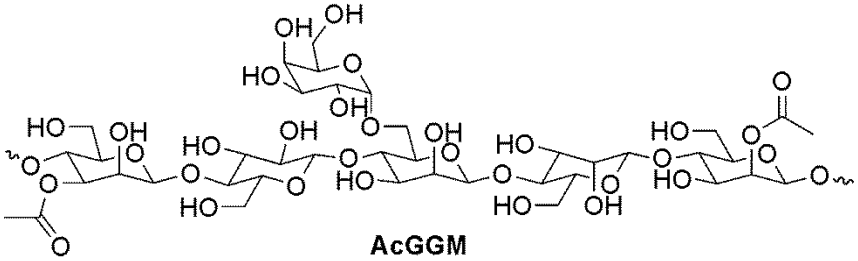

Figure 14. Structural features of water-soluble *O*-acetylgalactoglucomannans (AcGGM).

It is reported in literature that only the mannosyl units bear acetyl groups in position C-2 and C-3. Different ratios of distribution between the C-2 and C-3 position have been suggested. However, it has also been shown that acetyl groups can migrate between these positions and supposedly also to the C-6 position. [104] [105] Unfortunately, the large

number of different techniques applied makes a comparison between results difficult. [98] AcGGM has been reported to have an approximate degree of polymerization (DP) between 100-150, [96] equivalent to a molecular weight (M_w) around 16,000-24,000 Da and it is typically water-soluble. [98] However, it has to be considered that the starting material as well as the extraction and isolation methods strongly influence the molar mass.

In both softwoods and hardwoods, covalently linked to the polymer backbone is lignin, a macromolecule which consists of alkylphenols and with a complex three-dimensional structure. The basic chemical phenylpropane units of lignin are primarily syringyl, guaiacyl and *p*-hydroxy phenol as shown in Figure 15. This matrix comprises a variety of functional groups, such as hydroxyl, methoxyl and carbonyl, which impart a high polarity to the lignin macromolecule whose structure has been extensively investigated. [106]

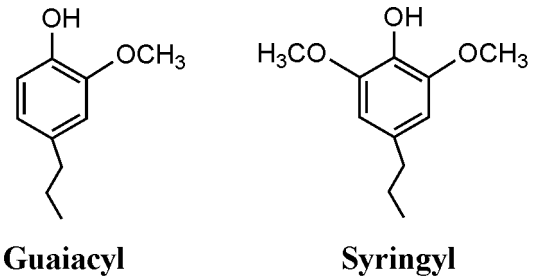

Figure 15. Schematic illustration of the main building units of lignin.

In recent years, the interest in hemicellulose as a renewable resource has rapidly grown. The multifunctional structure of AcGGM and its natural abundance makes it a good candidate for the preparation of value-added products such as, for example, films, [107] [108] [109] [110] bio-based fuels [111] [112] and hydrogels to use also for the treatment of polluted water. [113] [114] [115] [116] [117] [118] [119] Laszlo and Dintzis have shown that lignocellulosic materials have sorption capacity for a wide range of solutes, particularly divalent metal cations, which derives from their constituent polymers and structure, including hemicelluloses. [120] To date, hundreds works have been published on the use of polysaccharides, biosorbents and agricultural waste materials as sorbents for waste water treatment, either in their natural form or properly modified, but few studies in particular have been focused on AcGGM or AcGGM-based sorbents. [119] [44] [121] [122] [123]

Guar gum

Origin, structure, properties and applications of guar gum

Guar gum (GG), also called guaran, is a naturally occurring galactomannan polysaccharide extracted from the seed of the leguminous shrub *Cyamopsis tetragonoloba*. It is made up of a linear chain of β-D-mannopyranose joined by β-(1-4) linkage to which α-D-galactopyranosyl units are linked at every second mannose to give short side-branches (Figure 16).

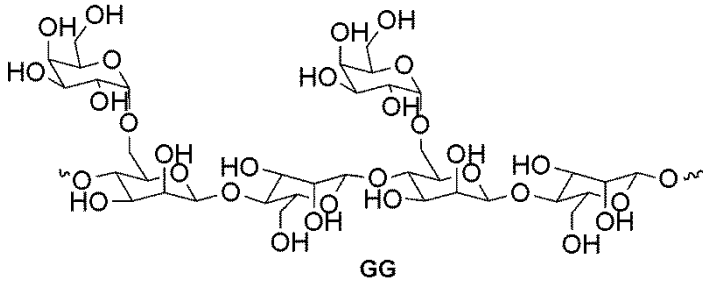

Figure 16. Structural features of guar gum (GG)

GG forms high viscosity colloidal dispersions in water at room temperature. Because of this property, native GG as well as its derivatives are commercially important and find use in diverse applications. An adverse property of GG is its susceptibility for biodegradation therefore it is rarely used in its natural form. Potentially, it can find use as adsorbent but its solubility in water limits its application. [124] [125] [126] To enhance the application spectrum, GG modification has been reported by grafting, derivatization, and network formation. After such modifications the dominant properties of the resultant products were those of the incorporated polymers therefore modifying GG chains to affect its physicochemical properties represents an attractive option. [127] [128]

GG-graft copolymers, nanocomposite materials as well as hydrogels have found application in the environmental field for the treatment of polluted water. In particular, they been used as flocculants and sorbents for the treatment of industrial wastewater containing heavy metal ions such as Cr^{6+}, Pb^{2+}, Cd^{2+}, Zn^{2+}, Cu^{2+}, and Fe^{2+}. They proved able to effectively remove heavy metal ions from water but to date few publications are available on the topic. [124] [129] [130] [128] [131] [132]

References

[1] R. P. Schwarzenbach, B. I. Escher, K. Fenner, T. B. Hofstetter, C. A. Johnson, U. von Gunten, B. Wehrli, *Science*, vol. 313, p. 1072, 2006.

[2] R. Schwarzenbach, T. Egli, T. B. Hofstetter, U. von Gunten, B. Wehrli, *Annu. Rev. Environ. Resour.*, vol. 35, pp. 109-136, 2010.

[3] R. P. Schwarzenbach, P. M. Gschwend, D. M. Imboden, Environmental Organic Chemistry, New York, 2003.

[4] W. J. Cosgrove, F. R. Rijsberman, «World Water Vision: Making Water Everybody's Business,» London, 2000.

[5] M. Ahmaruzzaman, *Adv. Colloid Interfac.*, vol. 166, pp. 36-59, 2011.

[6] I. Ali, M. Asim, T. A. Khan, *J. Environ. Manage.*, vol. 113, pp. 170-183, 2012.

[7] T. A. Kurniawan, G. Y. Chan, W.-H. Lo, S. Babel, *Sci. Total Environ.*, vol. 366, pp. 409-426, 2006.

[8] T. Basile, A. Petrella, M. Petrella, G. Boghetich, V. Petruzzelli, S. Colasuonno, D. Petruzzelli, *Ind. Eng. Chem. Res.*, vol. 50, pp. 8389-8401, 2011.

[9] D. Sud, G. Mahajan, M. P. Kaur, *Bioresource Technol.*, vol. 99, pp. 6017-6027, 2008.

[10] B. Pan, B. Pan, W. Zhang, L. Lv, Q. Zhang, S. Zheng, *Chemical Engineering Journal*, vol. 151, pp. 19-29, 2009.

[11] G. Crini, S. Bertini, G. Torri, A. Naggi, D. Sforzini, C. Vecchi, L. Janus, Y. Lekchiri, M. Morcellet, *J. Polym. Sci. Part A: Polym. Chem.*, vol. 68, pp. 1973-1978, 1998.

[12] B. Pan, W. Du, W. Zhang, X. Zhang, Q. Zhang, B. Pan, L. Lv, Q. Zhang, J. L. Chen, *Environ. Sci. Technol.*, vol. 41, pp. 5057-5062, 2007.

[13] M. Streat, L. Sweetland, *Trans. Inst. Chem. Eng.*, vol. B76, pp. 127-134, 1998.

[14] F. Danusso, P. Ferruti, *Polymer*, vol. 11, p. 88, 1970.

[15] P. Ferruti, M. Marchisio, R. Barbucci, *Polymer*, vol. 26, pp. 1336-1348, 1985.

[16] P. Ferruti, in *Polymeric Materials Encyclopedia*, Boca Raton, Florida, J. C. Salamone, CRC Press Inc, 1996.

[17] A. Manfredi, M. Suardi, E. Ranucci, P. Ferruti, *J. Bioact. Compat. Pol.*, vol. 22,

pp. 219-231, 2007.

[18] P. Ferruti, M. Marchisio, R. Duncan, *Macromol. Rapid Commun.,* vol. 23, pp. 332-355, 2002.

[19] P. Ferruti, *J. Polym. Sci. A Polym. Chem.,* vol. 51, pp. 2319-2353, 2013.

[20] N. Pattrick, S. Richardson, M. Casolaro, P. Ferruti, R. Duncan, *J. Contr. Rel.,* vol. 77, pp. 225-232, 2001.

[21] P. Ferruti, S. Manzoni, S. Richardson, R. Duncan, N. Pattrick, R. Mendichi, M. Casolaro, *Macromolecules,* vol. 33, pp. 7793-7800, 2000.

[22] E. Ranucci, P. Ferruti, E. Lattanzio, A. Manfredi, M. Rossi, P. R. Mussini, F. Chiellini, C. Bartoli, *J. Polym. Sci. Part A: Polym. Chem.,* vol. 47, pp. 6977-6991, 2009.

[23] E. Ranucci, L. Sartore, F. Bignotti, M. Marchisio, P. Bianciardi, F. Veronese, *Biomaterials,* vol. 15, pp. 1235-1241, 1994.

[24] J. Franchini, F. Ferruti, in *Polymeric gene delivery: Principles and Applications*, Mansoor M. Amiji, CRC Press, 2005.

[25] F. Bignotti, P. Sozzani, E. Ranucci, P. Ferruti, *Macromolecules,* vol. 27, pp. 7171-7178, 1994.

[26] E. Ranucci, G. Spagnoli, P. Ferruti, D. Sgouras, R. Duncan, *J. Biomat. Sci. Polym. Ed.*, vol. 2, pp. 303-315, 1991.

[27] P. Ferruti, S. Bianchi, E. Ranucci, F. Chiellini, V. Caruso, *Macromol. Biosci.,* vol. 5, pp. 613-622, 2005.

[28] B. Malgesini, I. Verpilio, R. Duncan, P. Ferruti, *Macromol. Biosci.,* vol. 3, pp. 59-66, 2003.

[29] P. Ferruti, E. Ranucci, S. Bianchi, L. Falciola, P. R. Mussini, M. Rossi, *J. Polym. Sci. A Polym. Chem.,* vol. 44, pp. 2316-2327, 2006.

[30] P. Ferruti, L. Oliva, R. Barbucci, M. C. Tanzi, *Inorg. Chim. Acta,* vol. 41, pp. 25-29, 1980.

[31] R. Barbucci, V. Barone, L. Oliva, P. Ferruti, T. Soldi, M. Pesavento, C. Bertoglio Riolo, in *Polymeric Amines and Ammonium Salts*, Pergamon Press: Oxford and New York, E. J. Goethals, 1980, p. 263.

[32] R. Barbucci, M. J. M. Campbell, M. Casolaro, M. Nocentini, G. Reginato, P.

Ferruti, *J. Chem. Soc. Dalton Trans.*, pp. 2325-2330, 1986.

[33] R. Barbucci, M. Casolaro, S. Corezzi, M. Nocentini, P. Ferruti, *Polymer*, vol. 26, pp. 1353-1358, 1985.

[34] M. Casolaro, F. Bignotti, L. Sartore, M. Penco, *Polymer*, vol. 42, pp. 903-912, 2001.

[35] R. Barbucci, M. Casolaro, V. Barone, P. Ferruti, M. Tramontini, *Macromolecules*, vol. 16, p. 1159–1164, 1983.

[36] R. Barbucci, M. Casolaro, N. Danzo, M. C. Beni, V. Barone, P. Ferruti, *Gazz. Chim. Ital.*, vol. 112, p. 105–113, 1982.

[37] P. Ferruti, C. Bertoglio Riolo, T. Soldi, M. Pesavento, *J. Polym. Sci. A Polym. Chem.*, vol. 27, pp. 2239-2248., 1982.

[38] M. Pesavento, T. Soldi, P. Ferruti, R. Barbucci, M. Benvenuti, *J. Appl. Polym. Sci.*, vol. 28, pp. 3361-3368, 1983.

[39] R. Barbucci, M. Benvenuti, M. Pesavento, P. Ferruti, *Polym. Commun.*, vol. 24, pp. 26-29, 1983.

[40] P. Ferruti, I. Domini, R. Barbucci, M. C. Beni, E. Dispensa, S. S. Sancasciani, M. A. Marchisio, M. C. Tanzi, *Biomaterials*, vol. 4, pp. 217-221, 1983.

[41] E. Ranucci, L. Sartore, E. Tempesti, P. Ferruti, *Mater. Eng.*, vol. 4, pp. 37-52, 1993.

[42] L. Sartore, M. Penco, F. Bigotti, C. Pedrotti, S. D'Antone, *Macromol. Symp.*, vol. 218, pp. 221-229, 2004.

[43] L. Sartore, M. Penco, S. Della Sciucca, A. D'Amore, S. D'Antone, *Macromol. Symp.*, vol. 247, p. 162–171, 2007.

[44] G. Crini, *Prog Polym Sci*, vol. 30, pp. 38-70, 2005.

[45] K. L. Larsen, *J. Inclusion Phenom. Macrocyclic Chem.*, vol. 43, pp. 1-13, 2002.

[46] H. Ueda, *J. Inclusion Phenom. Macrocyclic Chem.*, vol. 44, pp. 53-56, 2002.

[47] J. Szejtli, *Chem Rev.*, vol. 98, p. 1743, 1998.

[48] F. van de Manakker, T. Vermonden, C. F. van Nostrum, W. E. Hennink, *Biomacromolecules* , vol. 10, pp. 3157-3175, 2009 .

[49] M. Bender, M. Komiyama, Cyclodextrin Chemistry, Berlin: Springer Verlag, 1978.

[50] J. Szejtli, Cyclodextrins and their Inclusion Complexes, Budapest: Akademiai Kiado, 1982.

[51] K. Frömming, J. Szejtli, Cyclodextrins in Pharmacy, Dordrecht : Kluwer Academic Publishers, 1994.

[52] S. Li, W. Purdy, *Chem. Rev.,* vol. 92, pp. 1457-1470, 1992.

[53] K. Connors, *Chem. Rev.*, vol. 97, pp. 1325-1357, 1997.

[54] F. Hacket, J. Coteron, H. Schneider, V. Kazachenko, *Can. J. Chem.*, vol. 75, pp. 52-55, 1997.

[55] M. Ceccato, P. Lo Nostro, P. Baglioni, *Langmuir*, vol. 13, pp. 243-2439, 1997.

[56] H. Okumura, M. Okada, Y. Kawaguchi, A. Harada, *Macromolecules*, vol. 33, pp. 4297-4298, 2000.

[57] M. E. Davis, M. E. Brewster, *Nat. Rev. Drug Discovery*, vol. 3, p. 1023–1035, 2004.

[58] G. Wenz, B. H. Han, A. Müller, *Chem. Rev.*, vol. 106, pp. 782-817, 2006.

[59] T. Loftsson, M. Masson, M. E. Brewster, *J. Pharm. Sci.*, vol. 93, p. 1091–1099, 2004.

[60] M. E. Davis, M. E. Brewster, *Nat. Rev. Drug Discovery*, vol. 3, pp. 1023-1035, 2004.

[61] M. E. Brewster, T. Loftsson, *Adv. Drug Delivery Rev.*, vol. 59, pp. 645-666, 2007.

[62] V. J. Stella, V. M. Rao, E. A. Zannou, V. V. Zia, *Adv. Drug Delivery Rev.*, vol. 36, p. 3–16, 1999.

[63] S. Li, W. C. Purdy, *Chem. Rev.*, vol. 92, pp. 1457-1470, 1992.

[64] J. Hu, Z. Tao, S. Li, B. J. Liu, *Mater Sci*, vol. 40, pp. 6057-6061, 2005.

[65] C. Easton, *J. Pure Appl. Chem.*, vol. 77, pp. 1865-1871, 2005.

[66] H.-J. Buschmann, E. J. Schollmeyer, *Cosmet. Sci.*, vol. 53, pp. 185-191, 2002.

[67] H.-J. Buschmann, D. Knittel, E. Schollmeyer, *J. Inclusion Phenom. Macrocyclic Chem.*, vol. 40, pp. 169-172, 2001.

[68] A. R. Hedges, *Chem Rev*, vol. 98, pp. 2035-2044, 1998.

[69] L. Szente, J. Szetjli, *Trends Food Sci. Tech.*, vol. 14, pp. 137-142, 2004.

[70] J. Lu, M. A. Hill, M. Hood, D. F. Greeson, J. R. Horton, P. E. Orndorff, A. S.

Herndon, A. E. Tonelli, *J. Appl. Polym. Sci.,* vol. 82, pp. 300-309, 2001.

[71] H. Hashimoto, *J. Inclusion Phenom. Macrocyclic Chem.,* vol. 44, pp. 57-62, 2002.

[72] G. Crini, M. Morcellet, *J. Sep. Sci.,* vol. 25, pp. 789-813, 2002.

[73] C. Baudin, C. Pean, B. Perly, P. I. Goselin, *J. Environ. Anal. Chem.,* vol. 77, p. 233– 242, 2000.

[74] J. Solms, R. H. Egli, *Helv. Chim. Acta,* vol. 48, p. 1225–1228, 1965.

[75] N. Morin-Crini, G. Crini, *Prog. Polym. Sci.,* vol. 38, pp. 344-368, 2013.

[76] D. Li, M. Ma, «Cyclodextrin polymer separation materials.». Brevetto WO9822197, 28 May 1998.

[77] D. Li, M. Ma, *Clean Technol. Environ. Policy,* vol. 2, pp. 112-116, 2000.

[78] F. Trotta, «Cyclodextrin Nanosponges and Their Applications,» in *Cyclodextrins in Pharmaceutics, Cosmetics and Biomedicine: Current and Future Industrial Applications*, Hoboken, NJ, USA, John Wiley & Sons, 2011, p. 323–342.

[79] F. Trotta, M. Zanetti, R. Cavalli, *Beilstein J. Org. Chem.,* vol. 8, pp. 2091-2099, 2012.

[80] S. D. Mhlanga, B. B. Mamba, R. W. Krause, T. J. Malefetse, *J. Chem.Technol. Biot.,* vol. 82, pp. 382-388, 2007.

[81] S. Berto, M. C. Bruzzoniti, R. Cavalli, D. Perrachon, E. Prenesti, C. Sarzanini, F. Trotta, W. Tumiatti, *J. Incl. Phenom. Macrocyclic Chem.,* vol. 57, pp. 631-636, 2007.

[82] S. Berto, M. C. Bruzzoniti, R. Cavalli, D. Perachon, E. Prenesti, C. Sarzanini, F. Trotta, W. Tumiatti, *J. Incl. Phenom. Macrocyclic Chem.,* vol. 57, p. 637–643, 2007.

[83] R. Cavalli, A. K. Akhter, A. Bisazza, P. Giustetto, F. Trotta, P. Vavia, *Int. J. Pharm.,* vol. 402, pp. 254-257, 2010.

[84] L. D. Wilson, M. H. Mohamed, C. L. Berhaut, *Materials,* vol. 4, pp. 1528-1542, 2011.

[85] J. Szejtli, in *Comprehensive supramolecular chemistry,* vol. 3, Oxford, Pergamon, 1996, pp. 603-614.

[86] G. Crini, N. Morin, J. Rouland, L. Janus, M. Morcellet, S. Bertini, *Europ. Polym. J.*, vol. 38, pp. 1095-1103, 2002.

[87] G. Crini, H. Peindy, *Dyes Pigments,* vol. 70, pp. 204-211, 2006.

[88] S. Murai, S. Imajo, H. Inumaru, K. Takahashi, K. Hattori, *J. Colloid Interf. Sci.,* vol. 190, pp. 488-490, 1997.

[89] N. Li, Z. Mei, S. Chen, *Fresen Environ Bull,* vol. 18, pp. 2249-2253, 2009.

[90] Z. Yang, K. Chai, H. Ji, *Sep Purif Technol,* vol. 80, pp. 209-216, 2011.

[91] D. Fengel, G. Wegener, Wood: chemistry, ultrastructure, reactions, Berlin: de Gruyter, 1984.

[92] T. Vuorinen, R. Alén, «Carbohydrates,» in *Analytical methods in wood chemistry, pulping, and papermaking*, Berlin, Springer, 1999, pp. 37-76.

[93] F. Bertaud, B. Holmbom, *Wood Sci. Technol.,* vol. 38, pp. 245-256, 2004.

[94] A. Pranovich, J. Konn, B. Holmbom, «Variation in chemical composition of, earlywood and latewood in Norway spruce,» in *12th International Symposium on Wood and Pulping Chemistry*, University of Wisconsin-Madison, Madison, 2003.

[95] A. Sundberg, A. Pranovich, B. Holmbom, *J. Pulp Pap. Sci.,* vol. 29, pp. 173-178, 2003.

[96] T. Timell, *Wood Sci. Technol.,* vol. 1, pp. 45-70, 1967.

[97] T. Timell, Compression wood in gymnosperms – biobliography, historical background, determination, structure, chemistry, topochemistry, physical properties, origin, and formation of compression wood, Berlin: Springer, 1986.

[98] C. S. Willför, K. Sundberg, M. Tenkanen, B. Holmbom, *Carbohyd. Polym.* , vol. 72, pp. 197-210, 2008.

[99] B. C. Saha, *J. Ind. Microbiol. Biotechnol.,* vol. 30, pp. 279-291, 2003.

[100] J. D. McMillan, «Pretreatment of lignocellulosic biomass,» in *Enzymatic conversion of biomass for fuel production* , Washington, D.C. , American Chemical Society, 1993, pp. 292-323.

[101] J. Lundqvist, A. Jacobs, M. Palm, G. Zacchi, O. Dahlman, H. Stålbrand, *Carbohyd. Polym.,* vol. 51, pp. 203-211, 2003.

[102] B. Lindberg, K.-G. Rosell, S. Svensson, *Svensk Papperstidn,* vol. 76, pp. 383-384, 1973.

[103] J. Lundqvist, A. Teleman, L. Junel, G. Zacchi, O. Dahlman, F. Tjerneld, H. Stålbrand, *Carbohydrate Polymers,* vol. 48, pp. 29-39, 2002.

[104] F. Reicher, J. B. Corréa, P. A. J. Gorin, *Carbohyd. Res.,* vol. 135, pp. 129-140, 1984.

[105] R. Tanaka, F. Yaku, J. Iyoda, T. Koshijima, *Journal of the Japan Wood Research Society,* vol. 36, pp. 672-678, 1990.

[106] A. Demirbas, *J Hazard Mater,* vol. 157, pp. 220-229, 2008.

[107] N. M. L. Hansen, D. Plackett, *Biomacromolecules,* vol. 9, pp. 1493-1505, 2008.

[108] J. Hartman, A. C. Albertsson, J. Sjöberg, *Biomacromolecules,* vol. 7, pp. 1983-1989 , 2006.

[109] J. Hartman, A. C. Albertsson, M. Söderqvist Lindblad, J. Sjöberg, *J. Polym. Sci. A Polym. Chem.,* vol. 100, pp. 2985-2991, 2006.

[110] Y. Z. Ryberg, U. Edlund, A. C. Albertsson, *Biomacromolecules,* vol. 12, p. 1355–1362, 2011.

[111] J. Nigam, *J. Biotechnol.,* vol. 97, pp. 107-116, 2002.

[112] B. C. Saha, *J. Ind. Microbiol. Biot.,* vol. 30, pp. 279-291, 2003.

[113] J. Voepel, U. Edlund, A. C. Albertsson, *J. Polym. Sci. A Polym. Chem.,* vol. 47, pp. 3595-3606, 2009.

[114] M. Söderqvist Lindblad, A. C. Albertsson, E. Ranucci, M. Laus, E. Giani, *Biomacromolecules,* vol. 6, pp. 684-690, 2005.

[115] J. Yang, X. Zhou, J. Fang, *Carbohyd. Polym.,* vol. 86, pp. 1113-1117, 2011.

[116] X. F. Sun, H. Wang, Z. Jing, R. Mohanathas, *Carbohyd. Polym.,* vol. 92, pp. 1357-1366, 2013.

[117] M. Söderqvist Lindblad, E. Ranucci, A. C. Albertsson, *Macromol. Rapid Commun.,* vol. 22, pp. 962-967, 2001.

[118] J. Voepel, J. Sjöberg, M. Reif, A. C. Albertsson, U. K. Hultin, U. Gasslander, *J. Polym. Sci. A Polym. Chem.,* vol. 112, pp. 2401-2412, 2009.

[119] D. Sud, G. Mahajan, M. Kaur, *Bioresource Technol.,* vol. 99, pp. 6017-6027, 2008.

[120] J. A. Laszlo, F. R. Dintzis, *J. Appl. Polym. Sci.,* vol. 52, pp. 531-538, 1994.

[121] F. Fu, Q. Wang, *J. Environ. Manage.,* vol. 92, pp. 407-418, 2011.

[122] J. S. Han, «Stormwater filtration of toxic heavy metal ions using lignocellulosic materials selection process, fiberization, chemical modification and mat formation,»

in *2nd Inter-Regional Conference on Environment-Water 99*, U.S. Department of Agriculture, Forest Service. Forest Products Laboratory, Madison, Wisconsin .

[123] X. Li, X. Pan, *Journal of Biobased Materials and Bioenergy*, vol. 4.4, pp. 289-297, 2010.

[124] V. Singh, P. Kumari, S. Pandey, T. Narayan, *Bioresource Technol.*, vol. 100, pp. 1977-1982, 2009.

[125] J. Tripathy, D. K. Mishra, A. Srivastava, M. M. Mishra, K. Behari, *Carbohyd Polym*, vol. 72, pp. 462-472, 2008.

[126] R. S. Blackburn, *Environ. Sci. Technol.*, vol. 38, pp. 4905-4909, 2004.

[127] R. Barbucci, D. Pasqui, R. Favaloro, G. Panariello, *Carbohyd. Res.*, vol. 343, pp. 3058-3065, 2008.

[128] K. Chauhan, G. S. Chauhan, J.-H. Ahn, *Bioresource Technol.*, vol. 100, pp. 3599-3603, 2009.

[129] R. K. S. Lalita, *Carbohyd. Polym.*, vol. 83, pp. 1929-1936, 2011.

[130] E. S. Abdel-Halim, S. S. Al-Deyab, *Carbohyd. Polym.*, vol. 86, pp. 1306-1312, 2011.

[131] R. P. Singh, T. Tripathy, G. P. Karmakar, S. K. Rath, N. C. Karmakar, S. R. Pandey, N. T. Lan, *Current Science*, vol. 78, pp. 798-803, 2000.

[132] V. Singh, S. Pandey, S. K. Singh, R. Sanghi, *Sep. Purif. Technol.*, vol. 67, pp. 251-261, 2009.

CHAPTER 1

EDDA, L-LYSINE AND EDTA POLYMER MIMICS AS HYDROGELS FOR THE QUANTITATIVE AND REVERSIBLE REMOVAL OF HEAVY METAL ION WATER POLLUTANTS

Introduction

Water pollution is currently one of the foremost worldwide environmental issues. Traditional water purification methods such as selective precipitation and flotation have intrinsic limitations as regard the quantitative removal of harmful trace pollutants, whereas absorption methods using active carbons, chitosan, zeolites, clays, polystyrene, or other materials, preferably if available as agricultural or industrial wastes, are becoming increasingly popular. [1] [2] [3] However, no fully satisfactory absorbing material, that is, optimized as regard cost, selectivity, and quantitative removal ability, has been found yet. Every endeavor is being made to find novel sorbents with superior biocompatibility; eco-compatibility, that is, environmental friendly preparation process; biodegradability; and moderate cost; ability to deal with micropollutants, that is, showing fast and quantitative absorption even at low pollutant concentration; full reversibility of the absorption process making it economically convenient both for regeneration and metal recovery; and selectivity toward obnoxious metal ions with no alteration of the normal salt loading of life-compatible waters, for instance, waters for domestic use.

To this purpose PAA represent a valuable class of synthetic polymers. In fact, the synthetic process is carried out in aqueous solution, at room temperature and with no added catalysts or organic solvents. Under these conditions, the polyaddition reaction is remarkably selective and allows using as monomers a virtually unlimited range of functional amines and bisacrylamides, thus providing ample possibilities for metal ion chelation.

Electroanalytical techniques proved powerful tools for the physicochemical characterization of PAAs. [4] [5] [6] For example, the acid–base properties of a wide array of PAAs were investigated by potentiometry, [7] obtaining speciation diagrams as a tool for determining the pH range suitable for metal ion chelation. [6] Voltammetric techniques allowed both *in situ* studies of absorption kinetics by cyclic voltammetry (CV), differential pulse voltammetry (DPV), and square wave voltammetry (SWV), depending on the concentration range and on the rapidity requirements, as well as the evaluation of asymptotic residual pollutant traces by stripping voltammetry (SV) analysis.

[4] Furthermore, complexation constants were obtained by both potentiometric and voltammetric approaches. [8] [9] [10]

In this chapter the syntheses, characterization and the performance as heavy metal ion absorbers of four PAA hydrogels, EDDA1, EDDA2, LYMA and LMT85 are reported. EDDA1 and EDDA2 were prepared with N,N'-ethylenediaminodiacetic acid (EDDA) as monomer in order to exploit its known ability to complex Co^{2+} and Cu^{2+} ions. [11] [12] LYMA, whose repeating unit contained two amine and one carboxyl groups, was prepared with L-lysine as monomer due to its well-documented heavy metal ion complexing ability, the repeating unit of LMT85 carried two amine and five carboxyl groups, and it was designed as a mimic of EDTA.

The heavy metal ion set adopted as a benchmark was Mn^{2+}, Cu^{2+}, Cd^{2+}, Pb^{2+}, Zn^{2+}, Ni^{2+}, and Co^{2+}, corresponding to the DIN 38406-16 protocol for the voltammetric determination of heavy metals in tap waters. [13]

Experimental

Materials

Where not otherwise specified, all materials and solvents were purchased from Sigma Aldrich and used as received apart from 2,2-bis(acrylamido)acetic acid (BAC) which was synthesized as previously described. [14] NaOH (98.5%), $LiOH{\bullet}H_2O$ (99%), ethylenediaminediacetic acid (EDDA) (98%), (S,S)-ethylenediamine-N,N'-disuccinic acid (EDDS) trisodium salt solution (35%), N,N'-methylenebisacrylamide (MBA; 99%), 37% HCl aqueous solution, $Na_2S_2O_8$ (>99%), $Na_2S_2O_5$ (99%), $K_2S_2O_8$ (99%), phosphate-buffered saline (PBS) tablets, ethanol (99.5%), D_2O (99.9%), and L-lysine (Lys) were purchased from Sigma Aldrich and used as received.

Methods

NMR. ^{1}H and ^{13}C NMR spectra were run at room temperature on a Bruker Advanced 400 spectrometer operating at 400.132 and 100.623 MHz, respectively.

FTIR analysis. The hydrogels were dried under vacuum to constant weight and the FTIR spectra were collected using a Perkin Elmer 100 spectrometer. All spectra were calculated as means of 16 individual scans at 2 cm^{-1} resolution in the 4000-500 cm^{-1} interval with corrections for atmospheric water and carbon dioxide.

Thermal analyses. Differential scanning calorimetry (DSC) was carried out using a Mettler Toledo DSC823 (Mettler Toledo, Italy) equipped with a STAR^e Software and a FRS5 METTLER TOLEDO ceramic sensor. The instrument was calibrated with indium for melting point and heat of fusion. A heating rate of 20 °C min^{-1} was used. Standard aluminum sample pans were used and an empty pan was used as a reference. The analyses were performed in N_2 atmosphere (N_2 flow: 20 ml min^{-1}). A first heating cycle from 25 °C to 100 °C was followed by a cooling cycle from 100 °C to 30 °C and a second heating cycle from 30 °C to 300 °C.
Thermogravimetric (TG) analyses were performed on a Perkin Elmer TGA 4000 on 10 mg samples under nitrogen flow at 50 mL min^{-1}, from 30 °C to 850 °C at a heating rate of 20 °C min^{-1}.

Swelling degrees. The swelling degree of the hydrogels was evaluated in water, 0.01 M PBS at pH 7.4, KCl/HCl buffer at pH 2 and TRIS/HCl buffer at pH 9. All of the samples were dried to constant weight at 0.1 Torr before undergoing swelling experiments. Each sample was put into the test tube containing an excess of ethanol. The hydrogel was allowed to settle, the supernatant was carefully removed and replaced with either the swelling solvent. The solvent was then changed three times so as to remove any ethanol traces. The swelling degrees were evaluated at equilibrium according to eq 1:

$$SD\ [\%] = \frac{V_t}{V_0}\ x\ 100 \qquad (1)$$

where V_0 is the volume of the dry powder and V_t is the volume of the hydrogel at equilibrium time. In all tests, the percent mean variation coefficient, CV%, was lower than 5%. The reported values were the average of three experiments.

Electroanalytical Studies. The kinetics of Mn^{2+}, Cu^{2+}, Cd^{2+}, Pb^{2+}, Zn^{2+}, Ni^{2+}, and Co^{2+} absorption by PAA hydrogels were studied *in situ* by monitoring the corresponding voltammetric peak currents, proportional to the ion concentration in solution, on a working hanging mercury drop electrode (HDME). In particular:
(a) Square wave voltammetry (SWV) was adopted for Cu^{2+}, Cd^{2+}, Pb^{2+}, Zn^{2+}, Ni^{2+}, and Co^{2+} at intermediate to low concentrations, directly monitoring the corresponding reduction peaks. SWV rather than DPV (the ideal choice in equilibrium conditions) was chosen for its intrinsic rapidity to achieve sufficient resolution in the initial part of the absorption kinetic curves, considering that half-life times were in the order of a minute;

(b) Anodic stripping voltammetry (ASV), implying local preconcentration of the metal by ion reduction to metal amalgam in controlled conditions followed by DPV reoxidation, [10] [14] was adopted for Mn^{2+}, Cu^{2+}, Cd^{2+}, Pb^{2+}, and Zn^{2+} at the lowest concentrations;
(c) Adsorptive cathodic stripping voltammetry, implying local preconcentration of the metal by its adsorption as dimethylglyoxime complex onto mercury in controlled conditions followed by DPV reoxidation was adopted for Ni^{2+} and Co^{2+} at the lowest concentrations.

The experiments were carried out by an EcoChemie Autolab PGStat 12 or 308 potentiostat by GPES software, in the voltammetric conic cell of a Metrohm 663 VA Polarographic Stand, including a HMDE (drop size 2) as the working electrode, a platinum wire as the counter electrode, and an aqueous saturated calomel electrode (filled with a saturated Trace SelectVR KCl solution) as the reference electrode. The working cell was thoroughly cleaned with nitric acid and ultrapure water before each experiment. Ultrapure nitrogen bubbling allowed solution deaeration.

The background solutions were, depending on the experiment, as follows:

1. a pH 6.8 PBS made up by Na_2HPO_4 and KH_2PO_4 (Fluka and Carlo Erba, both = 99.5%);
2. a pH 6.8 asymmetric Tris(hydroxymethyl)aminomethane (TRIS) buffer made up by ultrapure α,α,α-tris-(hydroxymethyl)-methylamine (Aldrich), partially neutralized by a 0.1 M HCl standard solution (Fluka);
3. a pH 5.4 asymmetric acetate buffer made up by acetic acid partially neutralized by sodium hydroxide monohydrate (both Trace SelectVR Fluka).

pH 6.8 has been chosen as intermediate in the typical range of tap or drinking waters. The TRIS buffer was tested as an alternative to PBS since phosphates, particularly PO_4^{3-} species (which however is not the dominant one at the working pH) can lead to cation precipitation at sufficiently high concentrations. Actually, the linear dynamic range for the above voltammetric techniques in the experimental timescale was verified for all tested ions in PBS, the maximum operating concentration appearing to be 10^{-4} M for Cu^{2+}, Zn^{2+}, Cd^{2+}, 10^{-5} M for Co^{2+}, 10^{-6} M for Ni^{2+}, and 10^{-7} M for Pb^{2+}. On the other hand, also the TRIS buffer could be non-innocent as it might give some cation coordination effect, which however should be hardly competitive with the hydrogel for entropic reasons, hinging on a single coordinating site, the amino one, partly protonated at the working pH. Except for the case of Pb^{2+} where PBS had to be avoided, in all of the other cases, fast, regular, and reproducible absorption kinetics were recorded in both PBS

and TRIS, pointing to a negligible matrix effect. For further confirmation, some experiments were also repeated in acetate buffer. This implied a lower pH (5.4), which can however be found in some natural waters.

The absorption experiments were performed adding the PAA hydrogel as a powder to the buffer background solution (25 cm^3), whereas metal ions were added by small volumetric additions of the corresponding Fluka TraceCertVR metal standards to give initial metal concentrations ranging 0.00002-0.0005 M. The maximum absorption capacity of the hydrogels was evaluated for each metal ion equilibrating for 3 days under stirring 100 cm^3 of a 0.001 M solution of the selected ion (with nitrate counter anion) with the chosen hydrogel. The hydrogel was confined in highly porous paper bags so that it could be easily removed upon absorption. After the experiment, the residual concentration of the metal ion was determined by SWV using the multiple standard addition method while the metal-saturated hydrogels were dried and photographed to evidence chromatic changes. Parameters for SWV analysis were as follows: stirrer 2000 rpm, purge time 10 s, purge amplitude 0.05 V, equilibration time 3 s, start potential 0.05 V, end potential -1.25 V, voltage step 0.006 V, and frequency 20 V s^{-1}. Parameters for ASV analysis were as follows: stirrer 2000 rpm, purge time 300 s, purge amplitude 0.05 V, deposition potential -1.15 V, deposition time 90 s, equilibration time 10 s, start potential -1.15 V, end potential 0.05 V, voltage step 0.006 V, voltage step time 0.1 s, and sweep rate 0.06 V s^{-1}. Some experiments were run on a set of pollutants rather than on a single one, to evaluate preferential absorption. In selected cases, after following the absorption kinetics and recording the limiting concentration at infinite time, the reversibility of the absorption process was investigated by small progressive additions of concentrated nitric acid. A simultaneous potentiometric monitoring of the pH solution and voltammetric monitoring of the metal ion release was recorded.

For Mn^{2+}, monitored via ASV, a tailored ASV protocol was adopted. ASV analyses were carried out on solutions made up by 10 mL sample + 50 μL 25% NH_3 + 2.5 mL supporting electrolyte (0.1 M $Na_2B_4O_7$ + 0.3 M NaOH) + 10 μL Zn^{2+} solution (100 mg dm−3), thoroughly deaerated by N_2 bubbling. The standard addition method was applied, the stripping peak current intensities being linearly proportional to the bulk Mn^{2+} concentration. ASV parameters: stirring 2000 rpm, purge time 300 s, pulse amplitude -0.075 V, deposition potential -1.7 V, deposition time 90 s, equilibration time 5 s, potential scan from -1.62 to -1.25 V (SCE) [the Mn^{2+} stripping peak appearing at about -1.45 V (SCE)], voltage step 0.004 V, voltage step time 0.5 s, and sweep rate 0.008 V s^{-1}.

Mn^{2+} sorption kinetics were studied at different (hydrogel monomeric unit:metal) ratios and at different metal starting concentrations both by *in situ* ASV monitoring and by final ASV verification of the limiting residual metal concentration. While the latter was achieved by the same ASV reference protocol above reported, an *ad hoc* protocol had to be developed for the *in continuo* monitoring, implying pH 7 (as in natural waters), and the absence of ions potentially sorbed by the hydrogel. Accordingly, (a) the borax + ammonia buffer at pH 9.5–10 of the reference protocol was replaced with a 0.0065 M TRIS + 0.1 M TRIS hydrochloride buffer, corresponding to pH 6.8; (b) Zn^{2+} addition was omitted; (c) the preaccumulation step was reduced to optimize the quantity of metal deposited on the mercury drop (10 s at 0.0001 M, to be increased to 3, 60, and 90 s at lower concentration ranges). As a consequence of (a) and (b), the baseline was no longer horizontal and sensitivity was lower (detection limit 10^{-7} M instead of 10^{-9} M), but more than sufficient to follow the sorption kinetics, implying a fairly high metal concentration range.

Synthesis of EDDA1 Acrylamido-End-Capped Oligomer. EDDA (780.6 mg; 4.34 mmol) and LiOH•H_2O (369.2 mg; 8.71 mmol) were dissolved in 50%$^{v}/_{v}$ aqueous MeOH (8 mL). MBA (997.4 mg; 6.21 mmol) was then added and the mixture reacted at 30 °C, in the dark, for 72 hours. MeOH was evaporated under vacuum, the mixture diluted with H_2O (150 mL) and freeze-dried. The final product was recovered as a white powder. Yield: 2.1 g, 96.2%.

^{1}H NMR (400.13 MHz, D_2O, δ): 6.11 (br, 4H, -CH=C**H$_2$**), 5.66 (br, 2H, -C**H**=CH_2), 4.52 (s, 2H, CO-NH-C**H$_2$**-NH-CO terminal), 4.43 (s, 2H, CO-NH-C**H$_2$**-NH-CO polymer backbone), 3.02 (s, 4H, N-C**H$_2$**-COOH), 2.73 (br, 4H, C**H$_2$**-N), 2.52 (br, 4H, N-CO-CH_2-C**H$_2$**), 2.30 (br, 4H, N-CO-C**H$_2$**-CH_2).

^{13}C NMR (100.62 MHz, D_2O, δ): 179.29 (-CH_2-**C**OOH), 175.4 (NH-**C**O polymer backbone), 168.45 (N-**C**O terminal), 129.55 (**C**H=CH_2), 128.19 (CH=**C**H_2), 58.43 (**C**H_2-COOH), 51.08 (-**C**H_2-N), 51.18 (**C**H_2-CH_2-CO-N), 44.28 (NH-**C**H_2-NH), 32.12 (CH_2-**C**H_2-CO-N). SEC: $\overline{M}_n$= 2100, PDI= 1.

Synthesis of EDDA1 hydrogel. EDDA1 hydrogel was prepared from EDDA1 oligomer solution after MeOH stripping and the radical polymerization was initiated by $Na_2S_2O_5$ and $Na_2S_2O_8$ (both 0.5 mg/μL aqueous solutions, 1% $^{w}/_{w}$). After 24 hours at room temperature the hydrogel was washed with three H_2O/EtOH cycles, soaking the product

in the solvent (50 mL) for 12 hours and renewing it at regular time intervals within the following 48 hours. The hydrogel was then dried until constant weight. Yield: 0.22 g, 72%. Anal. calcd. for EDDA1: C 48.44, N 17.16, C/N calcd. ratio=2.75; found: C 41.38, N 14.28, C/N found ratio=2.90.

Synthesis of EDDA2 Acrylamido End-Capped Oligomer. EDDA (785.1 mg; 4.37 mmol) and LiOH•H_2O (368.1 mg; 8.71 mmol) were dissolved in H_2O (8 mL). MBA (501.9 mg; 3.13 mmol) was then added and the mixture reacted at 30 °C, in the dark, for 48 hours. BAC (648.3 mg; 3.13 mmol) and LiOH•H_2O (132.66 mg; 3.13 mmol) were added and the mixture reacted at 20 °C, in the dark, for 24 hours. The mixture was diluted with H_2O (150 mL) and freeze-dried. The final product was recovered as a white powder. Yield: 2.3 g, 95%.

^{1}H NMR (400.13 MHz, D_2O, δ): 6.17 (br, 4H, -CH=C**H$_2$**), 5.73 (br, 2H, -C**H**=CH_2), 5.52 (s, 1H, CH-COOH terminal), 5.44 (s, 1H, CH-COOH polymer backbone), 4.56 (s, 2H, -CO-NH-C**H$_2$**-NH-CO terminal), 4.47 (s, 2H, CO-NH-C**H$_2$**-NH-CO polymer backbone), 3.05 (s, 4H, N-C**H$_2$**-COOH), 2.77 (br, 4H, C**H$_2$**-N), 2.55 (br, 4H, N-CO-CH_2-C**H$_2$**), 2.35 (br, 4H, N-CO-C**H$_2$**-CH_2).

^{13}C NMR (100.62 MHz, D_2O, δ): 179.30 (N-CH_2-**C**OOH), 175.4 (NH-**C**O-CH_2-**C**O-NH polymer backbone), 174.69, 174.46 (CH-**C**OOH), 173.15 (**C**O-CH-COOH polymer backbone), 168.78 (**C**O-CH_2-**C**O terminal), 167.74 (**C**O-CH-COOH terminal), 129.51 (**C**H=CH_2), 128.28 (CH=**C**H_2), 58.16 (**C**H-COOH), 57.92 (**C**H_2-COOH), 51.21 (-**C**H_2-N), 50.24 (**C**H_2-CH_2-CO-N), 44.28 (NH-**C**H_2-NH), 32.01 (CH_2-**C**H_2-CO-N). SEC: $\bar{M}_n$= 1600, PDI= 1.15.

Synthesis of EDDA2 hydrogel. EDDA2 hydrogel was prepared employing EDDA2 oligomer mixture without freeze drying and following the same procedure described for the synthesis of EDDA1 hydrogel. Yield: 0.23 g, 76%. Anal. calcd. for EDDA1: C 46.88, N 15.89, C/N calcd. ratio=2.95; found: C 38.36, N 12.60, C/N found ratio=3.04.

Synthesis of LYMA hydrogel. L-lysine (1.597 g, 10.702 mmol) and sodium hydroxide (434.6 mg, 10.702 mmol) were added at 80 °C under vigorous stirring to a suspension of finely powdered MBA (2.5 g, 16.054 mmol) in water (5.3 mL). The resultant mixture became rapidly homogeneous. At this point, it was slowly cooled to 25 °C, gently stirred until the gel point, reached in 15 min, and then maintained at the same temperature for further 3 days to complete the reaction. After this time, the reaction mixture turned into a

transparent, fairly substantial gel that was crushed, acidified by adding 1 M hydrochloric acid (1 x 50 mL) and washed up three times for 30 min with, alternatively, water and ethanol (100 mL each). The rationale for these extractions was to subject the hydrogel to several swelling (in water) and deswelling (in ethanol) cycles, thus facilitating the expulsion of soluble impurities. Finally, the hydrogel was dried to constant weight at room temperature and 0.1 torr. Anal. calcd. for LYMA: C, 51.98%; N, 18.65%; C/N = 2.79. Found: C, 46.2%; N, 15.68%; C/N = 2.95.

Synthesis of LMT85 Acrylamido End-Capped Oligomer. NaOH (1.46 g, 36 mmol) was added to an EDDS trisodium salt solution (45.47 g, 45.99 mmol). MBA was added (5.12 g, 32.85 mmol) under vigorous stirring until complete dissolution, and the homogeneous reaction mixture thus obtained was kept 48 h at 50 °C in the dark, under nitrogen atmosphere. BAC (6.54 g, 32.85 mmol) and sodium hydroxide (1.09 g, 26.76 mmol) were added, and the reaction mixture allowed to react for 24 h at 25 °C. The solution was then diluted to 150 mL with doubly distilled water and the pH adjusted to 4 with 37% HCl. A portion of the mixture (0.5 mL) was purified by ultrafiltration through a membrane with a 500 molecular weight cutoff, freeze dried, and characterized by ^{1}H and ^{13}C NMR analyses. The remaining part did not undergo ultrafiltration and was directly freeze dried to be used in the next step. LMT85 acrylamido end-capped oligomer was analyzed as a hydrochloride salt.

^{1}H NMR (400 MHz, D_2O, δ, ppm): 6.18 (m, 2H, terminal C**H$_2$**); 5.70 (m, 1H, terminal C**H**); 5.62 (br, 1H, COOH-C**H**-NH-CO); 4.52 (br, 2H, CO-NH-C**H$_2$**-NH-CO); 3.87 (br, 1H, COOH-C**H**-CH_2-COOH); 3.76 (br, 2H, COOH-CH-C**H$_2$**-COOH); 3.30 (br, 2H, CO-C**H$_2$**-CH_2-N); 3.10 (br, 2H, CO-CH_2-C**H$_2$**-N); 2.60 (br, 2H, N-C**H$_2$**).

^{13}C NMR (100, MHz, D_2O, δ, ppm): 175.71 (**C**OOH-CH-CH_2-COOH); 172.97 (**C**OOH-CH-CO); 167.85 (NH-**C**O-CH_2-CH_2); 129.57 (terminal **C**H_2); 128.43 (terminal **C**H); 62.57 (COOH-CH-**C**H_2-COOH); 58.07 (COOH-**C**H-NH-CO); 48.90 (**C**H_2-N); 48.36 (NH-CO-CH_2-**C**H_2); 44.27 (NH-**C**H_2-NH); 31.22 (NH-CO-**C**H_2-CH_2).

Synthesis of LMT85 hydrogel. Acrylamido end-capped oligomer (5 g) was dissolved in doubly distilled water (4.05 mL). An aqueous solution (0.95 mL) of $K_2S_2O_8$ (50 mg, 0.19 mmol) was added to the above solution, the resulting mixture was heated to 50 °C for 20 seconds then kept at 25 °C for 24 h. The final product was a transparent hydrogel, which was finely ground, alternatively washed with H_2O and EtOH as above described for

LYMA, and finally dried in vacuum until constant weight. Yield: 3.0 g (60%). Anal calcd. for LMT85: C: 40.76%; N: 11.15%; ratio C/N = 3.66. Found: C: 32.4%; N: 9%; ratio C/N = 3.60.

Results and discussion

To the purpose of this study, no polymer family was better suited than PAAs, owing to their structural versatility, probably unique in stepwise polyaddition polymers, which enables to obtain highly sophisticated structures with simple and environmental friendly procedures starting from easily prepared and/or commercial products of low to moderate cost.

EDDA1 and EDDA2 were planned to obtain highly hydrophilic hydrogels with repeating units bearing EDDA residues, known for their complexing ability toward heavy metal ions such as Co^{2+} and Cu^{2+}. Following the same criteria LYMA was designed as a polymeric analog of L-lysine, known for its ability to complex several metal ions, in particular Cu^{2+} and Ni^{2+}. Finally, LMT85 was planned in order to obtain a polymeric mimic of EDTA, well known for its outstanding complexing ability toward heavy metal ions, able to absorb a wide range of heavy metals. For this reason EDDS, mimic of EDTA, was chosen as a monomer for the preparation of LMT85. Furthermore, it is worthwhile to mention that both L-lysine and EDDS were chosen also for their costs, far lower than that of EDDA.

EDDA1 was synthesized in two steps (Scheme 12). In the first step, a low molecular weight acrylamide end-capped oligomer was prepared by polyaddition of EDDA to excess MBA in 50%$^{v}/_{v}$ MeOH aqueous solution and in the presence of enough lithium hydroxide to neutralize all the carboxyl groups. Aqueous MeOH was used as solvent due to the poor solubility of MBA in water in the experimental conditions adopted. In the second step, MeOH was evaporated and the oligomer directly polymerized using $Na_2S_2O_5/Na_2S_2O_8$ redox couple as initiator.

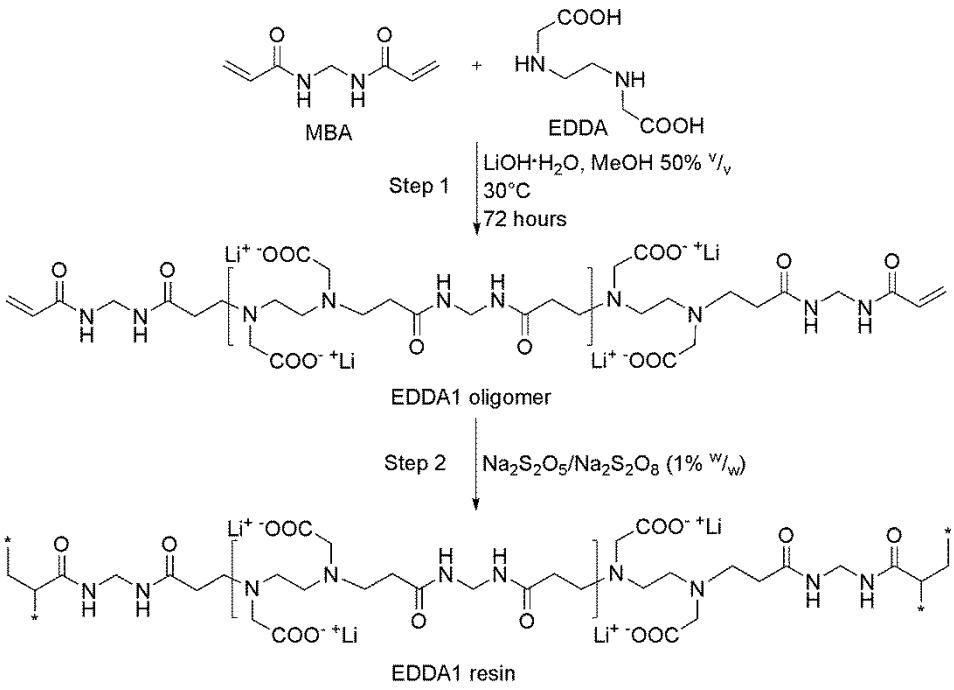

Scheme 12. Synthesis of EDDA1 hydrogel.

EDDA2 was prepared following a similar procedure. Here both MBA and BAC were used as bisacrylamides in order to increase the amount of carboxylic groups with respect to EDDA1 (Scheme 13). After the syntheses, both EDDA1 and EDDA2 were purified with three water/ethanol cycles that is, after swelling the crosslinked product in water, the solvent was replaced with ethanol and the procedure repeated twice so as to remove any uncrosslinked residue.

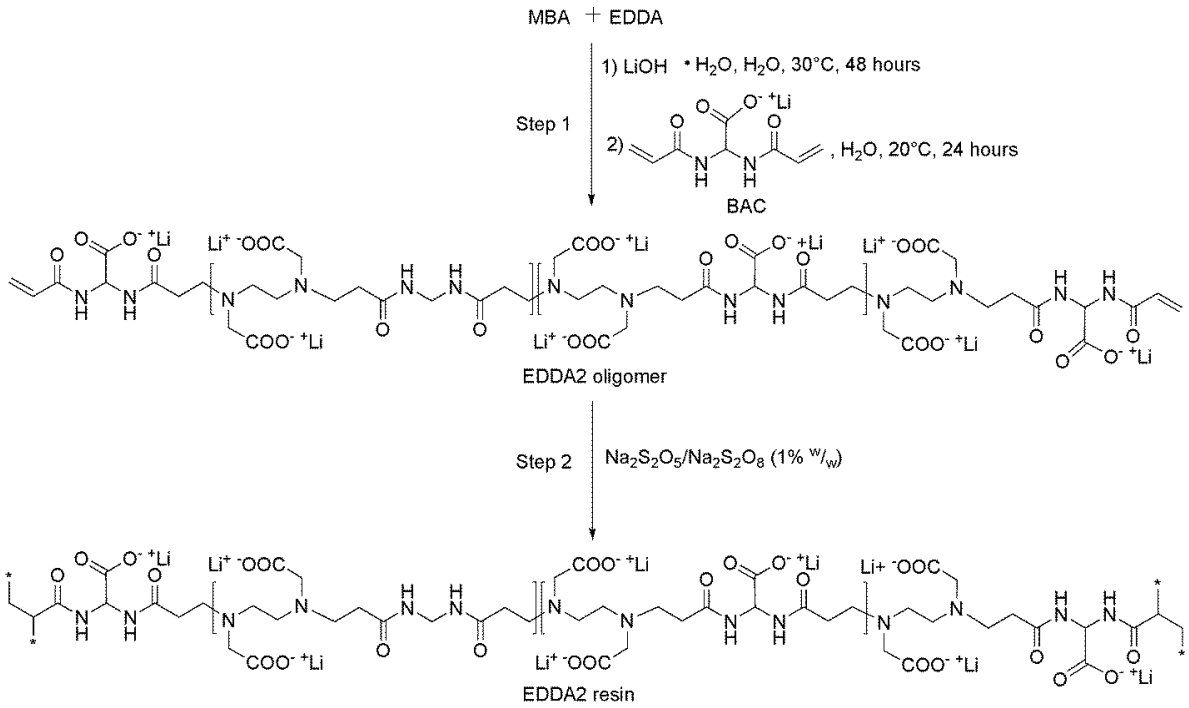

Scheme 13. Synthesis of EDDA2 hydrogel.

LYMA was prepared by polyaddition at room temperature in a pH 9 aqueous solution of L-lysine, by far the cheapest lysine isomer, with MBA (Scheme 14).

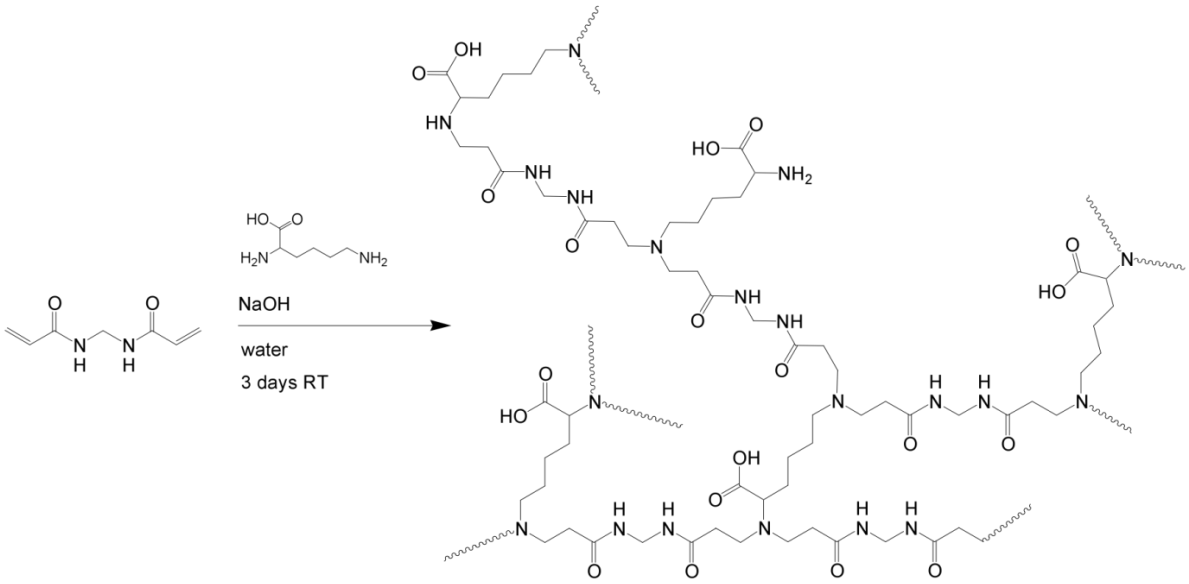

Scheme 14. Synthesis of LYMA hydrogel.

MBA is poorly soluble in water at room temperature and initial heating at 80 °C was necessary to dissolve it and let the reaction start, after which the reaction mixture became permanently homogeneous. L-lysine carries four amine hydrogen pertaining to two

primary amine groups of comparable basicity. Therefore, in Michael polyadditions with bisacrylamides it could act as tetrafunctional monomer yielding crosslinked products. However, in the working pH range, the molecule is zwitterionic, which significantly biases the reactivity of the amine groups. Therefore, 1 mole base per L-lysine mole was added in the polymerization mixture. The gel point was typically observed after 5 min, after which the reaction was allowed to proceed for further 3 days.

LMT85 was prepared in two steps (Scheme 15). In the first step, a low molecular weight end-capped oligomer was prepared by polyaddition of (S,S)-ethylenediamine-N,N'-disuccinic acid (EDDS) to excess BAC and MBA in water and in the presence of enough sodium hydroxide to neutralize all the carboxyl groups present in the monomers. In the second step, the oligomer was not isolated but directly cross-linked using $K_2S_2O_8$ as initiator at pH 5.5.

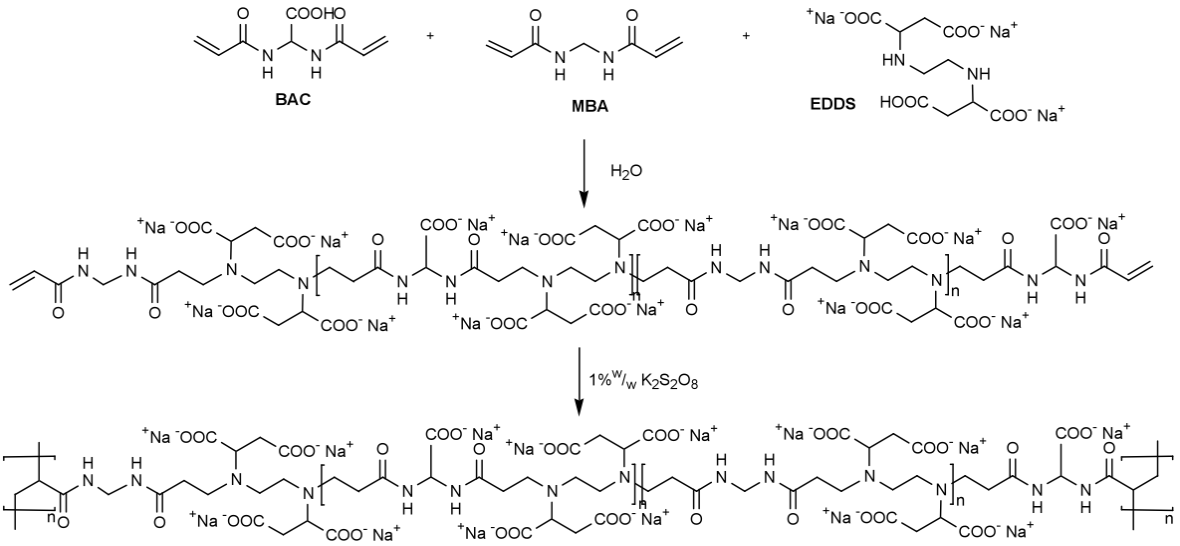

Scheme 15. Synthesis of acrylamido end-capped oligomer and of LMT85 hydrogel.

All of the products were characterized by FTIR analysis. In the case of EDDA1 and EDDA2, the FTIR analyses were carried out on both hydrogels and their oligomeric acrylamide end-capped precursors (Figure 17).

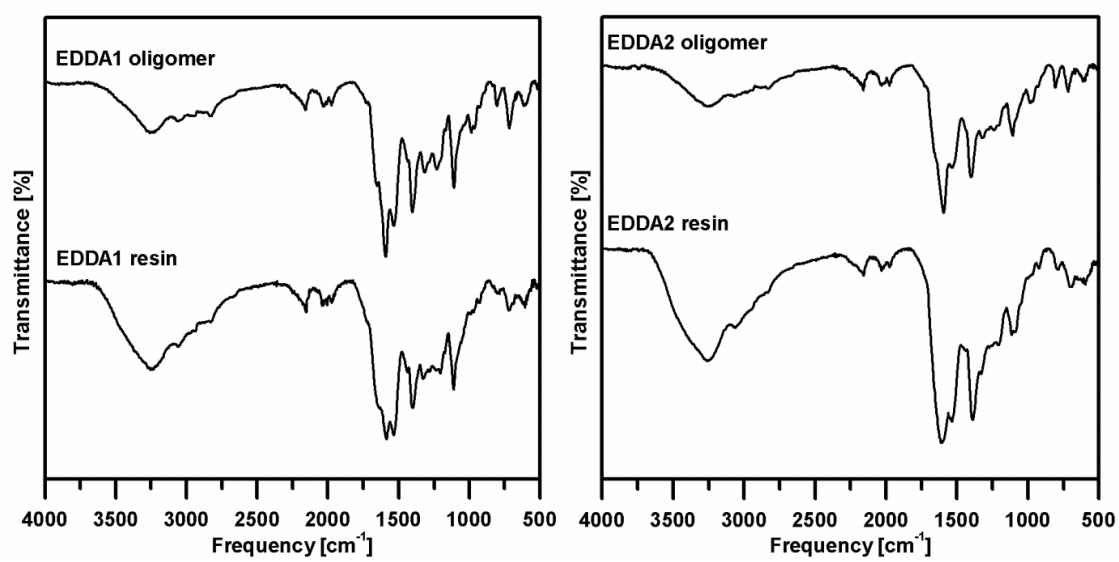

Figure 17. FTIR spectra of EDDA1 and EDDA2 acrylamido end-capped oligomers and hydrogels.

FTIR spectra of EDDA1 oligomer and hydrogel revealed peaks at 3275 and 3071 cm^{-1} due to NH amide stretching, at 2960 and 2838 cm^{-1} signals due to CH_2 asymmetric and symmetric stretching, respectively. At 1655 cm^{-1} is clearly visible an intense band due to amides C=O stretching, at 1595 and 1406 cm^{-1} $-COO^-$ asymmetric and symmetric stretching, respectively, are showed and at 1236 cm^{-1} tertiary amines CN stretching are visible. At 708 cm^{-1} a band due to amide NH out of plane wagging is showed. In the spectrum of EDDA1 oligomer is also visible a peak at 850 cm^{-1}due to alkene CH_2 wagging. This signal is hardly detectable in EDDA1 hydrogel spectrum, meaning that after the crosslinking reaction few unreacted vinyl bonds were left.

The signals found in EDDA1 oligomer and hydrogel spectra can be detected also for EDDA2 products at slightly different frequencies. Here, for EDDA2 oligomer and hydrogel NH amide stretching is present at 3262 and 3072 cm^{-1} and CH_2 asymmetric and symmetric stretching are at 2987 and 2840 cm^{-1}, respectively. Amides C=O stretching is visible at 1640 cm^{-1}, $–COO^-$ asymmetric and symmetric stretching are present at 1597 and 1405 cm^{-1}, respectively. Tertiary amines CN stretching is visible at 1246 cm^{-1} and a band due to amide NH out of plane wagging is showed at 710 cm^{-1}. In the spectrum of EDDA2 oligomer, a peak due alkene CH_2 wagging is also visible at 856 cm^{-1}. This signal is not detectable in EDDA2 hydrogel spectrum because apparently there were no unreacted vinyl bonds left.

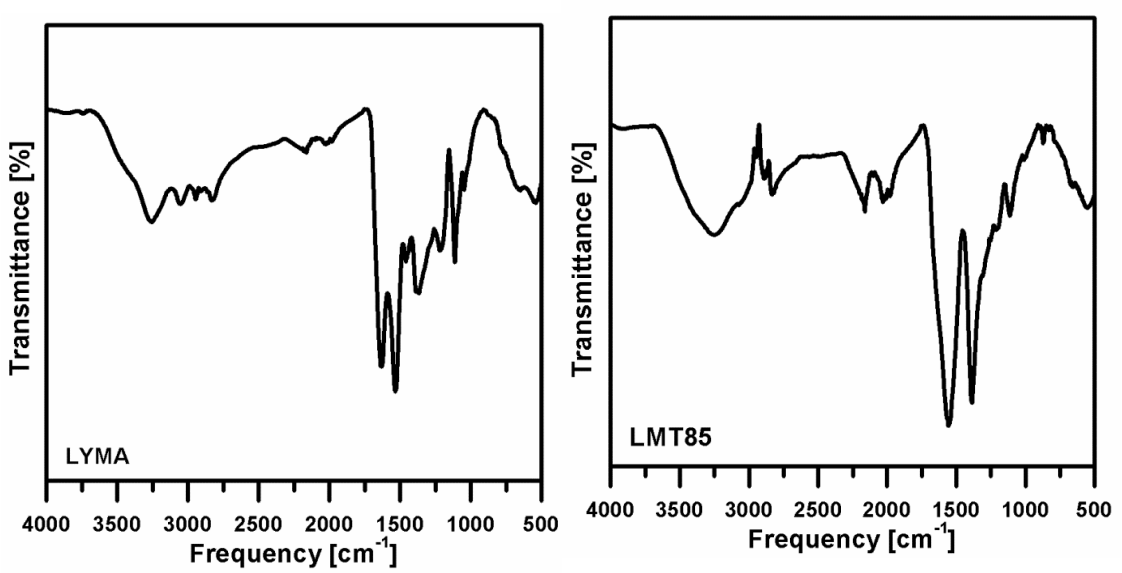

Figure 18. FTIR spectra of LYMA and LMT85.

FTIR spectrum of LYMA (Figure 18, left) showed NH amide stretching at 3263 and 3065 cm^{-1}, asymmetric and symmetric CH_2 stretching at 2844 and 2941 cm^{-1}, respectively, $-COO^-$ asymmetric and symmetric stretching at 1541 and 1390 cm^{-1}, respectively, C=O amide stretching at 1636 cm^{-1}, CN amine stretching at 1111 cm, NH amide out of plane wagging at 665 cm^{-1}.

FTIR spectrum of LMT85 (Figure 18, right) mainly showed EDDS signals such as $-COO^-$ asymmetric and symmetric stretching at 1559 and 1391 cm^{-1}, respectively. C=O amide stretching at 1655 cm^{-1} is overlapped to the strong band of $-COO^-$ asymmetric stretching, NH amide stretching are detectable at 3255 and 3053 cm^{-1}, asymmetric and symmetric CH_2 stretching are shown at 2894 and 2828 cm^{-1}, respectively, and NH amide out of plane wagging is visible at 664 cm^{-1}.

The thermal behavior of the hydrogels was evaluated by DSC and TG analyses. The DSC thermograms were obtained in the 30-300 °C range at a heating rate of 20 °C min^{-1} in N_2 atmosphere. The second run heating cycle, following a cooling cycle carried out at the same rate, of EDDA1 and EDDA2 hydrogels, LYMA and LMT85, is reported in Figure 19. All of the products showed no evidence of either melting phenomena or glass transition up to 200 °C. Above 200 °C they all showed exothermic thermal decompositions in spite of the inert atmosphere, with onset temperatures at 230.81 °C for EDDA1, 251.11 °C for EDDA2, 271.64 °C for LYMA and 239.21 °C for LMT85.

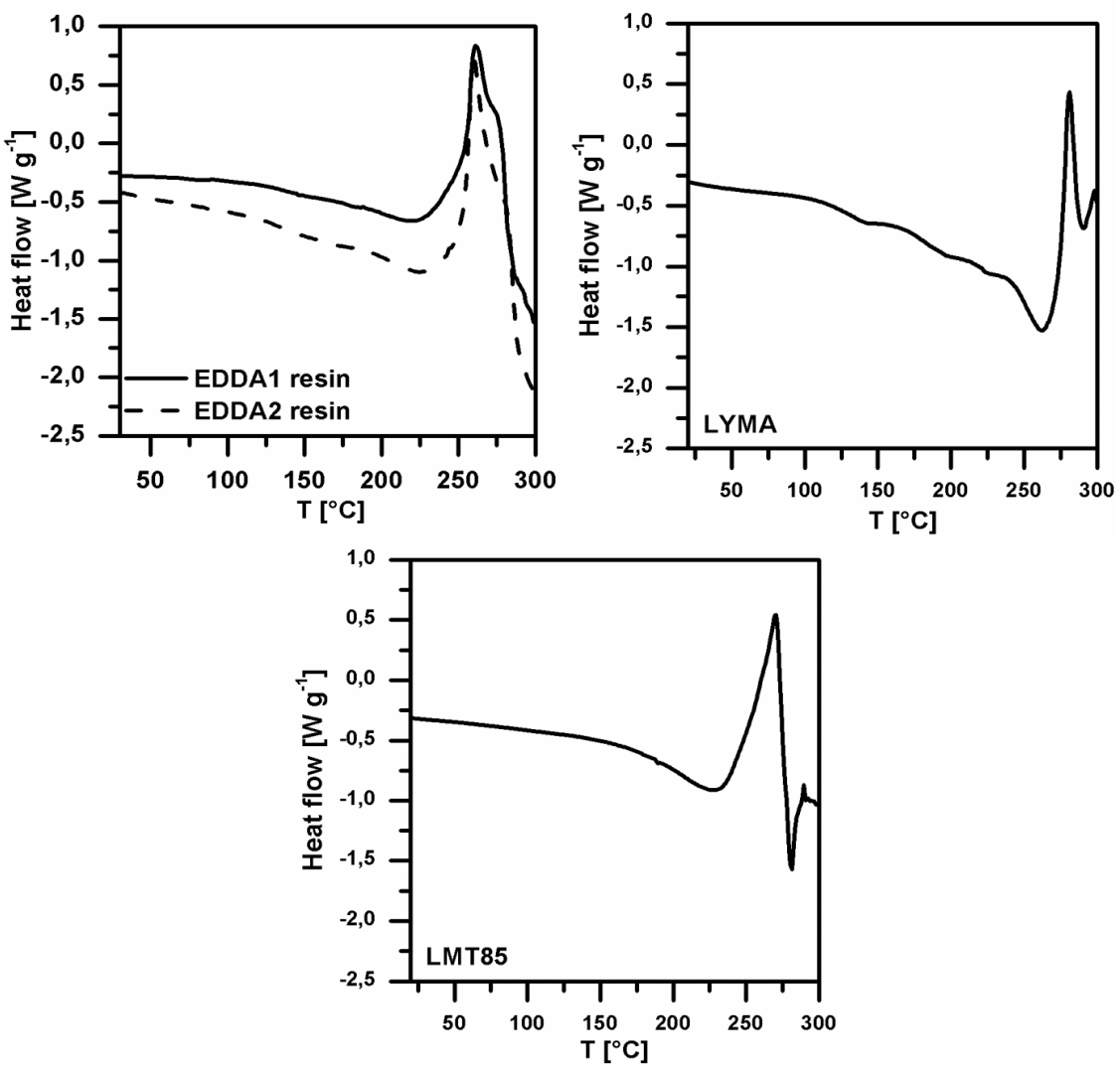

Figure 19. DSC second run curves for EDDA1, EDDA2, LYMA and LMT85 hydrogels.

TG analyses confirmed the behavior of the products upon heating (Figure 20). The analyses were performed in the 30-850 °C range at a heating rate of 20 °C min^{-1} in N_2 atmosphere. EDDA1 and EDDA2 hydrogels TG curves were characterized, apart from an initial slight weight loss due to dehydration in the 30-100 °C range (0.60% for EDDA1 hydrogel, 1.90% for EDDA2 hydrogel), by a massive degradation above 200 °C. The main thermal decomposition step was observed in the range 200-560 °C with a residual mass of 32.57% and 35.39% for EDDA1 and EDDA2, respectively. The highest decomposition rate equal to 8 % $°C^{-1}$ was observed at 300 °C for both hydrogels. LYMA showed a 0.34% weight loss at 100 °C due to dehydration and a massive degradation between 200 and 515 °C with a residual mass of 15%. The highest decomposition rate equal to 13 % $°C^{-1}$ was showed at 312 °C. LMT85 showed a 1.81% weight loss at 100 °C

due to dehydration and a main degradation step between 200 and 520 °C with a residual mass of 48.7%. The maximum decomposition rate of 9 % $°C^{-1}$ was at 295 °C.

In general, the thermal stability of EDDA1, EDDA2 and LMT85 hydrogels is comparable and higher than that of LYMA. Besides the chemical composition, the reason may be ascribed to the synthetic method adopted. In fact, EDDA1, EDDA2 and LMT85 were prepared by radical polymerization of pre-synthesized acrylamido end-capped PAA oligomers, thus leading to the formation of methylene chains that apparently lead to a better thermal stability than that of LYMA, prepared by Michael polyaddition of L-lysine to MBA.

The swelling behavior of EDDA1 and EDDA2, LYMA and LM85 hydrogels in H_2O, and buffers pH 7.4, pH 2 and pH 9 are shown in Figure 21. The swelling behavior of the hydrogels was evaluated on the products as dried fine powders in H_2O, ethanol, 0.01 M buffer solutions at pH 7.4, at pH 2 and pH 9 (Figure 21). It is apparent that while all of the products can be considered as highly hydrophilic, the water absorption of LMT85 is outstanding. This is, in fact, a superabsorbent polymer, in line with the commonly adopted definition for this category of products. [15] It may be observed that the number of ionizable groups per repeating unit, that is, the charge density at pH 5.5 (in doubly distilled H_2O) of LMT85 is particularly high, probably resulting in higher hydration shell and higher electrostatic repulsion compared to LYMA, EDDA1 and EDDA2 hydrogels. The same is observed at pH 2, 7.4 and 9. For EDDA1, EDDA2 and LMT85 hydrogels the swelling at pH 9 is slightly higher than those at pH 2 and 7.4 due to the presence of dissociated carboxylic groups whose electrostatic repulsion effect is apparently more significant than that of protonated amines. In general, the swelling degrees of EDDA1 and LYMA hydrogels, bearing less ionizable groups, are less sensitive to pH.

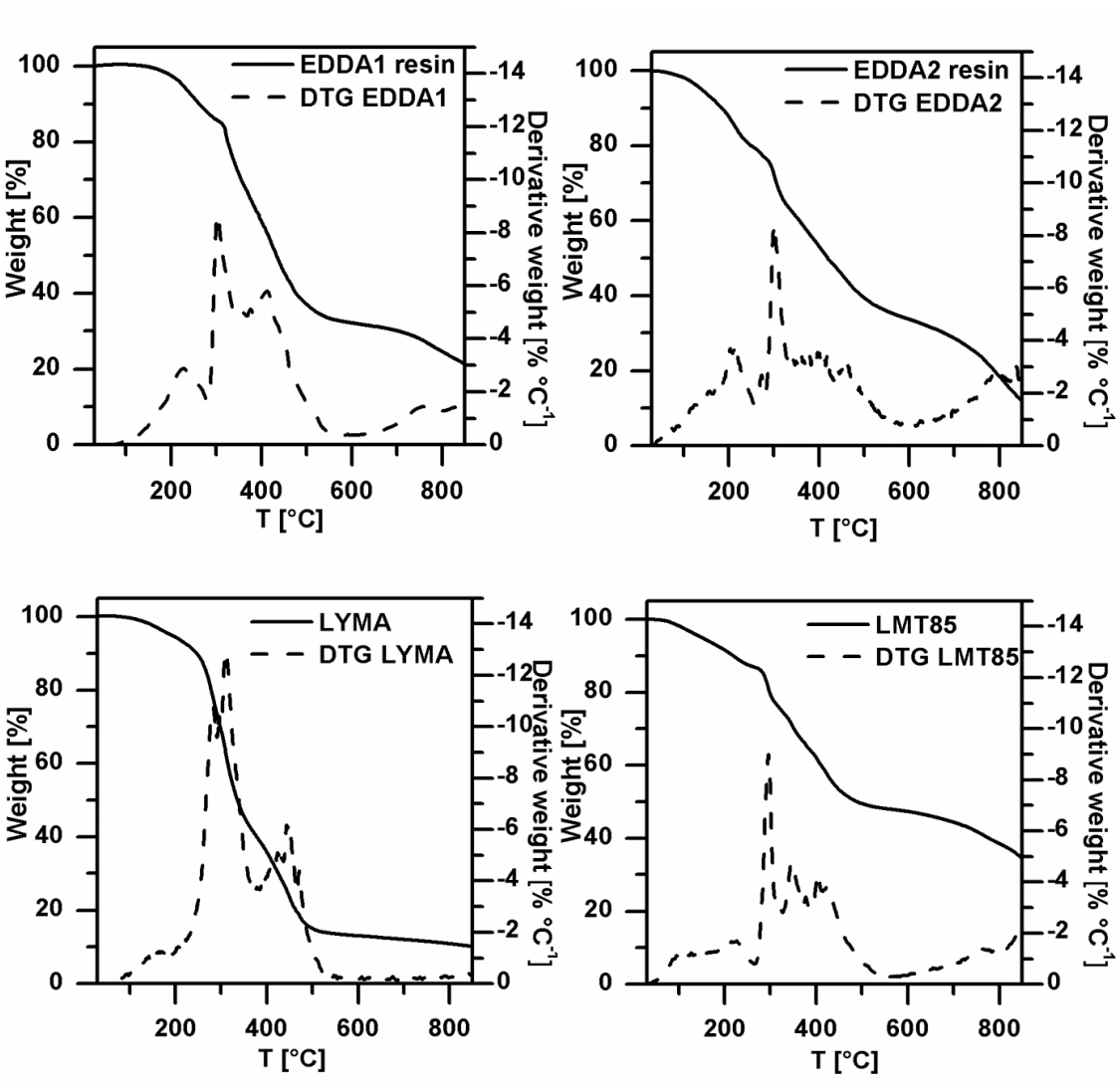

Figure 20. TG and DTG analyses for EDDA1 and EDDA2, LYMA and LMT85 hydrogels.

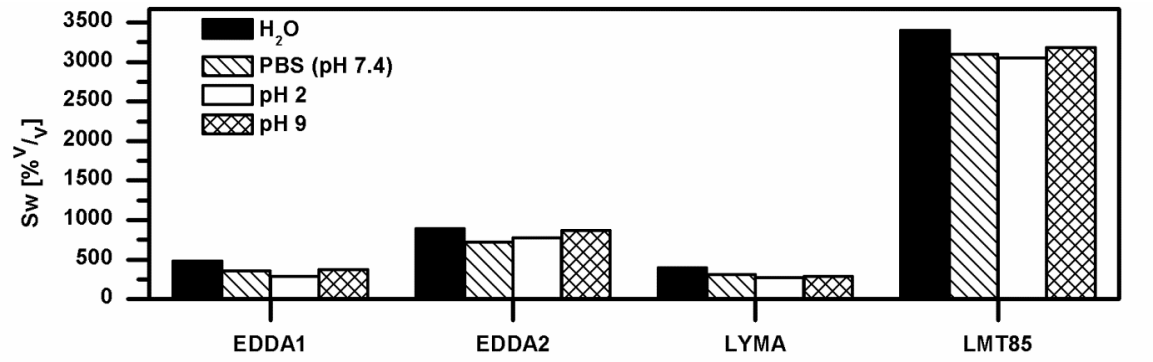

Figure 21. Swelling behavior of EDDA1, EDDA2, LYMA and LMT85 hydrogels: swelling percentage volume per volume (SW% $^{v}/_{v}$) are reported in H_2O, PBS at pH 7.4, KCl/HCl buffer at pH 2 and TRIS/HCl buffer at pH 9.

Batch tests of absorption capacity of excess metal ions showed that both EDDA1 and EDDA2 hydrogels were able to absorb either Co^{2+} and Cu^{2+}, with EDDA2 showing preferential absorption towards Co^{2+}. LMT85 absorbed all the tested ions whereas LYMA only absorbed Cu^{2+} and Ni^{2+}. The absorption capacities obtained (corresponding to 100-500 mg Me^{2+} g^{-1} hydrogel, depending on the metal atomic weights) were quite competitive with the literature data for other absorbing materials, considering both the absorption capacity and, in the case of LMT85, the wide range of metal ions efficiently absorbed that can be reasonably expected to extend far beyond the model metal series considered in this study. [1] [2] The same experiment also gave indication about the chromatic changes of the hydrogels upon metal absorption. As shown in
Figure 22, in some cases, particularly with Cu^{2+}, Co^{2+}, and Ni^{2+}, the absorption process resulted in intense and fast coloring (blue, pink/violet, and green, respectively). This feature may be in principle exploited in diagnostic kits or, if the hydrogels are used for water purification, adopted as indicator of their degree of exhaustion and, therefore, of the regeneration timing.

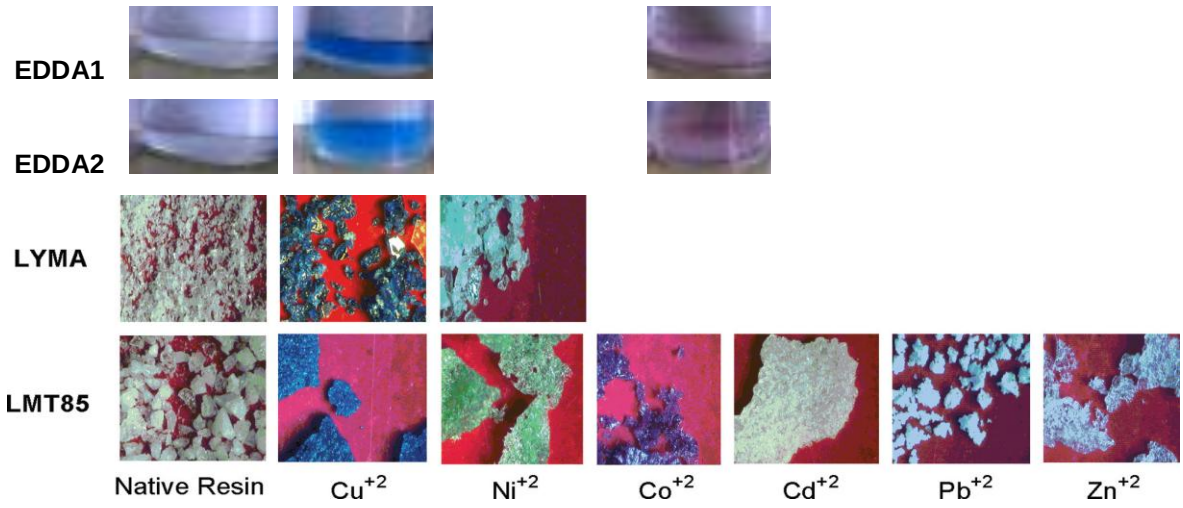

Figure 22. Chromatic changes of EDDA1, EDDA2, LYMA and LMT85 hydrogels upon ion absorption.

The absorption kinetics of single ions and their mixtures were investigated as a function of ion concentration and of the hydrogel repeating unit/metal ion ratio. Single absorption kinetics were obtained by in situ monitoring by either SWV or ASV on the HMDE (see for instance Figure 23), whereas ‘‘stripping’’ techniques (ASV for Mn^{2+}, Cu^{2+}, Cd^{2+}, Pb^{2+} and Zn^{2+}, and adsorptive stripping voltammetry (AdsV) for Co^{2+} and Ni^{2+}) were applied on the same electrode, to determine the asymptotic concentration values for the six ions.

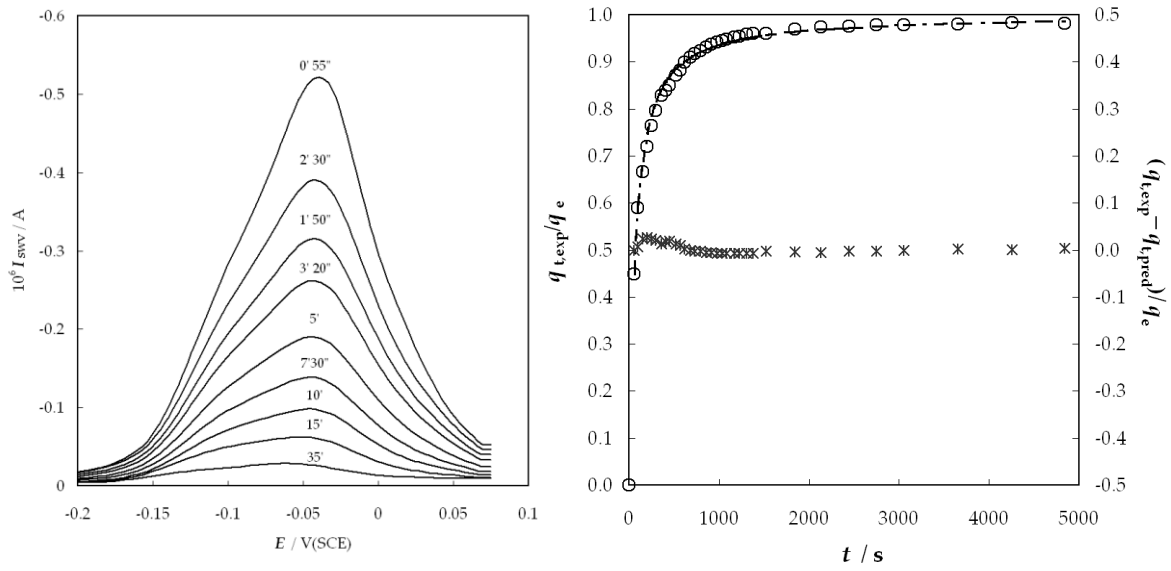

Figure 23. (left) *in situ* SWV monitoring of Cu^{2+} absorption from a 0.00005 M solution at pH 6.8 (phosphate buffer) by LYMA resin in 10:1 ratio (not all curves reported for sake of clarity); (right) fitting the same kinetics according to the pseudo-second order model: experimental q_t values (circles: experimental points; dash-and-dot line: predicted curve; stars: residuals)

In the above experiments, dilute metal ion solutions and high hydrogel repeating unit/metal ion ratios were purposely adopted, to verify the feasibility of quantitative removal of metal ions at very low concentrations. In particular, the starting concentration of metal ions ranged from 0.00025 (1 ppm) to 0.00005 M.

The absorption kinetics were found for most cases to fit a pseudosecond-order model, implying the following:

$$\frac{dq_t}{dt} = -k_2(q_e - q_t)^2 \qquad (1)$$

where q_t is the absorption capacity of the metal ion at time t (in mmol g^{-1}), q_e the same quantity at the equilibrium (in our case, at SWV peak current practically constant and at $t \geq 10\ t_{1/2}$ ($t_{1/2}$ = halving time), while k_2 is the pseudosecond-order constant (in g $mmol^{-1}$ s^{-1} or g $mmol^{-1}$ min^{-1}). Rearranging and integrating, eq 1 gives the following:

$$\frac{t}{q_t} = \frac{1}{q_e^2 k_2} + \frac{1}{q_e}\, t \qquad (2)$$

that can be used for linearization of the kinetic characteristics. An example, concerning Cu^{2+} absorption by LYMA, is provided in Figure 24. According to (2), the halving time is:

$$t_{1/2} = 1/(q_e k_2) \qquad (3)$$

A single case appeared not to fit within the above model but into the double exponential one, implying the presence of two kinds of absorption sites, a faster one and a slower one, it can be expressed by the following equation:

$$q_t = q_e - \frac{D_1}{m_{abs}}\exp\left(-k_{D_1} t\right) - \frac{D_2}{m_{abs}}\exp(-k_{D_2} t) \qquad (4)$$

where m_{abs} is the weight of absorbing material, k_{D1} and k_{D2} (with $k_{D1} > k_{D2}$) its absorption kinetic constants corresponding to the two different absorption modes, and D_1 and D_2 (in mmol dm^{-3}) modulating parameters of the corresponding two absorption rates. Approaching equilibrium, the third term of the equation prevails on the second one. Therefore, D_2 and k_{D2} can be obtained fitting the flat region of the experimental curve by eq 4. Subsequently, D_1 and K_{D1} were obtained by fitting the whole experimental curve (Figure 25) by the following linearized version of eq 3:

$$\ln(q_e - q_t) = ln\frac{D_2}{m_{abs}} - k_{D_2} t \qquad (5)$$

It is worthwhile noticing that the double exponential model is actually the sum of two first-order models, each of them being expressed by:

$$\frac{dq_t}{dt} = k_1(q_e - q_t) \qquad (6)$$

Giving after integration:

$$ln\frac{(q_e - q_t)}{q_e} = -k_1 t \qquad (7)$$

That is:

$$q_t = q_e - q_e\exp(-k_1 t) \qquad (8)$$

corresponding to (3) in the presence of a single absorption mode. In this frame, comparing the pre-exponential terms D/m_{ABS} in eq 3 with q_e in (8), the constants D_1 and D_2 appear to express the number of sorbed moles in each mode. From (3), we obtain for this model a halving time of:

$$t_{1/2} \approx ln2/k_{D_1} \qquad (9)$$

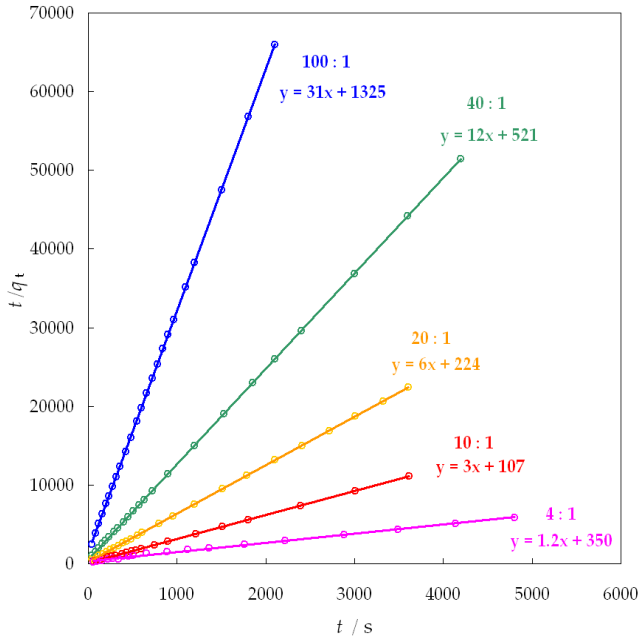

Figure 24. Pseudo-second order linearization of absorption kinetics of Cu^{2+} at different concentrations ($5 \cdot 10^{-4}$ M, $2 \cdot 10^{-4}$ M, $1 \cdot 10^{-4}$ M, $5 \cdot 10^{-5}$ M, $2 \cdot 10^{-5}$ M) and constant volume (V = 25 cm^3) by a constant amount of LYMA repeating units ($5 \cdot 10^{-5}$ moles). LYMA repeating units *vs* metal ion ratios are reported beside each straight line.

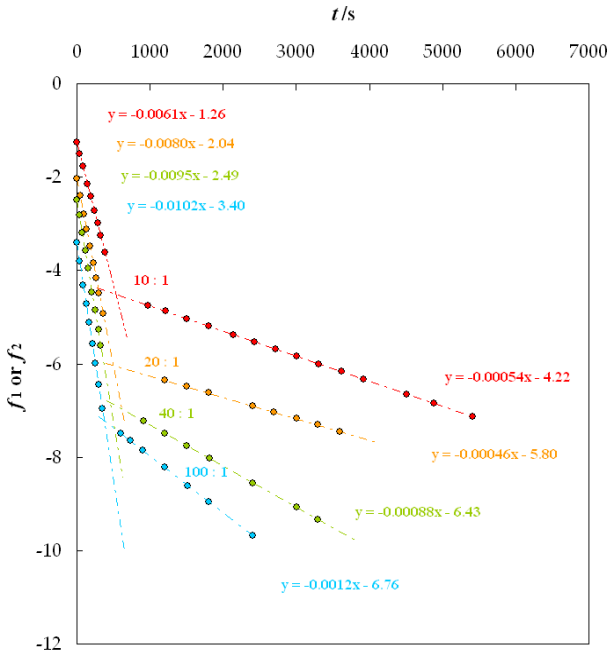

Figure 25. Double-exponential linearization of absorption kinetics of Ni^{2+} at different concentrations ($2 \cdot 10^{-4}$ M, $1 \cdot 10^{-4}$ M, $5 \cdot 10^{-5}$ M, $2 \cdot 10^{-5}$ M) and constant volume (V = 25 cm^3) by a constant amount of LYMA repeating units ($5 \cdot 10^{-5}$ moles). The LYMA repeating units *vs* metal ion ratios are reported beside each straight line.

Table 6 summarizes the results concerning Cu^{2+} absorption for EDDA1 and EDDA2 hydrogels. The concentration effects were evaluated. In particular, the apparent rate constant k_2 increased at constant hydrogel weight with increasing hydrogel to metal ratio, that is with the availability of coordinating sites. The same trend was observed for Co^{2+} absorption (Table 7). Furthermore, while EDDA1 showed similar k_2 values for both metals, EDDA2 showed significantly higher k_2 for Co^{2+} ions.

Table 6. A Synopsis of Experimental Kinetic Parameters for Cu^{2+} absorption by EDDA1 and EDDA2 in different experimental conditions.

#	Hydrogel	Cu^{2+} [mol L^{-1}]	Molar ratio[a]	q_e [mmol g^{-1}]	k_2 [g $mmol^{-1}$ s^{-1}]	$t_{1/2}$ [min]
TRIS buffer (pH 6.8)						
1	**EDDA1**	2.5×10^{-4}	1:2	5.86	0.104	3
2	**EDDA1**	2.5×10^{-5}	70:1	0.45	0.17	2.1
1	**EDDA2**	2.5×10^{-4}	1:2	6.25	0.001	11
2	**EDDA2**	2.5×10^{-5}	20:1	0.013	0.230	57.3

[a] mol hydrogel repeating unit/mol Cu^{2+}

Table 7. A Synopsis of Experimental Kinetic Parameters for Co^{2+} absorption by EDDA1 and EDDA2 in different experimental conditions.

#	Hydrogel	Co^{2+} [mol L^{-1}]	Molar ratio[a]	q_e [mmol g^{-1}]	k_2 [g $mmol^{-1}$ s^{-1}]	$t_{1/2}$ [min]
PBS (pH 6.8)						
1	**EDDA1**	2.5×10^{-4}	1:5	2.836	0.001	6.03
2	**EDDA1**	2.5×10^{-5}	20:1	0.172	0.842	0.12
1	**EDDA2**	2.5×10^{-4}	1:5	1.012	0.037	0.43
2	**EDDA2**	2.5×10^{-5}	20:1	0.016	3478	3×10^{-4}

[a] mol hydrogel repeating unit/mol Co^{2+}

Table 8 summarizes the results concerning Cu^{2+} absorption for LYMA and LMT85 hydrogels. The experiments in phosphate buffer allowed evaluating the concentration effects. In particular, the apparent rate constant k_2 regularly increased (a) at constant hydrogel weight, with increasing hydrogel to metal ratio, that is with the availability of coordinating sites (entries 4-7 in Table 11 for both LYMA and LMT85); (b) at constant metal concentration, with increasing hydrogel to metal ratio (entries 1 and 2 for LYMA; entries 2 and 5 for LMT85); (c) at constant hydrogel to metal ratio, with increasing metal concentration (entries 2-4 for LYMA, entries 1, 3, and 4 for LMT85). Moreover, comparing entries 2, 8, and 9 for LMT85, the other conditions being the same, the maximum rate is observed in phosphate buffer pH 6.8, whereas significantly lower rates were found in acetate buffer pH 5.4, consistently with a lower dissociation degree of the carboxyl groups, and in TRIS buffer, that might somewhat compete with LYMA in Cu^{2+} coordination.

Table 8. A Synopsis of Experimental Kinetic Parameters for Cu^{2+} absorption by LYMA and LMT85 in different experimental conditions.

#	Hydrogel	Cu^{2+} [mol L^{-1}]	Molar ratio[a]	q_e [mmol g^{-1}]	k_2 [g $mmol^{-1}$ min^{-1}]	$t_{1/2}$ [min]
Phosphate buffer (pH 6.8)						
1	**LYMA**	5×10^{-4}	4.10	0.860	0.23	5.02
2	**LYMA**		10.1	0.319	11.9	0.26
3	**LYMA**	5×10^{-5}	10.6	0.312	2.8	1.13
4	**LYMA**	2×10^{-4}	10.0	0.329	5.2	0.58
5	**LYMA**	10^{-4}	20.2	0.163	10.1	0.61
6	**LYMA**	5×10^{-5}	39.8	0.083	16.9	0.72
7	**LYMA**	2×10^{-5}	102	0.033	40.7	0.75
1	**LMT85**	5×10^{-5}	5.01	0.586	1.04	1.63
2	**LMT85**	5×10^{-4}	5.01	0.545	5.50	0.33
3	**LMT85**	0.00050	4.99	0.553	1.11	1.62
4	**LMT85**	2×10^{-4}	5.01	0.546	2.83	0.65
5	**LMT85**	10^{-4}	10.0	0.274	5.74	0.64
6	**LMT85**	5×10^{-5}	20.0	0.149	6.60	1.02
7	**LMT85**	2×10^{-5}	50.1	0.064	9.35	1.67
TRIS buffer (pH 6.8)						
8	**LYMA**	10^{-4}	9.95	0.345	0.80	3.64
8	**LMT85**		5.0	0.610	0.39	4.16
Acetate buffer (pH 5.4)						
9	**LMT85**	0.0001	5.0	0.613	0.32	5.16

[a] mol hydrogel/mol Cu^{2+}

Table 9 summarizes the results concerning Ni^{2+} absorption by both hydrogels. Ni^{2+} absorption kinetics by LYMA in PBS fitted the double exponential model, whereas in TRIS buffer (entry 7) they followed the usual pseudosecond-order model. As expected, the process proceeded faster with increasing ion concentration at constant hydrogel to metal ratio (entries 1-3) and increasing the amount of hydrogel at constant metal concentration (entries 2 and 4). In TRIS buffer Ni^{2+} absorption by LYMA was slower than that of Cu^{2+} (Table 8, entry 8). Ni^{2+} absorption by LYMA was also slower than that by LMT85 (entry 2). Ni^{2+} absorption by LMT85 followed pseudosecond-order kinetics and was slower than Cu^{2+} absorption in PBS but faster than Cu^{2+} absorption in TRIS buffer, probably due to some competition of TRIS in Cu^{2+} coordination.

Table 9. A synopsis of experimental kinetic parameters for Ni^{2+} absorption by LYMA and LMT85 in different conditions[a]

#	Hydrogel	Ni^{2+} [mol L^{-1}]	Molar ratio[b]	q_e [mmol g^{-1}]	D_1 [mmol L^{-1}]	k_{d1} [min^{-1}]	D_2 [mmol L^{-1}]	k_{d2} [min^{-1}]	$t_{1/2}$ [min]
Phosphate buffer (pH 6.8)									
1	**LYMA**	5 x 10^{-5}	11	0.316	0.000807	0.0046	0.0001442	0.0008	2.5
2	**LYMA**	10^{-4}	10	0.307	0.001549	0.0052	0.0001661	0.0007	2.2
3	**LYMA**	2 x 10^{-4}	10	0.319	0.004280	0.0060	0.0002241	0.0005	1.9
4	**LYMA**	10^{-4}	20	0.163	0.001911	0.0078	0.0000422	0.0004	1.5
5	**LYMA**	5 x 10^{-5}	40	0.082	0.001222	0.0093	0.0000200	0.0008	1.2
6	**LYMA**	2 x 10^{-5}	101	0.033	0.000509	0.0102	0.0000175	0.0012	1.1
#	**Hydrogel**	**Ni^{2+}** [mol L^{-1}]	**Molar ratio[b]**		**q_e** [mmol g^{-1}]		**k_2** [g $mmol^{-1}$ min^{-1}]		**$t_{1/2}$** [min]
Phosphate buffer (pH 6.8)									
1	**LMT85**	5 x 10^{-5}	5.0		0.552		0.84		2.2
TRIS buffer (pH 6.8)									
7	**LYMA**	10^{-4}	9.95		0.234		0.97		4.4
2	**LMT85**		5.0		0.561		0.81		2.2

[a] The amount of hydrogel repeating units per volume unit is the product of the entries in the third and fourth columns

[b] mol hydrogel/mol Ni^{2+}

Table 10 summarizes the results concerning Mn^{2+} absorption by LYMA and LMT85. In situ kinetic experiments were performed in a voltammetric cell with a TRIS+TRIS hydrochloride buffer at pH 6.8, affording simulation of a typical natural water pH while avoiding the presence of precipitating ions such as phosphates.

Extremely fast sorption was observed with both LMT85 and LYMA, with halving times in the order of 1 min for LMT85 and even less for LYMA, even starting with diluted metal solutions. In the presence of Mn2+ excess, LYMA and LMT85 showed absorption capacities of 0.10 g Mn^{2+} g^{-1} hydrogel and 0.18 g Mn^{2+} g^{-1} hydrogel, respectively. LYMA, in spite of showing lower sorption capacity in batch tests, appeared to give faster sorption than LMT85: the metal peak disappeared within approximately 1 min, so that the voltammetric monitoring protocol, albeit fast (affording about 1 scan min^{-1}), could not provide enough points for the subsequent kinetic analysis. Also the sorption process appeared quantitative. The residual Mn^{2+} concentrations after treatment using only slight excess hydrogel were below the ppm detection limit of the reference ASV protocol (1 ppb), well below the law limits (0.05 ppm in the USA). In the case of LMT85, good

linearization of the kinetic parameters was achieved by the pseudosecond-order kinetic model. A synopsis of the linearized kinetic characteristics is shown in Figure 26. All halving times were of the order of 1 min or less and regularly decreased with increasing LMT85 amount. The kinetic constants followed the opposite trend.

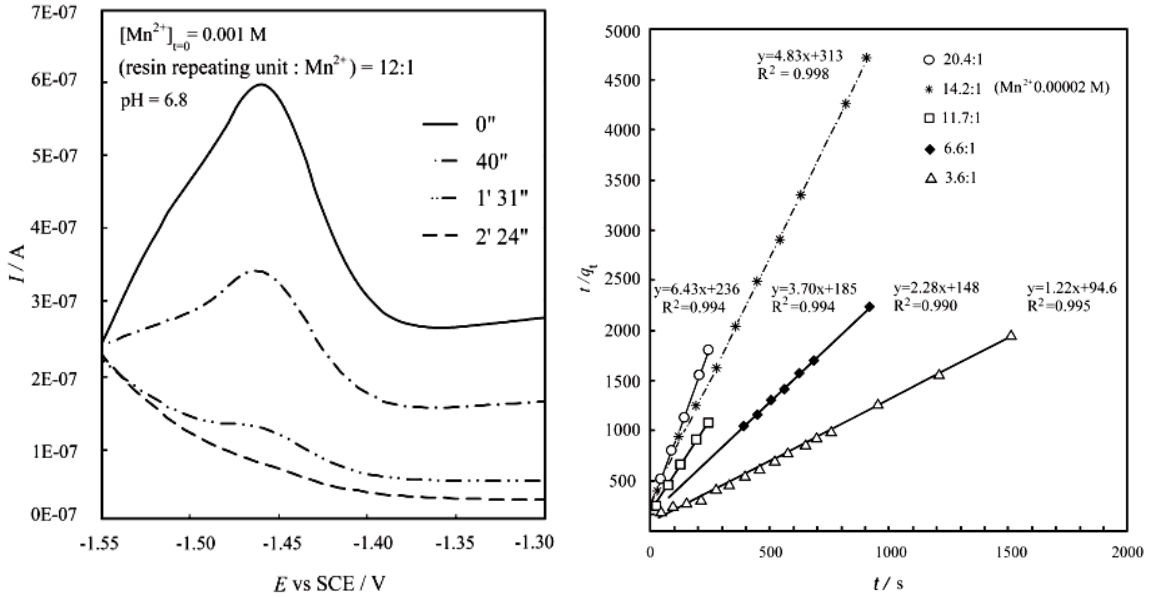

Figure 26. On the left: an example of fast Mn^{2+} sorption by LMT85, monitored by in situ ASV. On the right: a synopsis of the linearized kinetic characteristics.

Table 10. A synopsis of experimental kinetic parameters for Mn^{2+} absorption by LMT85 in different experimental conditions[a].

#	Hydrogel	Mn^{2+} [mol L^{-1}] x 10^{-5}	Molar ratio[b]	q_e [mmol g^{-1}]	k_2 [g $mmol^{-1}$ s^{-1}]	$t_{1/2}$ [min]
1	**LMT85**	9.54	20.4	0.156	0.18	0.61
2			11.7	0.270	0.074	0.83
3			6.6	0.440	0.035	1.08
4			3.6	0.817	0.016	1.29
5		1.91	14.2	0.207	0.075	1.08

[a] The amount of hydrogel repeating units per volume unit is the product of the entries in the third and fourth columns.

[b] mol hydrogel/mol Mn^{2+}.

The remaining four metal ions were complexed only by LMT85 hydrogel. The relevant experimental kinetic parameters are summarized in Table 11. The performance of LMT85 with Cd^{2+} was comparable to that with Cu^{2+}, whereas significantly lower kinetic constants, hence higher halving times, were observed with Zn^{2+}, Co^{2+}, and Pb^{2+}. As already mentioned, in the latter case, the phosphate buffer was avoided to prevent precipitation.

Figure 27 reports a comparison of the LMT85 absorbing efficiency towards all metal ions, in both PBS and TRIS buffers. On the whole, in all cases the fast absorption rates were observed in PBS, the fastest absorption was observed with Cu^{2+}. In TRIS buffer, the lower absorption rate observed in the case of Cu^{2+} and Co^{2+} can probably be ascribed to the previously mentioned competition by the buffer.

Table 11. A synopsis of experimental kinetic parameters for Cd^{2+}, Pb^{2+}, Co^{2+} and Zn^{2+} absorption by LMT85 in different experimental conditions[a].

#	Hydrogel	Cd^{2+} [mol L^{-1}]	Molar ratio[b]	q_e [mmol g^{-1}]	k_2 [g $mmol^{-1}$ min^{-1}]	$t_{1/2}$ [min]
PBS (pH 6.8)						
1	**LMT85**	5 x 10^{-5}	5.23	0.558	0.576	3.1
2	**LMT85**	10^{-4}	5.01	0.514	1.32	1.5
3	**LMT85**	5 x 10^{-4}	4.99	0.541	3.34	0.6
4	**LMT85**	2 x 10^{-4}	5.01	0.537	0.98	1.9
5	**LMT85**	10^{-4}	10.0	0.273	5.78	0.6
6	**LMT85**	5 x 10^{-5}	20.0	0.136	11.49	0.6
7	**LMT85**	2 x 10^{-5}	50.1	0.054	12.22	1.5
TRIS buffer (pH 6.8)						
8	**LMT85**	10^{-4}	5.0	0.581	0.66	2.6
#	**Hydrogel**	**Pb^{2+}** [mol L^{-1}]	**Molar ratio[b]**	**q_e** [mmol g^{-1}]	**k_2** [g $mmol^{-1}$ min^{-1}]	**$t_{1/2}$** [min]
TRIS buffer (pH 6.8)						
1	**LMT85**	10^{-4}	5.0	0.520	0.54	3.6
#	**Hydrogel**	**Co^{2+}** [mol L^{-1}]	**Molar ratio[b]**	**q_e** [mmol g^{-1}]	**k_2** [g $mmol^{-1}$ min^{-1}]	**$t_{1/2}$** [min]
Phosphate buffer (pH 6.8)						
1	**LMT85**	5 x 10^{-5}	5.0	0.558	1.01	1.8
TRIS buffer (pH 6.8)						
2	**LMT85**	10^{-4}	5.2	0.554	0.53	3.4

#	Hydrogel	Zn^{2+} [mol L^{-1}]	Molar ratio[b]	q_e [mmol g^{-1}]	k_2 [g mmol^{-1} min^{-1}]	$t_{1/2}$ [min]
Phosphate buffer (pH 6.8)						
1	**LMT85**	5 x 10^{-5}	5.2	0.557	0.57	3.1
2	**LMT85**	10^{-4}	5.1	0.564	0.38	4.7
3	**LMT85**	2 x 10^{-4}	5.0	0.570	0.42	4.2
4	**LMT85**	5 x 10^{-4}	5.0	0.561	1.59	1.1
TRIS buffer (pH 6.8)						
5	**LMT85**	0.00010	5.0	0.579	0.54	3.2

[a] The amount of hydrogel repeating units per volume unit is the product of the entries in the third and fourth columns.

[b] mol hydrogel/mol Me^{2+}.

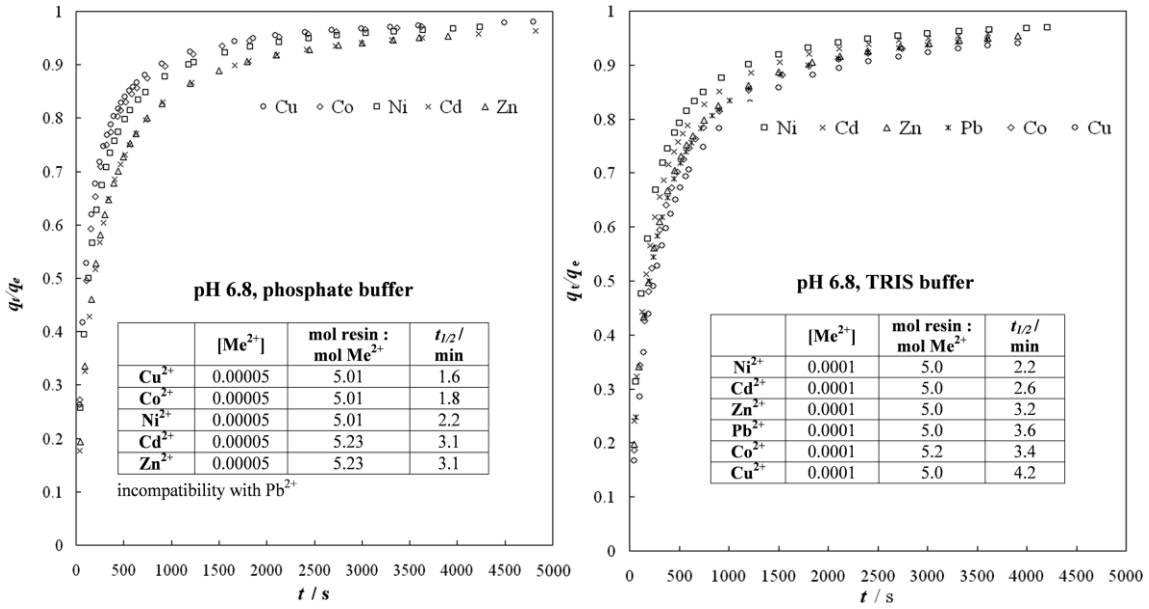

Figure 27. Comparison of the LMT85 absorbing efficiency toward all metal ions, in both phosphate and TRIS buffers. On the whole, in all cases, fast absorption rates were observed. In phosphate buffer, the fastest absorption was observed with Cu^{2+}. In TRIS buffer, the lower absorption rate observed in the case of Cu^{2+} and Co^{2+} can probably be ascribed to the previously mentioned competition by the buffer.

Experiments in multiple ion solutions confirmed the features evidenced in single ion absorption experiments. In fact, EDDA2 quickly removed Co^{2+} ions from the aqueous solution, with $t_{1/2}$=0.04 min, while Cu^{2+} ions were absorbed with $t_{1/2}$=4.18 min.

Table 12. A synopsis of experimental kinetic parameters for $Cu^{2+}$and Co^{2+} absorption by EDDA1 and EDDA2 hydrogels

Hydrogel	**Metal ion**	**Me^{2+}** [mol L^{-1}]	**Molar ratio**[a]	q_e [mmol g^{-1}]	k_2 [g $mmol^{-1}$ s^{-1}]	$t_{1/2}$ [min]
TRIS (pH 6.8)						
EDDA1	Co^{2+}	5 x 10^{-5}	60:1:1	0.059	0.021	0.22
	Cu^{2+}			0.059	0.01	0.45
EDDA2	Co^{2+}		60:1:1	0.051	8.869	0.04
	Cu^{2+}			0.048	0.084	4.18

[a] mol hydrogel repeating unit/mol Co^{2+}/mol Cu^{2+}

LYMA (Figure 28) selectively absorbed Cu^{2+} and Ni^{2+} with respect to other metal ions. The lack of absorption of Pb^{2+} and Cd^{2+} was particularly evident in acetate buffer, as the buffer was not competing with the absorbent. In contrast, LMT85 (Figure 28) absorbed all six ions with comparable speed and efficiency.

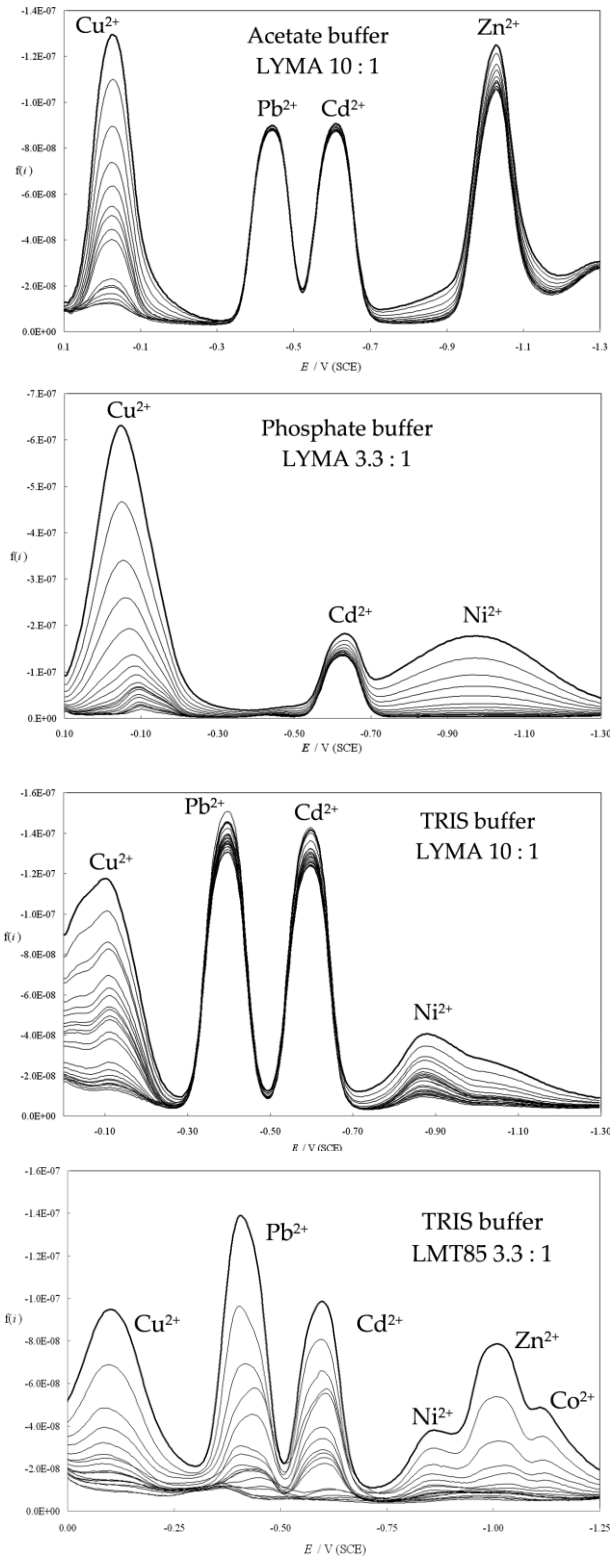

Figure 28. Absorption experiments with LYMA hydrogel in multiple metal solutions. Metal ion concentrations (from the top): 0.0000167, 0.00002, and 0.000025 M. Bottom: Absorption experiment with LMT85 hydrogel in multiple metal solution. Metal ion concentration was 0.000025 M.

With all of the hydrogels the absorption process was easily reversed by acidifying with excess mineral acids (Figure 29). The release was quantitative at pH 2 for EDDA1 and LYMA and at pH 0.8 for EDDA2 and LMT85, in accordance with the higher amounts of carboxylic groups present in the polymeric networks of the latter. This feature is particularly attractive for metal recover and/or hydrogel recycle after use.

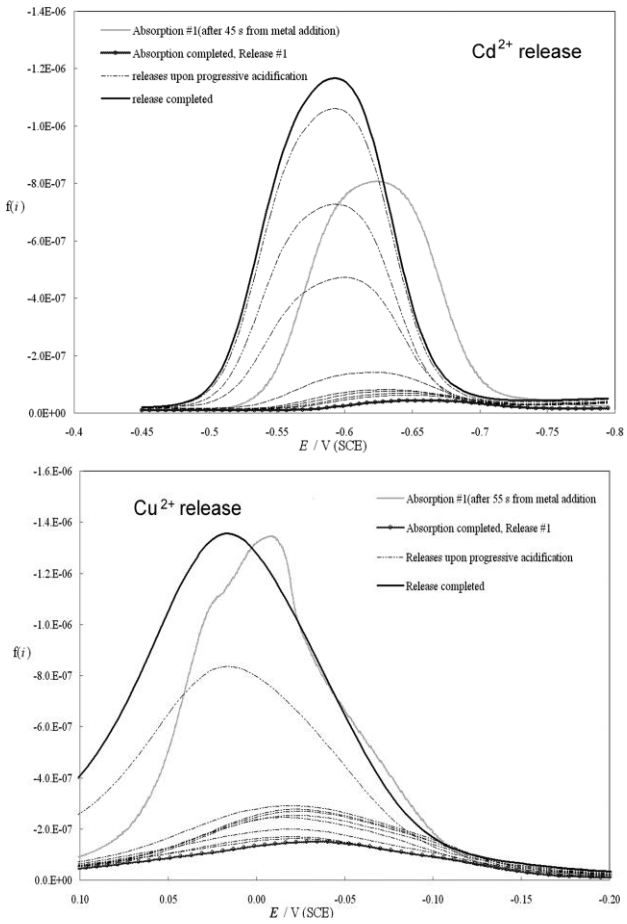

Figure 29. Examples of metal release from LMT85 (top) and LYMA (bottom) upon progressive acidification by small additions of concentrated nitric acid after absorption experiments.

Conclusions

The target of this study was to provide new multifunctional hydrogels for removing inorganic micropollutants from water. LYMA, LMT85, EDDA1 and EDDA2 were successfully synthesized as proved by elemental and FTIR analyses and showed thermal stability up to 200 °C. Furthermore, they exhibited the following relevant properties: the absorption capacity was apparently competitive with that of existing materials; the

absorption rate was fast even from dilute solutions down at least to 1 ppm; the metal ions were quantitatively removed by modest excess hydrogel; the absorption process was reversible, and the hydrogels were easily regenerated by acidification. The sorption of several metal ions imparted intense coloring to the hydrogels, a feature exploitable for analytical purposes, such as revealing on the spot the presence of the same ions in ponds or even running water by an environmental safe method, as well as monitoring the hydrogel exhaustion during water treatments, thus optimizing the timing of the regeneration process. Finally, all the hydrogels were obtained by simple eco-friendly procedures. Moreover, while EDDA1 and EDDA2 were prepared employing a quite expensive monomer (EDDA), LYMA and LMT85 were obtained at more moderate cost employing L-lysine, so far the cheapest isomer of lysine, and EDDS, mimic of EDTA. The scopes of the hydrogels were different. EDDA1 and EDDA2 hydrogels, EDDA mimics, proved able to maintain the complexing ability of EDDA after crosslinking, and absorbed both Co^{2+} and Cu^{2+} metal ions. Furthermore, EDDA2 proved selective for Co^{2+}. LYMA, the lysine mimic, proved remarkably selective for Mn^{2+}, Cu^{2+} e Ni^{2+} with respect to the other ions tested, which were negligibly absorbed. On the opposite, LMT85, the EDTA mimic, proved capable of rapidly and quantitatively absorbing all the seven ions tested either singly or in mixed solution and will likely prove capable in the future of absorbing a wide array of not yet considered metal ions. By concluding, EDDA1, EDDA2, LYMA and LMT85 hydrogels exhibited the expected metal complexing ability and their practical application for metal ion detection and removal in waters for domestic and agricultural use can be reasonably envisaged.

Acknowledgements

Project funded by Cariplo Foundation (Milan, Italy), call ‘‘Scientific and Technological Research for Advanced Materials’’ 2009.

References

[1] S. Babel, T. A. Kurniawan, *J. Hazard. Mater.*, vol. B97, pp. 219-243, 2003.

[2] T. A. Kurniawan, G. Y. S. Chan, W. Lo, S. Babel, *Sci. Total Environ.*, vol. 366, pp. 409-426, 2006.

[3] Y. A. Skorik, *Polym. Bull.*, vol. 68, pp. 1065-1078, 2012.

[4] P. Ferruti, E. Ranuci, S. Bianchi, L. Falciola, P. R. Mussini, M. Rossi, *J. Polym. Sci. A Polym. Chem.*, vol. 47, pp. 6977-6911, 2009.

[5] E. Emillitri, P. Ferruti, R. Annunziata, E. Ranucci, M. Rossi, L. Falciola, P. R. Mussini, F. Chiellini, C. Bartoli, *Macromolecules*, vol. 40, pp. 4785-4793, 2007.

[6] E. Ranucci, P. Ferruti, E. Lattanzio, A. Manfredi, M. Rossi, P. R. Mussini, F. Chiellini, C. Bartoli, *J. Polym. Sci. Part A: Polym. Chem.*, vol. 47, pp. 6977-6991, 2009.

[7] R. de Levie, Aqueous Acid-Base Equilibria and Titrations, Oxford: Oxford University Press, 1999.

[8] A. E. Martell, R. J. Motekaitis, Determination and Use of Stability Constants, Hoboken, New Jersey: Wiley-VCH, 1992.

[9] M. Kolthoff, J. I. Lingane, Polarography, New York: Interscience, 1952.

[10] *DIN 38406 Teil 16, "Verfahren zur Bestimmung von Zink, Cadmium, Blei, Kupfer, Thallium, Nickel, Cobalt, mittels Voltammetrie, E16 Deutsche Einheitsverfahren"*.

[11] K. H. Schrøder, B. G. Johnsen, *Talanta*, vol. 21, pp. 671-673, 1974.

[12] G. McLendon, R. J. Motekaitis, A. E. Martell, *Inorg. Chem.*, vol. 8, pp. 1993-1996, 1975.

[13] P. Ferruti, E. Ranucci, F. Trotta, E. Gianasi, G. E. Evagorou, M. Wasil, G. Wilson, R. Duncan, *Macromol. Chem. Phys.*, vol. 200, pp. 1644-1654, 1999.

[14] W. Joseph, Analytical Electrochemistry, Hoboken, New Jersey: Wiley-VCH, 2006.

[15] F. L. Buchholz, A. T. Graham, Modern Superadsorbent Polymer Technology, New York: Wiley, 1997.

CHAPTER 2

SYNTHESIS AND CHARACTERIZATION OF CYCLODEXTRIN-GRAFT-METHACRYLIC ACID-POLYAMIDOAMINE NANOSPONGES

Introduction

Great attention is currently given to specific organic water pollutants such as chlorinated organic compounds, which have potential significant impacts on human health and the environment. In particular, chlorinated volatile organic compounds (CVOC) have been proven to be carcinogenic to humans [1] and, as a rule, are listed among the substances that reduce the ozone layer. [2] Different technologies and processes have been investigated to remove CVOC from waters. Biological treatments, [1] advanced oxidation processes, [2] catalytic combustion, [3] electrochemical techniques, [4] and adsorption procedures have been most widely investigated. Adsorption is one of the most popular methods, now recognized as an effective, efficient and economic technology for water decontamination. The adsorbents may be of mineral, organic or biological origin: activated carbons, [5] [6] [7] [8] agricultural wastes, [9] biomass, [10] carbon nanotubes, [11] activated zeolites [12] and crosslinked polymers [13] are relevant examples. Cross-linked polymers able to absorb large amounts of water are commonly referred to as hydrogels. They are devoted increasing attention thanks to their unique properties such as, for example, high permeability to metabolites, hydrophilicity and consistency. Among the numerous molecules employed for the preparation of hydrogels, carbohydrates represent an important family thanks to their biocompatibility, nontoxicity and biodegradability. [14] CDs, torus-shaped cyclic oligosaccharides containing six to twelve glucose units connected by α-1,4-glycosidic bond, are well known for their ability to form inclusion compounds with various organic molecules thanks to their hydrophobic cavities which act as ideal binding sites. [15] [16] The smallest ones, α-, β and γ-CD, are also commercially available. Various CD and CD-containing polymers were prepared either immobilised on water-insoluble supports or as crosslinked materials, mainly employing β-CD which is the cheapest of the three. [14] [17] [18] [19] [20] [21] [22] [23] [24] After 1998, when the term was first used by Li and Ma, [25] [26] materials in which CD units are linked by many short moieties are commonly referred to as nanosponges. Nanosponges represent supermolecular structures in which CD units are connected by nanochannels forming a cage-like architecture. [27] [28] [29] They are nanoporous by definition and [26] [30] [31] are usually obtained from β-CD using different crosslinking agents, e.g.,

carbonyldimiidazole, triphosgene, diphenyl carbonate, or organic dianhydrides, [27] all normally demanding organic solvents. To date, only relatively few examples of α- and γ-CD nanosponges, characterized by different dimensional selectivity, are reported. [32]

Methacrylic acid (MA) is an important monomer widely used for the preparation of hydrogels. With its incorporation into the network, hydrogels can find numerous applications in various fields such as, for example, water treatment and removal of heavy metal ions. [33] [34] [35]

Poly(amidoamine)s (PAAs) are a family of biodegradable, biocompatible and environmental friendly synthetic polymers prepared in aqueous solution, at room temperature and with no added catalysts or organic solvents. [36] Crosslinked PAAs are prepared either using multifunctional amines as crosslinking agents or by radically polymerizing acrylamide end-capped PAA oligomers, pre-synthesized employing a controlled excess of bisacrylamide. PAAs are normally highly hydrophilic and, when crosslinked, give rise to hydrogels in aqueous media. [37] [36] [38] [39] [40] One of the synthetic strategies employed for the preparation of hydrogels with carbohydrates consists in the chemical grafting of vinylic monomers such as for example acrylonitrile, acrylic and methacrylic acid onto polysaccharides using various initiating systems and in the presence of a crosslinker. Following this method many cross-linked products were prepared from, for example, cellulose, chitosan and starch. [41] [42] Grafting onto carbohydrates is achieved growing a polymer chain on the active sites of the polysaccharide backbone. The radical copolymerization can start either on the carbohydrate active sites or on the monomer to be grafted and, in the latter case, the result is homopolymerization. [43] If CDs react with MA via free radical graft polymerization and a crosslinker such as an acrylamide end-capped PAA oligomer is added, novel insoluble nanosponges can be obtained. Moreover, these insoluble products can be easily separated from the solvent after use, providing ample possibilities for environmental applications and therapeutics.

To our knowledge, so far there is no report of nanosponges consisting of PAA, MA and CD. In this chapter, a series of PAA-MA-CD nanosponges was designed and synthesized in aqueous solution via crosslinking graft polymerization of MA onto either α- or β-CD in the presence of PAAs as crosslinkers. Structure and properties of the insoluble materials were determined by Fourier-transform infrared spectroscopy (FTIR), elemental analysis, differential scanning calorimetry (DSC) and thermogravimetric analysis (TGA). Moreover, with the aim of a potential application in the environmental field, preliminary

results on the sorption of CVOC from their aqueous solutions such as chloroform, halothane, and tetrachloroethylene are also reported.

Experimental

Materials

Solvents and reagents, unless otherwise indicated, were analytical-grade commercial products and were used as received. α-cyclodextrin (89.5%) was purchased from Alfa Aesar and β-cyclodextrin (95%) from Fluka. Methylenebisacrylamide (MBA) (96%) was obtained from Acros Organics. N,N'-2-methylpiperazine (MP) (95%), methacrylic acid (MA) (99%), NaOH (98.5%), $LiOH•H_2O$ (99%), $Na_2S_2O_5$ (99%),$Na_2S_2O_8$ (99%), ethanol (>99.8%) were supplied by Sigma Aldrich.

Methods

NMR. ^{1}H and ^{13}C NMR spectra of PAA oligomers were obtained using a Bruker Avance DPX-400 NMR operating respectively at 400.13 MHz and 100.40 MHz in D_2O.

Molecular weight. PAA oligomer size exclusion chromatography (SEC) traces were obtained with Toso-Haas TSK-gel G4000 PW and TSK-gel G3000 PW columns connected in series using a Waters model 515 HPLC pump equipped with a Knauer autosampler 3800, a light scattering and viscometer Viscotek 270 dual detector, a UV detector Waters model 486 operating at 230 nm and a refractive index detector (Waters, Model 2410). The mobile phase was a 0.1 M Tris buffer (pH 8.00 ± 0.05) with 0.2 M sodium chloride. The flow rate was 1 mL min^{-1} and the sample concentration was 1% ($^{w}/_{w}$).

FTIR analysis. The nanosponges were dried under vacuum to constant weight and the FTIR spectra were collected using a Perkin Elmer 100 spectrometer. All spectra were calculated as means of 16 individual scans at 2 cm^{-1} resolution in the 4000-600 cm^{-1} interval with corrections for atmospheric water and carbon dioxide.

Swelling degrees. The swelling degrees were evaluated in deionized H_2O and in 0.01 M PBS. Each nanosponge was weighted in a 10 ml test tube and suspended in an excess of ethanol. It was allowed to settle, the supernatant was carefully removed and replaced with either H_2O or 0.01 M PBS. The solvent was then changed three times so as to remove any

ethanol traces. The swelling degrees were evaluated at equilibrium according to the following equation:

$$SD\ (\%) = \frac{V_t}{V_{to}}\ x\ 100 \qquad (1)$$

where V_t is the volume of the nanosponge at equilibrium and V_{to} is the volume of the sample in ethanol.

Thermal analyses. DSC analyses were performed on a Mettler Toledo DSC823^e on 10 mg samples, under nitrogen flow at 20 mL min^{-1}, heating/cooling rate of 20 °C min^{-1}. Standard aluminium sample pans (Perkin-Elmer) were used and an empty pan was used as reference standard. A first heating cycle from 25 °C to 200 °C was followed by a cooling cycle from 200 °C to 25 °C and a second heating cycle from 25 °C to 200 °C. TG analyses were performed on a Perkin Elmer TGA 4000 on 10 mg samples under nitrogen flow at 50 mL min^{-1}, from 30 °C to 600 °C at a heating rate of 20 °C min^{-1}.

Absorption experiments. The experiments were carried out by an Autolab PGSTAT 12 or 128 potentiostat manufactured by EcoChemie, The Netherlands, with a General Purpose Electrochemical System software. The voltammetric cell was conical (20-50 cm^3 operating volume), including an AMEL disk working electrode made of glassy carbon (non catalytic reference, 0.071 cm^2) or silver (0.071 cm^2), a platinum wire as the counter electrode, an aqueous saturated calomel electrode (SCE, filled with a saturated Trace Select® KCl solution), as the reference electrode. To avoid leakage of chloride anions in the working solution, the electrode was inserted in a compartment with a porous sept filled with a 1 M KNO_3 aqueous solution, or with an aliquot of the working solution.

The working cell was thoroughly cleaned with nitric acid and ultrapure water before each experiment. The working electrode surface was cleaned with synthetic diamond powder (Aldrich, diameter 1 µm) on a wet Struers DP Nap cloth.

The background solution was H_2O (MilliQ® Millipore) with 0.1 M KNO_3 (ultrapure Fluka) as the supporting electrolyte.

The organohalide molecules studied were chloroform (≥ 99% Aldrich), tetrachloroethylene (≥ 99.9% Aldrich), chloroacetonitrile (> 99% Aldrich), halothane (≥ 99% Aldrich), benzyl chloride (> 99.5% Aldrich). Absorptions kinetics were observed *in situ* by square wave voltammetry SWV monitoring the corresponding voltammetric peak currents, proportional to the organohalide concentration in solution, on a working hanging

mercury drop electrode (HDME). [44]

In each experiment, after recording the voltammetric pattern of the buffer background solution (50 cm^3) previously deaerated by nitrogen bubbling, the organohalide was added so as to have a 10^{-3} M concentration in solution. Oxygen entrance was prevented and the organohalide reduction peak monitored until it was constant. Either the PAA-MA-CD resin (100 mg) or the soluble cyclodextrins (100 mg) were then added and SWV voltammograms recorded as a function of time until complete disappearance of the signal or for a time span sufficient for the kinetic study. Parameters for SWV analysis were as follows: stirrer 2000 rpm, purge time 10 s, purge amplitude 0.05 V, equilibration time 3 s, start potential 0.05 V, end potential -1.25 V, voltage step 0.006 V, and frequency 20 V s^{-1}.

Synthesis of MBAMP oligomer. MBA (7.76 g; 49.82 mmol) and MP (3.56 g; 34.87 mmol) were mixed in water (16.61 mL) and maintained at 40 °C, in the dark, under stirring. The mixture, which turned into a clear solution after 12 hours, was allowed reacting for totally 72 hours, then diluted with H_2O (150 mL) and freeze-dried. The final product was recovered as a white powder. Yield: 11.3 g, 99.8%. ^{1}H NMR (D_2O, 400.13 MHz, 298 K): δ (ppm) 6.14 (br, H1), 5.69 (br, H2), 4.62-4.44 (H4, H4'), 2.96-1.75 (br, -MP ring and -CH_2- polymer chain), 0.94 (br, H10). ^{13}C NMR (D_2O, 100.40 MHz, 298 K): δ (ppm) 175.19 (C15,C17), 168.61 (C3,C5), 129.50 (C2), 128.21 (C1), 58.61 (C8), 53.61 (C9), 52.90 (C11), 51.45 (C12), 49.76 (C13), 48.20 (C7), 44.24 (C4), 32.27 (C14), 30.76 (C6), 15.84 (C10). SEC: $\bar{M}_n$=4370, PDI=1.00. See Figure 30 for NMR assignment.

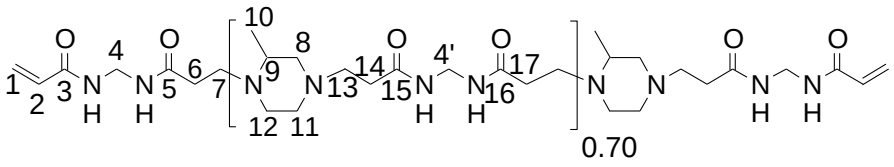

Figure 30. MBAMP atom labeling for NMR assignment.

Synthesis of PAA-MA-CD nanosponges. In a typical procedure, alpha2 was prepared by dissolving αCD (2137.59 mg; 1.97 mmol) and LiOH•H_2O (333.35 mg; 7.86 mmol) in H_2O (3 mL), in the dark and under nitrogen. MA (341.85 mg; 3.93 mmol) followed by MBAMP (327 mg; 0.44 acrylamide bonds mmol) were added and the polymerization initiated by $Na_2S_2O_5$ and $Na_2S_2O_8$ (each 0.5 mg/μL aqueous solutions, 1% $^w/_w$). After 24 hours at room temperature the nanosponge was soaked in deionized H_2O (100 mL)

followed by ethanol (100 mL). Three H_2O/ethanol washing cycles were carried out within for 48 hours and the product was then dried until constant weight. Yield: 1.47 g, 82.30%.

Nanosponges alpha4, alpha6, beta2, beta4 and beta9 were prepared following the same procedure described for alpha2 employing monomers and amounts listed here below. As redox initiator $Na_2S_2O_5$ and $Na_2S_2O_8$ 0.5 mg/μL aqueous solutions were used (1% $^{w}/_{w}$).

Alpha4: MBAMP oligomer (511.5 mg; 0.69 acrylamide bonds mmol), MA (489.82 mg; 5.63 mmol), LiOH•H_2O (477.64 mg; 11.27 mmol), αCD (1531.43 mg; 1.41 mmol), H_2O (3 mL). Yield: 1.30 g, 81.40%.

Alpha6: MBAMP oligomer (301.2 mg; 0.40 acrylamide bonds mmol), MA (647.36 mg; 7.45 mmol), LiOH•H_2O (631.27 mg; 14.89 mmol), αCD (1349.34 mg; 1.24 mmol), H_2O (3 mL). Yield: 1.26 g, 84.80%.

Beta2: MBAMP oligomer (267.2 mg; 0.36 acrylamide bonds mmol), MA (271.90 mg; 3.13 mmol), LiOH•H_2O (265.13 mg; 6.26 mmol), βCD (1868.44 mg; 1.56 mmol), H_2O (2.7 mL). Yield: 1.28 g, 83%.

Beta4: MBAMP oligomer (2000.3 mg; 2.68 acrylamide bonds mmol), MA (1793.23 mg; 20.63 mmol), LiOH•H_2O (1748.64 mg; 41.26 mmol), βCD (6161.43 mg; 5.16 mmol), H_2O (12 mL). Yield: 5.35 g, 83.70%.

Beta9: MBAMP oligomer (165.3 mg; 0.22 acrylamide bonds mmol), MA (399.70 mg; 4.60 mmol), LiOH•H_2O (389.60 mg; 9.20 mmol), βCD (610.38 mg; 0.51 mmol), H_2O (1.6 mL). Yield: 0.61 g, 82.10%.

Results and discussion

In this chapter, the feasibility of preparing cyclodextrin-containing nanosponges by free radical graft polymerization of either α- or β-cyclodextrin (CD) with methacrylic acid (MA) in the presence of a polyamidoamine (PAA) as crosslinker was demonstrated. A series of PAA-MA-CD nanosponges was synthesized employing various PAA/MA/CD ratios (Table 13). MA was grafted onto either α- or β-CD in water at pH≈12, using $Na_2S_2O_5$/$Na_2S_2O_8$ as a redox couple and MBAMP, a PAA oligomer pre-synthesized by polyaddition of the cheap N,N'-methylenebisacrylamide with 2-methylpiperazine (Scheme 16), was employed as a crosslinker. The mechanism proposed for the copolymerization of MA in the presence of CD and MBAMP is reported in Scheme 17. It

is known for many polysaccharides that the radicals resulting from the radical initiator generate active centers on the substrate abstracting hydrogens from the hydroxyl groups to form alkoxy radicals. These active centers radically initiate the polymerization of MA. Since a crosslinking agent, *e. g.* MBAMP, is present in the system, the final product is a nanosponge. The redox couple may initiate also MA homopolymerization increasing the soluble content of the nanosponges that for PAA-MA-CD nanosponges was around 20% (see Experimental part), apparently due to the loss of uncrosslinked MA. However, a contemporary loss of either CD and PAA cannot be excluded. Since the radical polymerization was carried out under basic conditions (~pH 11) it is possible that also the Michael addition of the alkoxide ions deriving from the dissociation of -OH groups with the acrylamide terminals of PAAs took place. [45]

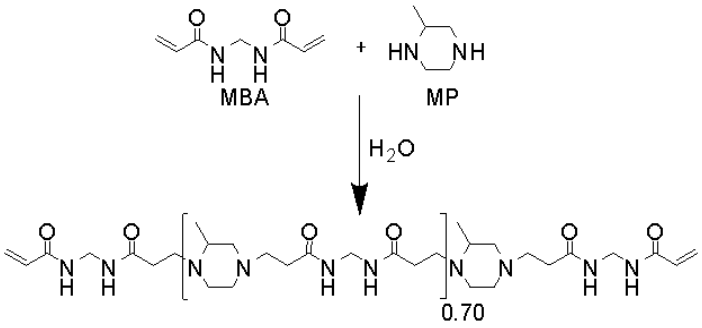

Scheme 16. Synthesis of MBAMP oligomer.

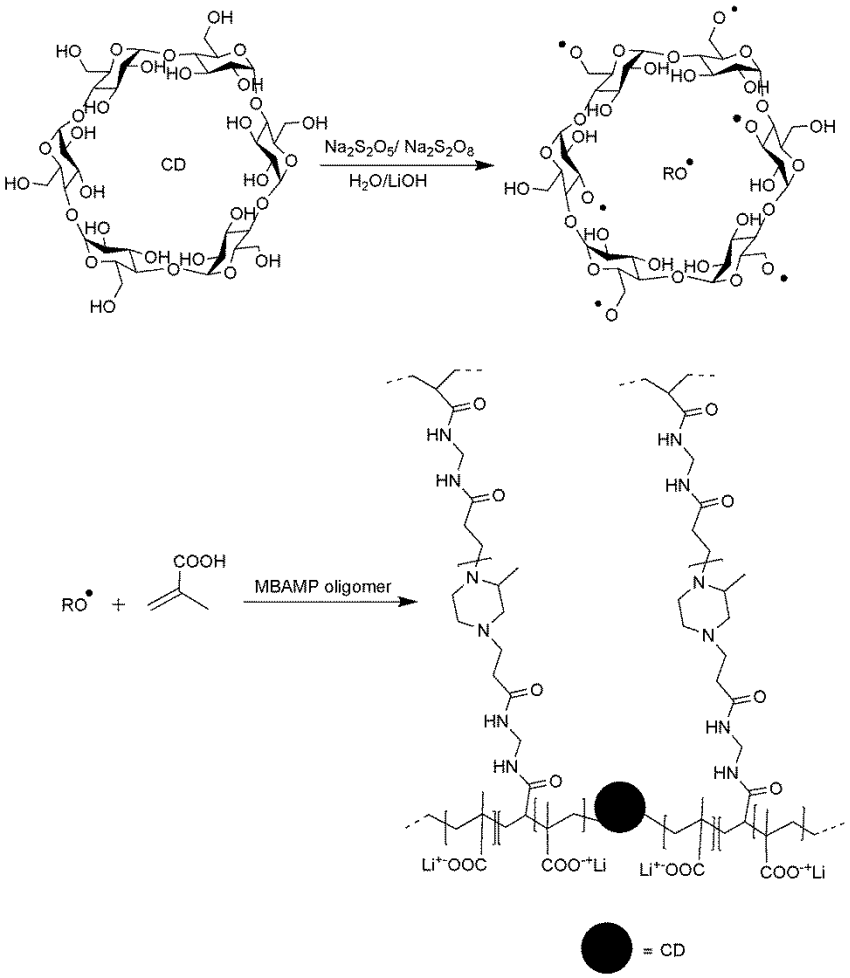

Scheme 17. General mechanism for radical graft polymerization of MA onto CD in the presence of MBAMP.

Table 13. Amounts of reagents used for the syntheses of PAA-MA-CD nanosponges.

Sample	**CD/MA/PAA acrylamide terminals [molar ratio]**	**CD content[a] [%^{w}/$_w$]**	**MA content [%^{w}/$_w$]**	**PAA content[a] [%^{w}/$_w$]**
Alpha2	1/2/0.22	76.17	12.18	11.65
Alpha4	1/4/0.49	60.47	19.34	20.20
Alpha6	1/6/0.33	58.72	28.17	13.11
Beta2	1/2/0.23	77.61	11.29	11.10
Beta4	1/4/0.52	61.89	18.01	20.09
Beta9	1/9/0.43	51.93	34.01	14.06

All nanosponge samples, irrespective of the synthetic pathway adopted, were purified by extensive washing with water/ethanol cycles, dried and analyzed by elemental analysis (Table 14). The C/N ratio values were always higher than that of the reference homopolymeric PAA nanosponge MBAMP, consistent with the presence of polyMA and CD in the nanosponge structure. Moreover, the found C/N ratio values were in all cases lower than the expected ones, indicating a preferential release of linear polyMA and CD in the extraction process. The N% values allowed for the calculation of the PAA content in the nanosponges and to compare it with feed data (Table 14).

Table 14. Results of the elemental analysis of PAA-MA-CD nanosponges.

Sample	**C%**		**N %**		**C/N**		**PAA**[a] **[%$^{w}/_{w}$]**	
	calc.[b]	found	calc.	found	calc.	found	feed[b]	found[c]
MBAMP	56.10	50.59	21.19	19.74	2.65	2.56	100	96.6
Alpha2	46.68	38.81	2.50	5.65	18.67	6.87	11.65	28.62
Alpha4	48.07	40.61	4.27	6.33	11.26	6.42	20.20	32.07
Alpha6	48.66	39.98	2.77	3.04	17.57	13.15	13.11	15.40
Beta2	46.44	46.85	2.28	6.94	20.37	6.75	11.10	35.16
Beta4	47.79	47.42	4.10	6.4	11.66	7.41	20.09	32.42
Beta9	49.24	50.18	2.86	4.82	17.22	10.41	14.06	24.42

[a] Theoretical molar composition of 100 g of product, [b] feeding data from Table 13.

The structural characterization of the synthesized nanosponges was performed by FTIR spectrophotometry (Figure 31).

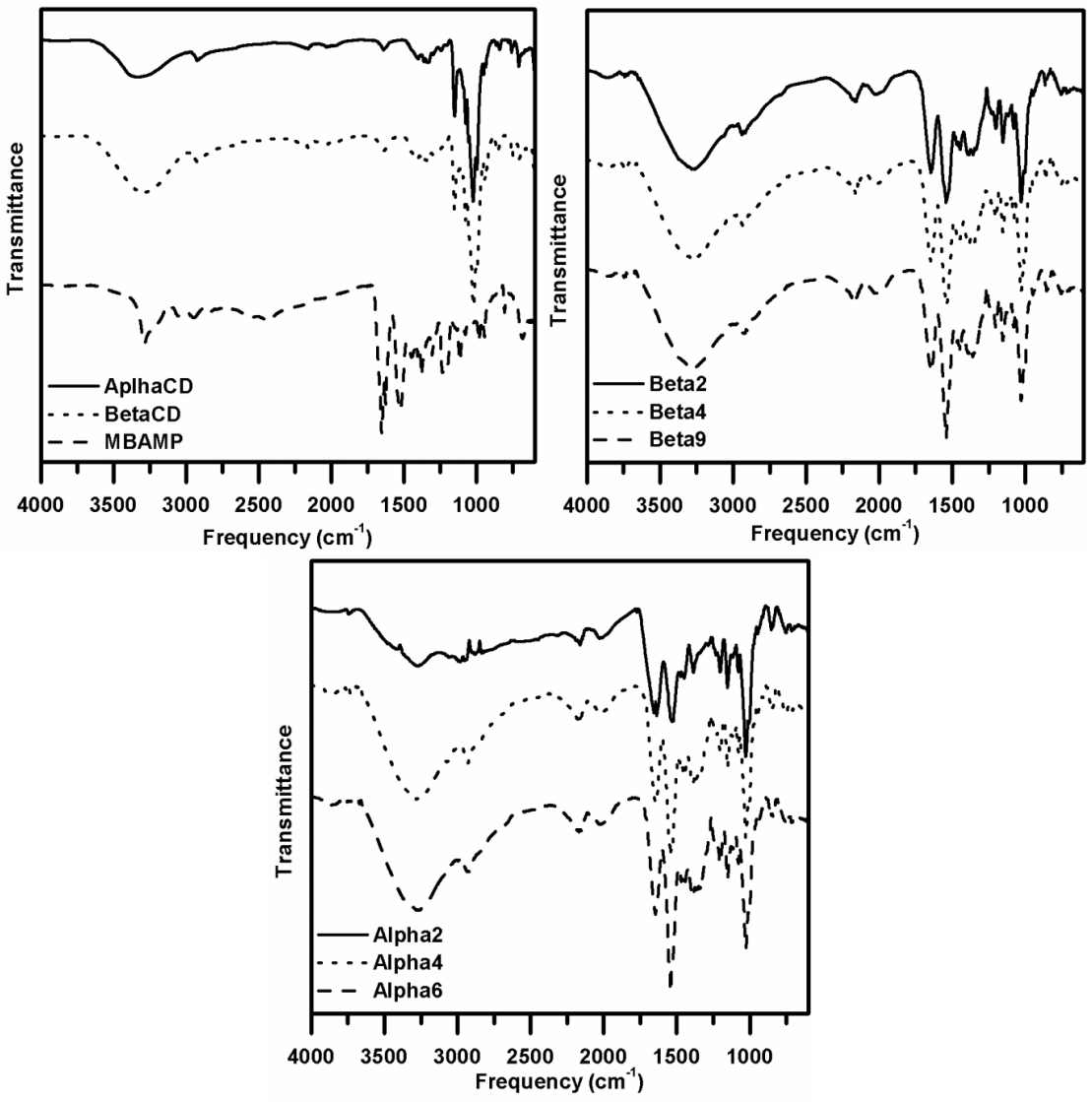

Figure 31. FTIR spectra for MBAMP and CD, PAA-MA-CD nanosponges containing αCD and PAA-MA-CD nanosponges containing βCD.

For CDs, O-H stretching vibration and in-plane bending vibration are observed at 3260 cm^{-1} and 1640 cm^{-1}, respectively. Absorption at 2925 cm^{-1} is attributable to the -CH_2- stretching vibration while C-O-C asymmetrical stretching vibration is visible at 1020 cm^{-1}.

For MBAMP, N-H stretching vibrations are visible at 3290 cm^{-1}, C=O amides stretching vibrations are detectable at 1654 cm^{-1}, NH bending at 1525 cm^{-1} and 3000 cm^{-1} while -CH_2- stretching vibrations are visible at 2950 cm^{-1}.

For PAA-MA-CD nanosponges peaks belonging to both CD, MA and MBAMP were visible. The absorption at 3260 cm^{-1} is attributable to the N–H and O–H stretching vibration. The peaks at 2920 and 1446 cm^{-1} are ascribed to the -CH_2- stretching vibration

and in-plane bending vibration, respectively. The peak at 1646 cm^{-1} is attributable to NH and C=O stretching vibration of amide units, to the stretching vibration of C=O from polyMA, and -OH in-plane bending vibration of CD units in the polymer. The peak at 1542 cm^{-1} can be assigned to the NH bending vibration of the amide units and it is overlapped with that of COO^- asymmetrical stretching. The intensities of these last two peaks increase from alpha2 to alpha9 and from beta2 to beta9, in accordance with the higher amount of MA in the reaction feed. The peak at 1029 cm^{-1} relates to C-O-C asymmetrical stretching vibration of CDs. Thus, all of the typical absorption peaks of both CD, polyMA and MBAMP are present in the spectra of the final products indicating that PAA-MA-CD nanosponges were successfully synthesized.

All nanosponges were thermally characterized by means of DSC and TGA analyses. The DSC second run heating cycle, following a cooling cycle carried out at the same rate, is reported in Figure 32. All of the samples showed weak endothermic peaks at 115 °C due to the loss of residual water and no evidence of glass transition temperatures or melting phenomena. A substantial thermal stability was observed in the temperature range investigated, with no dramatic decomposition events up to 200 °C.

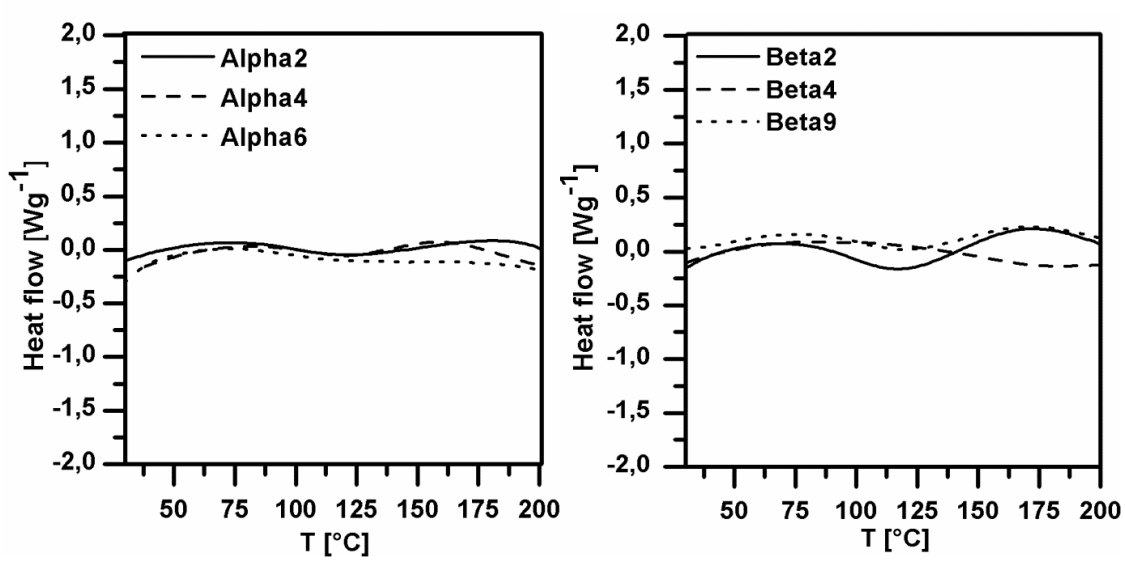

Figure 32. DSC second run curves for PAA-MA-CD nanosponges.

The thermal behaviors of PAA-MA-CD nanosponges were confirmed by thermogravimetric analysis (Figure 33). Their thermogravimetric pattern contrasted with those of the parent α- and β-CD that exhibit almost superimposable thermograms, showing thermal decomposition above 250 °C. [46] The thermogravimetric patterns of PAA-MA-CD nanosponges showed an initial loss of weight at 100 °C due to dehydration

and main thermal decompositions in the range 200-500 °C, with residual weights down to 10.1%. In general, nanosponges containing β-CD appeared more thermally stable than those prepared with α-CD showing lower weight losses in the temperature range investigated (Table 15). These results revealed that all of the samples were stable at temperatures up to 200 °C.

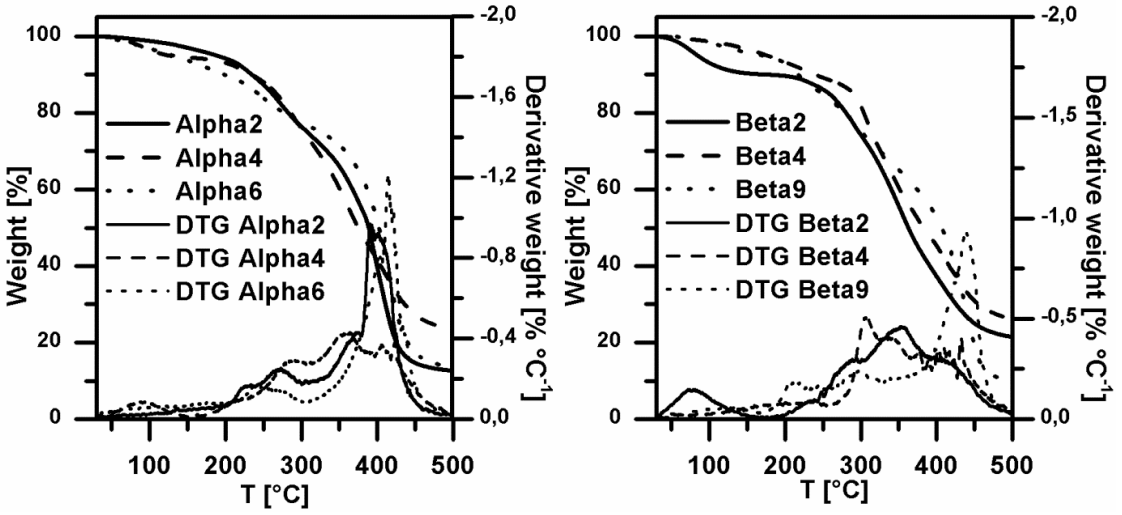

Figure 33. TG and DTG curves for PAA-MA-CD nanosponges.

Table 15. Results of the TG analyses. T_{max} represents the temperature of the highest weight loss rate.

Sample	**Dehydration (T=100 °C)**	**Main decomposition stage**		**Residual weight at 500 °C [%]**
	Weight loss [%]	T_{max} [°C]	Weight loss [%]	
Alpha2	1.23	393.1	81.6	12.6
Alpha4	3.55	362.3	69.4	23.6
Alpha6	3.24	411.9	76.2	13.6
Beta2	6.96	354.1	68.2	21.4
Beta4	1.36	306.2	67.1	26.1
Beta9	1.68	437.1	82.8	10.1

The swelling degree is a very important parameter that describes the amount of water retained by nanosponges. PAA-MA-CD nanosponges containing α-CD showed higher swelling in aqueous media than those containing β-CD (Figure 34). This behavior might

be ascribed to the fact that β-CD is characterized by a more rigid structure than α-CD. [47] In general, the swelling degrees were lower at higher MBAMP contents because MBAMP acts as crosslinking agent, giving tighter networks when present in larger amounts.

The swelling degrees of PAA-MA-CD nanosponges in PBS were lower than in water, indicating a shrinkage of the network when exposed to electrolyte solutions with counterions. It is known that an osmotic pressure difference exists between internal and external solutions of the gel network in aqueous solutions. [48] [49] In the presence of external ions, the ratio of ions between the interior of the nanosponge and the surrounding environment decreases and, for PAA-MA-CD nanosponges, the interactions of polyMA COO^- with external ions became more significant than the electrostatic repulsion of COO- within the network. Moreover, the presence of electrostatic interactions between COO^- and amine nitrogens of MBAMP cannot be excluded. As a consequence, the osmotic pressure difference decreases and results in a shrinkage of the network in PBS. [48] [50]

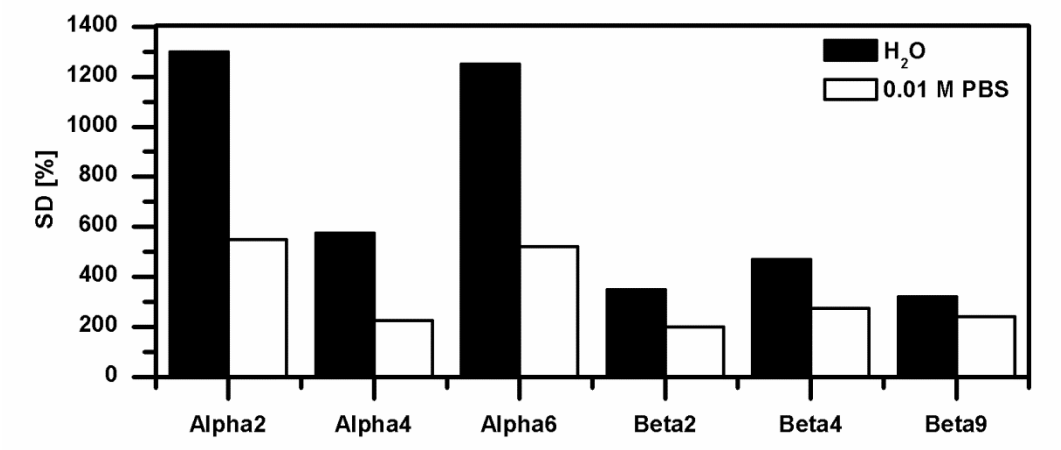

Figure 34. Swelling behavior of PAA-MA-CD nanosponges of different compositions. The percentage swelling degrees are reported on y-axis in water and 0.01M PBS.

One of potential applications of PAA-MA-CD nanosponges is the sorption of micropollutants from water, especially drinking water. Hydrocarbons, in particular halogenated compounds, are among the subjects of increasingly stringent restrictions concerning the organic content in drinkable water. These compounds are the products of many industrial processes and occur in traces in industrial waste water therefore it would be advantageous to have sorbents able to eliminate them. To this purpose, preliminary studies were carried out for investigating the absorption performance of PAA-MA-CD

nanosponges on chloroform, halothane and tetrachloroethylene. The results were obtained by *in situ* monitoring via SWV on the HDME from 10^{-5} M solutions (see for example Figure 35). The absorption kinetics were found for most cases to fit a pseudosecond-order model, implying the following:

$$\frac{dq_t}{dt} = -k_2(q_e - q_t)^2 \qquad (1)$$

where q_t is the absorption capacity of the metal ion at time t (in mmol g^{-1}), q_e the same quantity at the equilibrium (in our case, at SWV peak current practically constant and at t $\geq$ 10 $t_{1/2}$ ($t_{1/2}$ = halving time), while k_2 is the pseudosecond-order constant in g $mmol^{-1}$ s^{-1} or g $mmol^{-1}$ min^{-1}. Rearranging and integrating, eq 1 gives the following:

$$\frac{t}{q_t} = \frac{1}{q_e^2 k_2} + \frac{1}{q_e}t \qquad (2)$$

that can be used for linearization of the kinetic characteristics. According to (2), the halving time is:

$$t_{1/2} = 1/(q_e k_2) \qquad (3)$$

Table 16 and Figure 36 summarize the results of the kinetic studies.

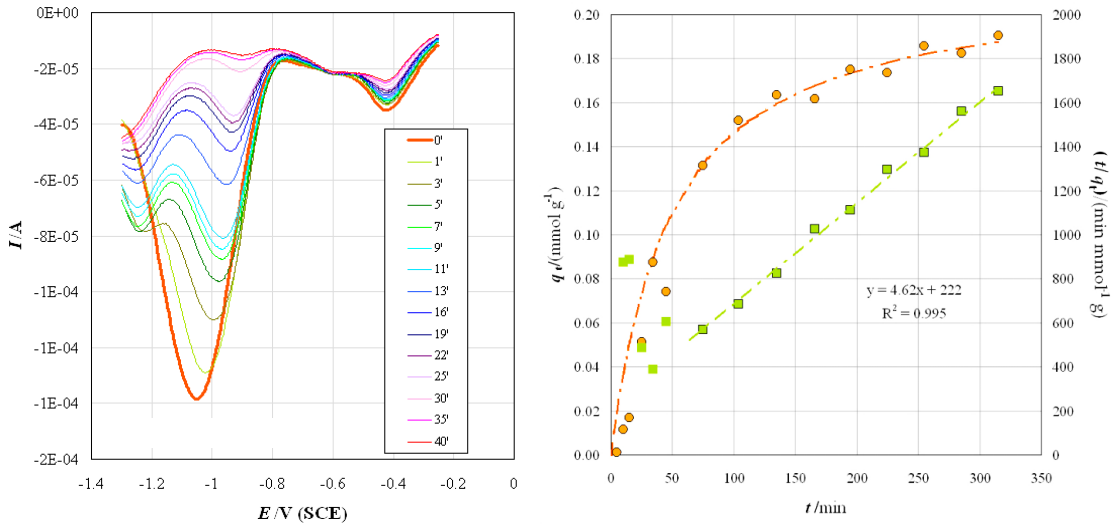

Figure 35. (a) *in situ* SWV monitoring of $CHCl_3$ absorption from 10^{-3} M solution by Beta4 nanosponge; (b) fitting the same kinetics according to the pseudo-second order model: experimental q_t values (circles: experimental points; line: predicted curve).

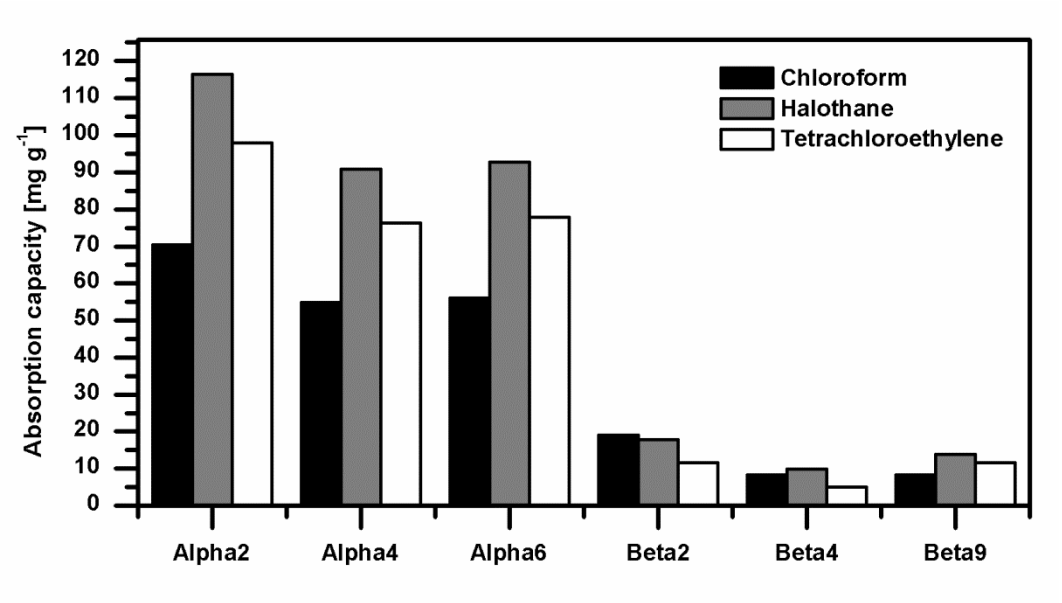

Figure 36. Absorption capacities in mg g^{-1} of PAA-MA-CD nanosponges.

Table 16. Experimental q_e [mmol g^{-1}] and q_e [mg g^{-1}], k_2 [g $mmol^{-1}$ min^{-1}] and $t_{1/2}$ [min] values and kinetic parameters for the absorptions of chloroform, halothane and tetrachloroethylene from 10^{-3} M aqueous solutions by PAA-MA-CD nanosponges based on the pseudo-second-order kinetic model.

Sample	**Chloroform**				**Halothane**				**Tetrachloroethylene**			
	q_e [mmol g^{-1}]	q_e [mg g^{-1}]	k_2	$t_{1/2}$	q_e [mmol g^{-1}]	q_e [mg g^{-1}]	k_2	$t_{1/2}$	q_e [mmol g^{-1}]	q_e [mg g^{-1}]	k_2	$t_{1/2}$
αCD	2.16 x 10^{-4}	0.03	1.85 x 10^{3}	2.5	2.57 x 10^{-4}	0.05	1.11 x 10^{3}	3.5	2.67 x 10^{-4}	0.04	98.5	38
βCD	1.41 x 10^{-4}	0.02	7.09 x 10^{2}	10	9.69 x 10^{-5}	0.02	2.72 x 10^{2}	38	1.59 x 10^{-4}	0.03	1.91 x 10^{2}	33
Alpha2	0.59	70.43	8.47 x 10^{-2}	20	0.59	116.45	1.69	1	0.59	97.84	8.47 x 10^{-2}	20
Alpha4	0.46	54.91	2.17 x 10^{-1}	10	0.46	90.80	2.17	1	0.46	76.28	8.70 x 10^{-2}	25
Alpha6	0.47	56.11	2.13 x 10^{-1}	10	0.47	92.77	2.13	1	0.47	77.94	2.13 x 10^{-1}	10
Beta2	0.16	19.10	1.04 x 10^{-1}	60	0.09	17.76	2.47 x 10^{-1}	45	0.07	11.61	3.17 x 10^{-1}	45
Beta4	0.07	8.36	2.38 x 10^{-1}	60	0.05	9.87	20	1	0.03	4.97	1.52	22
Beta9	0.07	8.36	2.38 x 10^{-1}	60	0.07	13.82	14.3	1	0.07	11.61	1.59	9

The sorption capacities of PAA-MA-CD nanosponges were compared to those of soluble α and β-CD. Both α and β-CD were able to form inclusion complexes with all of the organic molecules. In general, α-CD showed higher and faster absorption than β-CD. This is in agreement with the dimensions of the species adopted as a benchmark that better fit α-CD cavity, smaller than that of β-CD. Regarding PAA-MA-CD nanosponges, those containing α-CD (alpha2, alpha4, alpha6) showed much higher absorption capacities than those containing β-CD (beta2, beta4, beta9) towards the chosen pollutants. Moreover, nanosponges prepared using maximum amounts of CDs in the feed (alpha2 and beta2), showed the highest absorption capacities within their own series. Furthermore, the sorption capacities of PAA-MA-CD nanosponges were up to 2 x 10^3 times higher than those of the parent CDs and competitive with other materials employed to the same purpose. [51] [52] Due to the large amounts of sorbed pollutants, it is very likely that the organohalides molecules adopted as a benchmark were sorbed to a large extent into or onto PAA-MA-CD nanosponges also by other kinds of interactions than inclusion such as, for example, hydrogen bonding.

Conclusions

Crosslinking graft polymerization of methacrylic acid onto either α- and β-cyclodextrin in the presence of an acrylamide end-capped poly(amidoamine) oligomer was performed in aqueous medium, using the redox couple sodium persulphate/sodium metabisulfite as initiator. FTIR analyses indicated that PAA-MA-CD nanosponges were successfully synthesized. The crosslinked products were able to absorb up to 13 times their weight when swollen in water and higher amounts of PAA resulted in denser crosslinked networks with lower swelling degrees. Thermal analyses showed that the products were stable up to 200 °C, with weight loss mainly due to water evaporation entrapped within the polymer network. In preliminary sorption experiments PAA-MA-CD nanosponges exhibited sorption capacities toward chlorinated organic pollutants such as chloroform, halothane and tetrachloroethylene competitive with other materials employed to the same purpose. [51] [52] These findings offer new opportunities for the synthesis of more sophisticated CD-based (or PAA-based) materials with enhanced properties.

References

[1] D. T. Sponza, *Adv. Environ. Res.*, vol. 7, pp. 453-462, 2007.

[2] M. Vilve, S. Vilhunen, M. Vepsäläinen, T. A. Kurniawan, N. Lehtonen, H. Isomäki, M. Sillanpää, *Environ. Sci. Pollut. Res. Int.*, vol. 17, pp. 875-884, 2010.

[3] K. Everaert, J. Baeyens, *J. Hazard. Mater.*, vol. 109, pp. 113-139, 2004.

[4] X. Mao, A. Ciblak, K. Baek, M. Amiri, R. Loch-Caruso, A. N. Alshawabkeh, *Water Res.*, vol. 46, pp. 1847-1857, 2012.

[5] K. G. Babia, K. M. Koumenidesa, A. D. Nikolaoua, C. A. Makria, F. K. Tzoumerkasb, T. D. Lekkasa, *Desalination*, vol. 210, pp. 215-224, 2007.

[6] G. Heron, K. Parker, J. Galligan, T. C. Holmes, *Groundwater Monitoring & Remediation*, vol. 29, pp. 56-65, 2009.

[7] A. M. Morawski, R. Kalenczuk, M. Inagaki, *Desalination*, vol. 130, pp. 107-112, 2000.

[8] J.-J. Yu, S.-Y. Chou, *Chemosphere*, vol. 41, pp. 371-378, 2000.

[9] A. Adachi, S. Takagi, T. Okano, *Chemosphere*, vol. 46, pp. 87-92, 2002.

[10] I. Abe, T. Fukuhara, J. Maruyama, H. Tatsumoto, S. Iwasaki, *Carbon*, vol. 39, pp. 1069-1073, 2001.

[11] C. Lu, Y.-L. Chung, K.-F. Chang, *Water Res.*, vol. 39, pp. 1183-1189, 2005.

[12] R. López-Fonseca, B. de Rivas, J. I. Gutiérrez-Ortiz, A. Aranzabal, J. González-Velasco, *Appl. Cat. B-Environ.*, vol. 41, pp. 31-42, 2003.

[13] J.-W. Lee, H.-J. Jung, D.-H. Kwak, P.-G. Chung, *Water Res.*, vol. 39, pp. 617-629, 2005.

[14] G. Crini, *Prog. Polym. Sci.*, vol. 30, pp. 38-70, 2005.

[15] J. Szejtli, *Chem Rev.*, vol. 98, pp. 1743-1753, 1998.

[16] H. Dodziuk, Cyclodextrins, their complexes: chemistry, analytical methods, applications., Weinheim: wiley VCH, 2006.

[17] Y. Q. Fan, Y. Feng, L. S. Da, *Anal. Chem. Acta*, vol. 484, pp. 145-153, 2003.

[18] R. Allabashi, M. Arkas, G. Hormann, D. Tsiourvas, *Water Res.*, vol. 41, pp. 476-486, 2007.

[19] Í. X. García-Zubiri, G. González-Gaitano, J. R. Isasi, *J. Colloid Interf. Sci.*, vol. 307,

pp. 64-70, 2007.

[20] A. Romo, F. J. Penas, J. R. Isasi, I. X. Garciá-Zubiri, G. González-Gaitano, *React. Funct. Polym.,* vol. 68, pp. 406-413, 2008.

[21] J. C. Yua, Z. T. Jiang, H. Y. Liu, J. Yu, L. Zhang, *Anal. Chim. Acta,* vol. 477, pp. 93-101, 2003.

[22] G. Crini, S. Bertini, G. Torri, A. Naggi, D. Sforzini, C. Vecchi, L. Janus, Y. Lekchiri, M. Morcellet, *J. Polym. Sci. Part A: Polym. Chem.,* vol. 68, pp. 1973-1978, 1998.

[23] K. Salipira, B. Mamba, R. Krause, T. Malefetse, S. Durbach, "http://www.wrc.org.za," 1 January 2008. [Online].

[24] L. Janus, G. Crini, V. El-Rezzi, M. Morcellet, A. Cambiaghi, G. Torri, A. Naggi, C. Vecchi, *React. Funct. Polym.,* vol. 42, pp. 173-180, 1999.

[25] D. Li, M. Ma, "Cyclodextrin polymer separation materials.". Patent WO9822197, 28 May 1998.

[26] D. Li, M. Ma, *Clean Technol. Environ. Policy,* vol. 2, pp. 112-116, 2000.

[27] F. Trotta, "Cyclodextrin Nanosponges and Their Applications," in *Cyclodextrins in Pharmaceutics, Cosmetics and Biomedicine: Current and Future Industrial Applications*, Hoboken, NJ, USA, John Wiley & Sons, 2011, pp. 323-342.

[28] F. Trotta, M. Zanetti, R. Cavalli, *Beilstein J. Org. Chem.,* vol. 8, pp. 2091-2099, 2012.

[29] S. D. Mhlanga, B. B. Mamba, R. W. Krause, T. J. Malefetse, *J. Chem.Technol. Biot.,* vol. 82, pp. 382-388, 2007.

[30] S. Berto, M. C. Bruzzoniti, R. Cavalli, D. Perrachon, E. Prenesti, C. Sarzanini, F. Trotta, W. Tumiatti, *J. Incl. Phenom. Macrocyclic Chem.,* vol. 57, pp. 631-636, 2007.

[31] S. Berto, M. C. Bruzzoniti, R. Cavalli, D. Perachon, E. Prenesti, C. Sarzanini, F. Trotta, W. Tumiatti, *J. Incl. Phenom. Macrocyclic Chem.,* vol. 57, pp. 637-643, 2007.

[32] R. Cavalli, A. K. Akhter, A. Bisazza, P. Giustetto, F. Trotta, P. Vavia, *Int. J. Pharm.,* vol. 402, pp. 254-257, 2010.

[33] V. V. Panic, Z. P. Madzarevic, T. Volkov-Husovic, S. J. Velickovic, *Chem. Eng. J.,* vol. 217, pp. 192-204.

[34] N. B. Milosavljević, M. Đ. Ristić, A. A. Perić-Grujić, J. M. Filipović, S. B. Štrbac, Z. L. Rakočević, M. T. K. Krušić, *Colloid. Surface A,* vol. 388, pp. 59-69.

[35] Y. Qiu, K. Park, *Adv. Drug Deliver. Rev.,* vol. 64, pp. 49-60.

[36] P. Ferruti, *J. Polym. Sci. Part A. Polymer Chem.,* vol. 51, pp. 2319-2353, 2013.

[37] E. Ranucci, P. Ferruti, E. Lattanzio, A. Manfredi, M. Rossi, P. R. Mussini, F. Chiellini, C. Bartoli, *J. Polym. Sci. Part A: Polym. Chem.,* vol. 47, pp. 6977-6991, 2009.

[38] P. Ferruti, E. Ranucci, S. Bianchi, L. Falciola, P. R. Mussini, M. Rossi, "2006," *J. Polym. Sci. Part A: Polym. Chem.,* vol. 44, p. 2316–2327, 2006.

[39] P. Ferruti, E. Ranucci, A. Manfredi, N. Mauro, E. Ferrari, R. Bruni, F. Colombo, P. Mussini, M. Rossi, *J. Polym. Sci. Part A: Polym. Chem.,* vol. 50, pp. 5000-5010, 2012.

[40] A. Manfredi, E. Ranucci, S. Morandi, P. R. Mussini, P. Ferruti, *J. Polym. Sci. Part A: Polym. Chem.,* vol. 51, pp. 769-773, 2013.

[41] G. M. Patel, C. M. Patel, H. C. Trivedi, *Eur. Polym. J.,* vol. 35, pp. 201-209, 1999.

[42] R. E. Kirk, D. F. Othmer, in *Encyclopedia of Chemical Technology*, 4th ed., vol. 4, New York: John Wiley & Sons, Kroschwitz J. I., Howe-Grant M., 1992, p. 942.

[43] G. Gurdag, M. Yasar, M. A. Gurkaynak, *J. Appl. Polym. Sci.,* vol. 66, pp. 929-934, 1997.

[44] J. Wang, Analytical Electrochemistry, New Jersey: Wiley-VCH, 2006.

[45] S. Swaminathan, R. Cavalli, F. Trotta, P. Ferruti, E. Ranucci, I. Gerges, A. Manfredi, D. Marinotto, P. R. Vavia, *J. Incl. Phenom. Macrocycl. Chem.,* vol. 68, pp. 183-191, 2010.

[46] F. Giordano, C. Novak, J. R. Moyano, *Thermochim. Acta,* vol. 380, pp. 123-151, 2001.

[47] J. Szejtli, "Encyclopedia of Nanoscience, Nanotechnology," vol. 2, pp. 283-304.

[48] O. Okay, S. B. Sariisik, S. D. Zor, *J. Appl. Polym. Sci.,* vol. 70, pp. 567-575, 1998.

[49] C. Alvarez-Lorenzo, O. Guney, T. Oya, Y. Sakai, M. Kobayashi, T. Enoki, Y. Takeoka, T. Ishibashi, K. Kuroda, K. Tanaka, G. Wang, A. Yu, G. S. Masamune, T. Tanaka, *Macromolecules,* vol. 33, pp. 8693-8697, 2000.

[50] Y. Li, T. Tanaka, *Annu. Rev. Mater. Sci.,* vol. 22, pp. 243-277, 1992.

[51] I. Abe, T. Fukuhara, J. Maruyama, H. Tatsumoto, S. Iwasaki, *Carbon*, vol. 39, pp. 1069-1073, 2001.

[52] J.-H. Tsai, H.-M. Chiang, G.-Y. Huang, H.-L. Chiang, *J. Hazard. Mater.*, vol. 154, pp. 1183-1191, 2008.

CYCLODEXTRIN NANOSPONGES AS O-TOLUIDINE ABSORBENTS

Introduction

O-toluidine is an important organic intermediate used, *inter alia*, in the manufacture of dyestuffs, in the production of synthetic rubber, chemicals and pesticides, and also as a curing agent for epoxy resins. o-Toluidine is ubiquitous in the human environment, as a major component of tobacco smoke. [1] The release of o-toluidine occurring during its manufacturing and processing has produced increasing amounts of toluidine-containing wastewater that have been introduced into water bodies. Being it classified by the International Agency for Research on Cancer (IARC) as 'carcinogenic to humans' (group 1), [2] its efficient removal from water is required. Different technologies are currently available to efficiently remove o-toluidine from wastewater, including photodecomposition, [3]electrochemical treatment, [4] oxidation, [5] microbial digestion [6] and adsorption. Among them, adsorption is reckoned as one of the most attractive and effective purification techniques in wastewater treatment. In the case of anilines, including o-toluidine, different studies report on various adsorbents, such as for instance organo-clay, [7] [8]montmorillonite, [9] silica, [10] rubber tire, [11] zeolites, [12] activated carbon, which can be in granular, powder or fiber form [13] and polymeric adsorbents. [14] [15]

Cyclodextrins (CDs) are cyclic oligosaccharides formed by 6 (α-CD), 7 (β-CD) or 8 (γ-CD) glucopiranose units, well-known to possess a hydrophobic cavity with a remarkable ability to form inclusion complexes with organic molecules through host–guest interactions, and with a dimensional selectivity due to the different sizes of their inner cavity. [16] [17] [18]CD-containing polymers, either linear [19] or immobilized on solid supports [20] [21] [22] and crosslinked CD resins [23] [24] [25] [26] [27] [28] have been extensively studied as sorbents of organic pollutants with removal efficacy ranging within ample limits. [29]Since the late nineties, hyper-crosslinked CD in which CD units are linked by many short moieties, have commonly been referred to as nanosponges. [30] [31]Nanosponges represent supermolecular structures in which CD units are connected by nanochannel-forming channels, giving rise to cage-like architectures. [32] [33] [34] Nanosponges are nanoporous by definition and show very high inclusion constants with several organic pollutants, including aromatic and chlorinated compounds, [31] [35] [36] as well as aromatic amines. [37] Nanosponges are usually obtained from β-CD, the

cheapest CD on the market, and only relatively few examples of α- and γ-CD nanosponges, characterized by different dimensional selectivity, are reported. [38] Nanosponges can be obtained using different crosslinking agents, e.g., carbonyldimiidazole, triphosgene, diphenyl carbonate, or organic dianhydrides, all normally demanding organic solvents. Only recently, β-CD-based nanosponges were synthesized by means of a water-based process, consisting of the Michael-type polyaddition of α-CD, or a β-CD/2-methylpiperazine mixture, with 2,2-bis(acrylamido)acetic acid at pH >12. [39] Under these conditions, CD hydroxyls undergo addition reaction with bisacrylamides, acting as multifunctional monomers, in a way similar to the process at the base of poly(amidoamine) synthesis. [40] Following the same aqueous solution process, a small library of nanosponges were prepared by polyaddition of α-, β- and γ-CDs with 1,4-bis(acryloyl)piperazine, 2,2-bisacrylamidoacetic acid and a 2-methylpiperazine/2,2-bisacrylamidoacetic acid mixture, and their ability to selectively remove o-toluidine from water was investigated. O-toluidine sorption was monitored by Linear Sweep Voltammetry (LSV) on a multi-walled carbon nanotubes modified glassy carbon electrode. In fact, carbon-based electrodes showed very good performances for the determination of another similar compound, benzidine, and nanomaterials, in particular carbon nanotubes, were extensively used for the production of electroanalytical sensors. For these reasons, the use of carbon nanotubes for the detection of o-toluidine seemd to be the best choice. The aim of this paper is to report on these issues.

Experimental

Materials

Solvents and reagents, unless otherwise indicated, were analytical-grade commercial products and were used as received. α-CD (89.5%) was purchased from Alfa Aesar, β-CD (95%) from Fluka and γ-CD (97%) from ABCR. 2,2-bisacrylamidoacetic acid (BAC) and N,N'-bisacryloilpiperazine (BISPIP) were prepared as reported in literature. [41] [42] N,N'-2-methylpiperazine (MP) (95%), $LiOH•H_2O$ (99%), ethanol (>99.8%), methanol (99%) were supplied by Sigma Aldrich.

Methods

NMR. ^{1}H and ^{13}C NMR spectra of PAA oligomers were obtained using a Bruker Avance DPX-400 NMR operating respectively at 400.13 MHz and 100.40 MHz in D_2O.

Molecular weight. PAA oligomers size exclusion chromatography (SEC) traces were obtained with Toso-Haas TSK-gel G4000 PW and TSK-gel G3000 PW columns connected in series using a Waters model 515 HPLC pump equipped with a Knauer autosampler 3800, a light scattering and viscometer Viscotek 270 dual detector and a refractive index detector (Waters, Model 2410). The mobile phase was a 0.1 M Tris buffer (pH 8.00 ± 0.05) with 0.2 M sodium chloride. The flow rate was 1 mL min^{-1} and the sample concentration was 1% ($^{w}/_{w}$).

FTIR analysis. The nanosponges were dried under vacuum to constant weight and the FTIR spectra collected using a Perkin Elmer 100 spectrometer. All spectra were calculated means of 16 individual scans at 2 cm^{-1} resolution in the 4000-600 cm^{-1} interval with corrections for atmospheric water and carbon dioxide.

Thermal analyses. DSC analyses were performed on a Mettler Toledo DSC823^{e} on 10 mg samples, under nitrogen flow at 20 mL min^{-1}, heating/cooling rate of 20 °C min^{-1}. Standard aluminum sample pans (Perkin-Elmer) were used and an empty pan was used as reference standard. A first heating cycle from 25 °C to 200 °C was followed by a cooling cycle from 200 °C to 25 °C and a second heating cycle from 25 °C to 300 °C. TGA analyses were performed on a Perkin Elmer TGA 4000 on 10 mg samples under nitrogen flow at 50 mL min^{-1}, from 30 °C to 600 °C at a heating rate of 20 °C min^{-1}.

Swelling degrees. About 30 mg of finely ground dried sample were weighted in a 10 ml test tube and first suspended in ethanol (7 mL). The nanosponge was allowed to settle, the supernatant was carefully removed and replaced with either H_2O or 0.01 M PBS. The solvent was then changed three times so as to remove any ethanol traces. The swelling degree (SD) was evaluated at equilibrium according to the following equation:

$$SD\ (\%) = \frac{V_t}{V_{to}}\ x\ 100 \qquad \text{Eq. 1}$$

where V_t is the volume of the nanosponge at equilibrium and V_{to} is the volume of the dry sample.

O-toluidine absorption. The experiments were carried out using a potentiostat/galvanostat Autolab PG-Stat 12. The voltammetric cell was conical (5 cm^3 operating volume), including a Ag/AgCl electrode as reference, a Pt wire as counter and a multi-walled carbon nanotubes (MWCNT) modified glassy carbon electrode as working. The working electrode surface was initially cleaned with synthetic diamond powder (Aldrich, diameter 1 μm) on a wet Struers DP Nap cloth; subsequently 20 μL of 0.5 mg mL^{-1} MWCNT suspension in dymethylformamide were deposited on the glassy carbon electrode and dried at 25 °C until complete evaporation of the casting solvent.

The working cell was thoroughly cleaned with nitric acid and ultrapure water before each experiment.

The background solution was H_2O (MilliQ® Millipore) with 0.1 M HCl (ultrapure Fluka) as supporting electrolyte.

Absorptions kinetics were observed by LSV monitoring the corresponding voltammetric peak current, proportional to o-toluidine concentration in solution.

In each sorption kinetic, 0.6 mL of sorption solution were collected at different times. 0.6 mL of 0.2 M HCl were then added at each samples. Voltammograms were recorded registering the background and o-toluidine plots from the lowest concentration to the highest one. Peak heights were obtained after background subtraction. Parameters for SWV analysis were as follows: equilibration time 10 s, start potential + 0.6 V, end potential + 1.0 V, step potential 0.005 V, scan rate 0.01 V s^{-1}.

O-toluidine desorption. To recover and reuse the sorbent after o-toluidine absorption, CD nanosponges (30 mg) were soaked in MeOH 70% aqueous solution (20 ml) and shaken for 20 minutes. The nanosponges were then recovered, thoroughly rinsed with H_2O and reused for o-toluidine absorption. The absorption-desorption cycle was repeated twice.

Synthesis of ISA23 oligomer. BAC (5 g, 24.84 mmol) and LiOH•H_2O (1.05 g, 24.84 mmol) were dissolved in H_2O (8.35 mL) under magnetic stirring, in the dark and N_2 atmosphere. MP (1.85 g, 17.57 mmol) was added. The mixture turned into a clear solution after about 15 minutes and was allowed reacting for totally 72 hours, then diluted with H_2O (150 mL) and freeze-dried. The final product was recovered as a white powder. Yield: 99.8% (26.8 g). ^{1}H NMR (D_2O, 400.13 MHz, 298 K): δ (ppm) 6.16 (br, H1), 5.73 (br, H2), 3.41-2.54 (H6, H7, H13, H14, H17, H18 and CH_2 MP ring H4, H4'), 1.22 (br, H10). ^{13}C NMR (D_2O, 100.40 MHz, 298 K): δ (ppm) 173.08 (C19), 172.12 (C15,C16),

167.86 (C3,C5), 129.56 (C2), 128.39 (C1), 58.20 (C19), 55.94 (C9), 52.24 (C7, C13), 49.82, 48.97, 48.00 (CH_2 MP ring), 30.86 (C14, C17), 30.00 (C6), 14.22 (C10). (Figure 36a) SEC: $\bar{M}_n$=2000, PDI=1.45.

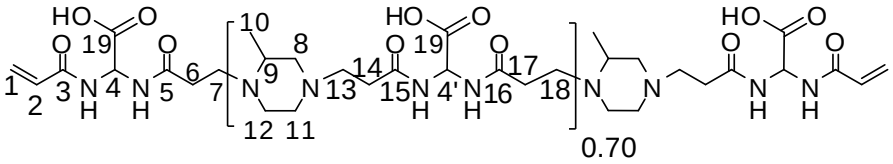

Figure 36a. Atom labeling for ISA23 oligomer.

Synthesis of ISA23 hydrogel. ISA23 oligomer (110 mg) was dissolved in H_2O (1 ml) under magnetic stirring, in the dark and N_2 atmosphere. $Na_2S_2O_5$ (2 µl of 0.33 mg/µl solution) and $Na_2S_2O_8$ (2 µl of 0.33 mg/µl solution) were added. The mixture turned into a soft hydrogels within 5 minutes and it was allowed to react for further 48 hours to complete the crosslinking reaction. The hydrogel was finely ground and purified by repeated water/ethanol extraction cycles. It was soaked in water (50 ml for 2 hours), the solvent was then hanged to ethanol (50 ml for 2 hours) and this extracting procedure was repeated three times. The extracted product was finally dried until constant weight. Yield: 61 % (67.1 mg).

Synthesis of ISA23-CD nanosponges. In a typical procedure, ISA23-βCD was prepared dissolving βCD (211.57 mg, 0.18 mmol) and LiOH•H_2O (22.7 mg, 0.54 mmol) in H_2O (0.16 mL) in a test tube. ISA23 (517.3 mg, 0.58 mmol double bonds) was dissolved in H_2O (0.37 mL) in a second test tube and the solution added to the first test tube under magnetic stirring. The mixture reacted at 25 °C for 24 hours. The final product appeared as a homogeneous, transparent and soft nanosponge, which was purified by repeated water/ethanol extraction cycles. The nanosponge sample was first soaked in deionized H_2O (50 mL) and allowed swelling for 2 hours, the pH was lowered to 5 with HCl 37% $^{w}/_{w}$ then the nanosponge was soaked in ethanol (50 mL) for 2 hours. This extracting procedure was repeated three times. The extracted product was finally dried until constant weight. Yield: 70.5% (513.85 mg).

ISA23-γCD was prepared following the same procedure described for ISA23-βCD. The monomers and reagents used and their amounts are reported below.

ISA23-γCD: γ-CD (205.36 mg, 0.15 mmol), LiOH•H_2O (20 mg, 0.47 mmol), H_2O (0.165 mL), ISA23 (465.4 mg, 0.52 mmol double bonds), H_2O (0.325 mL). Yield: 61.7% (670.76 mg).

Synthesis of BAC-CD and BISPIP-CD nanosponges. In a typical procedure, BAC-αCD was prepared dissolving α-CD (312.51 mg, 0.29 mmol) and LiOH•H_2O (35.7 mg, 0.84 mmol) in H_2O (0.16 mL) in a test tube. BAC (213.5 g, 1.06 mmol) and LiOH•H_2O (45 mg, 1.06 mmol) were dissolved in H_2O (0.18 mL) a second test tube then the solution was added to the first test tube under magnetic stirring. The mixture reacted at 25 °C for 24 hours. The final product appeared as a homogeneous, transparent and soft nanosponge, which was purified by repeated water/ethanol extraction cycles. The nanosponge sample was first soaked in deionized H_2O (50 mL) and allowed swelling for 2 hours, the pH was lowered to 5 with HCl 37% $^{w}/_{w}$ then the nanosponge as soaked in ethanol (50 mL) for 2 hours. This extracting procedure was repeated three times. The extracted product was finally dried until constant weight. Yield: 69% (526.01 mg).

BAC-βCD and BAC-γCD were prepared following the same procedure described for BAC-αCD. BISPIP-αCD, BISPIP-βCD and BISPIP-γCD were prepared following the same procedure described for BAC-αCD but BISPIP was dissolved in H_2O without adding LiOH•H_2O.

The monomers used and their amounts are reported here below.

BAC-βCD: β-CD (734.84 mg, 0.62 mmol), LiOH•H_2O (77.7 g, 1.83 mmol), H_2O (0.4 mL), BAC (377.3 g, 1.87 mmol), LiOH•H_2O (79.2 mg, 1.87 mmol), H_2O (0.3 mL). Yield: 76.2% (752.14 mg).

BAC-γCD: γ-CD (1030.52 mg, 0.77 mmol), LiOH•H_2O (158.4 mg, 3.74 mmol), H_2O (0.7 mL), BAC (384.8 mg, 1.92 mmol), LiOH•H_2O (81.5 mg, 1.92 mmol), H_2O (0.3 mL). Yield: 47.4% (1415.32 mg).

BISPIP-αCD: α-CD (312.74 g, 0.29 mmol), LiOH•H_2O (23.5 mg, 0.55 mmol), H_2O (0.16 mL), BISPIP (207.2 mg, 1.07 mmol), H_2O (0.18 mL). Yield: 52% (519.94 mg).

BISPIP-βCD: β-CD (741.58 mg, 0.62 mmol), LiOH•H_2O (75 mg, 1.77 mmol), H_2O (0.4 mL), BISPIP (359 mg, 1.85 mmol), H_2O (0.3 mL). Yield: 47.4% (1100.58 mg).

Results and discussion

The synthetic procedure adopted for the preparation of cyclodextrin nanosponges was based on the previous finding that under strongly alkaline conditions (pH≥12) CD participates in hydrogen-transfer stepwise polyadditions to activated double bonds either alone or in combination with amines, in the latter case yielding mixed CD-PAA crosslinked resins. [39] Under these conditions, CD's hydroxyl groups are partially ionized to alkoxides thus triggering the Michael addition. In the polyaddition reaction with either bisacrylamides or acrylamide end-capped PAA oligomers, CDs behave as multifunctional monomers leading to crosslinked products that in aqueous media give rise to highly swollen nanosponges, while maintaining the ability to form host-guest inclusion complexes with compounds whose molecular dimension matches the size of the inner cavity.

In this study, α-, β- and γ-CD based nanosponges in which the CD moieties are bridged by either BAC or BISPIP or PAA deriving moieties were obtained (Scheme 18). In the latter case, the PAA portions of the nanosponges stemmed from the polyaddition of a controlled excess of 2,2-bisacrylamidoacetic acid (BAC) with 2-methylpiperazine (MP) (ISA23, Scheme 19). ISA23 proved endowed with remarkable ion complexing properties and represents a good model of cost-effective amphoteric PAA. [43]

For the sake of simplicity, Scheme 18 implicitly assumes that the polyaddition involves only the primary CD hydroxyl groups, neglecting the secondary ones. This, however, was not proved and no data are at present available. In fact, the primary hydroxyl groups are less sterically hindered and generally more accessible, whereas the secondary ones are stronger acids, hence more easily ionized. [44] The CD/comonomer molar ratio in the monomer feed was adjusted so as to obtain products with the highest CD content in order to establish sound terms for comparison of their absorption capacities of different water pollutants. Nanosponges containing αCD with ISA23 or γCD with BISPIP were not obtained probably due to a prevalence of the degradation process competing with the cross-linking reaction. The feed compositions are reported in Table 17. All nanosponges were purified by extensive washing with water and ethanol then dried. Their composition was determined by elemental analysis (Table 18) and points to a CD content in the resin generally higher than the composition of the monomer feed.

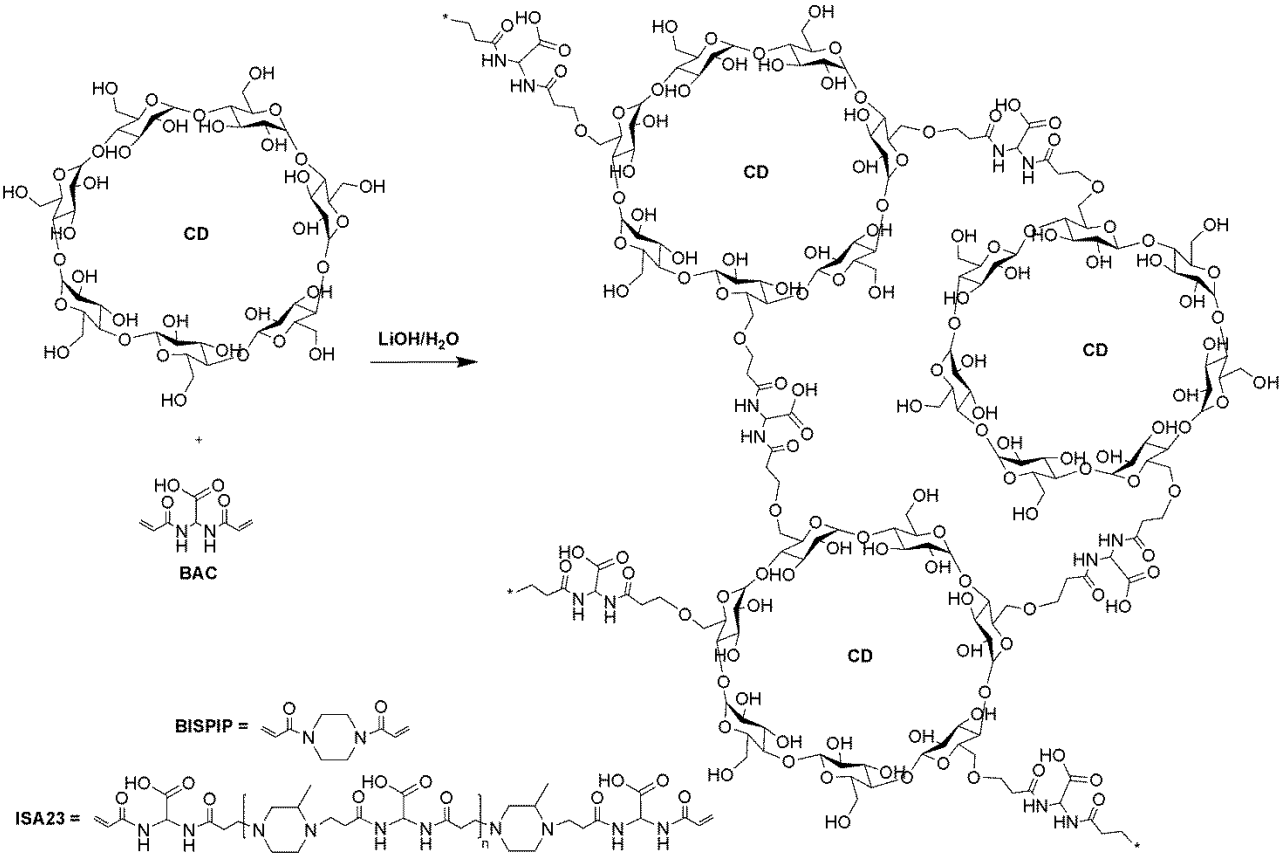

Scheme 18. Synthesis of BAC-CD, BISPIP-CD, ISA23-CD nanosponges. As an example the reaction of β-CD is shown.

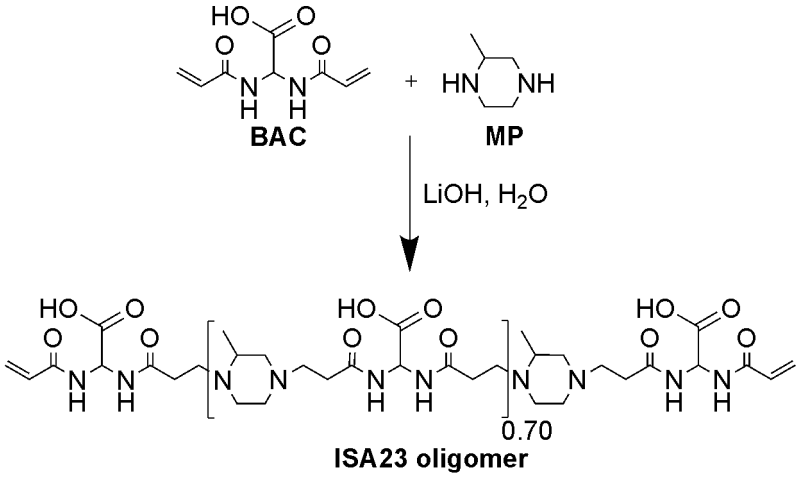

Scheme 19. Synthesis of ISA23 oligomer.

Table 17. Amounts of reagents used in the syntheses of BAC-CD, BISPIP-CD, ISA23-CD nanosponges.

Sample	**CD/acrylamide terminals** [molar ratio]	**-OH/acrylamide terminals** [molar ratio]	**CD content** [$^{w}/_{w}$%]	**Comonomer content** [$^{w}/_{w}$ %]
ISA23-βCD	0.31	6.43	48.06	51.94
ISA23-γCD	0.30	7.08	41.92	58.08
BAC-αCD	0.89	16.03	65.89	34.11
BAC-βCD	1.08	22.73	71.48	28.52
BAC-γCD	1.33	31.91	78.41	21.59
BISPIP-αCD	0.90	16.20	67.26	32.74
BISPIP-βCD	1.12	23.51	72.53	27.47

Table 18. Results of the elemental analysis of BAC-CD, BISPIP-CD, ISA23-CD nanosponges.

Sample	**C%**		**N %**		**C/N**		**CD** [mmol/g]		**CD [$^{w}/_{w}$ %]**	
	feed	found	feed	found	feed	found	feed	found	feed	found
ISA23-βCD	49.49	45.54	12.80	9.23	3.87	4.93	0.25	0.42	28.38	47.67
ISA23-γCD	49.35	42.96	12.44	10.32	3.97	4.16	0.23	0.32	29.83	41.50
BAC-αCD	46.17	42.42	6.12	4.82	7.55	8.80	0.58	0.68	56.38	66.10
BAC-βCD	45.74	42.12	4.93	4.03	9.27	10.45	0.57	0.63	64.70	71.51
BAC-γCD	45.46	40.55	3.91	3.05	11.63	13.30	0.56	0.60	72.63	77.82
BISPIP-αCD	51.82	44.29	6.13	4.72	8.45	9.38	0.59	0.69	57.35	67.07
BISPIP-βCD	50.27	44.13	4.87	3.96	10.33	11.14	0.58	0.64	65.83	72.64

BAC-CD, BISPIP-CD and ISA23-CD nanosponges were characterized by means of FTIR spectroscopy. All nanosponges show intense diagnostic bands typical of both CD pattern and of the addition product of either BAC, BISPIP or ISA23 (Figure 37). In particular, the CD frequencies observed at 3283, 2924, and 1024 cm^{-1} corresponds to -OH, -CH_2-, and C-O stretching. Meanwhile the frequencies for ISA23 addition products were observed at 1616 and 1515 cm^{-1} for amide C=O stretching and NH bending, respectively. BAC signals corresponding to amide C=O stretching and N-H bending were present at 1664 and 1515 cm^{-1}, respectively. BISPIP addition products were observed at 1616 and 1436 cm^{-1} (amide C=O and C-N stretching).

The -CH_2- groups, present in both structural units, give rise to C-H stretching bands at 2924 cm^{-1} and bending at 1380 cm^{-1}. The broad band typical of N-H amide stretching at 3283 cm^{-1} overlaps with OH stretching. In general, no signals corresponding to unreacted ISA23, BAC or BISPIP double bonds are visible. The only exception is ISA23-βCD showing a peak at 2973 cm^{-1} due to some residual vinyl bonds (CH bending).

Swelling experiments showed larger swelling in water than in 0.01 M PBS with all BAC-CD, BISPIP-CD and ISA23-CD nanosponges (Figure 38). Deswelling in the buffer solution is likely due to the ionic strength generated by the buffer salt. The swelling degrees increase when decreasing the cross-linking density that is, when increasing the –OH/acrylamide terminals molar ratio. Furthermore, differences observed within the series can be ascribed to the different hydrophilic/lipophilic balance associated to the different ratio among the hydrophilic bisacrylamide (or ISA23)-deriving residues and hydrophobic CD cavities.

Thermal stability is a major requirement for BAC-CD, BISPIP-CD and ISA23-CD nanosponges in view of the envisaged application as sorbents of volatile compounds. Thermal treatment might indeed represent an important step of the regeneration process. The thermal behavior of the resins was evaluated by DSC and TG analyses. For DSC analysis, the second run heating cycles following a cooling cycle carried out at the same rate are shown in Figure 39. DSC curves showed substantially flat curves in the range 20-150 °C, with no apparent transitions. In spite of the inert atmosphere, exothermic thermal decomposition occurred above 200 °C.

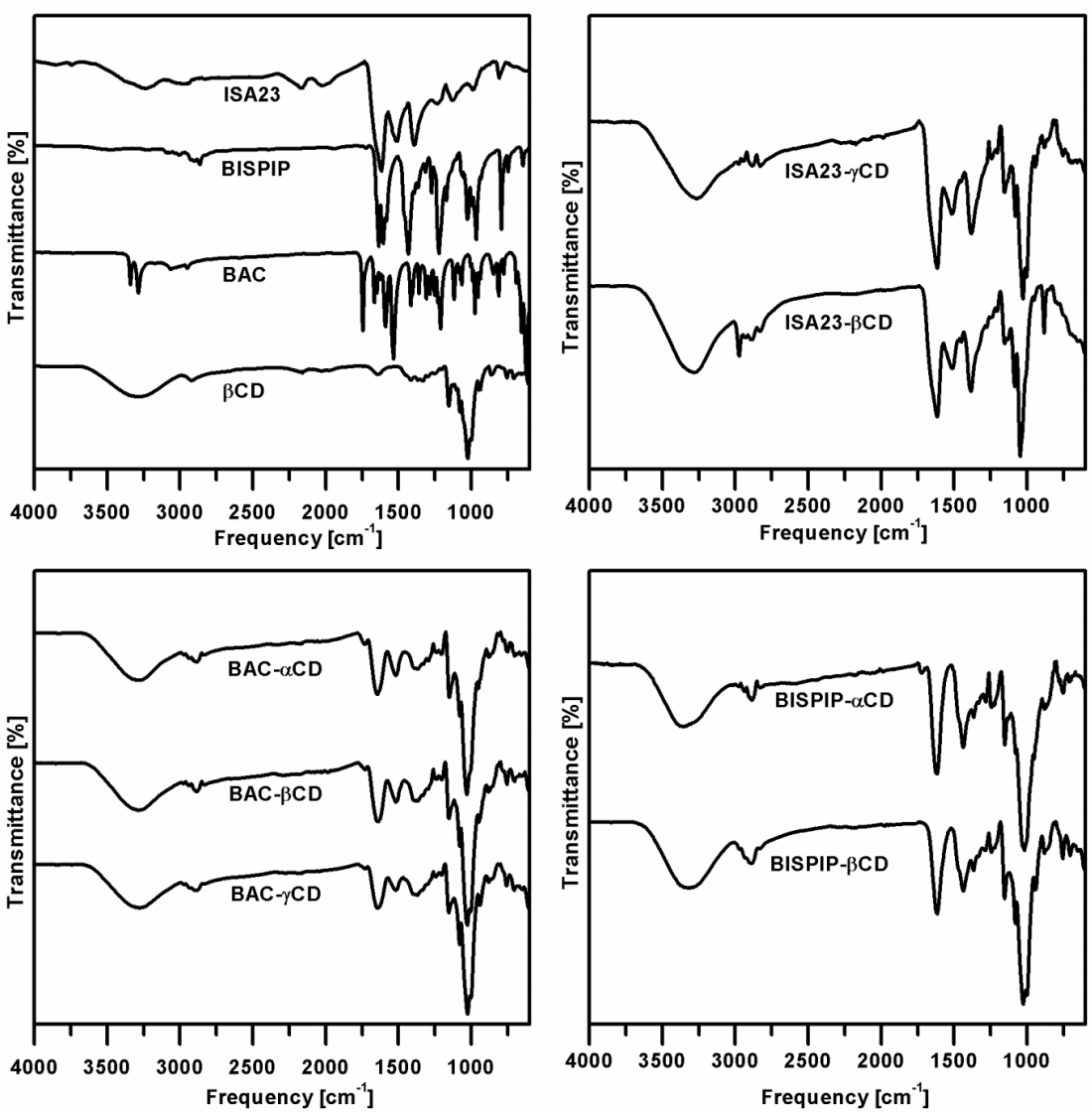

Figure 37. FTIR spectra of β-CD, ISA23 oligomer, and BAC-CD, BISPIP-CD, ISA23-CD nanosponges.

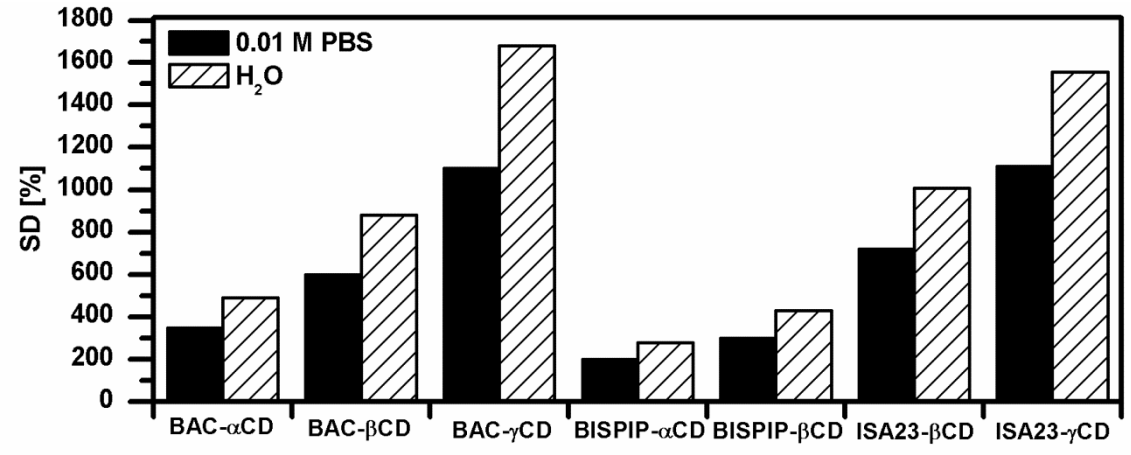

Figure 38. Swelling behavior of BAC-CD, BISPIP-CD and ISA23-CD nanosponges.

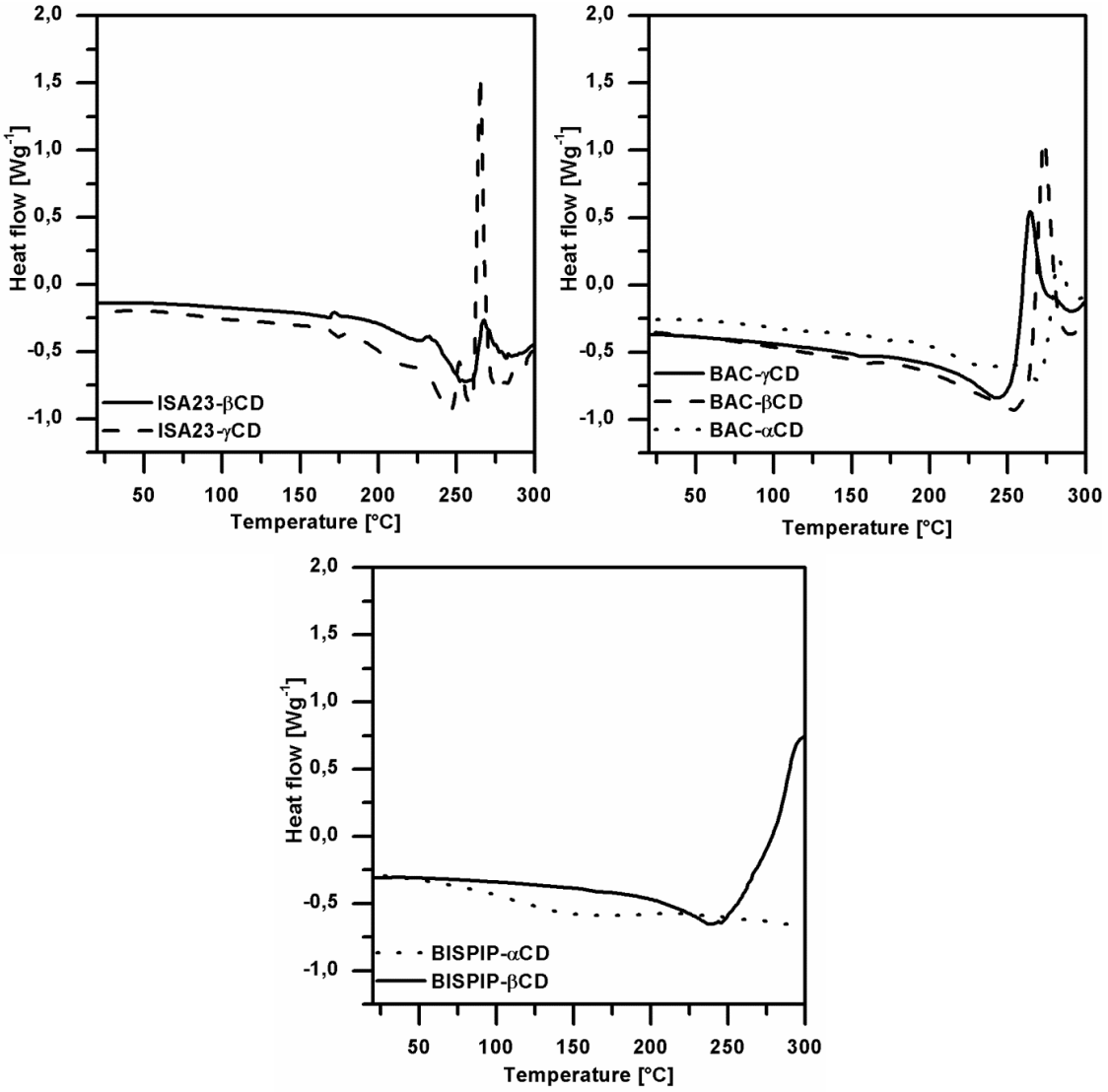

Figure 39. DSC thermograms of BAC-CD, BISPIP-CD and ISA23-CD nanosponges.

The thermal behaviors were confirmed by TG analyses. As reported for other CD-resins [45] the thermogravimetric pattern of BAC-CD, BISPIP-CD and ISA23-CD nanosponges contrasted with those of the parent CDs. α-, β- and γ-CD exhibited almost superimposable thermograms, showing complete decomposition before 400 °C. By contrast, all nanosponges showed a small loss of water at about 100 °C, followed by a main gradual decomposition stage between 150 °C and 500 °C, with a weight loss increasing sharply above 200 °C and further increasing up to about 80% at 600 °C (Figure 40 and Table 19). In some cases, DTG curves clearly show a peak at about 350 °C which can be ascribed to the decomposition of CDs embedded in the nanosponges. Peaks at lower temperatures can be attributed to the irregular thermal degradation of the nanosponges network. Overall, the thermal stabilities of the three nanosponge series are comparable and all of the products are stable up to 150 °C in nitrogen atmosphere.

Table 19. Results of the TG analyses. T_{max} represents the temperature of the highest weight loss rate.

Sample		**Dehydration (T=100 °C)**	**Main decomposition stage**		**Residual weight at 600 °C [%]**
		Weight loss [%]	T_{max} [°C]	Weight loss [%]	
ISA23	β	1.40	260.44	69.05	19.96
	γ	4.50	279.07	64.66	21.49
BAC	α	1.98	294.11	64.40	26.30
	β	1.80	286.96	63.36	27.30
	γ	2.27	278.64	66.61	22.41
BISPIP	α	0.67	298.35	58.94	32.72
	β	1.28	342.28	61.45	26.17

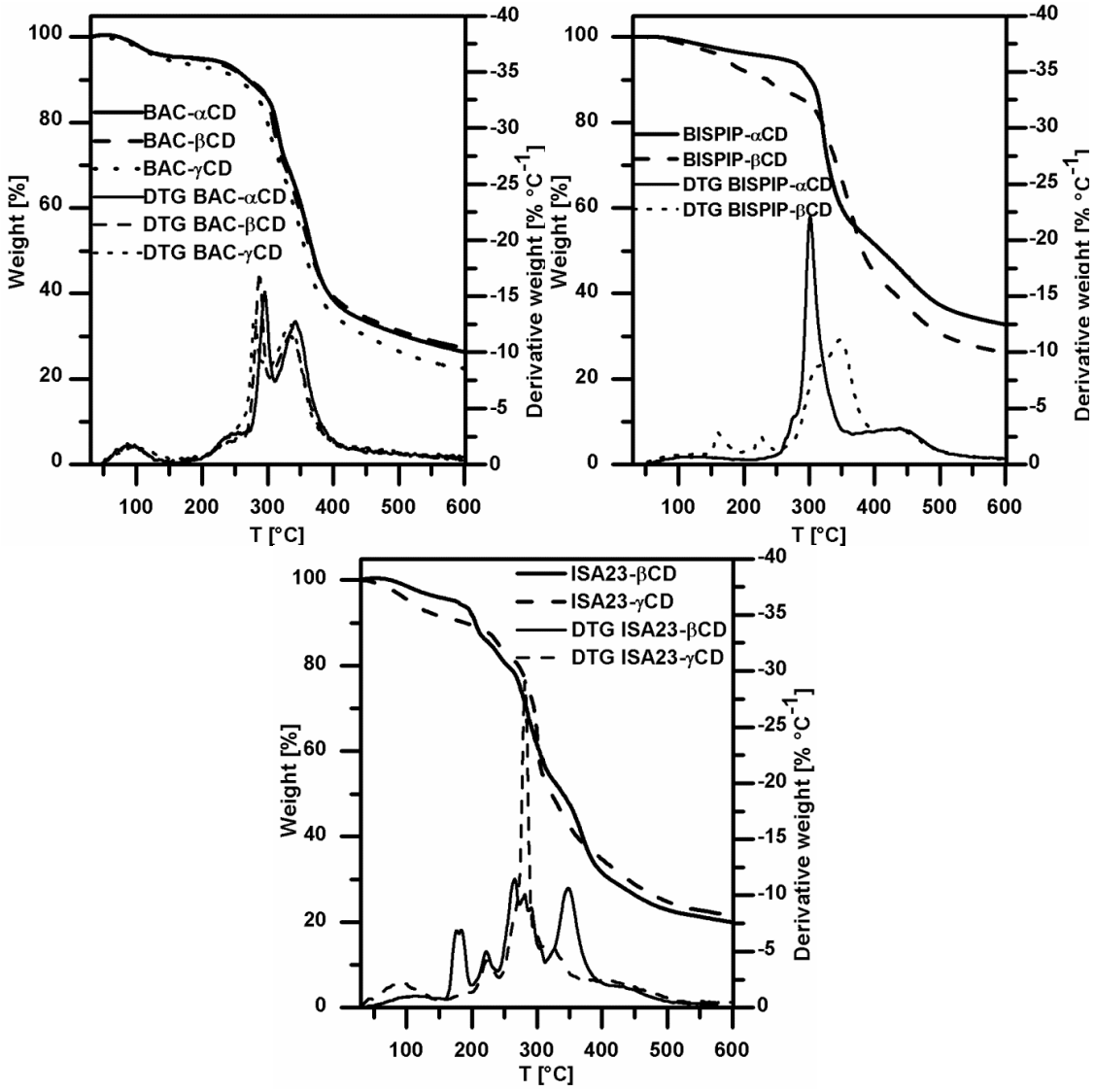

Figure 40. TG and DTG curves of BAC-CD, BISPIP-CD, ISA23-CD nanosponges.

One of potential applications of CD-based nanosponges is the sorption of organic micropollutants from water, especially drinking water. As stated by IARC, o-toluidine is carcinogenic to humans and [2] its efficient removal from water is required. To this purpose, preliminary studies were carried out for investigating the absorption performance of CD nanosponges on o-toluidine. The results were obtained by monitoring via LSV on MWCNT-modiifed glassy carbon electrode from 10^{-4} M solutions (about 10 ppm) (see for example Figure 41). The absorption kinetics were found for all cases to fit a mono exponential kinetic model, implying the following:

$$q_t = q_e - \frac{D}{m_{abs}} e^{-k_D t} \qquad (1)$$

where m_{abs} is the weight of the sample of the sorbing material, k_D is the relevant sorption rate, q_e is the equilibrium pollutant sorption capacity and D is a further parameter modulating the sorption rate. O-toluidine abatement percentage was calculated as follows:

$$Abatement\ [\%] = \frac{\text{Absorbed o-toluidine [mg]}}{\text{Initial o-toluidine [mg]}} \text{ x } 100 \qquad (2)$$

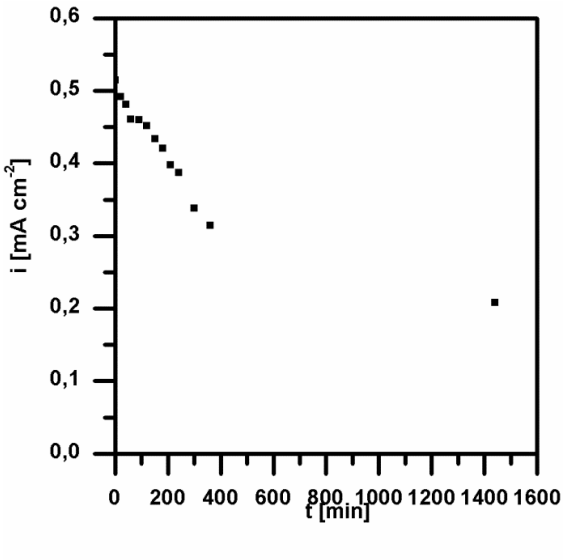

Figure 41. Monitoring of o-toluidine absorption from 10^{-4} M solution by βCD-BISPIP nanosponge.

The sorption capacities of the nanosponges were compared to those of soluble α-, β-, and γ-CD.

Among the three CDs, β-CD showed the highest sorption capacity because the dimensions of its cavity were particularly suitable for the formation of inclusion complexes with o-toluidine. As shown in Figure 42, for α-, β-, and γ-CD the sorption capacity in μmol g^{-1} towards o-toluidine was maintained and, in some instances, even improved once CDs were embedded into the nanosponges network. This suggested that the sorption behaviour of the nanosponges was not only due to the formation of inclusion complexes but it is very likely that o-toluidine was sorbed to a large extent into or onto their surface also by other kinds of interactions such as, for example, hydrogen bonding and van der Waals forces.

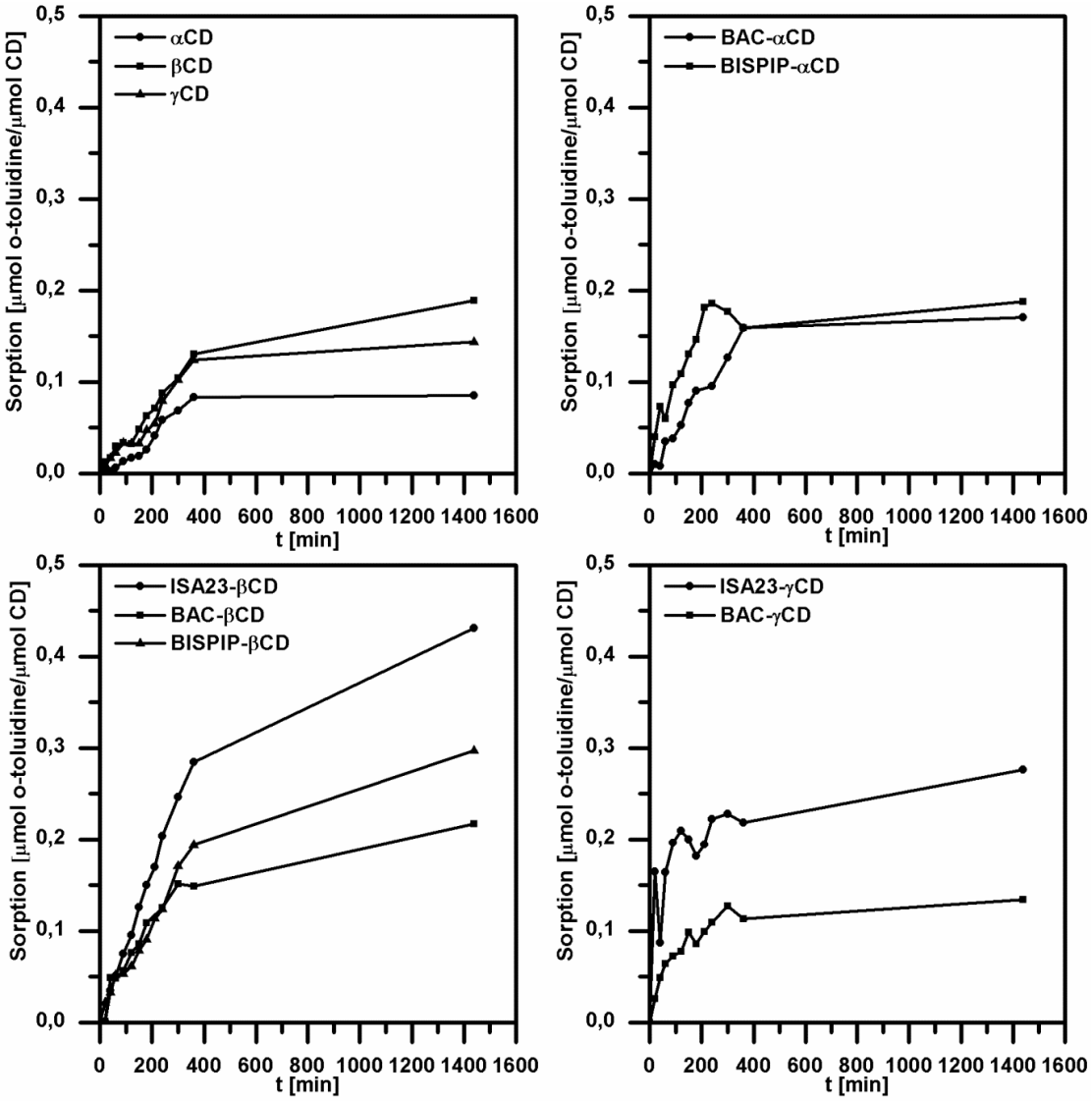

Figure 42. Sorption performance of soluble CDs and CD-containing nanosponges in μmol of o-toluidine per μmol of CD in the sorbent**.**

Overall, the best sorption performance was that of βCD-based nanosponges and, in particular, BISPIP-βCD, containing the highest amount of CD (Figure 43 and Table 20). BISPIP-βCD proved able to absorb up to 21.32 mg g^{-1} of toluidine with a 59.62% abatement (Figure 44). In spite of the lower CD content, ISA23-βCD performance was comparable to that of BISPIP-βCD, probably due to the sorption contribute of ISA23 itself (4.29 mg g^{-1}) as well as to the length of ISA23 polymer chains connecting CD units. In fact, compared to BAC and BISPIP, ISA23 binds CDs forming a wider network, as suggested also by the high ISA23-βCD swelling degree, therefore o-toluidine may be more easily accommodated into the cross-linked product. The same trend was observed for γCD-containing nanosponges. BAC-containing nanosponges did not show sorption

capacities significantly higher than those of BISPIP-containing nanosponges therefore it can be concluded that in these cases ionic interactions did not significantly contribute to the sorption process.

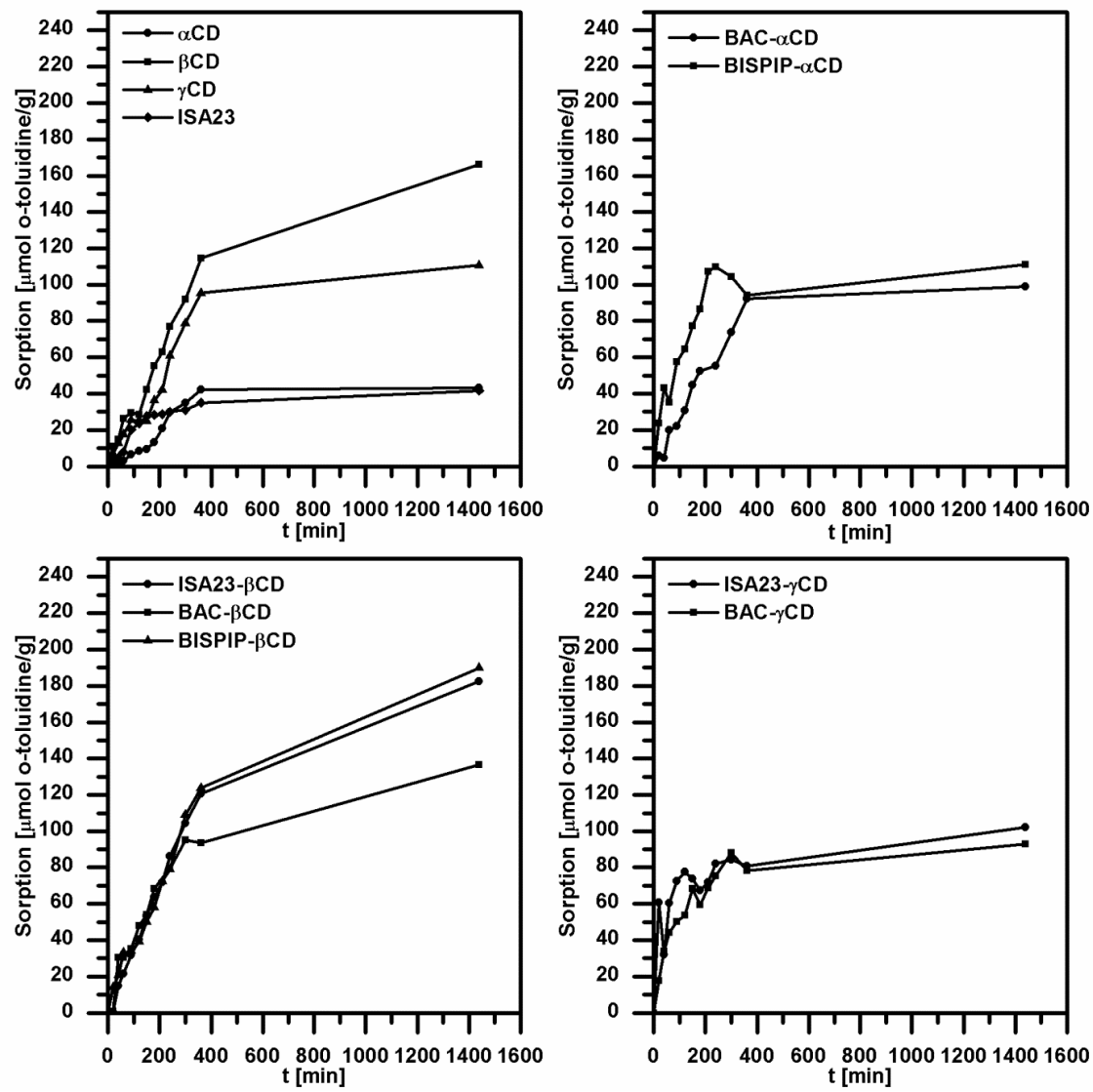

Figure 43. Sorption performance of soluble CDs, ISA23 hydrogel and CD-containing nanosponges in µmol of o-toluidine per g of sorbent.

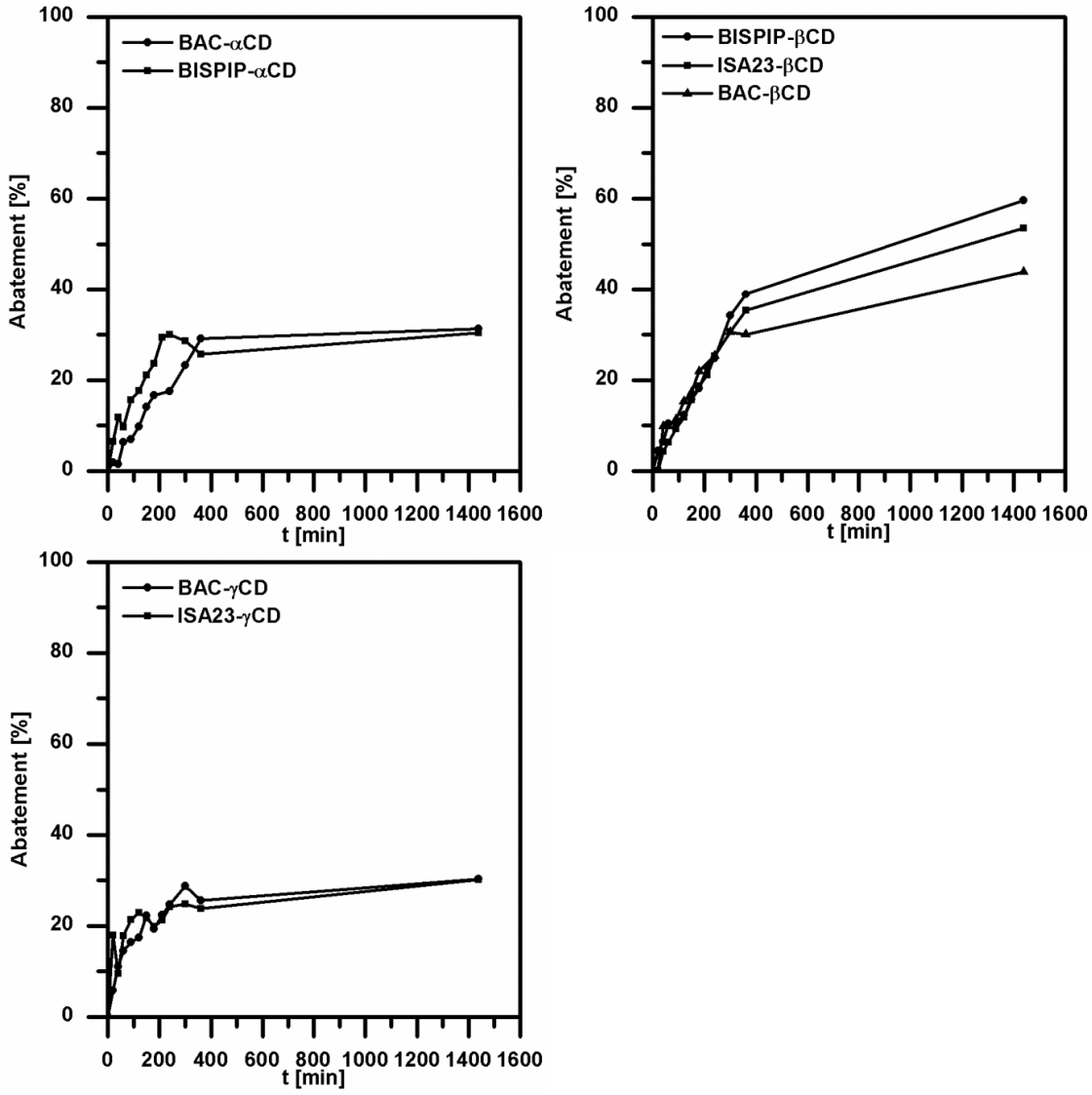

Figure 44. Abatement percentages of o-toluidine in water by PAA-CD nanosponges.

Table 20. Experimental q_e [µmol g^{-1}] and q_e [mg g^{-1}] values and kinetic parameters for the absorptions of o-toluidine from 10^{-4} M (10 ppm) aqueous solutions by CD-based nanosponges.

Sample	-toluidine				
	q_e [µmol g^{-1}]	q_e [mg g^{-1}]	D [µmol dm^{-3}]	$k_D \times 10^{-3}$ [min^{-1}]	$t_{1/2}$ [min]
αCD	47 ± 6	5.04 ± 0.64	1.6 ± 0.2	3.6 ± 0.9	223
βCD	174 ± 9	18.65 ± 0.96	5.3 ± 0.3	2.4 ± 0.3	294
γCD	117 ± 11	12.54 ± 1.18	3.6 ± 0.3	3.0 ± 0.6	243
ISA23	40 ± 2	4.29 ± 0.21	1.2 ± 0.1	6.6 ± 0.9	111
BAC-αCD	104 ± 7	11.14 ± 0.75	3.5 ± 0.2	4.1 ± 0.6	183
BISPIP-αCD	112 ± 7	12.00 ± 0.75	3.0 ± 0.2	8 ± 2	80
BAC-βCD	137 ± 5	14.68 ± 0.54	4.2 ± 0.2	3.4 ± 0.3	192
BISPIP-βCD	199 ± 10	21.32 ± 1.07	6.3 ± 0.3	2.3 ± 0.2	306
ISA23-βCD	188 ± 6	20.15 ± 0.64	5.7 ± 0.2	2.6 ± 0.2	277
BAC-γCD	88 ± 4	9.43 ± 0.43	2.7 ± 0.2	8 ± 1	78
ISA23-γCD	82 ± 6	8.79 ± 0.64	2.1 ± 0.4	19 ± 8	29

One of the important properties of a sorbent is its regeneration that allows the repeated use of the material itself. Since the interactions between o-toluidine and CD nanosponges were probably dominated by inclusion complex, Van Der Waals forces and hydrogen bonding, organic solvents were good candidates for the regeneration process. ISA23-βCD and BISPIP-βCD nanosponges, showing the highest sorption capacities, were regenerated by methanol extraction and o-toluidine sorption-desorption cycle was repeated twice. As shown in Figure 45, the sorption capacities slightly improved after the first regeneration treatment probably due to a rearrangement of the nanosponges network that enhanced o-toluidine sorption facilitating its inclusion into the sorbent. As a consequence, also the abatement percentages increased up to 70.70% (Figure 46). These results proved the stability and recyclable value of CD nanosponges.

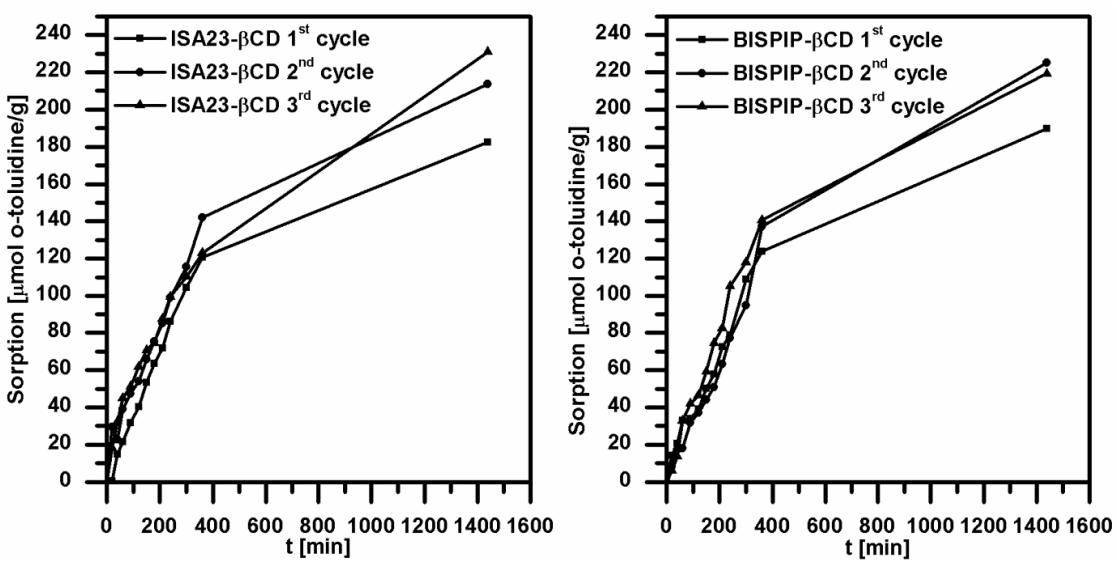

Figure 45. Absorption capacities of o-toluidine for ISA23-βCD and BISPIP-βCD nanosponges before (1st cycle) and after recycling (2nd and 3rd cycles).

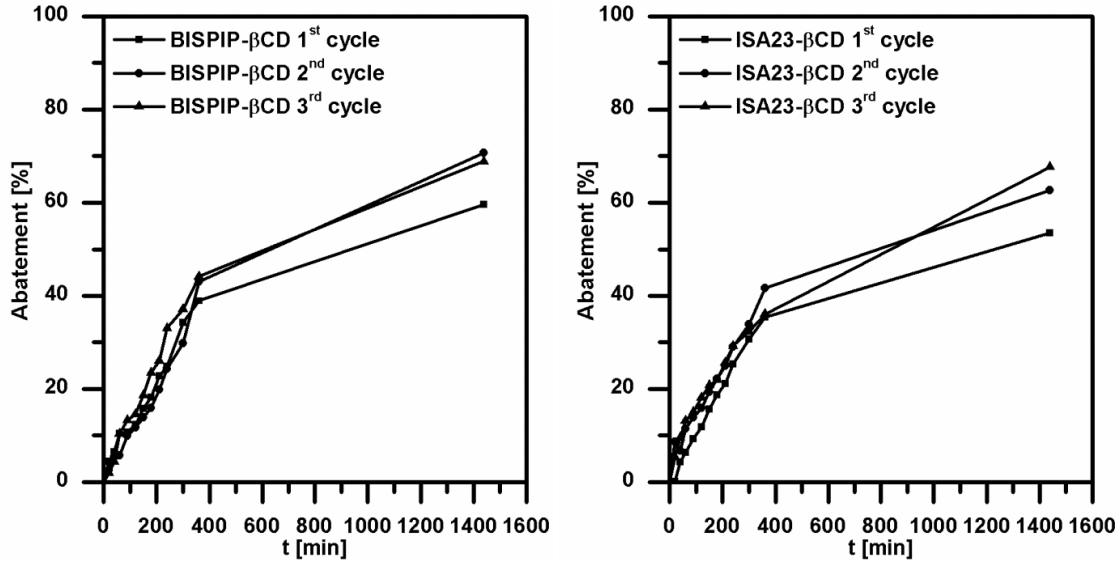

Figure 46. Abatement percentages of o-toluidine for ISA23-βCD and BISPIP-βCD nanosponges before (1st cycle) and after recycling (2nd and 3rd cycles).

Conclusions

CD nanosponges were planned to be covalently crosslinked by transversal bisacrylamide or PAA moieties and were successfully synthesized at moderate cost by eco-friendly procedures. CD nanosponges were characterized by high CD content and absorbed up to 17 times their weight when swollen in water. They proved thermally stable up to 150 °C, with weight loss mainly due to dehydration. In preliminary sorption experiments, CD nanosponges proved suitable for the removal *o*-toluidine from aqueous solutions with

absorption capacities in the range 82-199 μmol g^{-1} (8.79-21.32 mg g^{-1}) at an initial pollutant concentration of 10^{-4} M (~10 ppm). The sorbents could be regenerated with methanol and recycled without loss of absorption capacity proving competitive with other materials employed to the same purpose. [46]

The potential scalability and environmental sustainability of the synthetic processes let envisage a high potential for the design of different CD-based materials with interesting functional properties and in the light of these results it can be speculated that the CD-based nanosponges presented in this work showed interesting properties for applications in water treatment, especially for the removal of o-toluidine from water.

References

[1] S. I. a. r. United Nations Environment Programme, «"O-Toluidine", Progress on OECD chemicals programme (11)--SIAM 19,» Berlin, 2004.

[2] R. Baan, K. Straif, Y. Grosse, B. Secretan, F. El Ghissassi, V. Bouvard, L. Benbrahhim-Tallaa, C. Cogliano, *Lancet Oncol.*, vol. 9, pp. 322-323, 2008.

[3] S. Nevim, Ç. Zekiye, *J. Adv. Oxid. Technol.*, vol. 5, pp. 85-92, 2002.

[4] V. López-Grimau, M. Riera-Torres, M. Lopez Mesas, C. Gutiérrez-Bouzán, *Color. Technol.*, vol. 129, pp. 267-273, 2013.

[5] J. Anotai, P. Thuptimdang, C.-C. Su, M.-C. Lu, *Environ. Sci. Pollut. Res.* , vol. 19, pp. 169-176, 2012.

[6] Z. Liu, H. Yang, Z. Huang, P. Zhou, S.-J. Liu, *Appl. Microbiol. Biotechnol.*, vol. 58, pp. 679-682, 2002.

[7] A. Uribe, P. L. Bishop, N. G. Pinto, *J. Environ. Eng. Sci.* , vol. 1, pp. 123-133, 2002.

[8] P. Zhang, D. Sparks, *Soil Sci. Soc. Am. J.*, vol. 57, pp. 340-345, 1993.

[9] M. Essington, *Soil Sci.*, vol. 158, pp. 181-188, 1994.

[10] P. Voumard, Q. Zhan, R. Zenobi, *Langmuir*, vol. 11, pp. 842-848, 1995.

[11] V. K. Gupta, A. Nayak, S. Agarwal, *Chem. Eng. J.*, vol. 203, pp. 447-457, 2012.

[12] E. Titus, A. K. Kalkar, V. G. Gaikar, *Sep. Sci. Technol.*, vol. 37, pp. 105-125, 2002.

[13] O. Duman, E. Ayranci, *J. Hazard. Mater.* , vol. B120, pp. 173-181, 2005.

[14] H. Wang, J. Chen, Z. Zai, Y. Chen, Q. Zhang, *Chin. J. Environ. Chem.* , vol. 23, p. 188, 2004.

[15] C. Jianguo, L. Aimin, S. Hongyan, F. Zhenghao, L. Chao, Z. Quanxing, *J. Hazard. Mater.* , vol. B124, pp. 173-180, 2005.

[16] J. Szejtli, *Chem Rev.*, vol. 98, pp. 1743-1753, 1998.

[17] H. Dodziuk, Cyclodextrins and their complexes: chemistry, analytical methods, applications., Weinheim: Wiley, 2006.

[18] J. Szejtli, «Encyclopedia of Nanoscience and Nanotechnology,» vol. 2, pp. 283-304.

[19] L. Janus, G. Crini, V. El-Rezzi, M. Morcellet, A. Cambiaghi, G. Torri, A. Naggi, C. Vecchi, *React. Funct. Polym.*, vol. 42, pp. 173-180, 1999.

[20] H. Faraji, S. W. Husain, M. Helalizadeh, *J. Chromat. Sci.*, vol. 49, pp. 482-487, 2011.

[21] Y. Q. Fan, Y. Feng, L. S. Da, *Anal. Chim. Acta*, vol. 484, p. 145–153, 2003.

[22] R. Allabashi, M. Arkas, G. Hormann, D. Tsiourvas, *Water Res.*, vol. 41, pp. 476-486, 2007.

[23] G. Crini, L. Janus, M. Morcellet, G. Torri, N. Morin, *J. Polym. Sci. Part A: Polym. Chem.*, vol. 73, pp. 2903-2910, 1999.

[24] L. D. Wilson, H. M. H. Mohamed, C. L. Berhaut, *Materials*, vol. 4, pp. 1528-1542, 2011.

[25] H. Yamasaki, Y. Makihata, K. Fukunaga, *J. Chem. Technol. Biot.*, vol. 81, pp. 1271-1276, 2006.

[26] Í. X. García-Zubiri, G. González-Gaitano, J. R. Isasi, *J. Colloid Interf. Sci.*, vol. 307, pp. 64-70, 2007.

[27] A. Romo, F. J. Penas, J. R. Isasi, I. X. Garciá-Zubiri, G. González-Gaitano, *React. Funct. Polym.*, vol. 68, pp. 406-412, 2008.

[28] J. Yu, Z. Jiang, H. Liu, J. Yu, L. Zhang, *Anal. Chim. Acta*, vol. 477, pp. 93-101, 2003.

[29] G. Crini, *Progr. Polym. Sci.*, vol. 30, pp. 38-70, 2005.

[30] D. Li, M. Ma, «Cyclodextrin polymer separation materials». Brevetto WO9822197, 28 May 1998.

[31] D. Li, M. Ma, *Clean Technol. Environ. Policy*, vol. 2, pp. 112-116, 2000.

[32] F. Trotta, «Cyclodextrin Nanosponges and Their Applications,» in *Cyclodextrins in Pharmaceutics, Cosmetics and Biomedicine: Current and Future Industrial*

Applications, Hoboken, NJ, USA, Bilensoy John Wiley & Sons, 2011, pp. 323-342.

[33] F. Trotta, M. Zanetti, R. Cavalli, *Beilstein J. Org. Chem.*, vol. 8, pp. 2091-2099, 2012.

[34] S. D. Mhlanga, B. B. Mamba, R. W. Krause, T. J. Malefetse, *J. Chem. Technol. Biotechnol.*, vol. 82, p. 382–388, 2007.

[35] S. Berto, M. C. Bruzzoniti, R. Cavalli, D. Perachon, E. Prenesti, C. Sarzanini, F. Trotta, W. Tumiatti, *J. Incl. Phenom. Macro.*, vol. 57, pp. 637-643, 2007.

[36] S. Berto, M. C. Bruzzoniti, R. Cavalli, D. Perrachon, E. Prenesti, C. Sarzanini, F. Trotta, W. Tumiatti, *J. Incl. Phenom. Macro.*, vol. 57, pp. 631-636, 2007.

[37] Z.-Y. Sun, M.-X. Shen, G.-P. Cao, J. Deng, Y. Liu, L. Zhao, W.-K. Yuan, *J. Appl. Polym. Sci.*, vol. 402, pp. 254-257, 2010.

[38] R. Cavalli, A. K. Akhter, A. Bisazza, P. Giustetto, F. Trotta, P. Vavia, *Int. J. Pharm.*, vol. 402, pp. 254-257, 2010.

[39] S. Swaminathan, R. Cavalli, F. Trotta, P. Ferruti, E. Ranucci, I. Gerges, A. Manfredi, D. Marinotto, P. R. Vavia, *J. Incl. Phenom. Macrocycl. Chem.*, vol. 68, pp. 183-191, 2010.

[40] P. Ferruti, *J. Polym. Sci. A Polym. Chem.*, vol. 51, pp. 2319-2353, 2013.

[41] P. Ferruti, E. Ranucci, F. Trotta, E. Gianasi, G. E. Evagorou, M. Wasil, G. Wilson, R. Duncan, *Macromol. Chem. Phys.*, vol. 200, pp. 1644-1654, 1999.

[42] P. Ferruti, *Macromol. Synth.*, vol. 9, pp. 25-29, 1985.

[43] P. Ferruti, E. Ranucci, S. Bianchi, L. Falciola, P. R. Mussini, M. Rossi, *J. Polym. Sci. A Polym. Chem.*, vol. 44, pp. 2316-2327, 2006.

[44] T. Loftsson, M. E. Brewster, *J. Pharm. Sci.*, vol. 85, pp. 1017-1025, 1996.

[45] R. W. M. Krause, B. B. Mamba, F. M. Bambo, T. J. Malefetse, «Cyclodextrin polymers: Synthesis and application in water treatment,» in *Cyclodextrins: Chemistry and Physics*, Y. Hu, Transworld Research Network, Kerala, India., 2010.

CHAPTER 3

SYNTHESIS AND CHARACTERIZATION OF HYBRID POLY(AMIDOAMINE)/HEMICELLULOSE HYDROGELS

Introduction

Polymers from renewable resources have attracted an increasing amount of attention over the last two decades. [1] The use of renewable resources such as agricultural and industrial by-products with little or no economic value, produced in large quantities and that often represent a disposal problem, would open a new market for these by-products. [2]

Hemicelluloses, amorphous polysaccharides located in the secondary cell wall of woods and grasses, are among the most abundantly available renewable resources. In particular, the hemicellulose *O*-acetyl-galactoglucomannan (AcGGM) is the major hemicellulose in softwood. It is typically water-soluble, with relatively high acetylation degree and low molecular weight. [3] The properties of AcGGM can be modified changing its physical and chemical structures by different methods and its multifunctional structure together with its natural abundance make it a good candidate for the preparation of value-added products such as films, [4] [5] [6] [7] bio-based fuels [8] [9] and hydrogels. [10] [11] [12] [13] [14] [15] The same applies to spruce hydrolysate, an only partly upgraded mixture isolated from softwood refining processes, containing AcGGM as a major component and a smaller but significant amount of lignin.

Hydrogels are three-dimensional hydrophilic polymer networks able to absorb large amounts of water without dissolving. Thanks to their unique properties such as, for example, high permeability to small molecules, hydrophilicity and softness, they are attracting attention in various fields of medicine, biotechnology, and environmental protection. Hydrogels can be obtained from natural polysaccharides, including hemicellulose, using different approaches. [16]

The chemical and physical properties of polysaccharides, including cellulose, starch and hemicelluloses, can easily be modified by the radical graft copolymerization of vinyl monomers onto the polysaccharide backbone in the presence of radical initiators. [17] [18] [19] [20] [21] [22] [23] [24] The relevant reaction step in this processes is the abstraction by the initiator of hydrogen radicals generating alkoxy radicals capable to start the radical polymerization of the vinyl monomer. In the presence of suitable crosslinking agents, polysaccharide hydrogels are obtained. To this purpose, methacrylic acid (MA) is

an important monomer widely used for the preparation of hydrogels. MA-based hydrogels find numerous applications in various fields, from therapeutics to environmental applications.[25][26] If AcGGM reacts with MA via free radical graft polymerization and a crosslinker such as an acrylamido end-capped PAA oligomer is added, novel insoluble crosslinked copolymers can be obtained. [19]

Here we present hybrid hydrogels of hemicellulose, poly(amidoamine)s and poly(acrylic acid).

Poly(amidoamine)s (PAAs) constitute a family of highly hydrophilic, biodegradable and biocompatible synthetic polymers prepared in aqueous solution, at room temperature and with no added catalysts or organic solvents. A wide range of functional amines and bisacrylamides can be used as monomers for their syntheses. PAAs are endowed with the ability to give complexes with many heavy metal ions. [27] [28] [29] [30]

In this study, multifunctional hybrid PAA/AcGGM hydrogels were obtained by free radical graft copolymerization of acrylamido end-capped PAA oligomers acting as crosslinkers with MA onto either highly purified AcGGM or a less fractionated hemicellulose-rich spruce hydrolyzate, using the metabisulfite/ammonium peroxydisulfate redox system as initiator. The hydrogels samples were characterized by Fourier-transform infrared spectroscopy (FTIR), elemental analysis, thermal measurements and mechanical studies. The sorption of heavy metal ions such as Cu^{2+}, Cd^{2+}, Pb^{2+}, Zn^{2+}, Ni^{2+}, Co^{2+} and CrO_4^{2-} from aqueous solutions was also studied.

Experimental

Materials

All chemicals, unless otherwise indicated, were used as received. N,N´-methylenebisacrylamide (MBA) (99%), NaOH (99%), $LiOH•H_2O$ (99%), HCl (32%), 2-methylpiperazine (MP) (98%), glycine (Gly) (99%), methacrylic acid (99%), $Na_2S_2O_5$ (99%), $(NH_4)_2S_2O_8$ (99%), ethylenediaminetetraacetic acid disodium salt (EDTA-Na_2) (98.5%), Eriochrome® Black T (indicator grade), Murexide (for complexometry), NH_4Cl (≥99.5%), NH_4OH solution (28% NH_3 in H_2O, ≥99.9%), K_2CrO_4 (≥99%), Cu^{2+}, Ni^{2+}, Co^{2+} and Pb^{2+} nitrate (99.99% on metal basis) were purchased from Sigma Aldrich. Cd^{2+} nitrate (99.99% on metal basis) was purchased from Alfa Aesar. Zn^{2+} sulfate heptahydrate was purchased from Kebo. N,N´-dimethylethylenediamine (DMEDA) (85%) was purchased from Acros.

O-Acetylated galactoglucomannan (AcGGM) originating from spruce (*Picea abies)* was obtained from the thermomechanical pulping, purified and concentrated by ultrafiltration and freeze-dried. The carbohydrate composition was determined to 17% glucose, 65% mannose, 15% galactose using the method of Dahlman et al. [31] AcGGM had $\bar{M}_w$ =7500 (DP ~ 40), PDI=1.3 and a degree of acetylation of 0.30 as determined by size exclusion chromatography (SEC) according to a published protocol. [32] A spruce hydrolyzate, rich in AcGGM, was obtained in the hydrothermal treatment of wood chips as described elsewhere.35 The process liquor was subjected to ultrafiltration (with a regenerated cellulose membrane (PLAC Prepscale, Millipore) with a nominal cut-off 1000 Da) and freeze-dried. The hydrolyzate contained mostly AcGGM, 5% xylan and 15% lignin, with $\bar{M}_w$ =2500 and PDI = 3.

Methods

NMR. ^{1}H and ^{13}C NMR spectra of PAA oligomers were obtained using a Bruker Avance DPX-400 NMR operating respectively at 400.13 MHz and 100.40 MHz in D_2O.

Molecular weight. PAA oligomers size exclusion chromatography (SEC) traces were obtained with Toso-Haas TSK-gel G4000 PW and TSK-gel G3000 PW columns connected in series using a Waters model 515 HPLC pump equipped with a Knauer autosampler 3800, a light scattering and viscometer Viscotek 270 dual detector, a UV detector Waters model 486 operating at 230 nm and a refractive index detector (Waters, Model 2410). The mobile phase was a 0.1 M Tris buffer (pH 8.00 ± 0.05) with 0.2 M sodium chloride. The flow rate was 1 mL min^{-1} and the sample concentration was 1% ($^{w}/_{w}$).

FTIR analysis. The hydrogels were dried under vacuum to constant weight and the FTIR spectra were collected using a Perkin Elmer spectrometer 2000 with an Attenuated Total Reflectance (ATR) crystal accessory (Golden Gate). All spectra were calculated means of 16 individual scans at 2 cm^{-1} resolution in the 4000-600 cm^{-1} interval with corrections for atmospheric water and carbon dioxide.

Swelling degrees. The swelling degrees were evaluated in deionized H_2O, in 0.01 M PBS at pH 7.4, KCl/HCl buffer at pH 2 and TRIS/HCl buffer at pH 9 at 20 °C. The swelling percentage was determined by the following equation:

$$SD\ [\%] = \frac{m_{eq}}{m_0}\ x\ 100 \quad (1)$$

where m_{eq} is the weight of the sample at equilibrium and m_0 the weight of the dry sample.

Thermal analyses. DSC analyses were performed on a Mettler Toledo DSC823^e on 10 mg samples, under nitrogen flow at 20 mL min^{-1}, heating/cooling rate of 30 °C min^{-1}. A first heating cycle from 0 °C to 100 °C was followed by a cooling cycle from 100 °C to 0 °C and a second heating cycle from 0 to 400°C. TGA analyses were performed on a Perkin Elmer TGA 4000 on 10 mg samples under nitrogen flow at 50 mL/min, from 30 °C to 600 °C at a heating rate of 30 °C min^{-1}.

Dynamic mechanical analyses. Rheological characterizations were performed on a TA instrument model AR2000. Samples obtained via route 1 were prepared as discs with a 2 mm thickness and a 0.8 cm base diameter. Samples obtained via route 2 were prepared as discs with a 5 mm thickness and a 2.5 cm base diameter. All samples were allowed to swell to equilibrium for 72 hours. Sweep tests (strain-controlled) were performed at 25 °C with samples at 0.2% strain within a frequency range from 0.5 to 100 rad s^{-1}. A parallel plate geometry was used.

Heavy metal ion absorption. Metal ions absorption tests were carried out against Cu^{2+}, Co^{2+}, Pb^{2+}, Cd^{2+}, Zn^{2+}, Ni^{2+} and CrO_4^{2-}. Standardized aqueous solutions at 700 ppm were employed for all of the heavy metals. Pb^{2+} and Cd^{2+} absorption was tested also starting from 50 ppm solutions and CrO_4^{2-} from 4 ppm solutions. The absorption tests were performed using 10 mg of dried hydrogel in a 10 ml tube and swelling it until equilibrium in deionized water (10 mL) for 24 hours. After this time, the supernatant was replaced with the heavy metal aqueous solution and the hydrogel was incubated in such solution for further 12 hours. The initial and the final surnatant metal concentrations were determined via complexometric titration with EDTA for all of the metals while CrO_4^{2-} was measured photometrically after lowering to 2 the pH of the solution with HCl (λ_{max}= 350.9 nm) . [33]

EDTA-Na_2 standardization: a 1 x 10^{-4} M $ZnSO_4 \cdot 7H_2O$ solution was prepared, added with NH_4Cl/NH_3 buffer (pH~10) until alkaline pH and titrated with a 1 x 10^{-4} M EDTA-Na_2 solution using Eriochrome® Black T as indicator. Cd^{2+}, Pb^{2+} and Zn^{2+}aqueous solution concentrations were determined adding NH_4Cl/NH_3 buffer until alkaline pH in the presence of Eriochrome® Black T as indicator and titrating with the standardized EDTA-

Na_2 solution. Ni^{2+}, Co^{2+} and Cu^{2+}were titrated according to the same procedure described for Cd^{2+}, Pb^{2+} and Zn^{2+}employing Murexide as indicator.

Synthesis of MBAMP oligomer. MBA (7.76 g; 49.82 mmol) and MP (3.56 g; 34.87 mmol) were mixed in water (16.61 mL) and maintained at 40°C, in the dark, under stirring. The mixture, which turned into a clear solution after 12 hours, was allowed reacting for totally 72 hours, then diluted with H_2O (150 mL) and freeze-dried. The final product was recovered as a white powder. Yield: 11.3 g, 99.8%. ^{1}H NMR (D_2O, 400.13 MHz, 298 K): δ (ppm) 6.14 (br, H1), 5.69 (br, H2), 4.62-4.44 (H4, H4'), 2.96-1.75 (br, -MP ring and -CH_2- polymer chain), 0.94 (br, H10). ^{13}C NMR (D_2O, 100.40 MHz, 298 K): δ (ppm) 175.19 (C15,C17), 168.61 (C3,C5), 129.50 (C2), 128.21 (C1), 58.61 (C8), 53.61 (C9), 52.90 (C11), 51.45 (C12), 49.76 (C13), 48.20 (C7), 44.24 (C4), 32.27 (C14), 30.76 (C6), 15.84 (C10). SEC: $\bar{M}_n$=4370, PDI=1.00. See Figure 47 for NMR assignment.

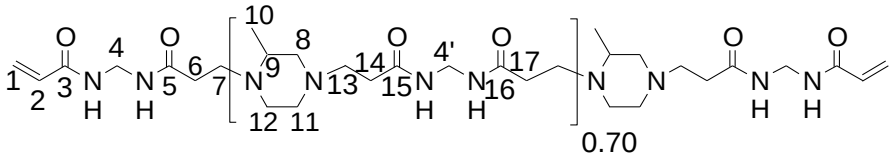

Figure 47. MBAMP atom labeling for NMR assignment.

Synthesis of MBAGD oligomer. MBAGD oligomer was prepared adding MBA (7.76 g; 49.82 mmol) followed by Gly (1.32 g; 17.44 mmol) together with LiOH•H_2O (746.72 mg; 17.44 mmol) and finally DMEDA (2.21 mL; 17.44 mmol) in a H_2O:MeOH=1:1 solution (16.61 mL) following the same procedure reported for MBAMP. The product was recovered as a light yellow powder. Yield: 11.59, 99.2%. ^{1}H NMR (D_2O, 400.13 MHz, 298 K): δ (ppm) 6.14 (br, H1), 5.69 (br, H2), 4.62-4.45 (H4, H4' and H4''), 3.02 (s, H18), 2.73-2.30 (br, -CH_2- polymer chain), 2.17 (s, H8, H8'). ^{13}C NMR (D_2O, 100.40 MHz, 298 K): δ (ppm) 178.76 (C19), 175.18 (C5, C3), 168.55 (C12, C12', C17), 129.56 (C2), 128.22 (C1), 57.41 (C7, C10), 53.00 (C9, C9'), 52.43 (C14, C15), 49.33 (C18), 44.35 (C4, C4', C4''), 41.65 (C8, C8'), 32.94 (C13, C16), 32.51 (C11, C6). SEC: $\bar{M}_n$= 1760, PDI =1.08. See Figure 48 for NMR assignment.

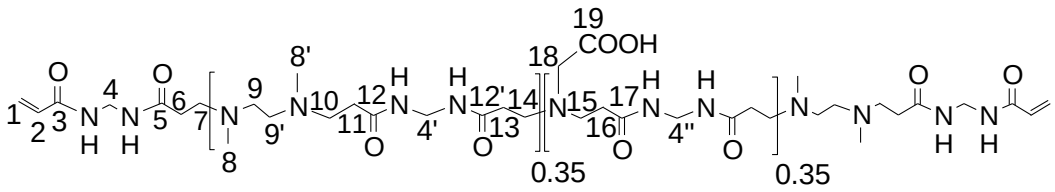

Figure 48. MBAGD atom labeling for NMR assignment.

Synthesis of PAA-MA-AcGGM hydrogels - route 1. In a typical procedure, MBAMP1 was prepared by dissolving AcGGM (100 mg; 0.52 hexose mmol) and LiOH•H_2O (59.35 mg; 1.4 mmol) in H_2O (2 mL), in the dark and under nitrogen. MA (10 mg; 0.12 mmol) followed by MBAMP (375.2 mg; 0.50 acrylamide bonds mmol) were added and the polymerization initiated by $Na_2S_2O_5$ and $(NH_4)_2S_2O_8$ (each 0.5 mg/µL aqueous solutions, 1% $^{w}/_{w}$). After 24 hours at room temperature the hydrogel was soaked in deionized H_2O (100 mL) for 48 hours, renewing the solvent at regular time intervals and dried until constant weight.

Hydrogels MBAMP, MBAGD and MBAGD1 were prepared following the same procedure described for MBAMP1 employing monomers and amounts listed here below. As redox initiator $Na_2S_2O_5$ and $(NH_4)_2S_2O_8$ 0.5 mg/µL aqueous solutions were used (1% $^{w}/_{w}$).

MBAMP: MBAMP oligomer (500 mg; 0.67 acrylamide bonds mmol), H_2O (1.5 mL).

MBAMP2: MBAMP oligomer (375.2 mg; 0.50 acrylamide bonds mmol), MA (55 mg; 0.63 mmol), LiOH•H_2O (92 mg; 2.17 mmol), hydrolyzate (55 mg; 0.24 hexose mmol), H_2O (1.5 mL).

MBAGD: MBAGD oligomer (500 mg; 0.70 acrylamide bonds mmol), H_2O (1.5 mL).

MBAGD1: MBAGD oligomer (375.2 mg; 0.53 acrylamide bonds mmol), MA (10 mg; 0.12 mmol), LiOH•H_2O (59.35 mg; 1.4 mmol), AcGGM (100 mg; 0.52 hexose mmol), H_2O (2 mL).

MBAGD2: MBAGD oligomer (375.2 mg; 0.53 acrylamide bonds mmol), MA (55 mg; 0.63 mmol), LiOH•H_2O (92 mg; 2.17 mmol), hydrolyzate (55 mg; 0.24 hexose mmol), H_2O (1.5 mL).

Synthesis of PAA-AcGGM hydrogel AcGGM1. AcGGM1 was prepared by dissolving AcGGM (150.9 mg; 0.78 hexose mmol) and NaOH (102.7 mg; 2.51 mmol) in H_2O (2.5 mL) at 40°C for 20 min. MBA (194.5 mg; 1.25 mmol) was then added under stirring and the mixture reacted at 25°C for 20 hours. The hydrogel was washed with deionized H_2O

(200 mL) for 48 hours renewing the solvent at regular time intervals and dried until constant weight. Yield: 0.26 g, 57.1%.

Results and discussion

The aim of this work was to demonstrate the feasibility of using differently purified hemicellulose fractions, isolated from hydrothermal treatments of spruce wood, for preparing hybrid hydrogels with poly(amidoamine)s (PAAs) and methacrylic acid (MA). The PAA portions of the hydrogels stemmed from the polyaddition of the cheap N,N'-methylenebisacrylamide with either 2-methylpiperazine (MBAMP, Scheme 20) or a mixture of glycine and N,N'-dimethylethylenediamine as amine counterparts (MBAGD, Scheme 20). MBAMP and MBAGD represent models of cost-effective either cationic or amphoteric PAAs. The synthetic pathway consisted of two steps. First, acrylamide-end-capped PAA oligomers were prepared employing a controlled excess of acrylamide, freeze-dried and recovered as fine powders (Scheme 20).

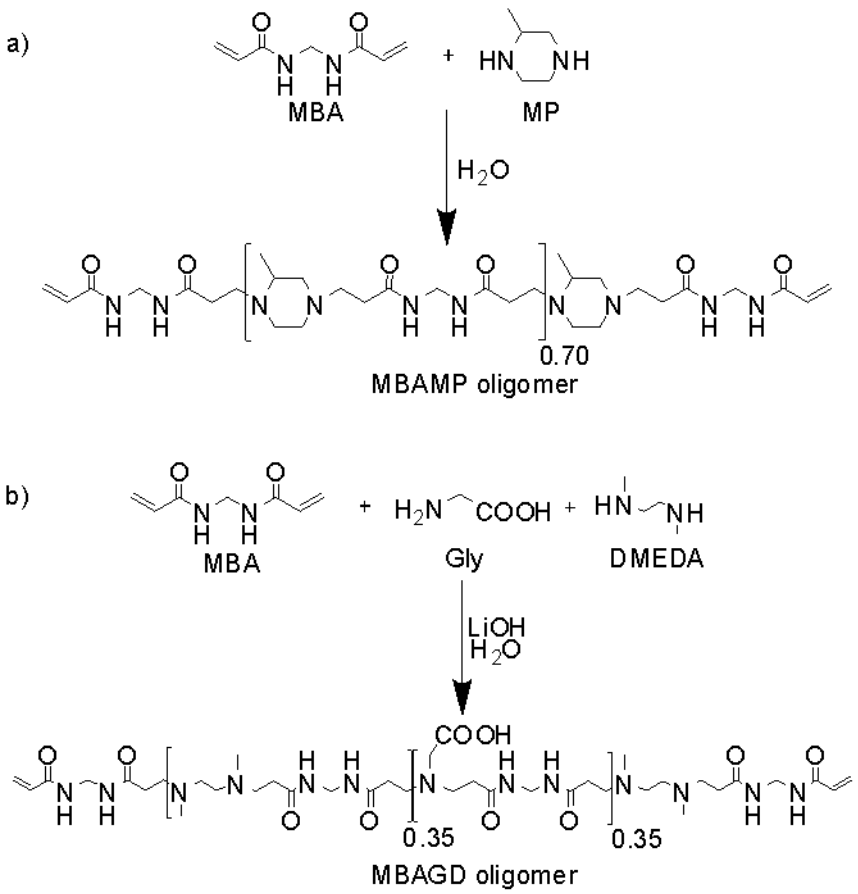

Scheme 20. Syntheses of acrylamide-end-capped PAA oligomers.

In the second step MA was grafted onto either AcGGM or spruce hydrolyzate in water using the metabisulfite/ammonium peroxydisulfate redox system as initiator, and reacted with either MBAMP or MBAGD as crosslinkers. The mechanism proposed for the copolymerization of MA in the presence of AcGGM and PAA oligomers is reported in Scheme 21. It is known for many polysaccharides that the radicals resulting from the radical initiator generate active centers on the substrate abstracting hydrogens from the hydroxyl groups to form alkoxy radicals. [19] These active centers radically initiate the polymerization of MA and when a crosslinking agent is present in the system, *e. g.* MBAMP or MBAGD, the final product is a hydrogel. In this system, the redox couple may initiate also MA polymerization, not contributing to the crosslinking density of the network therefore affecting the soluble content of the hydrogels.

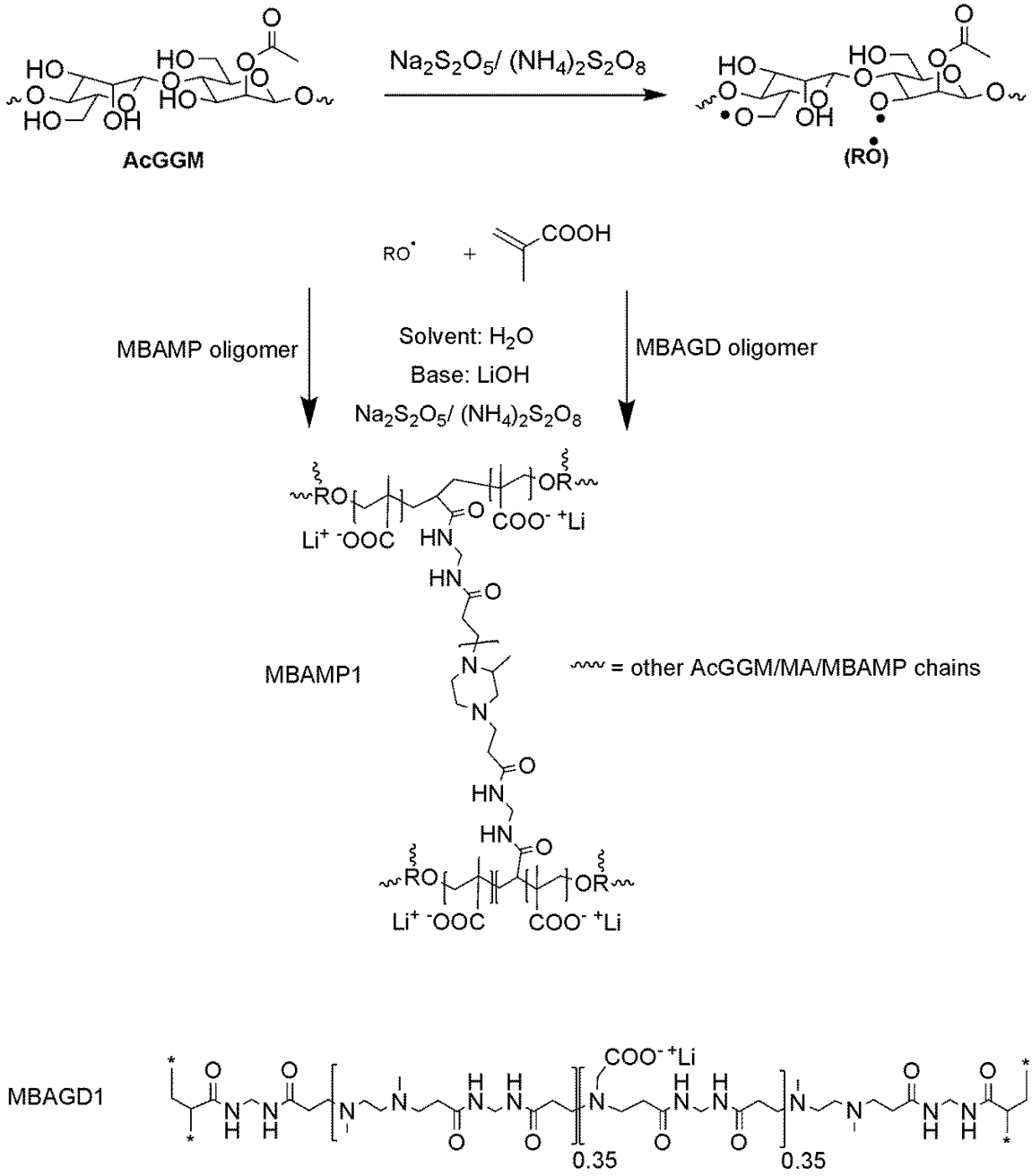

Scheme 21. Scheme of the PAA-MA-AcGGM and PAA-MA-Hydrolyzate hydrogel preparation. As an example, the preparation of MBAMP1 is reported.

Following this synthetic pathway two PAA-MA-AcGGM and two PAA-MA-Hydrolyzate hydrogels were obtained, namely MBAMP1, MBAGD1 and MBAMP2, MBAGD2, respectively. Their behavior was compared with that of the corresponding "homopolymeric" PAA hydrogels prepared under the same conditions but in the absence of either MA and AcGGM (MBAMP and MBAGD). Due to the solubility limit of AcGGM, its amount in the feeding was equal to 20.6%$^{w}/_{w}$ for both MBAMP1 and MBAGD1 (Table). The same applied for spruce hydrolyzate whose amount was equal to

11.3%$^{w}/_{w}$ for both MBAMP2 and MBAGD2 (Table). The PAA content in the feeding was always around 77%$^{w}/_{w}$ and the overall concentration of solids 25% (see Experimental). Polymerization experiments were also carried out with either PAA/AcGGM or PAA/MA mixtures, but resulted in poor products. The former, produced viscous seemingly uncross-linked mixtures which gave clear signs of degradation for prolonged reaction times. The latter turned into hard and apparently highly cross-linked solids with low, if any, water swelling ability. For this reason, the use of mixtures containing all of the three components (PAA, MA and either AcGGM or hydrolyzate) was necessary to obtain covalently cross-linked hydrogels able to swell in water. As a reference, an hydrogel without MA and PAA was prepared reacting AcGGM and MBA in water at pH≈11 (Table 21).

Table 21. Amounts of reagents used in the syntheses of PAA-MA-AcGGM and PAA-MA-Hydrolyzate hydrogels.

Sample	**Hexose units/MA/PAA acrylamide terminals [molar ratio]**	**AcGGM content[a] [%]**	**MA content[a] [%]**	**PAA content[a] [%]**
MBAMP	0/0/1	0.0	0.0	100.0
MBAMP1	1.04/0.24/1	20.6	2.1	77.3
MBAMP2	0.48/1.26/1	11.3	11.3	77.4
MBAGD	0/0/1	0.0	0.0	100.0
MBAGD1	1/0.23/1	20.6	2.1	77.3
MBAGD2	0.45/1.19/1	11.3	11.3	77.4
AcGGM1	1/1.60[b]	43.7	0	56.3[c]

[a] in the feed; [b] hexose/MBA ratio; [c] MBA content

All hydrogel samples, irrespective of the synthetic pathway adopted, were purified by extensive washing with water, dried and analyzed by elemental analysis (Table 22). The C/N ratio values were always higher than those of the reference homopolymeric PAA hydrogels (either MBAMP or MBAGD), consistent with the presence of polyMA and AcGGM in the hydrogel structure. Moreover, the found C/N ratio values were in all cases slightly lower than the expected ones, indicating a preferential release of linear AcGGM and polyMA in the extraction process. The N% values allowed for the calculation of the PAA content in the hydrogels and to compare it with feed data (Table 21).

Table 22. Results of the elemental analysis for all of the hydrogels.

Sample	C%		N %		C/N		PAA[a] [%$^{w}/_{w}$]	
	calc.[a]	found	calc.	found	calc.	found	feed[a]	found[b]
AcGGM	48.83	-	-	-	-	-	-	-
AcGGM1	51.80	42.38	10.63	7.83	4.87	5.41	56.3[c]	43.12 [c]
MBAMP	56.10	50.59	21.19	19.74	2.65	2.56	100	96.6
MBAMP1	50.37	48.47	15.59	15.99	3.23	3.03	77.3	81
MBAMP2	50.50	46.49	15.29	14.96	3.29	3.11	77.4	76
MBAGD	51.59	47.91	20.18	21.17	2.56	2.26	100	88.3
MBAGD1	48.26	45.96	16.72	16.52	2.88	2.78	77.3	78
MBAGD2	48.22	44.42	16.40	15.20	2.94	2.92	77.4	71.8

[a]feeding data from Table 1 and 2, [b] calculated values, [c] MBA content, [d] not determined.

The structural characterization of the synthesized hydrogels was performed by FTIR spectrophotometry. Spectra of PAA-MA-AcGGM (MBAMP1 and MBAGD1) and PAA-MA-Hydrolyzate (MBAMP2 and MBAGD2) hydrogels showed intense diagnostic bands typical of the PAA pattern, such as the amide C=O stretching (1642 cm^{-1} for MBAMP1, 1637 cm^{-1} for MBAGD1), N-H bending and C-N stretching overlapped with carboxylate C=O symmetric stretching of polyMA $–COO^-$ at 1529 cm^{-1} for MBAMP1 and 1528 cm^{-1} for MBAGD1, which prevail over the remaining portion of the spectra. Asymmetric $–COO^-$ stretching are also visible at 1446 cm^{-1} for MBAMP1-2 and 1454 cm^{-1} for MBAGD1-2. Due to the low AcGGM content, C-O-C stretching are hardly detectable at 1072 cm^{-1} and 1040 cm^{-1} for MBAMP1-2 and 1071 cm^{-1} and 1039 cm^{-1} for MBAGD1-2. C-O-C splitting is here due to the presence of ramifications on the -C- atoms next to -O- that, due to synthetic strategy adopted, cannot be excluded nor controlled. [34] In this frequency range *tert*-amine C-N stretching are also present. Methylene chains gave rise to C-H stretching bands in the 2970-2800 cm^{-1} region and to scissoring in the 1350-1480 cm^{-1} range. The broad band typical of –OH stretching at 3264 cm^{-1} is also clearly visible, overlapped with amides N-H stretching.

In contrast to what observed in the case of PAA-MA-AcGGM and PAA-MA-Hydrolyzate hydrogels, the FTIR spectra of AcGGM1 (Figure 49) showed very strong C-O stretching bands at 1025 cm^{-1} due to AcGGM besides the diagnostic bands typical for MBA. This accounts for the higher AcGGM content. The band at 809 cm^{-1} is originated from AcGGM C-C stretching while that at 882 cm^{-1} can be attributed to residual alkene deformation.

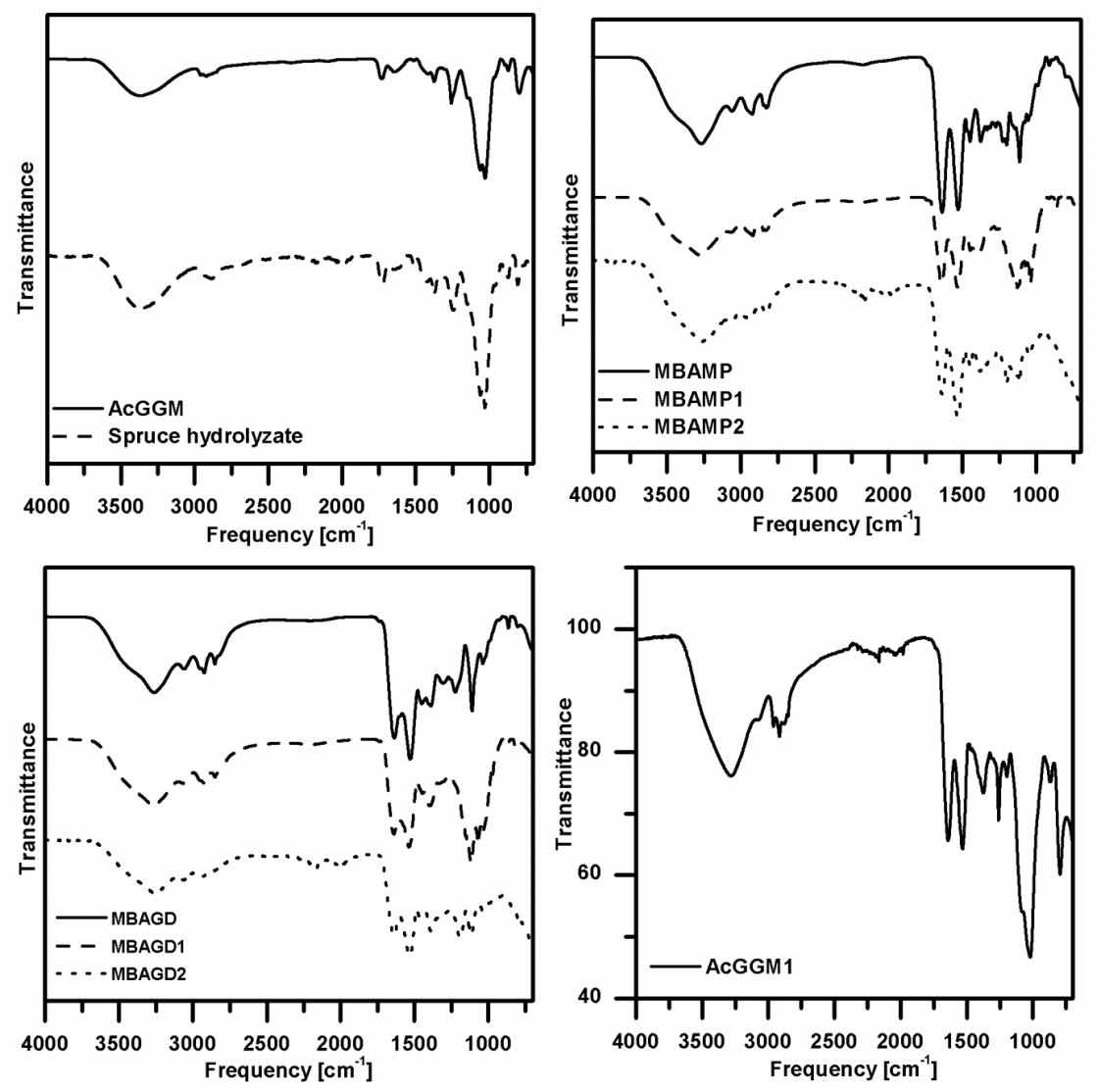

Figure 49. FTIR spectra for PAA, PAA-MA-AcGGM, PAA-MA-Hydrolyzate, AcGGM1 hydrogels and AcGGM and spruce hydrolyzate as references.

All hydrogels were thermally characterized by means of DSC and TG analyses. The DSC second run heating cycle, following a cooling cycle carried out at the same rate, is reported in Figure 50. For comparison purposes, thermograms of the reference materials are also reported. All samples showed no evidence of glass transition temperatures or melting phenomena, in agreement with the behavior of both reference PAA hydrogels and AcGGM. A substantial thermal stability was observed in the temperature range investigated, with no dramatic decomposition events.

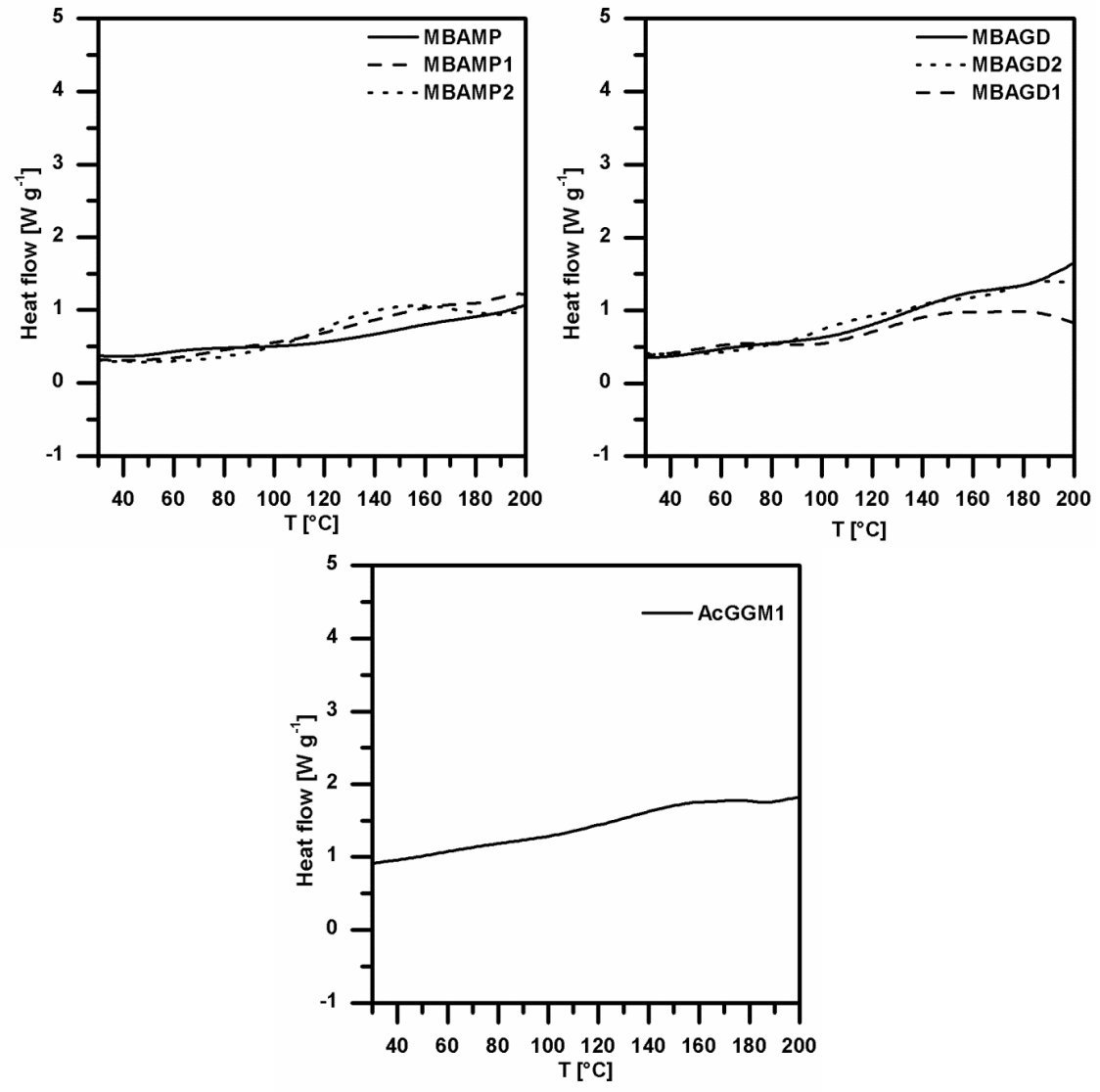

Figure 50. DSC second run curves for PAA, PAA-MA-AcGGM and PAA-MA-Hydrolyzate hydrogels.

The thermal behaviors of PAA-MA-AcGGM and PAA-MA-Hydrolyzate hydrogels samples were confirmed by thermogravimetric analysis. The results of the TG analyses are shown in Table 23. The TGA curves of the hydrogels (Figure 51) were characterized by weight losses due to dehydration at 100 °C and main thermal decompositions in the range 200-450 °C, with residual masses down to 13.7%. The introduction of AcGGM and MA in the reaction mixture apparently increased the thermal stability with respect to the "homopolymeric" PAA hydrogels. In fact, in most cases the weight losses of PAA-MA-AcGGM and PAA-MA-Hydrolyzate were lower than those of MBAMP and MBAGD. For AcGGM1 (Figure 51) the main degradation occurred between 250 °C and 450 °C with residual masses down to 21.3%.

These results revealed that all of the samples were stable at temperatures up to 200 °C.

Table 23. Results of the TG analyses. T_{max} represents the temperature of the highest weight loss rate.

Sample	**Dehydration (T=100 °C)**	**Main decomposition stage**		**Residual weight at 600 °C [%]**
	Weight loss [%]	T_{max} [°C]	Weight loss [%]	
MBAMP	0.5	285.6	76	18.5
MBAMP1	0.1	280	70.7	23.3
MBAMP2	1.2	282.8	74.9	13.7
MBAGD	0.2	300.4	77.4	17.7
MBAGD1	0.1	300.4	70.6	23
MBAGD2	0.5	271.7	65.8	23.1
AcGGM1	1.3	290.5	68.2	21.3

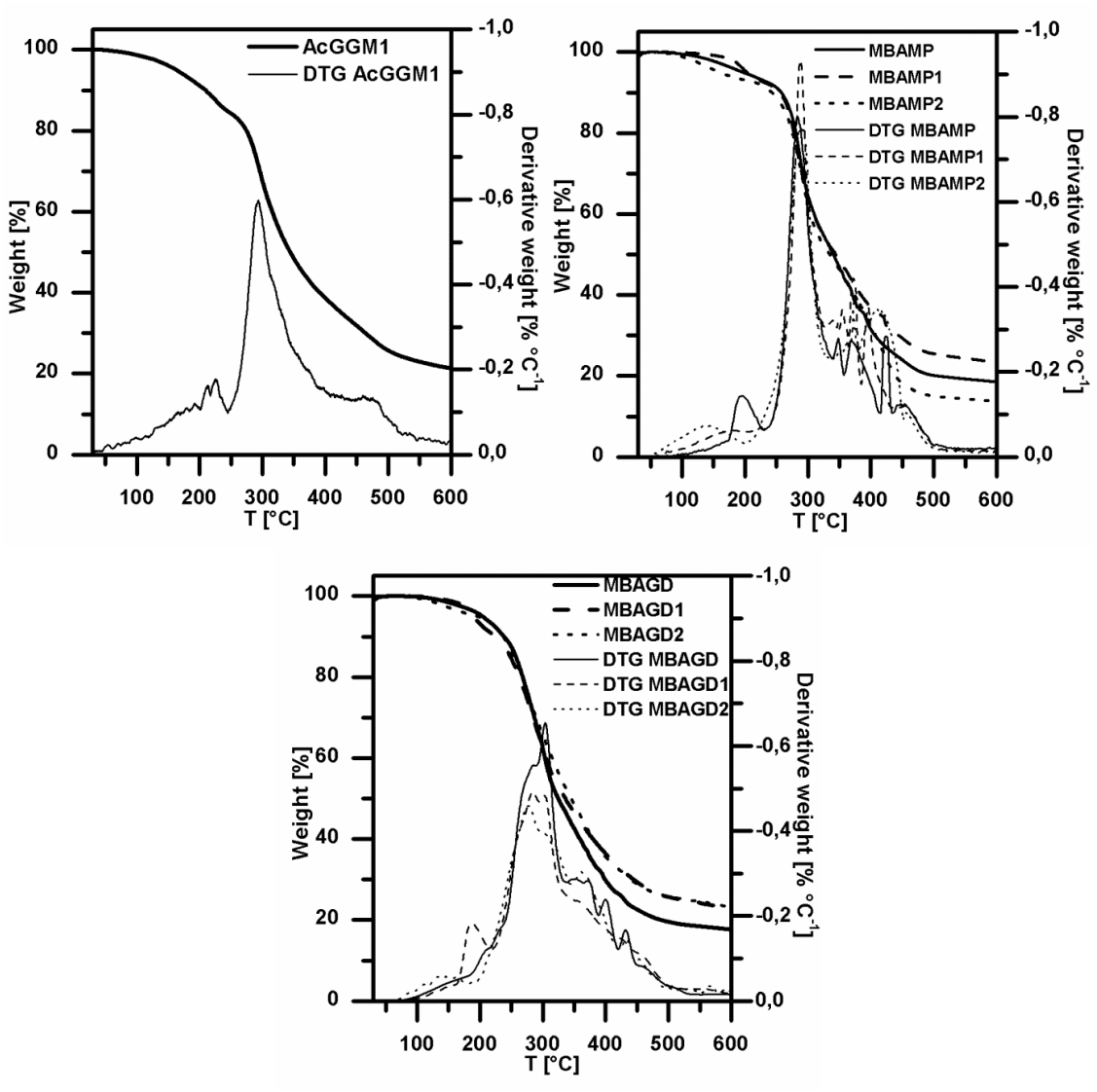

Figure 51. TGA thermograms for AcGGM1, PAA-MA-AcGGM and PAA-MA-Hydrolyzate hydrogels.

The swelling behavior of the synthesized hydrogels was evaluated in water and buffers at pH 2 and 9 (Figure 52). PAA-MA-AcGGM hydrogels were more swellable in aqueous media than PAA-MA-Hydrolyzate hydrogels. This might be ascribed to the higher crosslink density. Furthermore, all hydrogels containing MA and either AcGGM or hydrolyzate swelled more than both AcGGM1 and "homopolymeric" PAA hydrogels MBAMP and MBAGD. This effect might be attributed to the hydrophilic nature of AcGGM and to the presence of carboxylic groups on the polyMA chains. All hydrogels showed larger swelling in water than in buffer solutions, probably due to their higher ionic strength.

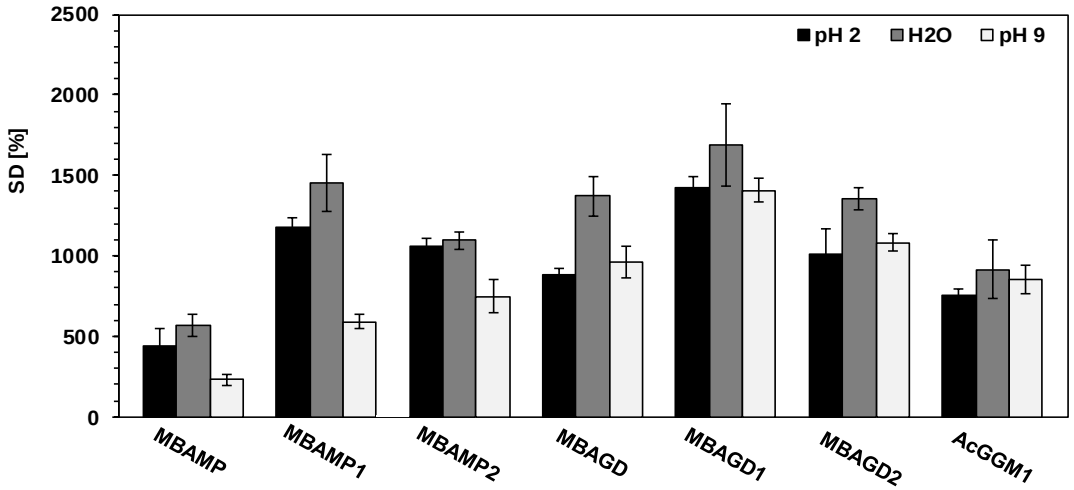

Figure 52. Swelling behavior of hydrogels of different compositions. The percentage swelling degrees are reported on y-axis in water, pH 2 and pH 9.

All hydrogel samples appeared as highly swollen, soft and pliable materials, which could be easily handled but did not withstand large stresses. They were characterized by dynamic mechanical analysis in the shear stress mode, within the frequency sweep in the range 0-100 rad/sec and with an applied 0.2 N compressive force. The observed trends of the storage and loss modulus versus frequency are reported in Figure 53. The storage modulus (G') and loss modulus (G'') values are summarized in Table 24. All samples showed very low G' values, consistent with the low compressive force applied. In all cases, the storage modulus was higher than the loss modulus (G'') over the entire frequency range, indicating that the elastic response of the materials prevailed over the viscous one, and that they displayed a solid-like behavior. MBAMP hydrogels showed higher moduli than MBAGD hydrogels, consistent with the observed higher hydrophilicity and swellability of the latter glycine-containing PAAs. PAA-MA-AcGGM hydrogels showed lower moduli that PAA-MA-Hydrolyzate hydrogels, consistent with the swelling degrees. The same applies to AcGGM1.

Table 24. Shear storage moduli for PAA-MA-AcGGM hydrogels (prepared via route 1) and PAA-AcGGM hydrogels (prepared via route 2).

Sample	**G' [KPa]**	**G'' [KPa]**
MBAMP	24.0	0.3
MBAMP1	4.0	0.2
MBAMP2	10.8	3.7
MBAGD	0.7	0.02
MBAGD1	0.2	0.006
MBAGD2	3.9	0.2
AcGGM1	7.1	0.6

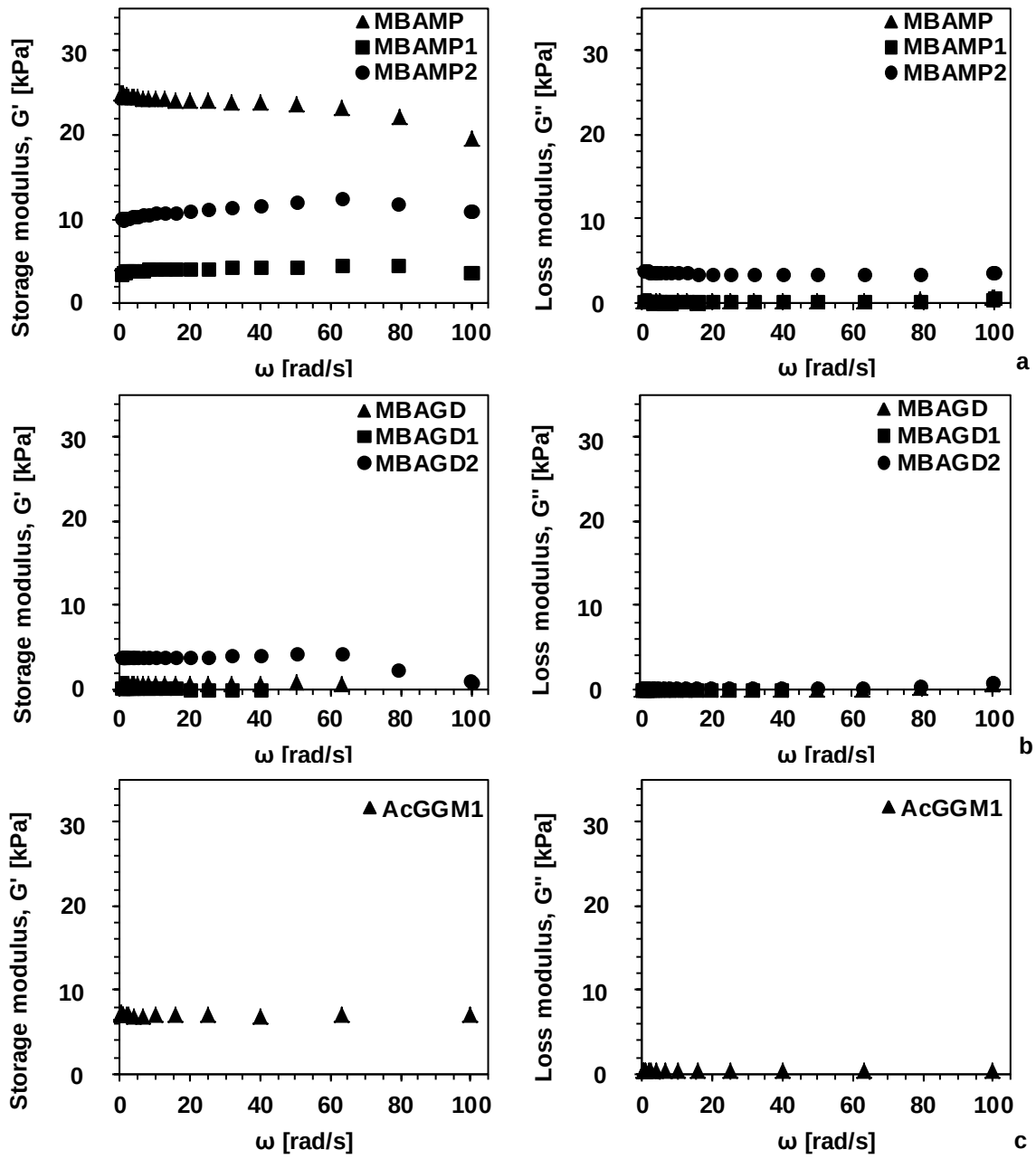

Figure 53. Shear storage and loss moduli at 0.2 N compressive force for PAA-MA-AcGGM (MBAMP1, MBAGD1), PAA-MA-Hydrolyzate (MBAMP2, MBAGD2) hydrogels and AcGGM1.

Preliminary investigations concerning the heavy metal ion absorption capacity of the hydrogels were carried out in batch, by incubating swollen hydrogel samples with single heavy metal ion aqueous solutions until equilibrium concentrations were achieved. The initial and final ion concentrations of Cd^{2+}, Pb^{2+}, Zn^{2+}, Ni^{2+}, Cu^{2+} and Co^{2+} were determined via complexometric titration with ethylenediaminetetraacetic acid (EDTA) while CrO_4^{2-} was determined by UV-vis spectrophotometry. A first series of absorption

tests was carried out in 700 ppm single metal aqueous solutions in order to determine the hydrogel absorption capacity (Figure 54). The abatement percentage was calculated as follows:

$$A\,[\%] = \frac{\text{Absorbed } Me^{2+}\,[mg]}{\text{Initial } Me^{2+}\,[mg]} \times 100 \qquad \text{Equation 2}$$

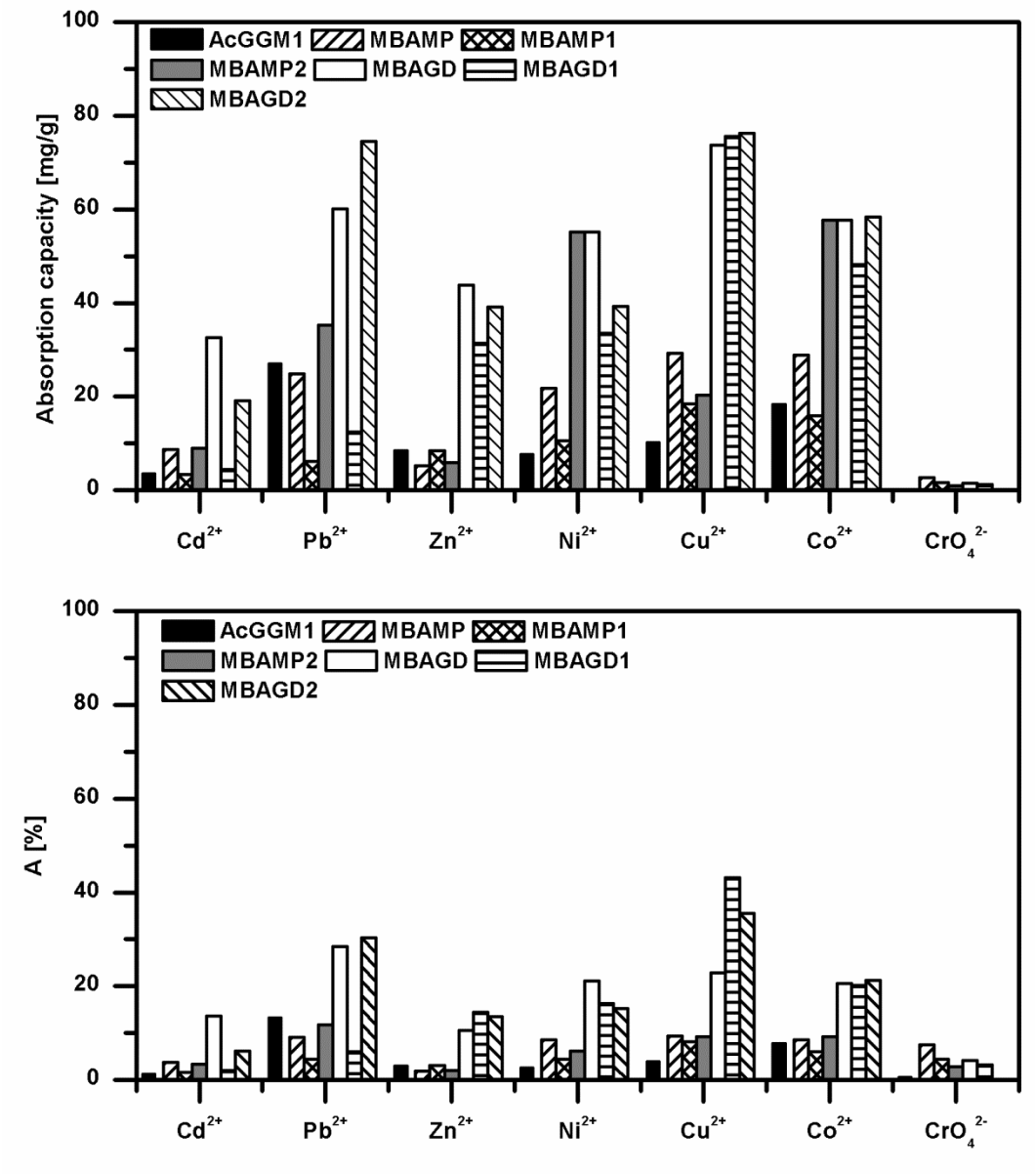

Figure 54. Absorption capacities and abatements of AcGGM1, PAA-MA-AcGGM and PAA-MA-Hydrolyzate hydrogels at an initial metal ion concentration of 700 ppm.

Several relevant correlations between the observed capacities and the peculiar structural features of hydrogels were identified. The ion absorption capacities varied dramatically by varying the amine composition and was mainly driven by the PAA content. In particular, glycine-containing hydrogels (MBAGD, MBAGD1 and MBAGD2) exhibited higher Me^{2+} complexing ability than the remaining hydrogels, suggesting a cooperative effect of the amine and carboxyl functions in ion complexation (Figure 54). For the same reason, MBAMP and MBAGD showed lower complexing abilities than MBAMP2 and MBAGD2, respectively, due to the higher $–COO^-$ content of these last two. In general, the order of absorption affinity towards Me^{2+} was $Cu^{2+}>Co^{2+}>Zn^{2+}\approx Ni^{2+}>Pb^{2+}>Cd^{2+}$, almost in agreement with the stability constants for amine complexes. [35]

The absorption performance of the hydrogels towards the negatively charged noxious pollutant CrO_4^{2-} was studied. CrO_4^{2-} was absorbed by AcGGM1, MBAGD, PAA-MA-AcGGM and PAA-MA-Hydrolyzate hydrogels to a less extent than MBAMP hydrogel, model of a cationic PAA, probably due to the lower PAA content and to the presence of AcGGM and $–COO^-$ groups of polyMA chains, that did not significantly contribute to the absorption of the negatively charged ions. For these reasons, CrO_4^{2-} abatement percentages of MBAMP series were higher than those of MBAGD series.

As shown in Figure 55, in some cases and particularly with Cu^{2+}, Ni^{2+} and Co^{2+}, the sorption process resulted in intense and fast coloring (blue, green and pink, respectively). This feature may be in principle exploited in diagnostic kits or adopted as indicator of the degree of exhaustion and, therefore, of the regeneration timing, if the hydrogels are used for water purification.

Figure 55. Color changes of MBAGD1 (a) and MBAMP1 (b) upon Cu^{2+}, Ni^{2+} and Co^{2+}absorption. Native resins on the left.

In the case of Cd^{2+}, Pb^{2+} and CrO_4^{2-}, the performance of all hydrogels was investigated also in the low concentration range, in order to identify their potential for ion abatement in dilute solutions. Absorptions from Cd^{2+} and Pb^{2+} 50 ppm single metal solutions and 4 ppm CrO_4^{2-} solutions demonstrated that the hydrogel complexing ability strongly depended on the metal ion concentration since the percent absorption decreased though without following a regular trend (Figure 56).

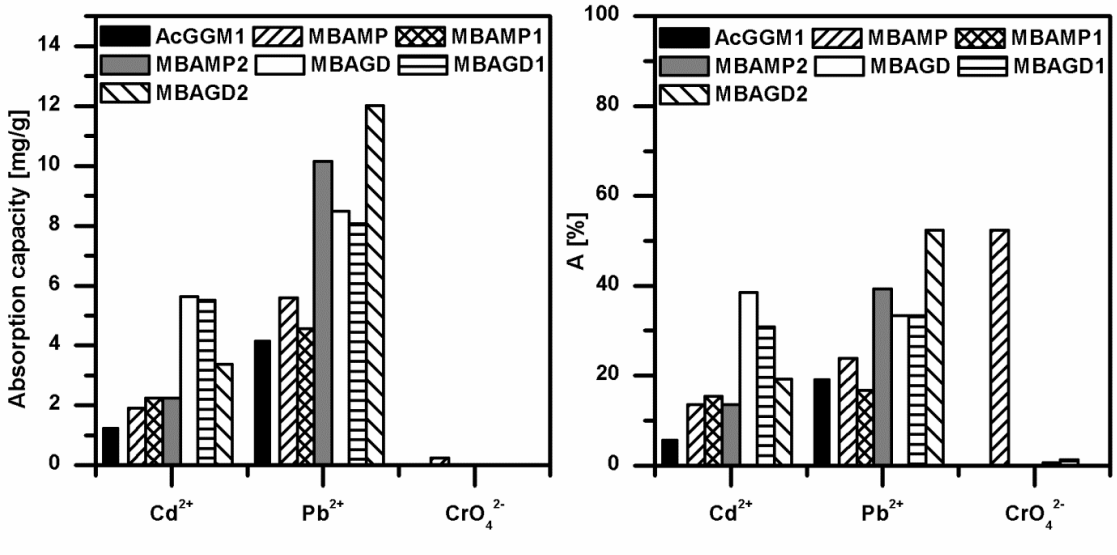

Figure 56. Absorption capacities and abatements of AcGGM1, PAA-MA-AcGGM and PAA-MA-Hydrolyzate hydrogels at an initial metal ion concentration of 50 ppm for Cd^{2+} and Pb^{2+} and 4 ppm for CrO_4^{2-}.

For PAA-MA-AcGGM and PAA-MA-Hydrolyzate hydrogels the abatement of Cd^{2+} varied between 12 to 38.5% whereas the Pb^{2+} abatement ranged from 16 to 52% (Figure 56). The most efficient series was MBAGD, containing dissociated glycine in the polymer chain, while AcGGM1 hydrogel showed lower abatements. The absorption capacities obtained were in some cases quite competitive with those of other materials reported in literature. [36] [37] [16] In the case of CrO_4^{2-} the abatement percentages were significant for MBAMP (52.4%) and lower for MBAGD (0.64%) and MBAGD1 (1.33%) while the remaining products showed no absorption towards CrO_4^{2-} in such diluted solutions.

Conclusions

Hybrid hydrogels were obtained by reacting softwood hemicellulose, either highly purified (AcGGM) or less fractionated (hydrolyzate), with poly(amidoamine)s (PAAs) and methacrylic acid (MA) by graft polymerization of MA onto AcGGM or hydrolyzate, in the presence of acrylamide end-capped PAA oligomers as crosslinkers and $(NH_4)_2S_2O_8/Na_2S_2O_5$ as a radical initiator. Due to the solubility limits of both AcGGM and hydrolyzate in water, their maximum amount in the reaction mixture was equal to 20.6%$^{w}/_{w}$ and 11.3%$^{w}/_{w}$, respectively. Elemental, FTIR and mechanical analyses proved

that the cross-linked products were successfully obtained. PAA-MA-AcGGM hydrogels proved more swellable in aqueous media than PAA-MA-Hydrolyzate products, probably due to lower crosslinking degrees. As a consequence, PAA-MA-AcGGM hydrogels showed lower G' moduli than PAA-MA-Hydrolyzate products.

Preliminary studies concerning the heavy metal ions absorption capacity of all hydrogels showed that they were able to remove Cd^{2+}, Pb^{2+}, Zn^{2+}, Ni^{2+}, Cu^{2+} and Co^{2+} from aqueous solutions with absorption capacities up to 76.3 mg/g. Furthermore, they proved able to completely abate Cd^{2+} and Pb^{2+} from more diluted (50 ppm) solutions. In most cases, their absorption performances improved increasing both PAA and carboxyl groups content, albeit without following a regular trend, leading to the conclusion that the absorption was significantly driven by PAAs. The same trend was observed for the removal of Cr^{6+} as CrO_4^{2-}. In this case, the sorption of the negatively charged ions was mainly driven by the amine groups on PAA chains. Overall, the absorption capacities shown were in some cases quite competitive with those of other sorbents reported in literature. [16] Moreover, the absorption of several metal ions imparted intense coloring to the resins, a feature exploitable for analytical purposes such as real-time detection of the presence of ions. All hydrogels were obtained at moderate cost by eco-friendly procedures according to a synthetic process characterized by potential scalability and environmental sustainability, and employing a renewable resource such as the purified AcGGM and its less fractionated form, spruce hydrolyzate. The results obtained that let envisage a high potential for the design of different hemicellulose-based materials with interesting functional properties.

Acknowledgments

The Swedish research council FORMAS (project nr. 2011-1542) is thanked for financial support.

References

[1] L. Yu, K. Dean, L. Li, *Prog. Polym. Sci.*, vol. 31, pp. 576-602, 2006.

[2] E. Abdel-Halim, S. S. Al-Deyaba, *Carbohyd. Polym.*, vol. 86, pp. 1306-1312, 2011.

[3] C. S. Willför, K. Sundberg, M. Tenkanen, B. Holmbom, *Carbohyd. Polym.*, vol. 72, pp. 197-210, 2008.

[4] N. M. L. Hansen, D. Plackett, *Biomacromolecules*, vol. 9, p. 1493.1505, 2008.

[5] J. Hartman, A. C. Albertsson, J. Sjöberg, *Biomacromolecules,* vol. 7, pp. 1983-1989, 2006.

[6] J. Hartman, A. C. Albertsson, M. Söderqvist Lindblad, J. Sjöberg, *J. Appl. Polym. Sci.,* vol. 100, pp. 2985-2991, 2006.

[7] Y. Z. Ryberg, U. Edlund, A. C. Albertsson, *Biomacromolecules,* vol. 12, pp. 1355-1362, 2011.

[8] J. J. Nigam, *Biotechnol.,* vol. 97, pp. 107-116, 2002.

[9] B. C. Saha, *J. Ind. Microbiol. Biot.,* vol. 30, pp. 279-291, 2003.

[10] J. Voepel, U. Edlund, A. C. Albertsson, *J. Polym. Sci. A Polym. Chem.,* vol. 47, pp. 3595-3606, 2009.

[11] M. Söderqvist Lindblad, A. C. Albertsson, E. Ranucci, M. Laus, E. Giani, *Biomacromolecules,* vol. 6, pp. 684-690, 2005.

[12] J. Yang, X. S. Zhou, J. Fang, *Carbohyd. Polym.,* vol. 86, pp. 1113-1117, 2011.

[13] X. F. Sun, H. Wang, Z. Jing, R. Mohanathas, *Carbohyd. Polym.,* vol. 92, pp. 1357-1366, 2013.

[14] M. Söderqvist Lindblad, E. Ranucci, A. C. Albertsson, *Macromol. Rapid Commun.,* vol. 22, pp. 962-967, 2001.

[15] J. Voepel, J. Sjöberg, M. Reif, A. C. Albertsson, U. K. Hultin, U. Gasslander, *J. Appl. Polym. Sci.,* vol. 112, pp. 2401-2412, 2009.

[16] G. Crini, *Progr. Polym. Sci.,* vol. 30, pp. 38-70, 2005.

[17] G. M. Patel, C. P. Patel, H. C. Trivedi, *Eur. Polym. J.,* vol. 35, pp. 201-208, 1999.

[18] G. Gurdag, M. Yasar, M. A. Gurkaynak, *J. Appl. Polym. Sci.,* vol. 66, pp. 929-934, 1997.

[19] X.-W. Peng, J.-L. Ren, L.-X. Zhong, F. Peng, R.-C. Sun, *J. Agr. Food Chem.,* vol. 59, pp. 8208-8215, 2011.

[20] X.-W. Peng, L.-X. Zhong, J.-L. Ren, R.-C. Sun, *J. Agr. Food Chem.,* vol. 60, pp. 3909-3916, 2012.

[21] Z. L. Liu, H. Hu, R. X. Zhou, *J. Polym. Sci., Part A: Polym. Chem.,* vol. 42, pp. 4370-4378, 2004.

[22] G. R. Mahdavinia, A. Pourjavadi, H. Hosseinzadeh, M. J. Zohuriaan, *Eur. Polym. J.,* vol. 40, pp. 1399-1407, 2004.

[23] A. Pourjavadi, A. M. Harzandi, H. Hosseinzadeh, *Eur. Polym. J.,* vol. 40, pp. 1363-1370, 2004.

[24] G. Gurdag, M. Yaşar, M. A. Gurkaynak, *J. Appl. Polym. Sci.,* vol. 66, pp. 929-934, 1997.

[25] V. V. Panic, Z. P. Madzarevic, T. Volkov-Husovic, S. J. Velickovic, *Chem. Eng. J.,* vol.

217, pp. 192-204.

[26] N. B. Milosavljević, M. Đ. Ristić, A. A. Perić-Grujić, J. M. Filipović, S. B. Štrbac, Z. L. Rakočević, M. T. Kalagasidis Krušić, *Colloid. Surface A*, vol. 388, pp. 59-69.

[27] P. Ferruti, *J. Polym. Sci. Pol. Chem.*, vol. 51, pp. 2319-2353, 2013.

[28] P. Ferruti, E. Ranucci, S. Bianchi, L. Falciola, P. R. Mussini, M. Rossi, *J. Polym. Sci. Part A: Polym. Chem.*, vol. 44, pp. 2316-2327, 2006.

[29] P. Ferruti, E. Ranucci, A. Manfredi, N. Mauro, E. Ferrari, R. Bruni, F. Colombo, P. Mussini, M. Rossi, *J. Polym. Sci. Part A: Polym. Chem.*, vol. 50, pp. 5000-5010, 2012.

[30] A. Manfredi, E. Ranucci, S. Morandi, P. R. Mussini, P. Ferruti, *J. Polym. Sci. Part A: Polym. Chem.*, vol. 51 , pp. 769-773, 2013.

[31] O. Dahlman, A. Jacobs, A. Liljenberg, A. I. Olsson, *J. Chromatogr.*, vol. 891, pp. 157-174, 2000.

[32] A. Jacobs, O. Dahlman, *Biomacromolecules*, vol. 2, pp. 894-905, 2001.

[33] S. D. A., D. M. West, Complex-formation titrations. Fundamentals of Analytical Chemistry, 3rd , Holt-Saunders International Edition, 1976, pp. 272-285.

[34] R. Silverstein, F. Webster, Spectroscopic Identification of Organic Compounds, 6th, J. Wiley Publisher , 1998.

[35] Stability constants for Metal-ion complexes, London: The Chemical Society, 1964.

[36] S. K. R. Yadanaparthi, D. Graybill, R. von Wandruszka, *J. Hazard. Mater.*, vol. 171, pp. 1-15, 2009.

[37] K. G. Bhattacharyya, S. S. Gupta, *Adv. Colloid Interfac.*, vol. 140, pp. 114-131, 2008.

[38] S. Babel, T. A. Kurniawan, *J. Hazard. Mater.*, vol. B97, pp. 219-243, 2003.

[39] F. Fu, Q. Wang, *J. Environ. Manage.*, vol. 92, pp. 407-418, 2011.

CHAPTER 4

SYNTHESIS AND CHARACTERIZATION OF GUAR GUM/POLY(AMIDOAMINE) HYDROGELS

Introduction

Heavy metals into aquatic ecosystem have become a matter of attention due to their toxicological effects. Numerous studies concerning their removal from aqueous solutions have been attempted.

Chemical precipitation is one of the most common conventional treatment methods adopted but it requires large excess of chemicals and generates volumetric sludge increasing the cost. Other available treatment technologies such as ion exchange, electrolysis and reverse osmosis require high capital investment and running cost. Absorption provides an attractive alternative for the treatment of contaminated water, especially if the adsorbent is not expensive and does not require any additional pre-treatment step before its application. It has been found superior compared to the other techniques in terms of initial cost, flexibility and simplicity of design as well as ease of operation.

Employing as sorbents renewable resources such as agricultural and industrial by-products with little or no economic value, produced in large quantities, that often represent a disposal problem, would open a new market for these by-products and they could be used for treating contaminated water. [1]

Hydrogels, polymeric three-dimensional networks known to swell in aqueous solutions that can find application in many different fields, can be obtained from renewable resources such as, for example, cellulose, chitosan, starch and agricultural wastes. These materials have spurred great interest in various biomedical, industrial and environmental applications. [2] [3] [4] [5] [6] [7] [8]

Guar gum (GG) is a hydrophylic, non-ionic polysaccharide extracted from the endospermic seed of the plant *Cyamopsis tetragonalobus*. GG belongs to the large family of galactomannans and consists of a D-galacto-D-mannan which hydrates in cold water to form a highly viscous solution where the single polysaccharide chains interact with each other in a complex way. [9] Since GG is a low-cost, easily available and non-toxic polysaccharide, it is widely applied in many industrial fields. [10] In particular, thanks to its property of producing highly viscous aqueous solutions, GG is commonly used as a thickening agent in cosmetics and food industry. To enhance its application spectrum, GG modification has been reported by various methods such as grafting, derivatization, and

network formation. [1] [11] The chemical cross-linking of GG has been performed with glutaraldehyde, phosphating agents, polyethylene glycol diglycidyl ether and, in some instances, in combination with polyacrylic acid in order to obtain polyelectrolyte hydrogels with mouldable physical properties. [11] [12] [13] [14] As for other carbohydrates, GG-containing hydrogels can be also prepared via Michael-type polyaddition of the polysaccharide to monomers bearing activated double bonds at pH≥11. [15] Under these conditions, GG acts as a multifunctional monomer via its hydroxyl groups leading to the formation of crosslinked products.

Poly(amidoamine)s (PAAs) constitute a family of biodegradable, biocompatible, hence environmental friendly synthetic polymers prepared in aqueous solution, at room temperature and with no added catalysts or organic solvents. [16] Crosslinked PAAs, prepared using multifunctional amines as crosslinking agents, are normally highly hydrophilic give rise to hydrogels in aqueous media. The ability of linear PAAs to form coordination complexes with heavy metal ions [16] is shared by crosslinked PAAs, which proved able to quantitatively and reversibly adsorb many different heavy metal ions, including Cu^{2+}, Cd^{2+}, Pb^{2+}, Zn^{2+}, Ni^{2+}, $Mn^{2+}$and Co^{2+} from aqueous solutions. [16] [17] [18] [19]

If GG is reacted in aqueous solution at pH≥11with mixtures of amines and bisacrylamides, cross-linked products where GG chains are bridged by PAA moieties can be readily obtained.

This chapter reports on the preparation and characterization of a family of GG-PAA hydrogels synthesized by Michael addition of GG and amines to either N,N'-methylenebisacrylamide (MBA) or 2,2-bisacrylamidoacetic acid (BAC) at pH>11 in water. Structure and properties of the hydrogels were determined by Fourier-transform infrared spectroscopy (FTIR), elemental analysis, thermal measurements and mechanical studies. Additionally, with the aim of a potential application in the environmental field, preliminary results on the sorption of heavy metal ions such as Cu^{2+}, Cd^{2+}, Zn^{2+}, Ni^{2+} and Co^{2+} from aqueous solutions are also reported, together with the sorption performances after repeated sorption-desorption cycles.

Experimental

Materials

Solvents and reagents, unless otherwise indicated, were analytical-grade commercial products and were used as received. N,N'-methylenebisacrylamide (MBA) (96%) was obtained from Acros Organics. Guar gum (GG), HCl (37%), N,N'-2-methylpiperazine (MP) (95%), L-lysine (≥97%), N,N-dimethylethylenediamine (N,N-DMEDA) (≥98%), N,N'-dimethylethylenediamine (N,N'-DMEDA) (≥98%), LiOH•H_2O (99%), (*S,S*)-Ethylenediamine-N,N′-disuccinic acid trisodium salt solution (~35%), Eriochrome Black T®, Murexide, ethanol (>99.8%) were supplied by Sigma Aldrich.

Methods

FTIR analysis. The hydrogels were dried under vacuum to constant weight and the FTIR spectra were collected using a Perkin Elmer spectrometer 2000. All spectra were calculated as means of 16 individual scans at 2 cm^{-1} resolution in the 4000-600 cm^{-1} interval with corrections for atmospheric water and carbon dioxide.

Thermal analyses. DSC analyses were performed on a Mettler Toledo DSC823^e on 10 mg samples, under nitrogen flow at 20 mL min^{-1}, heating/cooling rate of 20 °C min^{-1}. Standard aluminium sample pans (Perkin-Elmer) were used and an empty pan was used as reference standard. A first heating cycle from 25 °C to 200 °C was followed by a cooling cycle from 200 °C to 25 °C and a second heating cycle from 25 °C to 200 °C. TGA analyses were performed on a Perkin Elmer TGA 4000 on 10 mg samples under nitrogen flow at 50 mL min^{-1}, from 30 °C to 600 °C at a heating rate of 20 °C min^{-1}.

Swelling degrees. In order to examine the swelling capacity, each hydrogel was weighted in a 10 ml test tube and suspended in an excess of ethanol. It was allowed to settle (hydrogel volume at t=0: V_{to}), the supernatant was carefully removed and replaced with either H_2O or 0.01 M PBS. The solvent was then changed three times so as to remove any ethanol traces. The swelling degrees were evaluated at equilibrium according to the following equation:

$$SD\ (\%) = \frac{V_t}{V_{to}}\ x\ 100 \qquad \text{Eq. 1}$$

where V_t is the volume of the hydrogel at equilibrium and V_{to} is the volume of the dry sample.

Heavy metal ions absorption experiments. Metal ions sorption tests were carried out against Cu^{2+}, Co^{2+}, Cd^{2+}, Zn^{2+} and Ni^{2+} standardized aqueous solutions at 1000 and 50 ppm. The absorption tests were performed using 10 mg of dried hydrogel in a 10 ml tube and swelling it until equilibrium in deionized water (10 mL) for 24 hours. After this time, the supernatant was replaced with the heavy metal aqueous solution and the hydrogel was incubated in such solution for further 5 hours. The initial and the final surnatant metal concentrations were determined via complexometric titration with EDTA.[36] EDTA-Na_2 standardization: 1 x 10^{-4} M $ZnSO_4 \cdot 7H_2O$ solution was prepared with the salt previously placed under vacuum for 24 hours. The solution was added with NH_4Cl/NH_3 buffer (pH~10) until alkaline pH and titrated with a 1 x 10^{-4} M EDTA-Na_2 solution using Eriochrome® Black T as indicator. $Cd^{2+}$and Zn^{2+}aqueous solution concentrations were determined adding NH_4Cl/NH_3 buffer until alkaline pH in the presence of Eriochrome® Black T as indicator and titrating with the standardized EDTA-Na_2 solution. Ni^{2+}, Co^{2+} and Cu^{2+} were titrated according to the same procedure described for Cd^{2+} and Zn^{2+}employing Murexide as indicator. The amount of adsorbed metal ion per gram of sorbent was calculated according to Eq. 2:

$$Absorption\ capacity\ [mg\ Me^{2+}\ g^{-1}] = \frac{Me^{2+}{}_{t=0}\,[mg] - Me^{2+}{}_{t=5\ hours}\,[mg]}{Dry\ hydrogel\,[g]} \qquad \text{Eq. 2}$$

Regeneration and recycle of the hydrogels for heavy metal ions absorption. After absorption of the heavy metal ion the hydrogel was withdrawn from the solution and washed with deionized water (10 ml x 2). Thereafter, it was rinsed with 0.01 M HCl (10 ml x 2) in order to remove the adsorbed metal ions and washed again with water (10 ml x 2). The hydrogel was then reused in the absorption experiments. The absorption-desorption process was repeated 4 times and the amount of absorbed metal ion was calculated according to Eq. 2.

Synthesis of GG-PAA hydrogels. In a typical procedure, GG-MP-MBA was prepared dissolving GG (1501.8 mg; 8.34 mmol) and $LiOH \cdot H_2O$ (711.2 mg; 16.78 mmol) in H_2O (40 mL). MP (1716.6 mg; 16.28 mmol) followed by MBA (4002.2 mg; 25.7 mmol) were added and the mixture reacted for 6 days, in the dark at 25 °C. The hydrogel was soaked in deionized H_2O (100 mL), the pH lowered to 5 with HCl 37% and the product was then

extracted with ethanol (100 mL). Three H_2O/ethanol washing cycles were carried out within 48 hours. The hydrogel was then dried until constant weight. Yield: 2.93 g, 37.94%.

Hydrogels GG-MP-BAC, GG-EDDS-MBA, GG-EDDS-BAC, GG-N,N'-DMEDA-MBA, GG-DMEDA-BAC, GG-DMEDA-MBA, GG-Lys-MBA were prepared following the same procedure described for GG-MP-MBA employing monomers and amounts listed here below.

GG-MP-BAC: GG (1503.4 mg; 8.34 mmol), LiOH•H_2O (711.1 mg; 16.78 mmol), MP (1716.6 mg; 16.28 mmol), BAC (5202.4 mg; 25.7 mmol), LiOH•H_2O (710.9 mg; 16.59 mmol), H_2O (40 mL). Yield: 3.40 g, 38.48%.

GG-EDDS-MBA: GG (1503.4 mg; 8.34 mmol), LiOH•H_2O (711.1 mg; 16.78 mmol), EDDS (11 mL; 16.28 mmol), LiOH•H_2O (658.0 mg; 15.52 mmol), MBA (4110.9 mg; 25.60 mmol), H_2O (30 mL). Yield: 2.92 g, 27.57%.

GG-EDDS-BAC: GG (1504.1 mg; 8.35 mmol), LiOH•H_2O (712.7 mg; 16.82 mmol), EDDS (11 mL; 16.28 mmol), LiOH•H_2O (658.5 mg; 15.54 mmol), BAC (5222.7 mg; 25.80 mmol), LiOH•H_2O (1075.3 mg; 25.37 mmol), H_2O (30 mL). Yield: 4.31 g, 35.40%.

GG-N,N'-DMEDA-MBA: GG (1503.6 mg; 8.35 mmol), LiOH•H_2O (715.6 mg; 16.88 mmol), N,N'-DMEDA (1.80 mL; 16.31 mmol), MBA (4015.4 g; 25.00 mmol), H_2O (40 mL). Yield: 3.93 g, 56.30%.

GG-DMEDA-BAC: GG (1506.6 mg; 8.36 mmol), LiOH•H_2O (714.2 mg; 16.85 mmol), N,N-DMEDA (1.80 mL; 16.31 mmol), BAC (5193.0 mg; 25.65 mmol), LiOH•H_2O (1075.3 mg; 25.37 mmol), H_2O (40 mL). Yield: 3.06 g, 37.50%.

GG-DMEDA-MBA: GG (1505.2 mg; 8.35 mmol), LiOH•H_2O (713.5 g; 16.83 mmol), N,N-DMEDA (1.80 mL; 16.31 mmol), MBA (4123.9 mg; 25.68 mmol), H_2O (40 mL). Yield: 2.71 g, 38.10%.

GG-Lys-MBA: GG (1501.3 mg; 8.35 mmol), LiOH•H_2O (709.8 g; 16.75 mmol), Lys (1256.1 mg; 8.34 mmol), MBA (4177.5 mg; 26.01 mmol), H_2O (40 mL). Yield: 2.97 g, 42.30%.

Results and discussion

The aim of this work was to demonstrate the feasibility of using guar gum in the synthesis of hybrid hydrogels with poly(amidoamine)s (PAAs) to potentially use as sorbents of heavy metal ions from wastewater. The PAA portions of the hydrogels stemmed from the polyaddition of either the cheap N,N'-methylenebisacrylamide (MBA) or 2,2-bisacrylamidoacetic acid (BAC) with either 2-methylpiperazine (MP), N,N-dymethylehtylenediamine (DMEDA), N,N'-dymethylehtylenediamine (N,N'-DMEDA), ethylenediaminodisuccinic acid (EDDS) or Lysine (Lys) as amine counterparts (Scheme 22). The PAA portions, though not always specifically endowed with remarkable ion complexing properties, represent good models of cost-effective either cationic or amphoteric PAAs. The synthetic route employed for the preparation of the hydrogels capitalized on the general reactivity of bisacrylamides in Michael addition, known to proceed with both primary and secondary amines at pH>7 and with alcohols at pH≥11. In particular, the devised process consisted in the reaction, carried out in aqueous solutions, of GG with either MBA or BAC and, as amine counterparts, either MP, or DMEDA, or N,N'-DMEDA, or EDDS or Lys. Due to solubility limits, the GG content in the feed varied from 12.36%$^{w}/_{w}$ for GG-EDDS-BAC to 21.65%$^{w}/_{w}$ in GG-Lys-MBA (Table 25). All hydrogel samples were purified by extensive washing with water/ethanol cycles, dried and analyzed. As showed by elemental and FTIR analyses, GG proved capable to efficiently react with bisacrylamides and amines under the experimental conditions adopted.

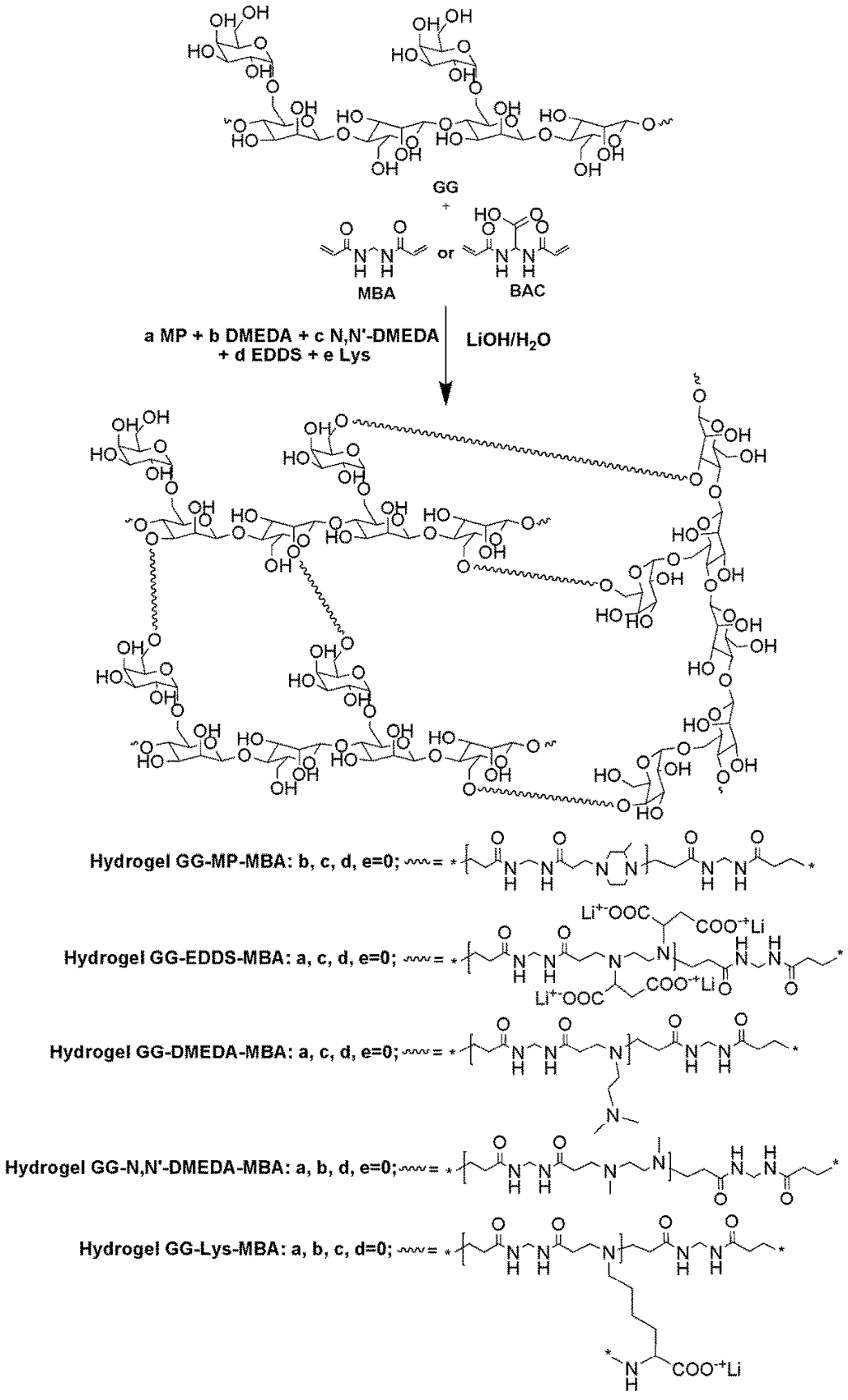

Scheme 22. Synthesis of GG-PAA hydrogels via Michael addition in water at pH≥11. As examples, only products prepared with MBA as a bisacrylamides are shown.

The results of the elemental analysis (Table 26) showed that the C/N ratio values of GG-PAA hydrogels were slightly higher than the calculated ones, indicating a preferential release of either linear PAA, bisacrylamide or amine in the purification process, and consistent with the presence of GG in the hydrogel structure.

Table 25. Amounts of reagents used in the syntheses of GG-PAA hydrogels.

Sample	GG/amine/ bisacrylamide [molar ratio]	OH/amine/ bisacrylamide [reactive functions ratio]	GG content [$^{w}/_{w}$%]	PAA content [$^{w}/_{w}$%]
GG-MP-BAC	1/ 1.95/ 3.08	1/ 0.43/ 0.68	17.85	82.15
GG-MP-MBA	1/ 1.95/ 3.08	1/ 0.43/ 0.68	20.80	79.20
GG-EDDS-BAC	1/ 1.95/ 3.08	1/ 0.43/ 0.69	12.36	87.64
GG-EDDS-MBA	1/ 1.95/ 3.08	1/ 0.43/ 0.69	13.60	86.40
GG-N,N'-DMEDA-MBA	1/ 1.95/ 2.99	1/ 0.43/ 0.67	21.50	78.50
GG-DMEDA-BAC	1/ 1.95/ 3.07	1/ 0.43/ 0.68	18.48	81.52
GG-DMEDA-MBA	1/ 1.95/ 3.07	1/ 0.43/ 0.68	21.25	78.75
GG-Lys-MBA	1/ 1/ 3.11	1/ 0.33/ 0.69	21.65	78.35

Table 26. Results of the elemental analysis of GG-PAA hydrogels.

Sample	C [%]		N [%]		C/N	C/N
	feed	found	feed	found	feed	found
GG-MP-BAC	49.12	40.95	14.45	9.17	3.40	4.47
GG-MP-MBA	53.09	47.50	17.13	10.91	3.10	4.35
GG-EDDS-BAC	43.51	40.40	10.22	6.34	4.26	6.37
GG-EDDS-MBA	43.64	42.94	10.58	7.24	4.12	5.93
GG-N,N'-DMEDA-MBA	51.39	48.08	17.09	12.67	3.01	3.79
GG-DMEDA-BAC	48.01	42.20	14.67	9.17	3.27	4.60
GG-DMEDA-MBA	51.44	46.76	17.10	10.86	3.01	4.31
GG-Lys-MBA	50.45	46.63	14.42	10.83	3.50	4.30

GG-PAA hydrogels were characterized by FTIR spectrophotometry and the results are shown in Figure 57. For comparison purposes the FTIR spectrum of GG is also reported. For each GG-PAA hydrogel a very strong band generally at 1025 cm^{-1} and due to guar gum C-O stretching is clearly visible. The broad band in the range of 3500–3200 cm^{-1} due to O–H stretching is also detectable and overlapped with amides N-H stretching. Amides also showed an intense C=O stretching band close to 1640 cm^{-1}. Hydrogels containing

COO^- functions such as GG-Lys-MBA, GG-EDDS-BAC, GG-EDDS-MBA, GG-DMEDA-BAC showed also asymmetric and symmetric $-COO^-$ stretching. While asymmetric $-COO^-$ stretching is overlapped wit NH amides bend, the symmetric $-COO^-$ stretching peak counts also for C-H scissoring and tertiary amines CN stretching. For these reasons, it is not possible to distinguish the different signals but, in general, those of BAC-containing hydrogels are more intense than those of MBA-containing products. For GG-EDDS-BAC hydrogel, amide C=O stretching is hardly detectable due to the high intensity of the nearby asymmetric $-COO^-$ stretching peak which prevails in this region of the spectrum. $-CH_2-$ bend give rise to a broad band between 1000 and 800 cm^{-1}, in general more intense for GG-PAA hydrogels than native GG due to the presence of methylene groups deriving from the crosslinking reaction, but also to C-H stretching bands in the 2970-2800 cm^{-1} region and to scissoring in the 1480-1350 cm^{-1} range.
In Table 27 the diagnostic bands detectable in GG-PAA spectra and their frequencies are reported.

Table 27. FTIR analysis: diagnostic peaks of GG-PAA hydrogels and their frequencies.

Sample	**Amide C=O str. [cm^{-1}]**	**Asymmetric $-COO^-$ str. and NH amide bend [cm^{-1}]**	**Symmetric $-COO^-$ str. and tertiary amine CN str. [cm^{-1}]**	**C-O str. [cm^{-1}]**
GG-MP-BAC	1615	1519	1392	1026
GG-MP-MBA	1648	1529	1372	1025
GG-EDDS-BAC	-	1575	1394	1025
GG-EDDS-MBA	1637	1551	1384	1025
GG-N,N'-DMEDA-MBA	1645	1533	1373	1025
GG-DMEDA-BAC	1618	1506	1379	1026
GG-DMEDA-MBA	1648	1533	1378	1028
GG-Lys-MBA	1638	1533	1380	1023

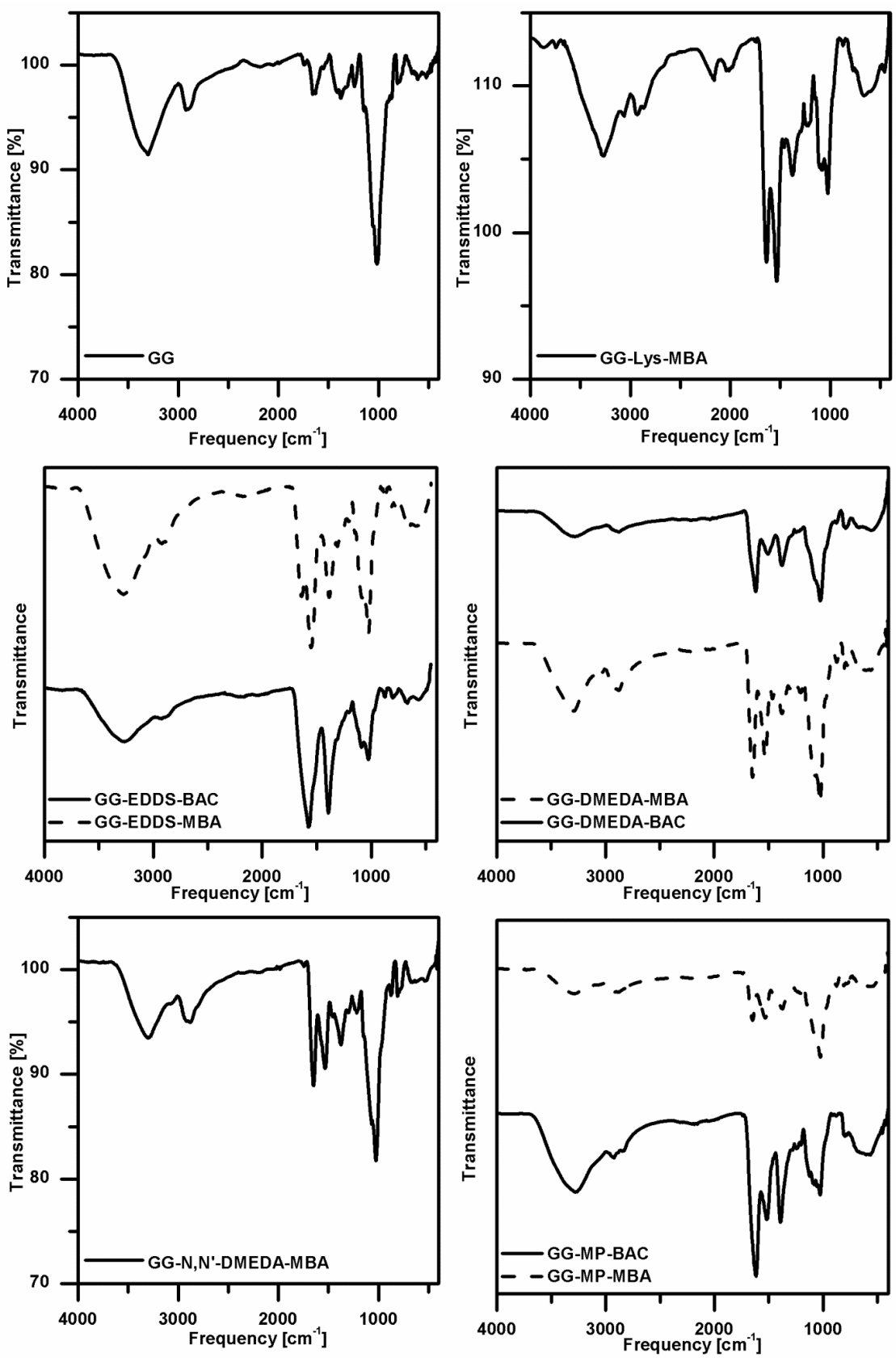

Figure 57. FTIR analyses of GG and GG-PAA hydrogels.

GG-PAA hydrogels were thermally characterized by means of DSC and TGA analyses. The DSC second run heating cycle, following a cooling cycle carried out at the same rate, is reported in Figure 58. For comparison purposes, GG thermogram is also reported. All samples showed no evidence of glass transition temperatures or melting phenomena in the temperature range investigated. A substantial thermal stability was observed up to 200 °C, with no dramatic decomposition events. Above 200 °C and in spite of the inert atmosphere, in some cases exothermic thermal decomposition occurred (Figure 58). The thermal behaviors of GG-PAA hydrogels samples were confirmed by thermogravimetric analysis (Figure 59). The TGA curves of GG and GG-PAA hydrogels were characterized by weight losses up to 13.17% at 100 °C due to dehydration and main thermal decompositions in the range 200-550 °C, with residual masses down to 6.57%. The thermal stability of GG-PAA hydrogels was comparable to that of GG, with 10% lower weight losses in the main decomposition stage. The only exception was GG-DMEDA-MBA whose thermal decomposition occurred at higher temperatures, between 350 °C and 550 °C, but with a considerably higher weight loss equal to 91.93% (Table 28). These results revealed that all of the samples were considerably thermally stable at temperatures up to 200 °C.

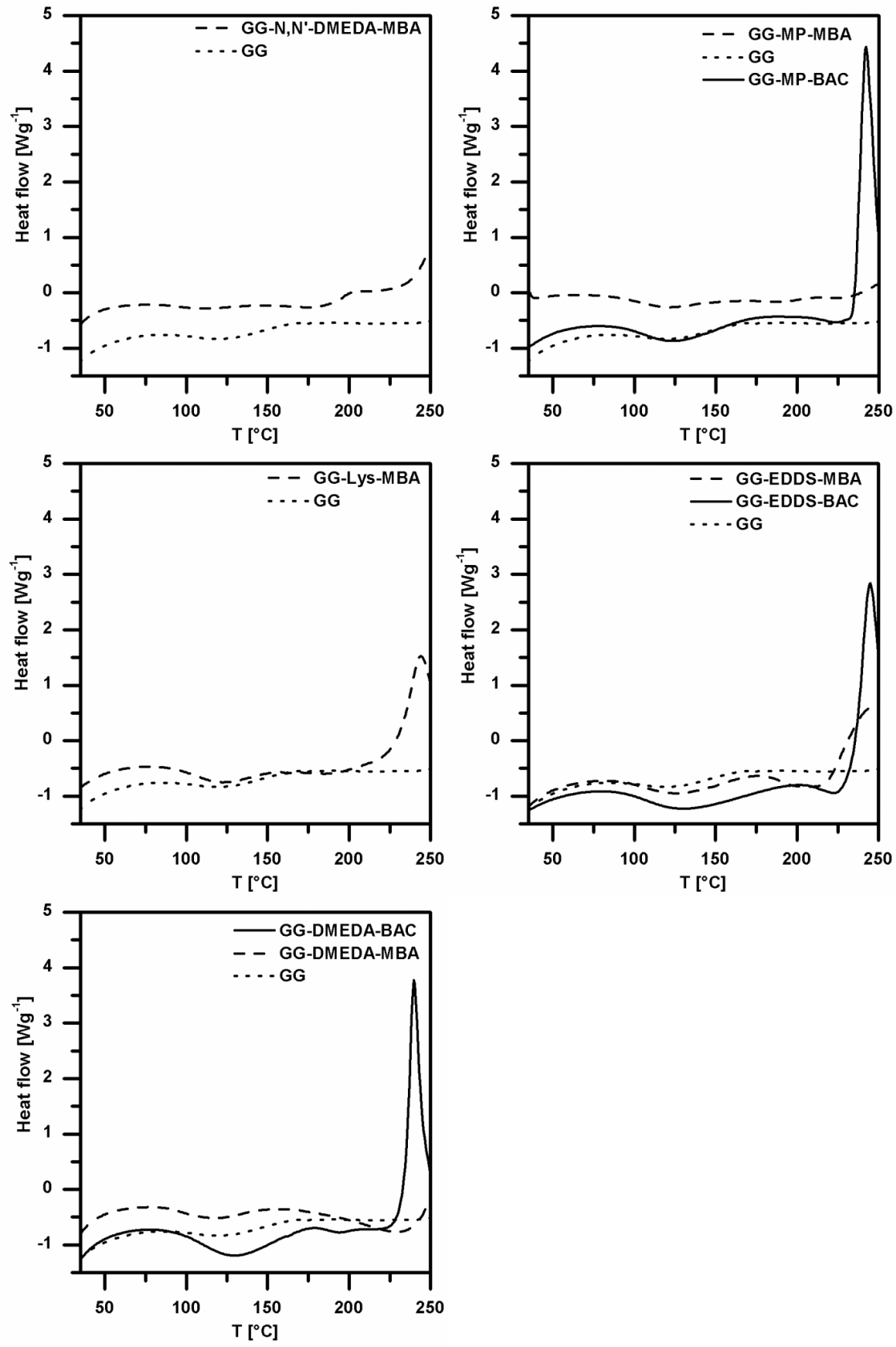

Figure 58. DSC second run curves for GG and GG-PAA hydrogels.

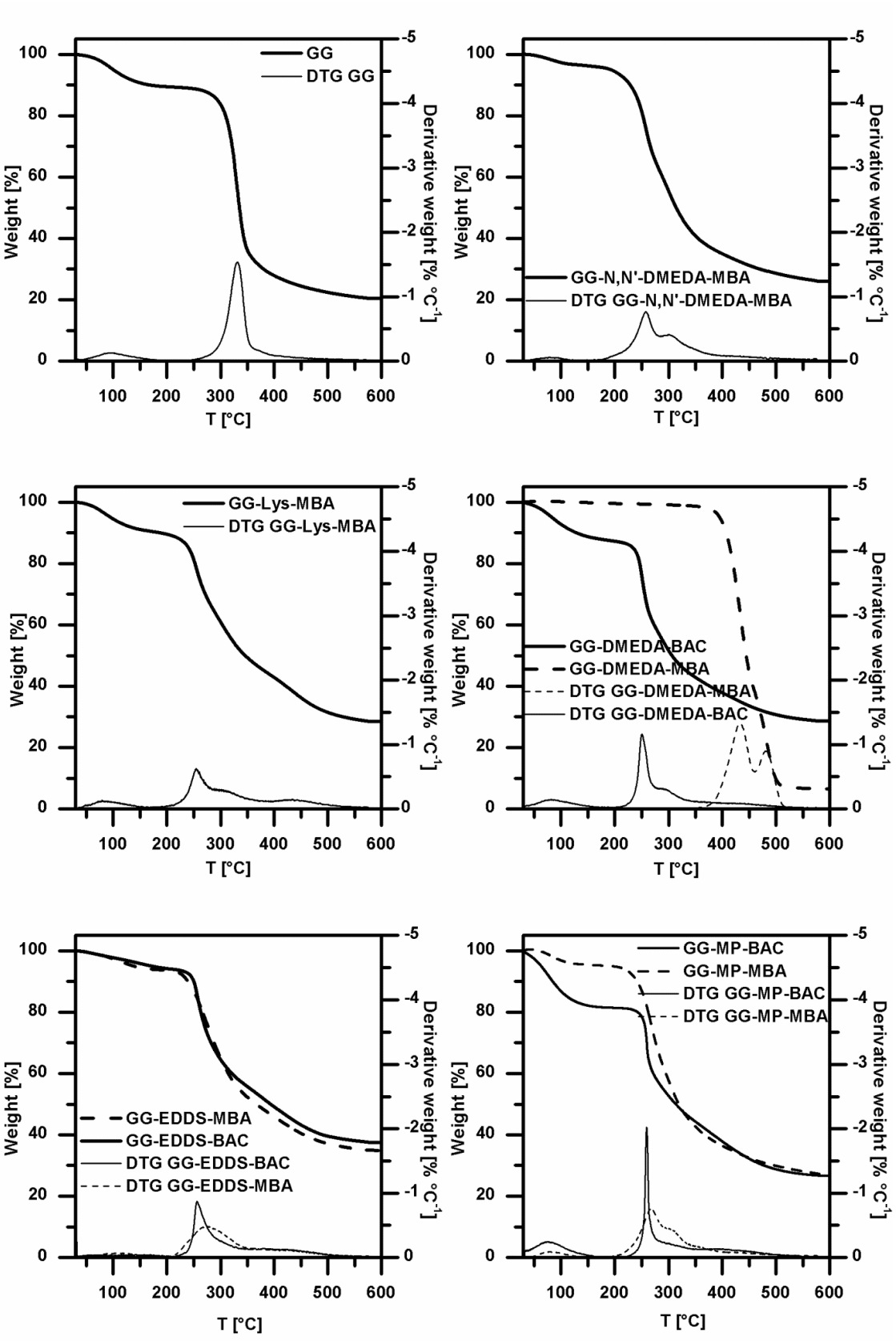

Figure 59. TGA thermograms for GG and GG-PAA hydrogels.

Table 28. Results of the TG analyses. T_{max} represents the temperature of the highest weight loss rate.

Sample	Dehydration (T=100 °C)	Main decomposition stage			Residual weight at 600 °C [%]
	Weight loss [%]	T range [°C]	T_{max} [°C]	Weight loss [%]	
GG	4.95	250-500	329.58	66.41	20.45
GG-MP-BAC	13.17	200-500	259.17	52.64	26.70
GG-MP-MBA	3.13	200-500	267.45	64.97	27.31
GG-EDDS-BAC	2.27	200-500	253.51	54.59	37.50
GG-EDDS-MBA	2.65	200-500	273.84	56.57	34.93
GG-N,N'-DMEDA-MBA	2.68	200-500	258.16	65.75	26.05
GG-DMEDA-BAC	7.23	200-500	248.56	56.59	28.65
GG-DMEDA-MBA	0	350-550	432.38	91.93	6.57
GG-Lys-MBA	5.48	200-500	262.98	58.10	28.49

The swelling behavior of the hydrogels was evaluated on the products as dried fine powders in H_2O and 0.01 M buffer solution (Figure 60). It is apparent that while all of the products can be considered as highly hydrophilic, the water absorption of GG-EDDS-BAC was outstanding. This is, in fact, a superabsorbent polymer, in line with the commonly adopted definition for this category of products. [20] It may be observed that the number of ionizable groups, that is, the charge density at pH 5.5 (in doubly distilled H_2O) of GG-EDDS-BAC is particularly high, probably resulting in higher hydration shell and higher electrostatic repulsion than the other GG-PAA hydrogels. As a consequence, hydrogels prepared with BAC showed higher swelling degrees than those prepared with MBA as a bisacrylamide. The same trend is observed at pH 7.4. Furthermore, the most of hydrogels showed larger swelling in water than in buffer solution, probably due to the higher ionic strength induced by the buffer salts. It is known that an osmotic pressure difference exists between internal and external solutions of the gel network in aqueous media. [21] [22] In the presence of external ions, the ratio of ions between the interior of the hydrogel and the surrounding environment decreases and, for GG-PAA hydrogels, the interactions with external ions became more significant than the electrostatic repulsion within the network. Moreover, the presence of electrostatic interactions between COO^- and amine nitrogens within the hydrogel network cannot be excluded. As a consequence, the osmotic pressure difference decreases and results in a shrinkage of the network in PBS. [21] [23] In the case of GG-MP-MBA and GG-N,N'-DMEDA-MBA, the swelling

in PBS is slightly higher than in water while for GG-DMEDA-MBA the values are very similar. Since no $–COO^-$ functions are present in these cationic hydrogels, the behavior is probably due to the electrostatic repulsions among amine nitrogens in the hydrogel network that either balance or are more significant than interactions with external ions.

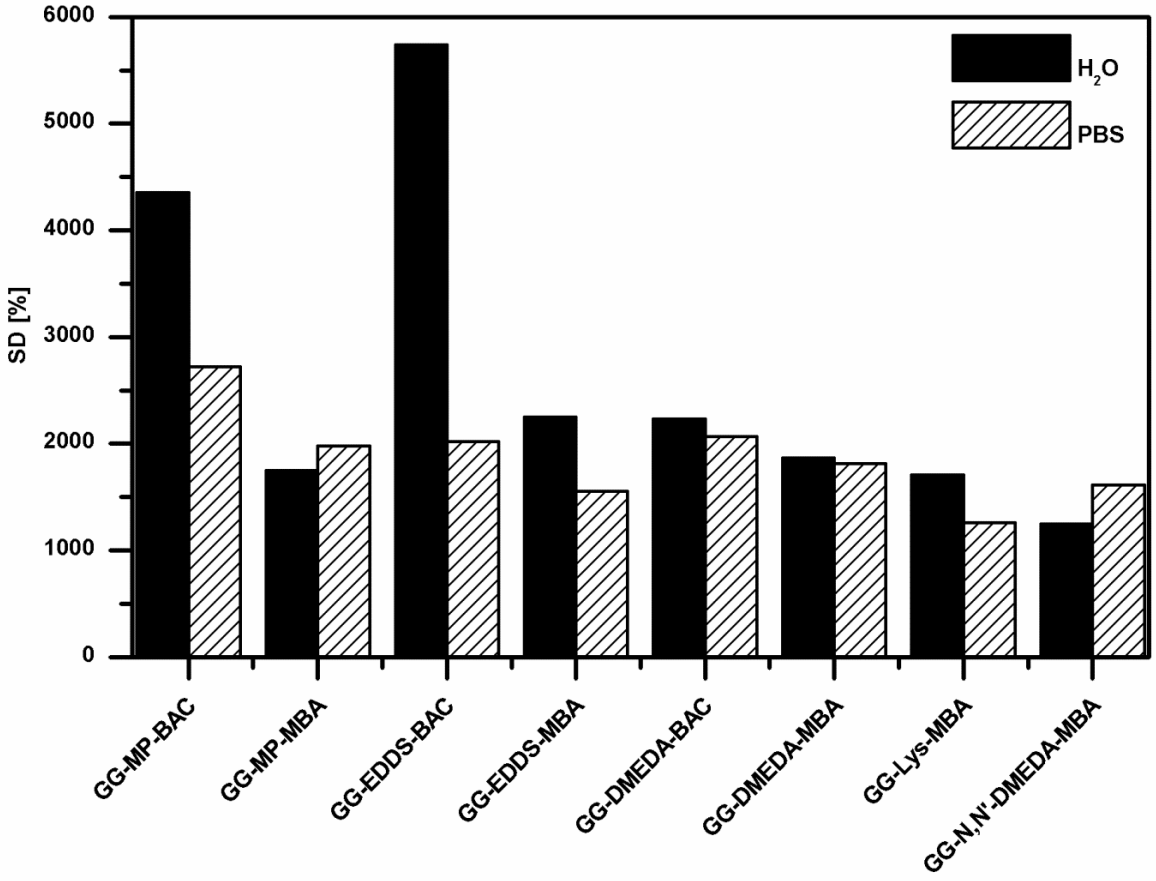

Figure 60. Swelling behavior of GG-PAA hydrogels: swelling percentage volume per volume (SD% $^{v}/_{v}$) are reported in H_2O and PBS at pH 7.4.

Preliminary investigations concerning the heavy metal ion absorption capacity of the hydrogels were carried out in batch, incubating swollen hydrogel samples with single heavy metal ion aqueous solutions until equilibrium concentrations were achieved. The initial and final ion concentrations of Cd^{2+}, Zn^{2+}, Ni^{2+}, Cu^{2+} and Co^{2+} were determined via complexometric titration with ethylenediaminetetraacetic acid (EDTA). Batch tests of absorption capacity of excess metal ions from 1000 ppm aqueous solutions showed that GG-PAA hydrogels were able to absorb all the tested ions (Figure 61). The absorption capacities obtained, corresponding to 10-130 mg Me^{2+} g^{-1} hydrogel (depending on the metal atomic weights), were competitive with the literature data for other absorbing materials considering both the absorption capacities and the wide range of metal ions

absorbed, which is reasonably expected to extend beyond the model metal series considered in this study. [24] [25] [26] [27]

Several relevant correlations between the observed capacities and the peculiar structural features of hydrogels were identified. In general, ion absorption capacities changed dramatically by varying the amine composition. In particular, EDDS-containing hydrogels exhibited overall the highest ion complexing ability. Furthermore, BAC-containing hydrogels showed higher absorption capacities than hydrogels prepared with MBA as a bisacrylamide, suggesting a cooperative effect of amine and carboxyl functions in ion complexation. For the same reason, GG-EDDS-BAC generally showed the highest complexing capacity. The abatement percentage, calculated by equation 2, followed the same trend as the absorption capacities, increasing with increasing the amount of metal ion absorbed. For Cu^{2+} the abatement varied between 24.3% and 60.9%, for Co^{2+} between 14.4% and 54.3%, for Ni^{2+} between 8.6% and 75.6%, for Zn^{2+} between 0% and 45.4% and for Cd^{2+} between 9% and 74.9%. The highest abatements were reached by GG-EDDS-BAC towards Ni^{2+} (75.6) and Cd^{2+} (74.9). Overall, the more versatile hydrogel was GG-EDDS-MBA showing abatement percentages always above 52% (Figure 61).

$$A\,[\%] = \frac{\text{Absorbed } Me^{2+}\,[mg]}{\text{Initial } Me^{2+}\,[mg]} \times 100 \qquad \text{Equation 2}$$

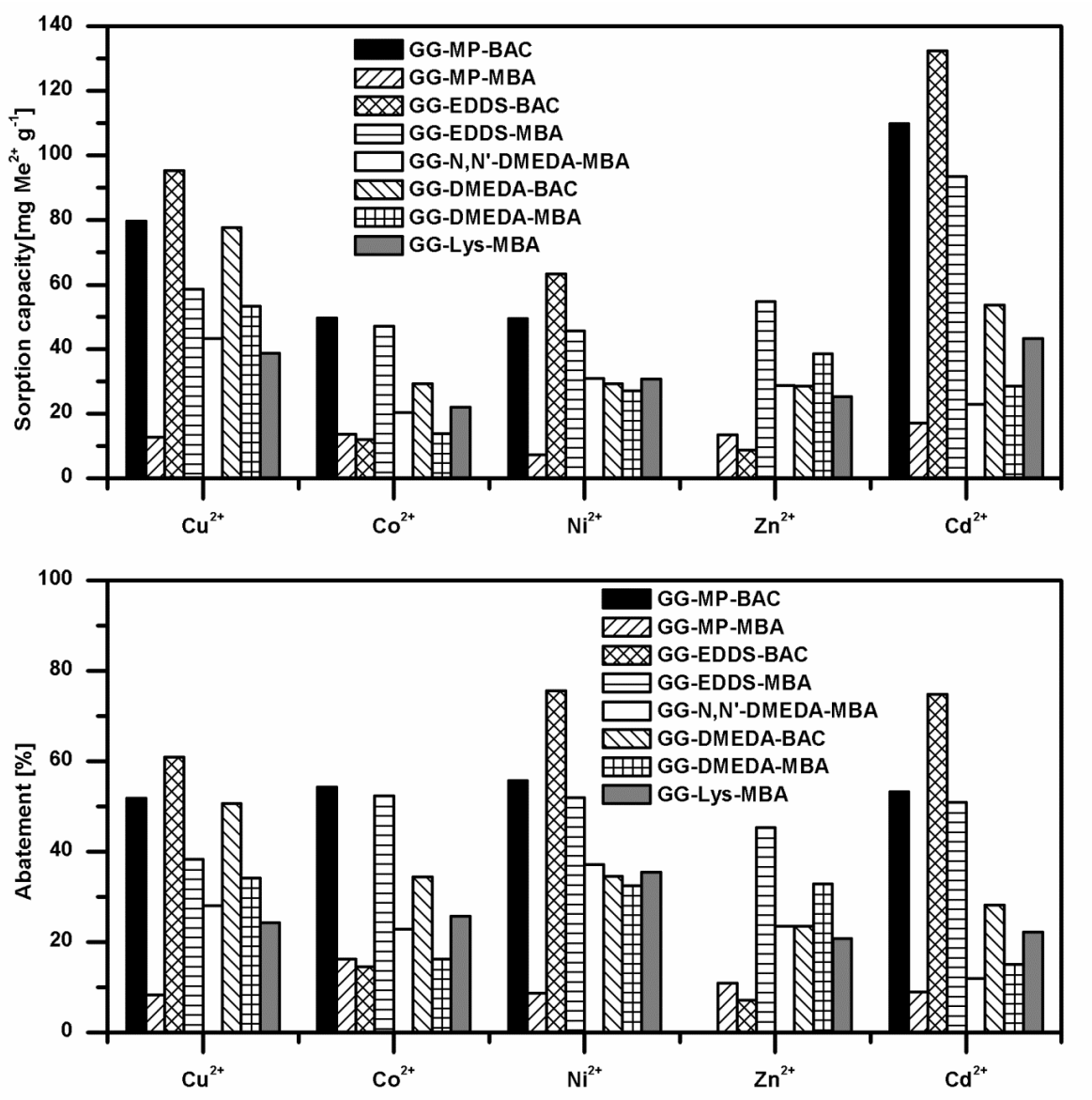

Figure 61. Absorption capacities and abatement percentages of GG-PAA hydrogels at an initial metal ion concentration of 1000 ppm.

The same experiment also gave indication about the chromatic changes of the resins upon metal ion absorption. In some cases and particularly with Cu^{2+}, Co^{2+}, and Ni^{2+}, the absorption process resulted in intense and fast coloring of the hydrogels (blue, pink, and green, respectively). As an example, in Figure 62 the chromatic changes of GG-EDDS-BAC hydrogel are shown. This feature may be in principle exploited in diagnostic kits or, if the resins are used for water purification, adopted as indicator of their degree of exhaustion and, therefore, of the regeneration timing.

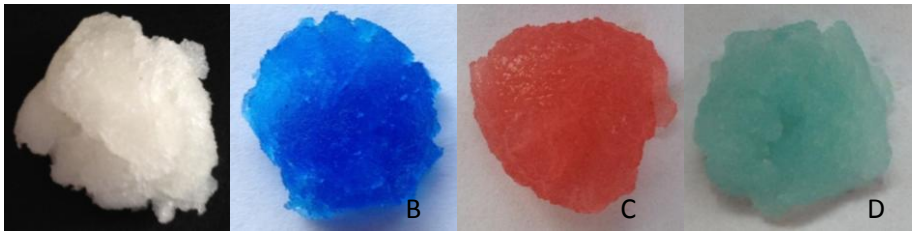

Figure 62. Chromatic changes of GG-EDDS-BAC upon ion absorption. Native resin (left), resin upon Cu^{2+} (B), Co^{2+} (C) and Ni^{2+} (D) adsorption.

In the case of GG-EDDS-BAC, GG-EDDS-MBA, GG-DMEDA-BAC, GG-DMEDA-MBA and GG-MP-BAC, showing the highest absorption capacities towards specific heavy metal ions, the absorption performance towards selected ions was investigated also in the low concentration range (50 ppm) in order to identify their potential for ion abatement in dilute solutions. In particular, for each metal ion, the two hydrogels showing the best performances at an initial metal ion concentration of 1000 ppm were studied also on diluted solutions. Absorptions from 50 ppm single metal ion solutions (Figure 63) demonstrated that the hydrogel complexing ability strongly depended on the metal ion concentration since the absorption capacity decreased with decreasing the metal ion concentrations down to 1/6, if compared to the results obtained with 1000 ppm initial ion concentration. The abatement percentages followed the opposite trend and with Cu^{2+}, Co^{2+}, Ni^{2+} and Zn^{2+} reached 100%, meaning that the whole amount of heavy metal ion in solution was absorbed by the hydrogel. With Cd^{2+} the absorption percentages were always higher than 55%.

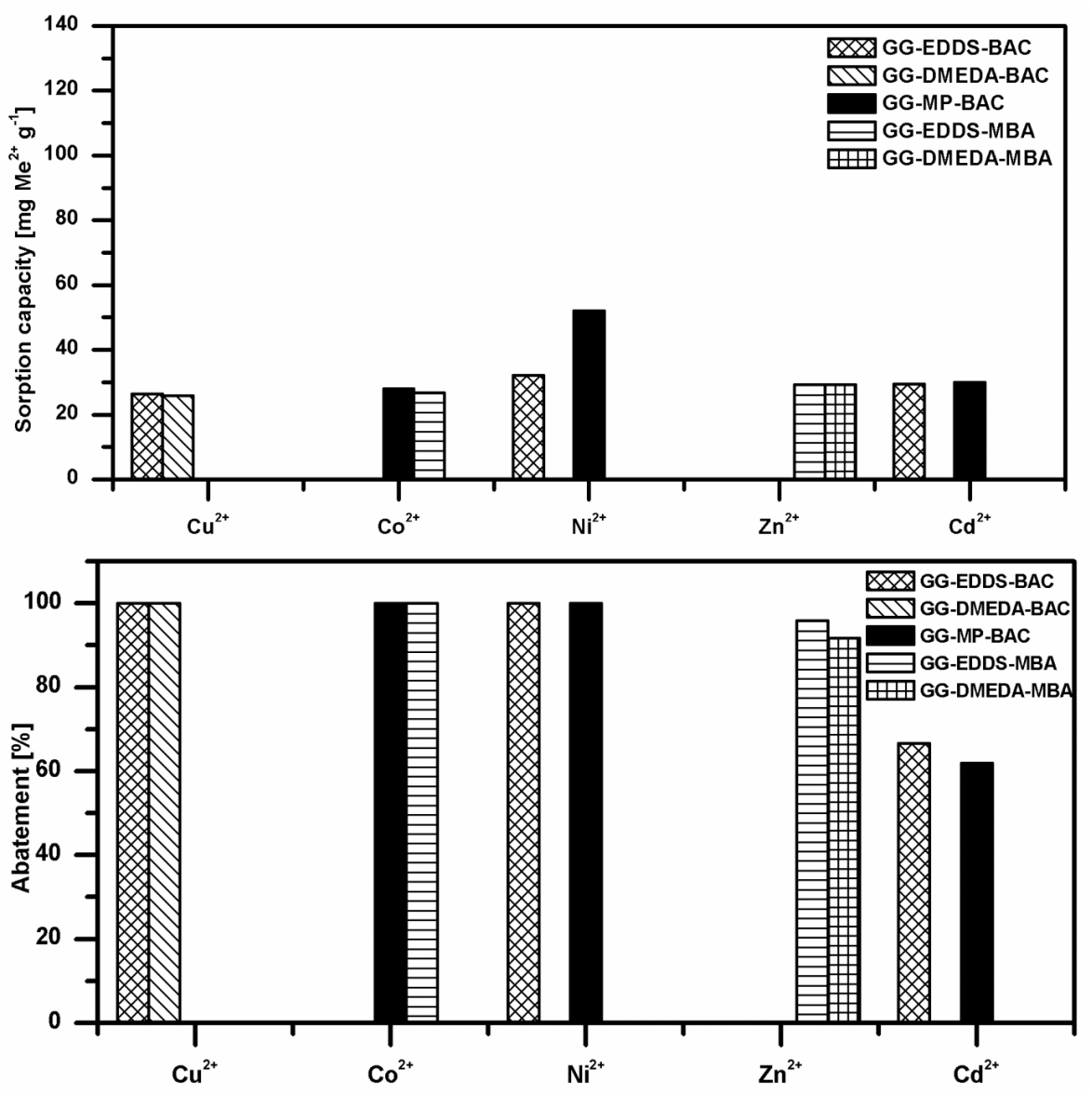

Figure 63. Absorption capacities and abatement percentages of GG-PAA hydrogels at an initial metal ion concentration of 50 ppm. For each metal ion, the two hydrogels showing the best performances at an initial metal ion concentration of 1000 ppm were studied also on diluted solutions at 50 ppm.

The possibility of recycling the absorbent with small regeneration additional costs, avoiding therefore its immediate disposal, is one of the most important characteristics for materials with application in the environmental field. For this reason, the absorption performance of GG-PAA hydrogels was studied also on a series of four consecutive absorption-desorption cycles. Figure 64 illustrates the adsorption and desorption behaviors of GG-PAA hydrogels. For each heavy metal ion, the hydrogels showing the most promising results in the absorption experiments were selected for this study.

Between each cycle, the material was regenerated by washing with 0.01 M HCl, thoroughly rinsed with water hence re-employed for the absorption of the selected metal ion from fresh 1000 ppm aqueous solution. In diluted HCl solution, the protons compete with metal ions for amines and carboxyl groups, therefore are responsible for the easy desorption of metal ions. This also suggests that the main adsorption mechanism is ion exchange.

For all of the hydrogel tested, the absorption capacity slightly decreased after the first absorption cycle, probably due to the extraction of residual soluble fractions that contributed to enhance the absorption capacity of the hydrogels. The absorption performance of each GG-PAA hydrogel studied remained then unchanged until the last absorption cycle, thus indicating that reuse has little influence on the metal ion uptake.

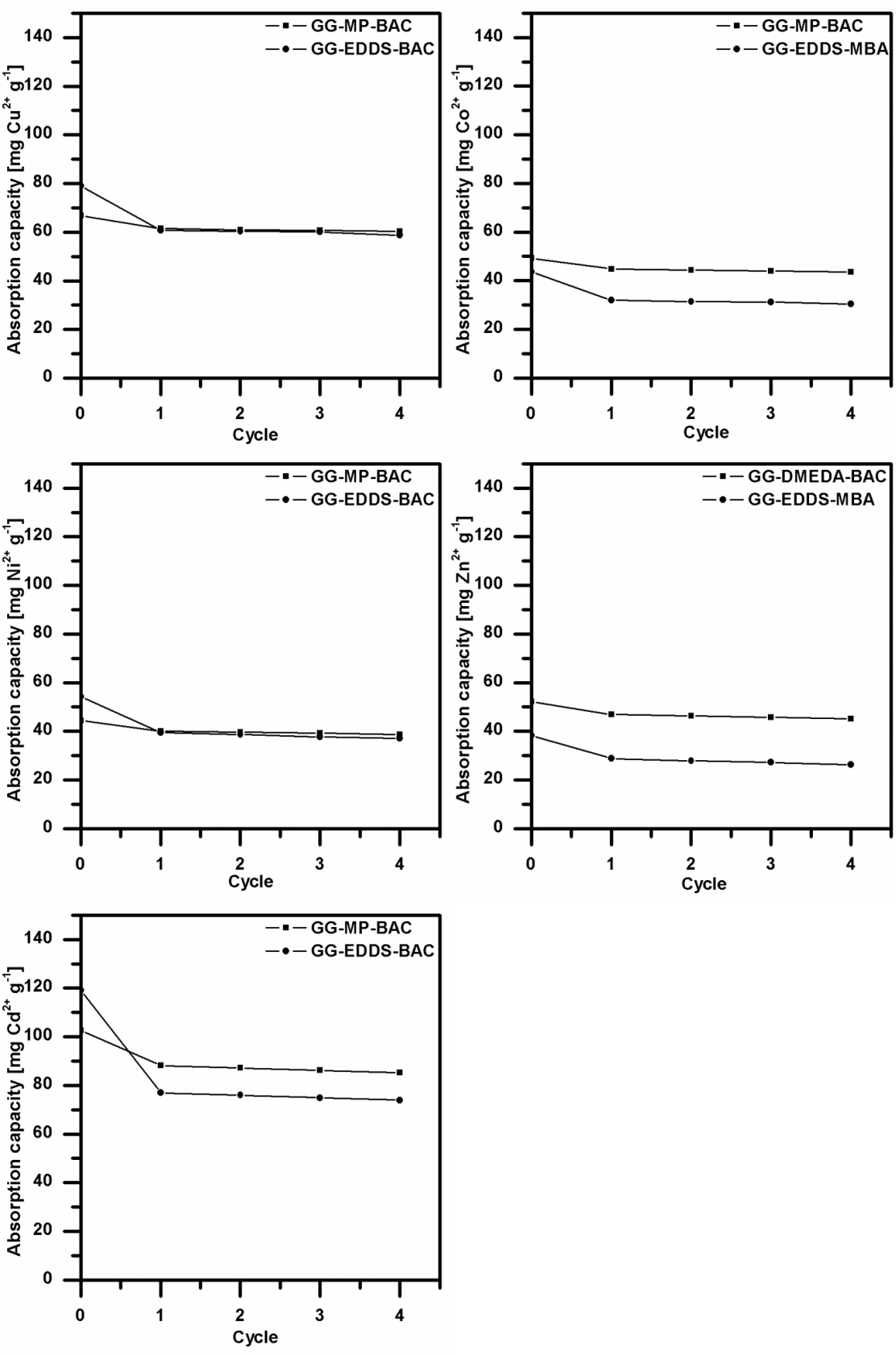

Figure 64. Absorption capacities for GG-PAA hydrogels recycling on four consecutive absorption-desorption cycles.

Conclusions

This work reports on the synthesis and characterization of hydrogels obtained from guar gum (GG) and poly(amidoamine)s (PAA). GG-PAA hydrogels with different characteristics were prepared by Michael polyaddition reacting GG with either N,N'-methylenebisacrylamide (MBA) or 2,2-bisacrylamidoacetic acid (BAC) and amine counterparts such as 2-methylpiperazine (MP), N,N-dymethylehtylenediamine (DMEDA), N,N'-dymethylehtylenediamine (N,N'-DMEDA), ethylenediaminodisuccinic acid (EDDS) or Lysine (Lys) in alkaline aqueous solution. GG-PAA hydrogels proved highly swellable in aqueous media, being able to sorb up to 58 times their dry weight, and thermally stable up to 200 °C.

Preliminary studies concerning their heavy metal ions absorption capacity showed that GG-PAA hydrogels were able to remove Cd^{2+}, Zn^{2+}, Ni^{2+}, Cu^{2+} and Co^{2+} from aqueous solutions with absorption capacities from 10 to 130 mg/g at an initial ion concentration of 1000 ppm. Furthermore, they proved able to completely abate heavy metals from 50 ppm solutions and are competitive with other materials reported in literature. [24] [25] [26] [27]

In most cases, their absorption performances improved increasing the $–COO^-$ content, leading to the conclusion that the absorption was significantly driven by PAAs. Finally, the absorption of several metal ions imparted intense coloring to the resins, a feature exploitable for analytical purposes such as real-time detection of the presence of ions. All GG-PAA hydrogels were obtained at moderate cost by eco-friendly procedures, with a potentially scalable synthetic process that let envisage a high potential for the design of different GG-based materials with interesting functional properties.

References

[1] E. Abdel-Halim, S. Al-Deyab, *Carbohyd. Polym.,* vol. 86, pp. 1306-1312, 2011.

[2] X. Peng, L. Zhong, J. Ren, R. Sun, *J. Agr. Food Chem.,* vol. 60, pp. 3909-3916, 2012.

[3] G. S. Chauhan, S. Mahajan, *J. Appl. Polym. Sci.,* vol. 86, pp. 667-671, 2002.

[4] H. A. Shawky, A. El-Hag Ali, R. A. El Sheikh, *J. Appl. Polym. Sci.,* vol. 99, pp. 2904-2912, 2006.

[5] A. Q. Dong, J. Xie, W. M. Wang, L. P. Yu, Q. Liu, Y. P. Yin, *J. Hazard. Mater.,* vol.

181, pp. 448-454, 2010.

[6] D. W. O'Connell, C. Birkinshaw, T. F. O'Dwyer, *Bioresource Technol.*, vol. 99, pp. 6709-6724, 2008.

[7] B. Kannamba, K. L. Reddy, B. V. AppaRao, *J. Hazard. Mater.*, vol. 175, pp. 939-948, 2010.

[8] K. Kadirvelu, M. Kavipriya, C. Karthika, M. Radhika, N. Vennilamani, S. Pattabhi, *Bioresour. Technol.*, vol. 87, pp. 129-132, 2003.

[9] R. H. W. Wientjes, M. G. H. Duits, R. J. J. Jongschaap, J. Mellema, *Macromolecules*, vol. 33, pp. 9594-9605, 2000.

[10] P. A. Todd, P. Benfield, L. K. Goa, *Drugs*, vol. 39, pp. 917-928, 1990.

[11] R. Barbucci, D. Pasqui, R. Favaloro, G. Panariello, *Carbohyd. Res.*, vol. 343, pp. 3058-3065, 2008.

[12] I. Gliko-Kabir, B. Yagen, A. Penhasi, A. Rubinstein, *J. Control. Release*, vol. 15, pp. 1019-1025, 1998.

[13] I. Gliko-Kabir, A. Penhasi, A. Rubinstein, *Carbohydr. Res.*, vol. 316, pp. 6-13, 1999.

[14] Y. Huang, H. Yu, C. Xiao, *Carbohyd. Polym.*, vol. 69, pp. 774-783, 2007.

[15] S. Swaminathan, R. Cavalli, F. Trotta, P. Ferruti, E. Ranucci, I. Gerges, A. Manfredi, D. Marinotto, P. R. Vavia, *J. Incl. Phenom. Macro.*, vol. 68, pp. 183-191, 2010.

[16] P. Ferruti, *J. Polym. Sci.Pol. Chem*, vol. 51, pp. 2319-2353, 2013.

[17] P. Ferruti, E. Ranucci, S. Bianchi, L. Falciola, P. R. Mussini, M. Rossi, *J. Polym. Sci.Pol. Chem*, vol. 44, pp. 2316-2327, 2006.

[18] P. Ferruti, E. Ranucci, A. Manfredi, N. Mauro, E. Ferrari, R. Bruni, F. Colombo, P. Mussini, M. Rossi, *J. Polym. Sci.Pol. Chem*, vol. 50, pp. 5000-5010, 2012.

[19] A. Manfredi, E. Ranucci, S. Morandi, P. R. Mussini, P. Ferruti, *J. Polym. Sci.Pol. Chem*, vol. 51 , pp. 769-773, 2013.

[20] F. L. Buchholz, A. T. Graham, Modern Superadsorbent Polymer Technology, New York: Wiley, 1997.

[21] O. Okay, S. B. Sariisik, S. D. Zor, *J. Appl. Polym. Sci.*, vol. 70, pp. 567-575, 1998.

[22] C. Alvarez-Lorenzo, O. Guney, T. Oya, Y. Sakai, M. Kobayashi, T. Enoki, Y. Takeoka, T. Ishibashi, K. Kuroda, K. Tanaka, G. Wang, A. Yu, G. S. Masamune, T. Tanaka, *Macromolecules*, vol. 33, pp. 8693-8697, 2000.

[23] Y. Li, T. Tanaka, *Annu. Rev. Mater. Sci.*, vol. 22, pp. 243-277, 1992.

[24] T. A. Kurniawan, G. Y. S. Chan, W. Lo, S. Babel, *Sci. Total Environ.*, vol. 366, pp. 409-426, 2006.

[25] K. Chauhan, G. S. Chauhan, J.-H. Ahn, *Bioresource Technol.*, vol. 100, pp. 3599-3603, 2009.

[26] A. Khan, F. Mahmood, S. Ahmed, M. Khokhar, *J. Sol-Gel Sci. Techn.*, vol. 27, pp. 221-224, 2003.

[27] J. Tripathy, D. K. Mishra, A. Srivastava, M. M. Mishra, K. Behari, *Carbohyd. Polym.*, vol. 72, pp. 462-472, 2008.